FORCE COMMUTATED INVERTERS FOR CONVERSION AND CONTROL OF MHD POWER

THESIS SUBMITTED FOR THE DEGREE OF

Doctor of Philosophy

IN

ELECTRICAL ENGINEERING

BY

MOHIBULLAH

DEPARTMENT OF ELECTRICAL ENGINEERING
Z. H. COLLEGE OF ENGINEERING & TECHNOLOGY
ALIGARH MUSLIM UNIVERSITY
ALIGARH (INDIA)

May 1988

ACKNOWLEDGEMENTS

I wish to express my sincere thanks and appreciation to all concerned staff in the School of Electrical Engineering, University of Sydney, Sydney, and the Department of Electrical Engineering, Aligarh Muslim University, Aligarh who have given me all possible assistance and encouragement during the preparation of this thesis.

My special thanks are due to G.J. Sanders, S. Ramakrishnan and V.J. Gosbell for their supervision guidance and valuable suggestions through out the course of this work. The author is indebted to Professor H.K. Messerle, the Head of School, for providing all possible facilities in the school. I also extend my special thanks to Prof. M.S. Beg, Prof. S.A. Abbasi, Prof. M.T. Ahmad, Prof. G. Mehboob and Prof. R.K. Gupta for their encouragement and guidance.

I wish to express deep appreciations to my colleagues particularly to John Voumard, Susilo Matair, Rob Lang and N.D. Heip with whom the author had useful discussions.

The author is thankful to Dr. M. Ramamoorty, Visiting Fellow and Mr. Trivor Kearney, Professional Officer, School of Electrical Engineering, for useful discussions and suggestions in experimental work.

I am indebted to the University of Sydney for the

provision of Postgraduate Research Award while the study was being carried out.

The author extends his feelings of gratitude towards all his family members, specially his wife, son and brother, Mr. Waliullah, for their patience and cooperation during this study.

Finally, the author wishes to extend his thanks to all those, who gladly helped him, in one way or the other to bring this work in its present form.

ABSTRACT

The work reported in this thesis pertains to the problems associated with a forced commutated inverter for the integration of an MHD generator into an A.C. power network. The study illustrates the feasibility of using a simple square wave inverter to convert and control the output power of an MHD duct feeding into a power system.

Power flow equations have been derived treating MHD-inverter link as a single machine connected to infinite bus. Operating point is located for the maximum power transfer from an MHD duct with particular values of series reactor and phase shift angle. Modified power flow equations are derived with filters added to eliminate harmonics. A computer programme has been prepared to simulate the connection of either a square wave or a PWM inverter to the MHD duct.

A simple scheme has been presented for the simulation of MHD inverter link in the laboratory. The results of digital simulation are verified with the experimental setup. The detailed design of inverter and associated components is presented for the inter-connection of the 2MW, 20 electrode pair MHD test facility. An experiment is conducted to predict the approximate length of a rewirable fuse wire for the protection of semiconductor devices of known I^2t ratings.

An automatic feedback controller for power control from an MHD duct has been designed, fabricated and tested. The steady state and dynamic response of the simulated system is demonstrated. The transient interaction of a multiple-electrode MHD generator with a force commutated inverter is described. Time dependent computer model of the MHD generator has been used for the determination of V-I characteristics. Sudden load changes have been considered from operating point and transients have been studied for various cases of interest.

TABLE OF CONTENTS

CHAPTER 1 : INTRODUCTION

1.1 General Introduction

1.2 MHD Generator-Power System Integration

1.3 Scope and Outline of the thesis

CHAPTER 1

INTRODUCTION

1.1 General Introduction

Magnetohydrodynamic (MHD) direct energy conversion was first observed by Michael Faraday in 1932. The phenomenon was experimentally verified by him, by sensing, through galvonometer, the emf induced in the saline and hence conducting water of river Thames due to its flow in the magnetic field of the earth [1,2]. The extraction of electrical energy from such a natural source could not gain momentum as the conductivity of water is quite low and the earth's magnetic field very weak to yield appreciable amount of electrical power. Besides the Thames river investigations, most of the Faraday's work was with conductive liquid metals, like murcury. It was some times late in the 19th century that the electrical properties of thermally ionised gases and their interaction with magnetic field were studied and the feasibility of MHD generation was realised. After the World War II, Magnetohydrodynamics (MHD) emerged as one component of developing interests in the understanding and utilization of ionized gases or plasmas under high temperature conditions. Kinetic theory of gases, statistical mechanics and quantum theories were developed in large part as explanations of what happened in gas discharge tubes [3].

In 1940 Karlovitz patented the design of an MHD device and around 1950's, Dr. Arthur R. Kantrowitz and young researchers did the original work for the MHD power generation [3]. In the year 1959 AVCO,s first generator, the Mark-I was built by Dr. Richard J. Rosa [4,5]. From 1960 to mid seventies number of test and experimental facilities were setup with international exchange of informations [6].

The characteristics of an MHD generator like its compactness, simplicity and high power density makes it specially suitable for a variety of applications in the military area. That is why it was developed during the world war II as mentioned above. An MHD system has no moving parts, operates at high temperature and has low weight to power ratio. As such it is found to be very appropriate for space applications like space vehicles, space power systems, space plateforms in addition to power systems in aircrafts and ship propulsion. A unique use of an MHD generator is as a portable source of power for emergency, standby or mobile requirements including temporary power for scientific experiments in isolated areas [2].

The area in MHD development that has received the maximum international attention and has a potential for power generation is the MHD conversion in fossil fuel based systems. Inspite of advent of other energy sources coal still remains the most important fuel for power generation all over the world

and about 79 percent of electrical power is supplied by thermal power plants[7]. With the increasing energy demands and diminishing reserves of natural fossil fuels, lot of time and energy has been spent in evaluating the alternative concepts in the energy conversion techniques. In mid seventies Energy Conservation Alternatives Study (ECAS) was conducted and the results proved that open cycle, coal-fired, direct preheat MHD systems have potentially one of the highest coal-pile to bus-bar efficiency and also one of the lowest cost of electricity (COE) among the various advanced power plant concepts using coal or coal derived fuels [8]. For better efficiency and cheap-er electrical power generation an MHD generator and associated components could be coupled to an existing conventional steam plant as a topping cycle and could be optimized for full load operation as a base load plant [9]. However occasional demands for part load operation may also occur during emergencies.

A first stage coal fired MHD plant is projected to achieve a cycle efficiency of 48 to 52 percent compared to conventional plants of about 29 to 35 percent and second stage MHD generation is expected with an overall efficiency of 60 percent. The consumer cost of electricity per KWh with MHD system will be approximately 18 to 20 percent lower than the conventional thermal power plants. and the fuel saving between 20 to 30 percent with less heat wastage per unit

of the useful power generated [10].

In addition to cost and efficiency consideration, MHD technology has also been viewed for commercial applications because of its better thermal and air pollution control features. The improved efficiency in MHD plants implies a reduction of pollutents. A further reduction is achieved with the emission control schemes. NO_x once formed in the combustor can be efficiently reduced along the flow path in the MHD channel with the optimised distribution of temperature, pressure and velocity. SO_x is automatically removed as seed material combines with sulphur as the gas steam cools [11]. It is reported that 99 percent oxides of sulphur out of the gases emitted from the MHD generator are eliminated and thus the pollution kept within the permissible limits. Also two stage cyclonic combustor with ammonia injection reduces the NO_x emission well below the permissible limits. Waste disposal involves several million tonnes of ash per year from any normal power station at present. A reduction in coal consumption implies considerable ash reduction [12]. Further studies are being carried out and new technologies are being developed for better environmental and pollution control [13,14].

Because of the above promising potentials Magneto-hydrodynamic power generation from the fossil fuels is

emerging as the most effective energy conversion method [15]. The construction of a commercial fuel-fired MHD generator unit with a capacity of 500 MW has already begun at the site of the Ryazan Central Power Station (USSR). The commissioning is planned in near future. At the outset of 1990's the first fuel-fired commercial power generating MHD unit having a capacity of 500-1000 MW is expected to be installed [16].

MHD involves many disciplines. The knowledge of disciplines such as, gasdynamics, thermodynamics, plasma physics, Electromagnetics, fluid mechanics etc. is necessary for the analysis and design of MHD power generators. International cooperation is very much helpful in the system design, material development, plasma effects, component design and development, diagnostics and power system integration. Tr mendous progress has already been made in these areas and commercial generators for large scale integration of MHD power into existing power grid are expected very soon. MHD activities in various countries depend upon the type of systems being considered and the level of efforts involved. The international liason group on MHD electrical power generation is providing exchange of informations between the specialist's of various countries. Research and development work has been stepped up at an advance level to commercialize this technology by the end of this century in many

countries of the world particularly, USA, USSR, Japan, Netherland, China, Australia and India [17-26].

1.2 MHD Generator Power System Integration

MHD power is delivered in direct current form which could be used directly in the normal chemical processes without the need for d.c./a.c. inversion but most economic and useful application of MHD generation is for the interconnection of MHD generator with electrical supply utility for bulk power transmission. Interfacing MHD power plants with the stablished electric utility grid depends upon the ability to afficiently and reliably invert d.c. power to conventional a.c. power. Therefore the inverter systems, which accomplish this process are an important subsystem of an MHD power plant. They should be efficient, reliable economical and carefully controlled systems. So far two types of inverter systems have been developed, namely, a rotary inverter and the other is a static inverter.

A novel rotary inverter system makes use of a parallel connected rotary motor (PCRM) driving a conventional alternator [27]. The design, fabrication, testing and stability studies of such a system has already been performed [28,29]. A conceptual design of an MHD motor is also proposed [30]. The advantages of rotary inverter systems are that -

(i) all the electrode-pairs of an MHD generator can be connected to a single machine while maintaining electrical isolation between electrode pairs,

(ii) the system provides a means of control to obtain the desired distribution of load along the MHD channel,

(iii) the system does not require elaborate filtering equipment and

(iv) owing to its mechanical inertia, the inverter system decouples the MHD generator from sudden load disturbances.

In this system MHD power is first converted into mechanical power which in turn is converted to electrical power. Therefore this system is somewhat costly and inefficient.

Static inverters provide a direct electrical connection between the a.c. and d.c. systems by means of solid state thyristor switches. The use of solid state inverters in conventional applications has achieved maturity but more performance data from inverters operating with MHD generators under full load, partial load and transient conditions must be acquired for optimal MHD inverter design for maximum power transfer. MHD inverter requirements include high power factor, low harmonic power, d.c. and a.c. transient protection and a.c. power control.

Static line commutated inverters have an stablished technology and are being operated at power levels of hundreds of magawatts in high voltage d.c. transmission. Therefore earlier studies are mainly devoted to line commutated inverters for interfacing MHD generator to power grid and they are referenced elsewhere [31]. Recent studies with line commutated inverters include series capacitive compensation for improved power factor, increased commutation stability and Hall voltage isolation [32]. A line commutated inverter system has also been used as load regulator of the MHD generator [33]. Stable operation of the MHD-inverter link has been studied and significant harmonic reduction has been achieved with higher pulse numbers [34,35]. The inverter system was connected with static VAR generator and oscillation behaviour and its elemination by current rate feedback is described [36]. Transient interaction and stability studies of a multiple-electrode MHD generator have appeared [37]. Despite all the efforts for better performance, power factor compensation is necessary because of low power factor and inorder to operate near unity power factor at maximum conversion efficiency approximately 1.5 MVA of power factor correction must be provided for each MW of power generated [44]. Line commutated inverters cannot work with isolated loads.

Static forced commutated inverter systems are an

emerging technology with many advantages namely

(a) the a.c. power factor can be steplessly controlled over any required range,

(b) better voltage and harmonic control,

(c) commutation failure induced faults are minimised,

(d) fast system response and

(e) better stability.

With the above advantages, extensive theoretical and experimental studies must be made. However, so far, world wide research in this area has been rather meagre and publications on this subject have been limited to a very small number of papers such as [38] to [46].

Reference [38] is the comparative study of the performance of line and forced commutated inverters, References[39] and [40] describe an inverter system having two controls (a) notch width control to determine the ratio between the MHD generator d.c. output and the a.c. line voltage and (b) a phasing control to regulate the angle, leading or lagging, between the inverter output and the a.c. line voltage. The process of voltage regulation produces varying harmonics which are cancelled in the specially designed magnetics. Reference [41] discusses about the tradeoffs of voltage and current source inverter technologies.

References [42], [43] and [44] are the studies concerning MHD channel - inverter interactions including fault protection, open and closed loop control and stability. Reference [45] describes the requirements of MHD, inverter and utility grid for successful operation using PWM techniques. Reference [46] describes some unique consideration of four electrode consolidation inverter systems with computer control.

Above mentioned references are mostly related with design testing and fabrication of forced commutated inverters upto few mega-watts. MHD generation at commercial levels is in the range of 500 to 2000 MW at the first stage and therefore above informations may not be sufficient to provide answers to many questions that may come up about the integration of MHD generators into a.c. network using forced commutated inverters. Therefore detailed investigations must be made for the switching losses, fluid dynamic coupling, harmonic control under variable operation, stability and maximum power transfer from MHD duct with desired power factor.

1.3 Scope and outline of the thesis

The work reported in this thesis pertains to the problems associated with the force commutated inverter for the integration of an MHD generator into an a.c. power network. Special attention has been paid to evolve a simple control

system and improved power factor for the conversion and control of MHD power. The theoretical and experimental studies presented, illustrate the feasibility of using a simple square wave inverter to convert and control the output power of an MHD duct feeding into a power system under maximum power transfer and unity power factor conditions.

Power flow equations have been derived treating MHD inverter link as a single machine connected to infinite bus. The operating point is located for the maximum power transfer from an MHD duct with particular values of the series reactor and the phase shift angle. Modified power flow equations are derived with filters added to eliminate harmonics. A computer programme has been prepared to simulate the connection of either a square wave or a PWM inverter to the MHD duct. Quasi static changes in fluid dynamic conditions have been allowed for, by considering the variation in the MHD output voltage and the internal resistance. Detailed theoretical and experimental results are presented in graphical and tabulated forms. Inverter and associated components have been designed and special fuse protection provided.

An automatic feedback controller for power control from MHD duct has been designed, fabricated and tested.. Excellent response under steady state as well as dynamic condition is demonstrated with a single control loop and a

simple logic circuitary. The V-I characteristics of an MHD generator have been computed using a time dependent computer model of the generator. The results are then utilized for power control of the generator under various operating conditions. A voltage source inverter (VSI) interface is considered for transient studies of the generator inverter link. The stability studies are also carried out with sudden load changes from operating point.

The organization of the thesis is as follows :

Chapter 2 : This chapter is devoted for the digital simulation of MHD generator inverter link. The analysis of an MHD generator-inverter link has been made to reduce switching losses by using a square wave inverter working at line frequency. A single controller has been used to transfer maximum power from HMHD generator-inverter link to the infinite bus at the desired power factor and without any power factor correction needed. Generalized power flow equations have been derived which can connect za square wave or PWM inverter to an MHD duct with any electrode configuration. Modified power flow equations with filters have been also derived. The quasi static changes in the fluid dynamic conditions have been allowed for by considering the variations in the MHD output voltage and the internal resistance from the operating point. The detailed digital computer study is

carried out for the variation of real and reactive powers with quasi static changes in the fluid dynamic conditions. The control of power to an a.c. system with input and output parameters using phase shift is also studied. Results of the digital simulation are plotted and tabulated.

Chapter 3 : This chapter describes a scheme to simulate the MHD-inverter link in the laboratory. The experimental resuls are obtained and compared with those of the digital simulation in the last chapter. An inverter has been designed to interconnect 2MW, 20 electrode pair MHD-test facility to a.c. grid. Special design considerations are made to choose the inductor for the commutation circuit for high frequency operation. A digital computer study is made to show the current variation under different operating conditions for safe inverter operation. Finally a special test is conducted to predict the approximate length of a rewirable fuse wire in water to be used for protection of power electronic devices. The changes in the input parameters of the MHD duct are made to control the power manually using phase shifting transformer.

Chapter 4 : This chapter is devoted for the design, fabrication and testing of an automatic feedback controller to demonstrate the steady state and the dynamic response of the simulated system. In order to predict the behaviour of

the feedback controller, the digital simulation of the controller is done using a 1st order controller in a closed loop system to achieve greater accuracy, improved dynamic response and reduced effects of disturbances. The digital computer study neglects the resistances in the system and time constants involved in the firing circuit and power transducer. The mathematical model of the controller is obtained and then simulated on the digital computer following step by step calculations to determine the approximate parameters of the controller. An analogue simulation is done to evaluate exact parameters. The feedback controller is then designed and fabricated. The transient response of the controller is calculated and experimentally verified for a step change in the MHD duct voltage and the resistance. The steady state response of the simulated system is also determined experimentally. Theoretical and experimental results are compared. The control logic has been designed and fabricated with CMOS integrated circuits for a low power consumption and a high noise immunity.

Chapter 5 : This chapter is devoted to the theoretical calculations of the V-I curves using the time dependent model of the MHD generator for different modes of loading. These curves are used for digital simulation of power control as described in Chapter 2. A segmented Faraday generator with fine segmentation to minimize Hall effect is considered in

this chapter. Calculations are made for 2MW (thermal), 20 electrode pair generator. The results of the steady state analysis is compared with the results in Chapter 3. The transient interaction of a multiple electrode MHD generator with a force commutated inverter system is described. The transient behaviour with a step change in current is also described. A voltage source inverter (VSI) interface is considered with the above computer model with a d.c. input filter in order to limit the inverter ripple injection to the MHD channel and the influence of the channels voltage ripple on the converter. A set of current and voltage equations are derived for the MHD generator inverter link. Digital simulation is carried out with these equations for the transient analysis of the above system.

The duct is subjected to sudden load changes from operating point to near open circuit and short circuit conditions and results are obtained for space and time variation of temperature, pressure, velocity, mach number, current and voltage. Also the results are obtained with different input capacitor and an optimum size of the same is suggested for the chosen system.

Chapter 6 : This is the concluding chapter. It summarizes the results obtained in the previous chapters and proposes further research work.

In carrying out this study the following objectives are persued.

(i) The analysis is generalised to include any type of force commutated inverter for the conversion and control of MHD duct power.

(ii) The results obtained are such that they can be experimentally verified with a laboratory generator of 2 MW (thermal) with 20 electrode pairs.

CHAPTER 2 : DIGITAL SIMULATION OF MHD GENERATOR INVERTER LINK

2.1 Introduction

2.2 Simulation of MHD Generator

2.3 Simulation of Inverter

2.4 Simulation with filters

2.5 Computational procedure

2.6 Results of digital simulation

2.7 Summary and conclusion

C H A P T E R 2

dDIGITAL SIMULATION OF MHD GENERATOR INVERTER LINK++

2.1 Introduction

The primary aim of an MHD generator-inverter based power system is to maximise the conversion of chemical energy of fossil fuel to electrical energy being supplied to an a.c. power grid. In order to achieve this goal, it is necessary to understand the nature of the MHD generator-inverter link and utility grid interaction when connected to a power system.

The studies so far reported in literature relate to the experimental aspect of the design, fabrication and initial operation of a force commutated inverter with voltage and displacement control [40-46]. The real power is controlled by changing the phase angle (δ) between the inverter output and bus voltage. Whereas reactive power is controlled by changing the inverter voltage using pulse width modulation (PWM) technique. This means operating an inverter at a higher frequency than the line frequency. In doing so varying amounts of

---

++The material presented in this chapter has led to the authors publication number 3,7 and part of publication number 1 mentioned in the list of publications attached.

harmonics are produced. The switching losses caused at the high power level are also increased. This chapter is devoted for the following studies :

- The analysis of an MHD generator-inverter link has been made to reduce switching losses by using a square wave inverter working at line frequency.

- The use of only a single controller to transfer maximum power from MHD generator-inverter link to the infinite bus at the desired power factor and without any power factor correction.

- Deriving the generalised power flow equations which can connect a square wave or PWM inverter to an MHD duct with any electrode configuration.

- Deriving the modified power flow equations with filters.

This chapter includes the derivation of the generalised power flow equations for the simulation of single electrode pair of an MHD generator inverter link in practical operating conditions. The condition for maximum power transfer to infinite bus is obtained taking into account the quasistatic changes in the fluid dynamic conditions. The MHD generator-inverter link is treated as a single machine connected to infinite bus as shown in figure

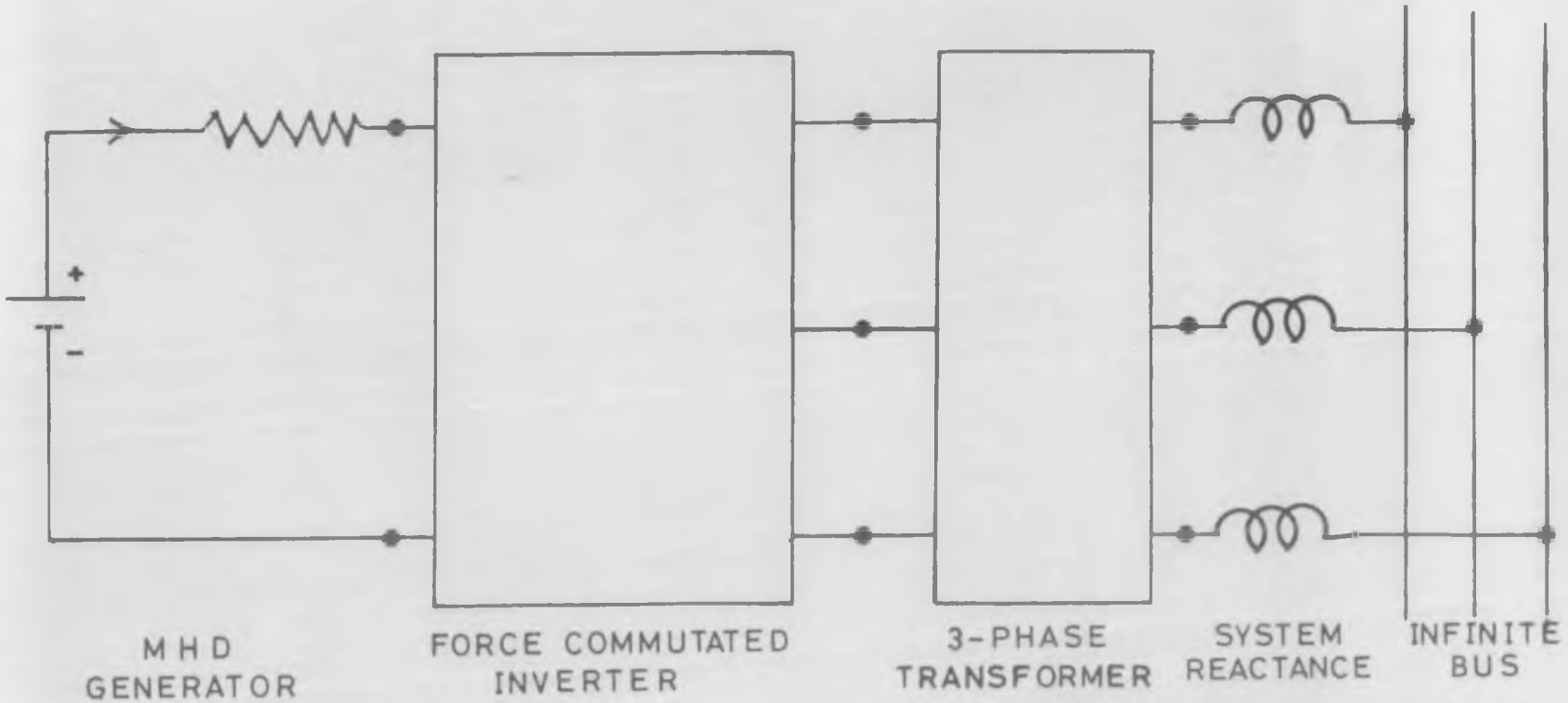

FIG. 2.1. BLOCK DIAGRAM OF MHD GENERATOR-INVERTER LINK.

2.1. Simple computer programmes have been developed to study the variation of real and reactive powers with quasi static changes in fluid dynamic conditions.

2.2 Simulation of an MHD generator

An MHD generator is a multi-electrode device. Each electrode pair can be represented by an equivalent circuit with a voltage source V_d in series with internal gas resistance R_d as shown in figure 2.2 [47]. In general V_d and R_d are variables and differ from their normal design values of V_o and R_o depending upon the loading conditions of other electrode pairs and other variables like temperature, pressure, magnetic field intensity, seeding rate etc. For the present analysis only single electrode pair V-I characteristic has been approximated by straight line. The VI characteristic is assumed to be bound within the region enclosed between two straight parallel lines as shown in figure 2.3.

2.2.1 Simplifying assumptions

For the simplified analysis the following assumptions are made for one electrode-pair V-I characteristic [47].

(i) V-I characteristic of one electrode pair is linear.

(ii) Magnetic field intensity in the generator channel is constant.

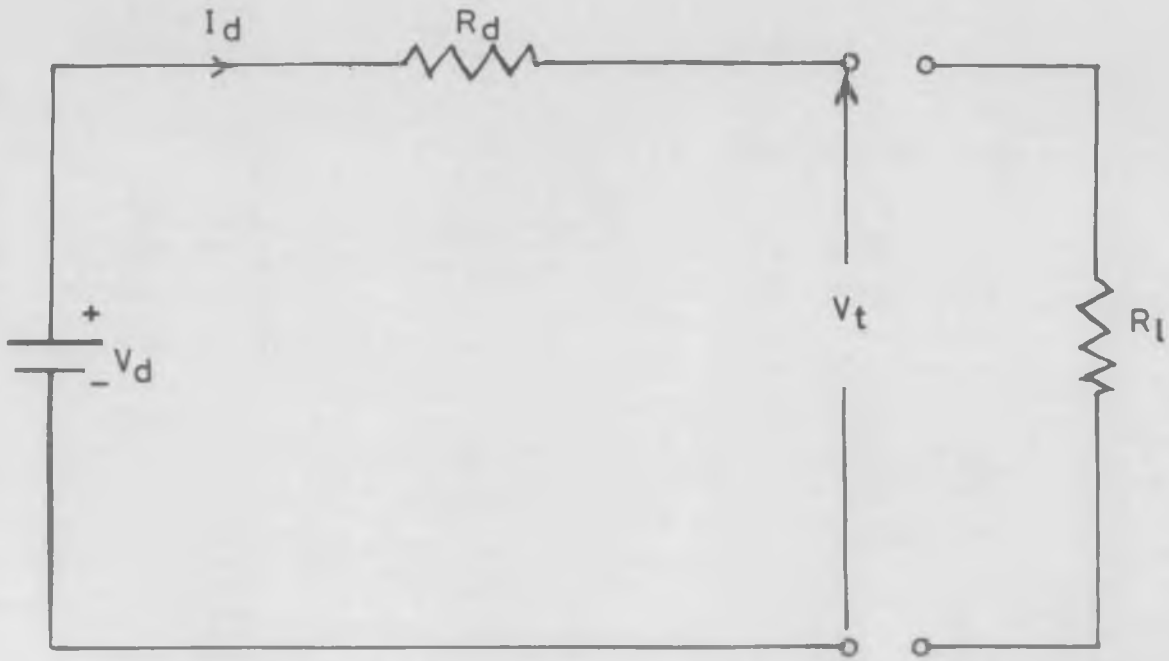

FIG.2.2. SIMPLIFIED EQUIVALENT CIRCUIT OF ONE ELECTRODE PAIR.

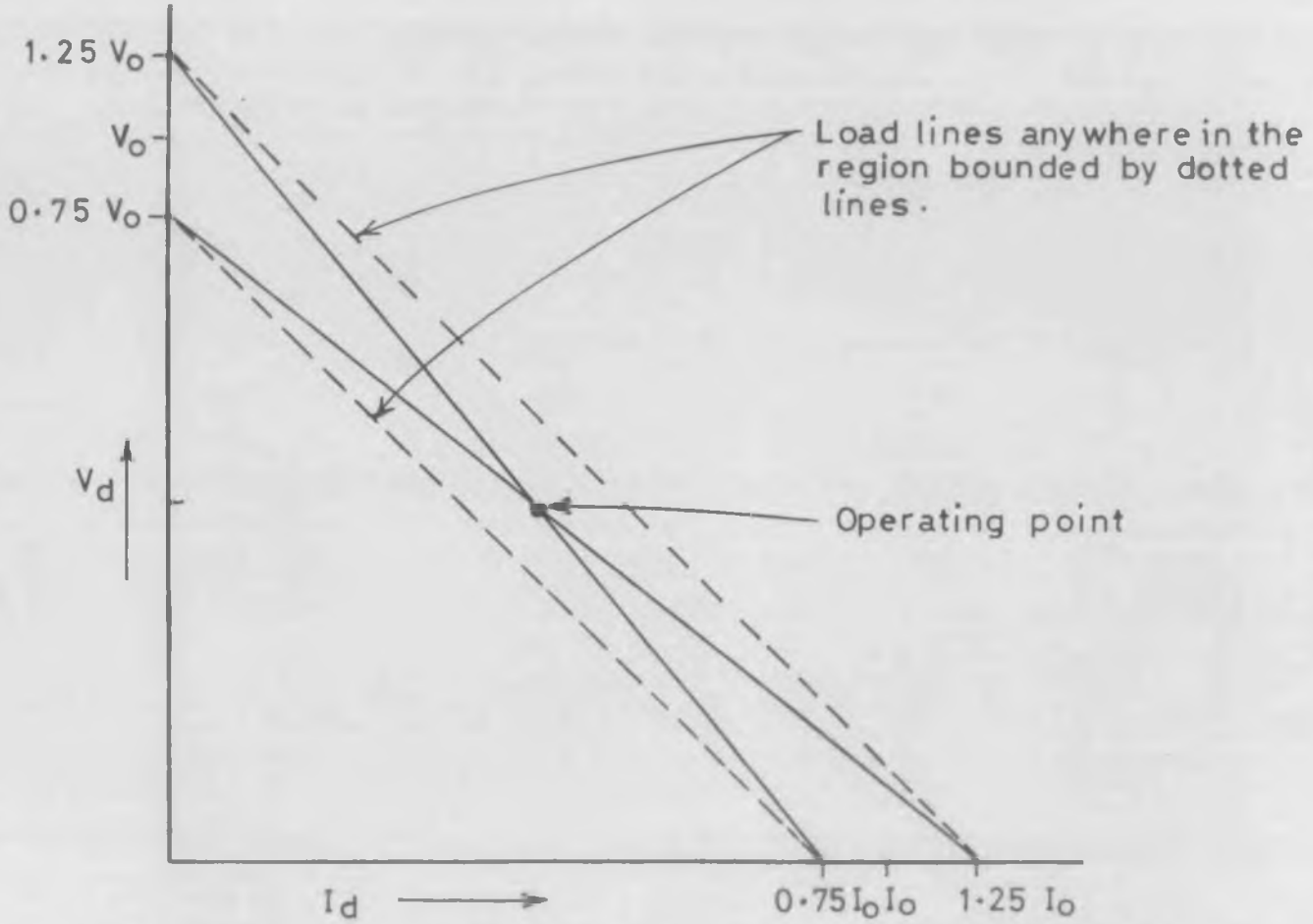

FIG.2.3. ASSUMED V-I CHARACTERISTICS OF SINGLE ELECTRODE PAIR.

(iii) Gas dynamical parameters are constant.

(iv) Generator inlet fluid dynamic conditions and seeding rate are constant.

(v) Individual pairs of electrodes are not dynamically coupled.

(vi) End effects and electrode effects are neglected.

2.2.2 MHD Equations

When the MHD generator is operating at any value of duct voltage and resistance other than the normal designed value, the open circuit voltage V_o and the internal gas resistance R_o of an electrode pair can be expressed in terms of the respective rated values as [28].

$$V_d = MV_o \quad \text{and} \quad R_d = NR_o \tag{2.1}$$

where letters M and N define the deviation from rated values.

Now terminal voltage of one electrode pair at any load, R_l can be expressed as follows [34].

$$V_t = V_d - I_d R_d \tag{2.2}$$

Combining the equations (2.1) and (2.2), we get

$$V_t = MV_o - I_d NR_o \tag{2.3}$$

For simplified analysis as discussed in section 2.2.1, M and N both are taken unity. Therefore

$$V_t = V_o - I_d R_o \qquad (2.4)$$

From figure 2.2 it can be seen that the power delivered from MHD generator electrode pair at any load is given as :

$$P_d = V_t . I_d = (V_o - I_d R_o) . I_d \qquad (2.5)$$

and maximum power transfer will take place when R_1 equals R_o and is given as

$$P_{dmax} = V_o / 4R_o \qquad (2.6)$$

This condition of maximum power transfer corresponds to a loading parameter of 0.5. In practice, however, the loading parameter required for optimum enthalpy extraction will differ from this value.

2.2.3 Perunit base quantities on MHD side

The selection of base values is made in order to reduce the calculations. To simplify the computational work, the base values are selected tin such a fashion that the perunit values of rated voltage and current yield the unit power [48]. The MHD generator-inverter link is a dual system i.e. on MHD side the quantities are d.c. whereas the

output of the inverter is a.c. Therefore the base values for both the sides are chosen separately. In this analysis, the operating point is chosen such that the maximum power is transferred to infinite bus. Therefore base power is chosen as given by Equation (2.6) and other values for the same condition are

$$\text{base voltage,} \quad V_b = V_o/2 \ \text{volts} \tag{2.7}$$

$$\text{base current,} \quad I_b = V_o/2R_o \ \text{amps} \tag{2.8}$$

and $$\text{base impedance,} \quad R_b = V_b/I_b = R_o \ \text{ohms} \tag{2.9}$$

2.3 Simulation of Inverter

MHD inverter link is connected to infinite bus via transformer and reactor as shown in figure 2.4 (a). The real and reactive power flow equations for the above power system represented by the equivalent circuit as shown in figure 2.4 (b), can be derived as under. The complex power flow from the inverter to infinite bus is given as

$$P + jQ = \underline{E}_1 \underline{I}_1^* \tag{2.10}$$

where $$\underline{E}_1 = E_1 (\cos \delta + j \sin \delta) \tag{2.11}$$

and $$\underline{I}_1^* = \frac{E_1 \sin \delta}{X_s} + j \frac{E_1 \cos \delta - E_b}{X_s} \tag{2.12}$$

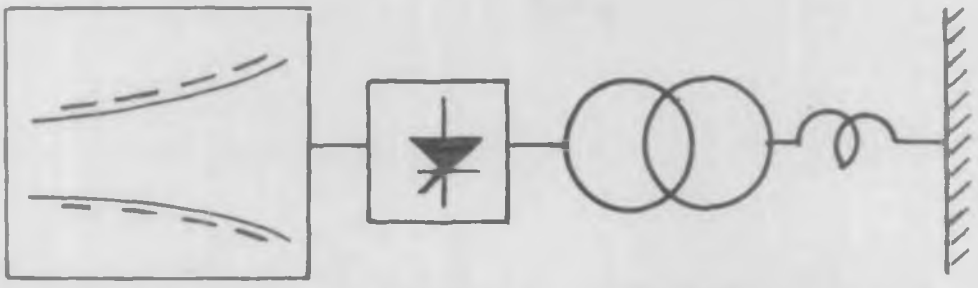

(a)

FIG.2.4.LINE DIAGRAM OF MHD. GENERATOR INVERTER LINK.

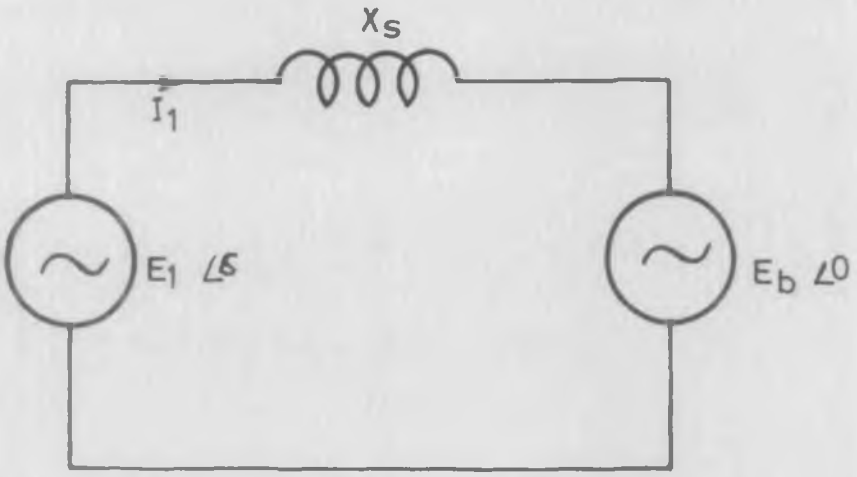

(b)

FIG.2.4. SIMPLIFIED EQUIVALENT CIRCUIT.

Giving the real and reactive power flow to infinite bus as [49].

$$P = \frac{E_1 E_b \sin \delta}{X_s} \tag{2.13}$$

$$Q = \frac{E_1^2}{X_s} - \frac{E_1 E_b \cos \delta}{X_s} \tag{2.14}$$

If the losses are neglected in the inverter then power delivered from the MHD generator equals the output power of the inverter.

2.3.1 Relation between d.c. and a.c. quantities

The duct voltage can be written as follows

$$E_1 = K V_t \tag{2.15}$$

where E_1 is the rms value of the fundamental amplitude of the inverter voltage per phase and K is a constant. K depends upon the type of the inverter. Using equations (2.2) and (2.4), we can rewrite equation (2.15) as

$$E_1 = K (V_d - I_d R_d) \tag{2.16}$$

or

$$E_1 = K (V_o - I_d R_o) \tag{2.17}$$

Above Equations give the idea how inverter voltage changes

with MHD duct loading and gas resistance. From Equations (2.5), (2.13) and (2.15), it can be deduced that

$$I_d = \frac{3K\ E_b}{X_s} \text{ Sin } \delta \tag{2.18}$$

Now from equations (2.4), (2.15) and (2.18) we can rewrite new values of V_t and E_1 as follows

$$V_t = (V_o - \frac{3K\ E_b}{X_s} .\ \text{Sin } \delta . R_o) \tag{2.19}$$

and

$$E_1 = K\ (V_o - \frac{3K\ E_b}{X_s} .\ \text{Sin } \delta . R_o) \tag{2.20}$$

Equations (2.13) and (2.14) can be obtained on substitution of the value of E_1 from equation (2.20).

$$P = \frac{K\ (V_o - \frac{3KE_b}{X_s} .\ \text{Sin } \delta . R_o) . E_b . \text{Sin } \delta}{X_s} \tag{2.21}$$

$$Q = \frac{K^2\ (V_o - \frac{3KE_b \text{Sin } \delta}{X_s} .\ R_o)^2}{X_s} -$$

$$\frac{K\ (V_o - \frac{3KE_b \text{Sin } \delta . R_o}{X_s})\ E_b \text{ Cos } \delta}{X_s} \tag{2.22}$$

Equations (2.21) and (2.22) give the power flow from inverter

to infinite bus. They depend upon the type of inverter, internal voltage and the resistance of the MHD generator, bus voltage, system reactance and displacement angle δ.

2.3.2 Perunit base quantities on a.c. side

For the dual system the base quantities are derived for the power equivalence criteria i.e. power transfer from d.c. side is the same on a.c. side neglecting inverter losses.

Let E_B and I_B be chosen as the a.c. bus voltage and current per phase, then total power is given :

$$\text{base power, } P_B = 3E_B I_B = V_o^2/4R_o \tag{2.23}$$

$$\text{base current, } I_B = \frac{V_o}{4R_o} \cdot \frac{1}{3E_B} \tag{2.24}$$

$$\text{base impedance, } Z_B = E_B/I_B = 12\, R_o \left(\frac{E_B}{V_o} \right)^2 \tag{2.25}$$

2.3.3 Simulation with square wave inverter

The most simple form of a force commutated inverter is a square wave inverter. The constant K defined in equation (2.15), for a square wave inverter with centre tapped supply is $\sqrt{2}/\pi$ [50]. Therefore we can rewrite the equations (2.18) to (2.22) for a square wave inverter on per unit basis by dividing the respective base quantities as described in Section 2.2.3.

$$I_{d_{pu}} = \frac{6\sqrt{2}}{\pi} \cdot \frac{E_b}{V_o} \cdot \frac{R_o}{X_s} \cdot \sin\delta \qquad (2.26)$$

$$V_{t_{pu}} = 2 - \frac{6\sqrt{2}}{\pi} \cdot \frac{E_b}{V_o} \cdot \frac{R_o}{X_s} \cdot \sin\delta \qquad (2.27)$$

$$E_{1_{pu}} = \frac{\sqrt{2}}{\pi} \cdot \left[2 - \frac{6\sqrt{2}}{\pi} \cdot \frac{E_b}{V_o} \cdot \frac{R_o}{X_s} \cdot \sin\delta\right] \qquad (2.28)$$

$$P_{pu} = \left[\frac{6\sqrt{2}}{\pi} \cdot \frac{E_b}{V_o} \cdot \frac{R_o}{X_s} \cdot \sin\delta\right] \cdot \left[2 - \frac{6\sqrt{2}}{\pi} \cdot \frac{E_b}{V_o} \cdot \frac{R_o}{X_s} \cdot \sin\delta\right] \qquad (2.29)$$

$$Q_{pu} = \left[\frac{\sqrt{2}}{\pi}\left(\frac{R_o}{X_s}\right) \cdot \left\{2 - \frac{6\sqrt{2}}{\pi} \cdot \frac{E_b}{V_o} \cdot \frac{R_o}{X_s} \cdot \sin\delta\right\}\right] \cdot \left[\frac{\sqrt{2}}{\pi}\left\{2 - \frac{6\sqrt{2}}{\pi} \cdot \frac{E_b}{V_o} \cdot \frac{R_o}{X_s} \cdot \sin\delta\right\} - \frac{2E_b}{V_o} \cdot \sin\delta\right]$$

The above equations predict the performance of the MHD generator-inverter link at any loading conditions. They are solved using digital computer. The computer programs are listed in Appendix A.

2.4 Simulation with filters

A converter is considered to be the source of harmonic voltages and currents on both the sides of the converter i.e. a.c. and d.c. side. Filters are added to reduce as far as

practicable these harmonic voltages and currents. It is recommended for economy to use a twelve pulse converter with filters than to use a converter of higher pulse number with permissible reduction in harmonics [51].

A filter circuit is a series combination of an inductance and a capacitance tuned to a specific harmonic frequency. It forms a short circuit path under series resonance for that perticular harmonic so that the harmonic voltage collapses. Such short circuiting path can be provided in parallel to the system for every particular harmonic to be suppressed [52].

2.4.1 Location and type of filters

Filters are located on both the sides of the converter. Filters on the a.c. side may be connected either on the primary (network) side of the converter transformers or preferably on the tertiary winding. The tertiary has a voltage lower than the primary winding and the filters are to be insulated for lower surge voltage and cost less [52].

The filters can be a series or shunt type. The series filters must carry the full current of the main circuit and must be insulated throughout for full voltage to ground. The shunt filters can be grounded at one end. They carry only the harmonic current for which they are tuned plus a fundamental component much smaller than the main current. Hence a shunt filter is much cheaper than a series filter of equal

effectiveness. A.C. shunt filters have another advantage over the series filters. At fundamental frequency the former supplies the needed reactive power whereas the latter consumes it.

2.4.2 Modified power flow equations with filters

For further analysis only the shunt filters connected to the reactor as shown in figure 2.5 is considered. Following equation can therefore be written in Matrix form

$$\begin{bmatrix} (Z_n/2) + Z_f & -Z_f \\ -Z_f & (Z_n/2)+Z_f \end{bmatrix} \begin{bmatrix} I_1 \\ I_b \end{bmatrix} = \begin{bmatrix} E_1 \\ E_b \end{bmatrix} \qquad (2.31)$$

where

$Z_n = X_s$ = Total network reactance per phase including line reactor at power frequency.

$Z_f = (X_c - X_l)$ = Net filter reactance per phase at power frequency

Using equation (2.31) we can write the following :

$$I_1 = \frac{E_1 (Z_f + Z_n/2) - E_b Z_f}{\{(Z_n/2)+Z_f\}(Z_f+Z_n/2)-Z_f^2} \qquad (2.32)$$

where $Z_n/2 = jX_s/2$

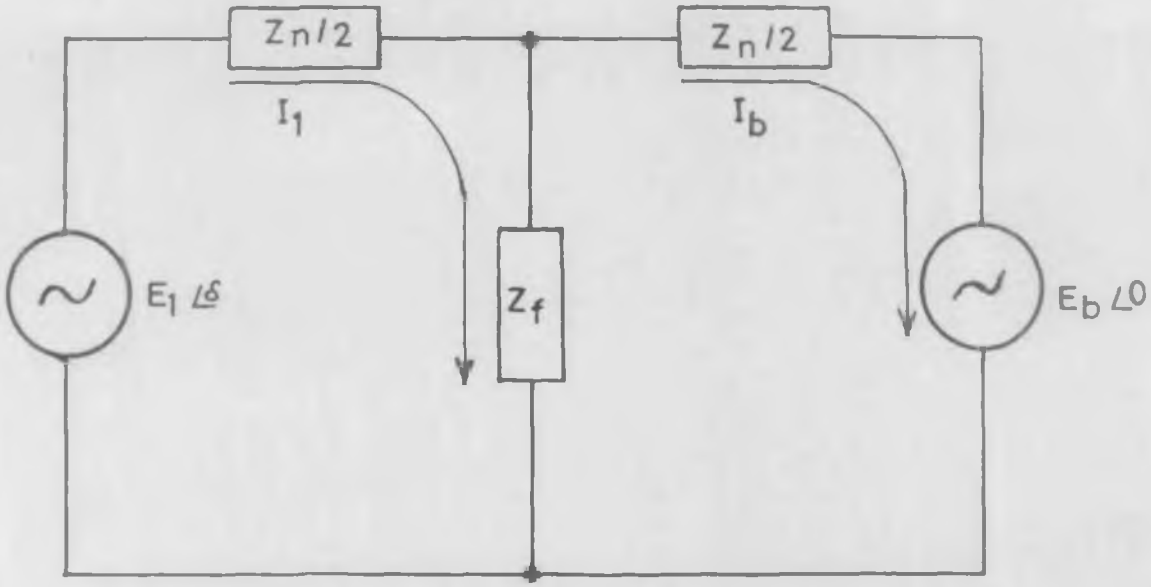

FIG.2.5.SIMPLIFIED EQUIVALENT CIRCUIT WITH FILTER.

$Z_f = j(X_1 - X_c) \simeq -jX_c$ because at power frequency capacitive reactance is predominant.

substituting above values of Z_f and Z_n and writing the complex conjugate of I_1

$$I_1 = \frac{-E_1 \text{ Sin } \delta \{(X_s/2)-X_c\}}{(X_s X_c + X_s^2/4)} - j \frac{E_1 \text{ Cos } \delta\{(X_s/2)-X_c\}+E_b X_c}{(X_s X_c - X_s^2/4)} \qquad (2.33)$$

using equations (2.10) to (2.14) we can write the modified power flow equations as follows

$$P = \frac{E_1 E_b \text{ Sin } \delta}{X_s'} \qquad (2.34)$$

$$Q = \frac{E_1^2}{X_s''} - \frac{E_1 E_b \text{ Cos } \delta}{X_s'} \qquad (2.35)$$

where

$$X_s' = X_s (1 - X_s/4X_c)$$

and

$$X_s'' = X_s (1/2 - 2X_c/X_s)/(1 - X_c/X_s)$$

Equation (2.6) to (2.30) can now be modified on perunit basis as discussed in section 2.2.3 to allow for the filter currents as follows :

$$I_{d_f} = \frac{6\sqrt{2}}{\pi} \cdot \frac{E_b}{V_o} \cdot \frac{R_o}{X_s'} \cdot \text{Sin } \delta \qquad (2.36)$$

$$V_{t_f} = 2 - \frac{6\sqrt{2}}{\pi} \cdot \frac{E_b}{V_o} \cdot \frac{R_o}{X_s'} \cdot \text{Sin } \delta \qquad (2.37)$$

$$E_{1_f} = \frac{\sqrt{2}}{\pi}\left[2 - \frac{6\sqrt{2}}{\pi} \cdot \frac{E_b}{V_o} \cdot \frac{R_o}{X_s'} \cdot \text{Sin } \delta\right] \qquad (2.38)$$

$$P_f = \left[\frac{6\sqrt{2}}{\pi} \cdot \frac{E_b}{V_o} \cdot \frac{R_o}{X_s'} \cdot \text{Sin } \delta\right].\left[2 - \frac{6\sqrt{2}}{\pi} \cdot \frac{E_b}{V_o} \cdot \frac{R_o}{X_s'} \cdot \text{Sin } \delta\right] \qquad (2.39)$$

$$Q_f = \left[\frac{\sqrt{2}}{\pi}\left(\frac{R_o}{X_s'}\right)\left\{2 - \frac{6\sqrt{2}}{\pi} \cdot \frac{E_b}{V_o} \cdot \frac{R_o}{X_s'} \cdot \text{Sin } \delta\right\}\right].$$

$$\left[\frac{\sqrt{2}}{\pi}\left\{2 - \frac{6\sqrt{2}}{\pi} \cdot \frac{E_b}{V_o} \cdot \frac{R_o}{X_s''} \cdot \text{Sin } \delta\right\} - \left(\frac{2E_b}{V_o}\right).\text{Cos } \delta\right] \qquad (2.40)$$

The above equations predict the performance of MHD generator-inverter link at any loading condition with filter. The computer program is listed in table B-13 in appendix B and results are given in section 3.4.2 of next chapter.

2.5 Computational procedure

Computation is carried out on the digital computer using the finite difference method. In this method step by step calculations are carried out with the assumption that different quantities remain constant over small finite intervals [53]. The operating point is chosen as shown in figure

2.3 and the design values are taken as initial parameters. The operating point is such that the power transfer is maximum. These design values are designated as V_o, I_o and R_o. The changes in the input and output parameters of the MHD-inverter link are studied from this operating point. Simple programs are developed directly from the equations derived in sections 2.3.3 and 2.4.2. This sort of work has not been reported so far. Therefore simple computer programs were developed and the results verified by actual calculations. Every digital simulation study used separate program. A few of these programs are listed in appendix A. A simple flow chart for the control of power from MHD duct is shown in figure 2.6.

2.6 Results of digital simulation

2.6.1 Variation in Electrical parameters with phase shift

1. Variation of current and voltage with phase shift

The variation of MHD duct voltage and current is computed as a function of phase shift and results are plotted as shown in figure 2.7 for three different values of the system reactance. Equations (2.26) and (2.27) are computed for phase shift of 0 to 180° and system reactances of 0.225, 0.45 and 0.90 PU. When system reactance is taken as 0.45 PU duct voltage and current is 1 PU. The program is shown in list

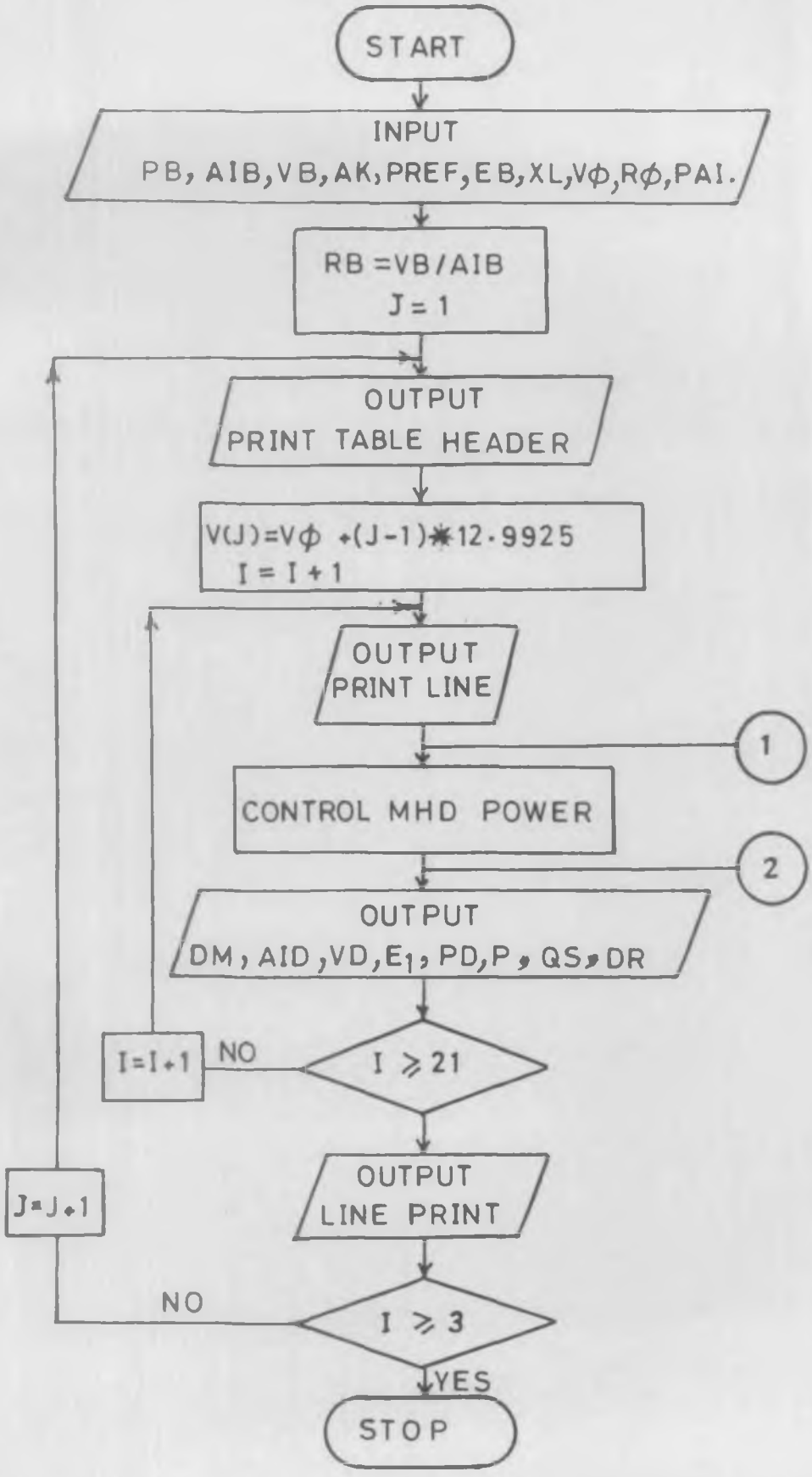

FIG. 2.6. FLOW CHART FOR MHD POWER CONTROL

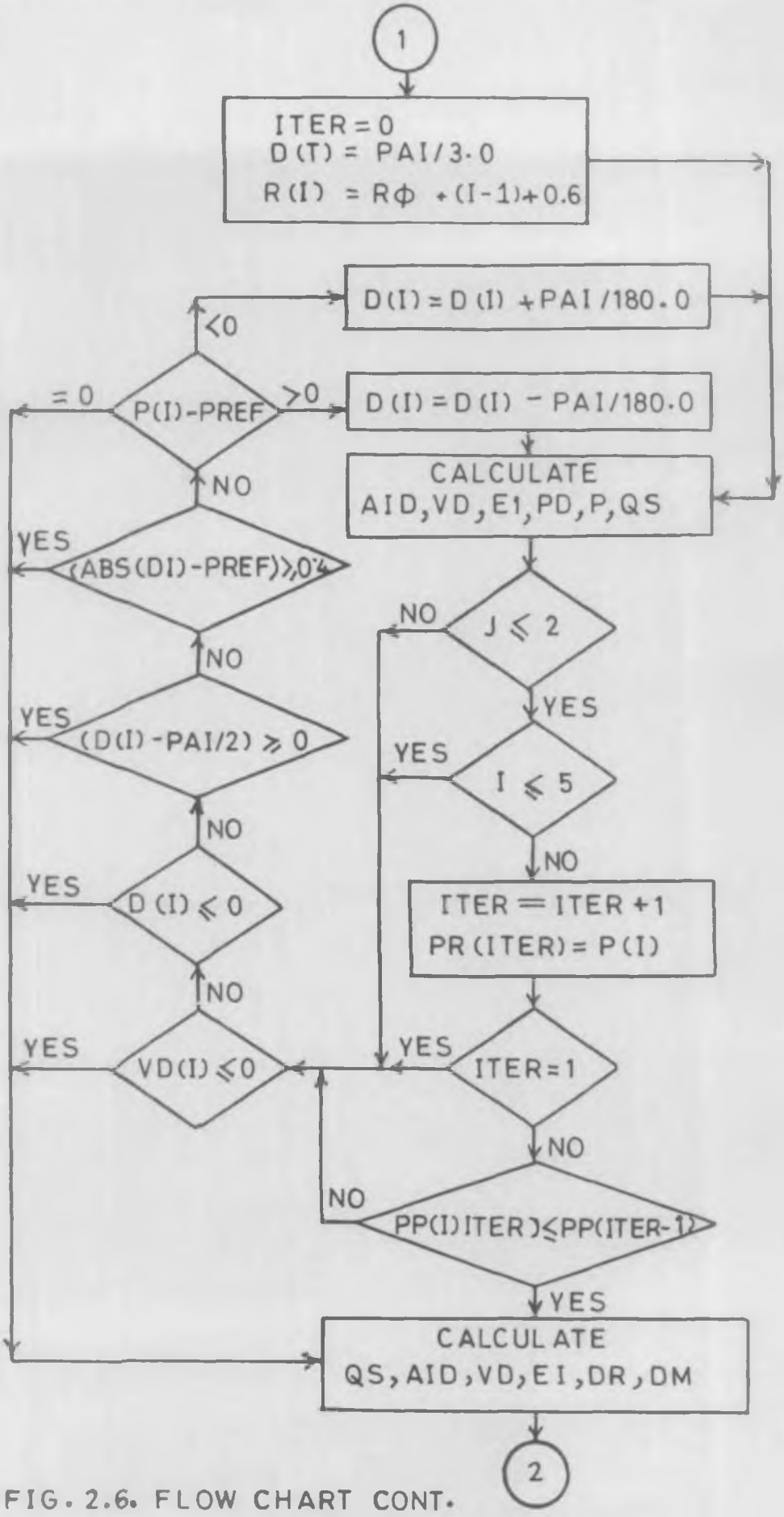

FIG. 2.6. FLOW CHART CONT.

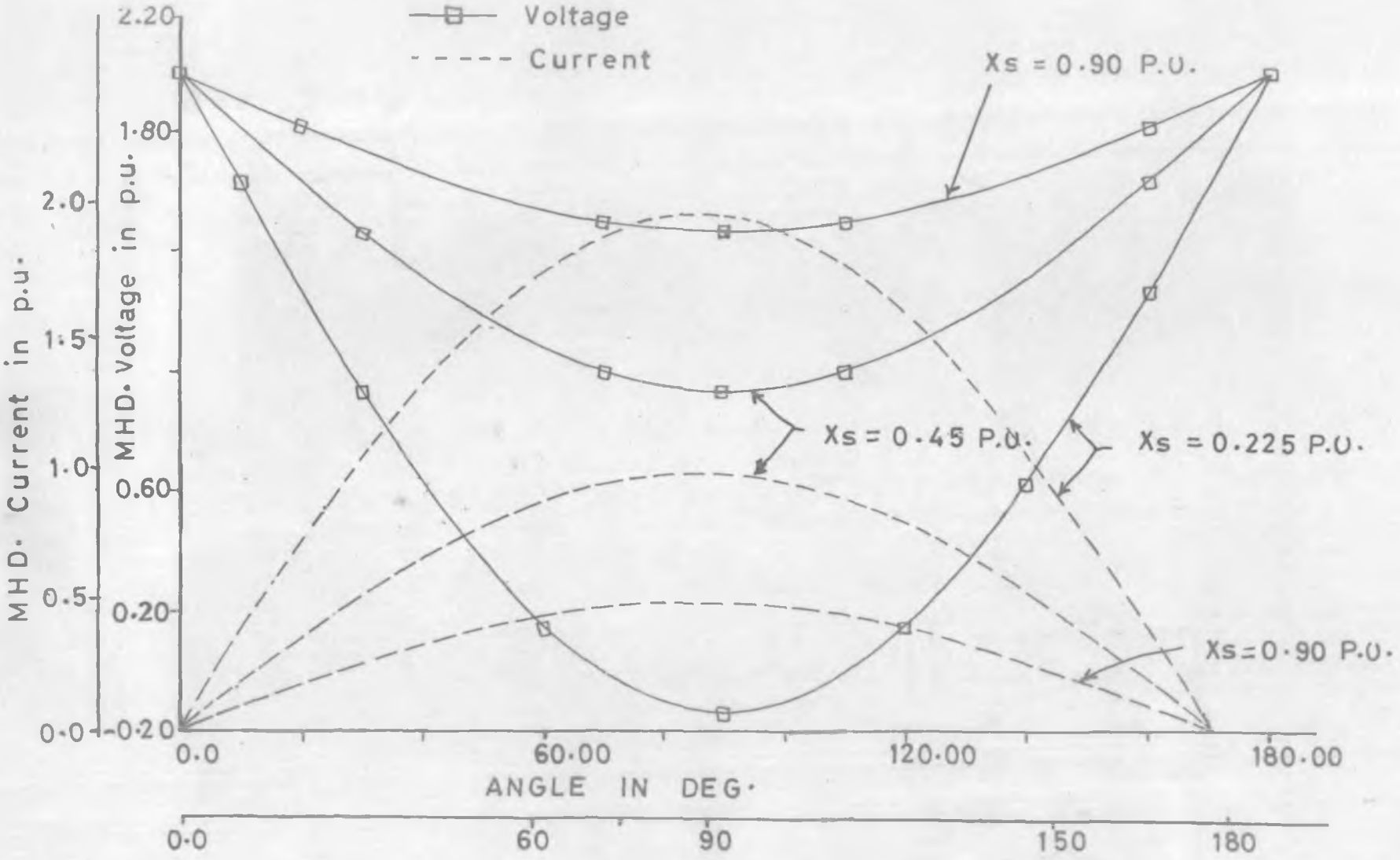

FIG. 2.7. VARIATION OF MHD VOLTAGE AND CURRENT WITH PHASE SHIFT .

A-2 and the results are tabulated in tables A-3, A-4 and A-5 in appendix A.

2. Variation of real and reactive power with phase shift

Equations (2.29) and (2.30) are computed as a function of phase shift and graphed in figure 2.8. As seen from the graph, real power remains constant between phase shift of 60° to 120° for system reactance of 0.45 PU and reactive power is zero at 60 phase shift. For other values of system reactance the variation is shown in figure 2.8 and tabulated in tables A-3 to A-5 in appendix A.

3. Comments

Equations (2.18) to (2.22) are generalised equations and can be used for any type of forced commutated inverter. However, considering the points mentioned in section 2.1, these equations have been modified for square wave inverter for the present analysis. For the system reactances more than 0.45 per unit real and reactive power, both decrease whereas if the system reactance is reduced, the variation of real and reactive power is shown in figure 2.8.

Therefore the operating point for the maximum power transfer from MHD duct is chosen for the case when reactive power is zero at 60° phase shift and 0.45 PU system reactance. At this operating point the power factor is unity i.e. reac-

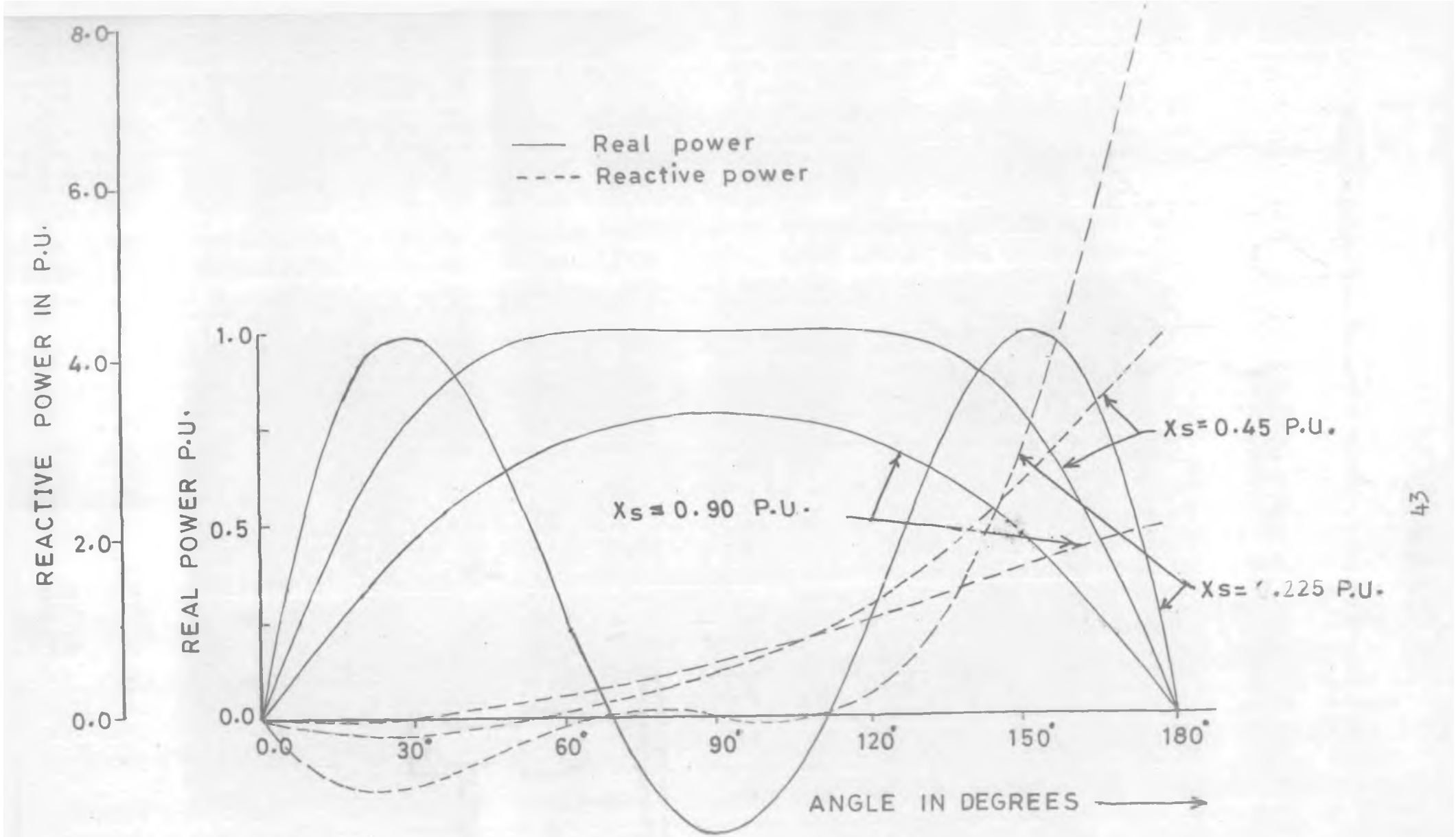

FIG. 2.8. VARIATION OF REAL AND REACTIVE POWER WITH PHASE SHIFT.

tive power is zero and no power factor correction is needed. Inverter components have small size because of zero reactive power. This is the desired point of operation as the power transfer is maximum and voltage and current remain approximately as 1 PU. Also the size and cost of inverter is minimized.

2.6.2 Variation of real and reactive power with changes in duct voltage and resistance as a function of phase shift

The MHD process being unsteady therefore the gas resistance and duct voltage may change from operating value. This quasi-static change in fluid dynamic condition is considered as a function of phase shift. The changes in internal resistance and duct voltage are considered as $\pm$ 25 percent from the operating point.

In order to control MHD power, the variation of real and reactive power is computed for above changes in internal resistance and duct voltage and plotted as shown in figure 2.9. It can be observed that with the change in voltage, real and reactive power variation is more compared to change in internal resistance. Figure 2.10 shows the variation of real and reactive power for fixed voltage and changes in internal resistance.

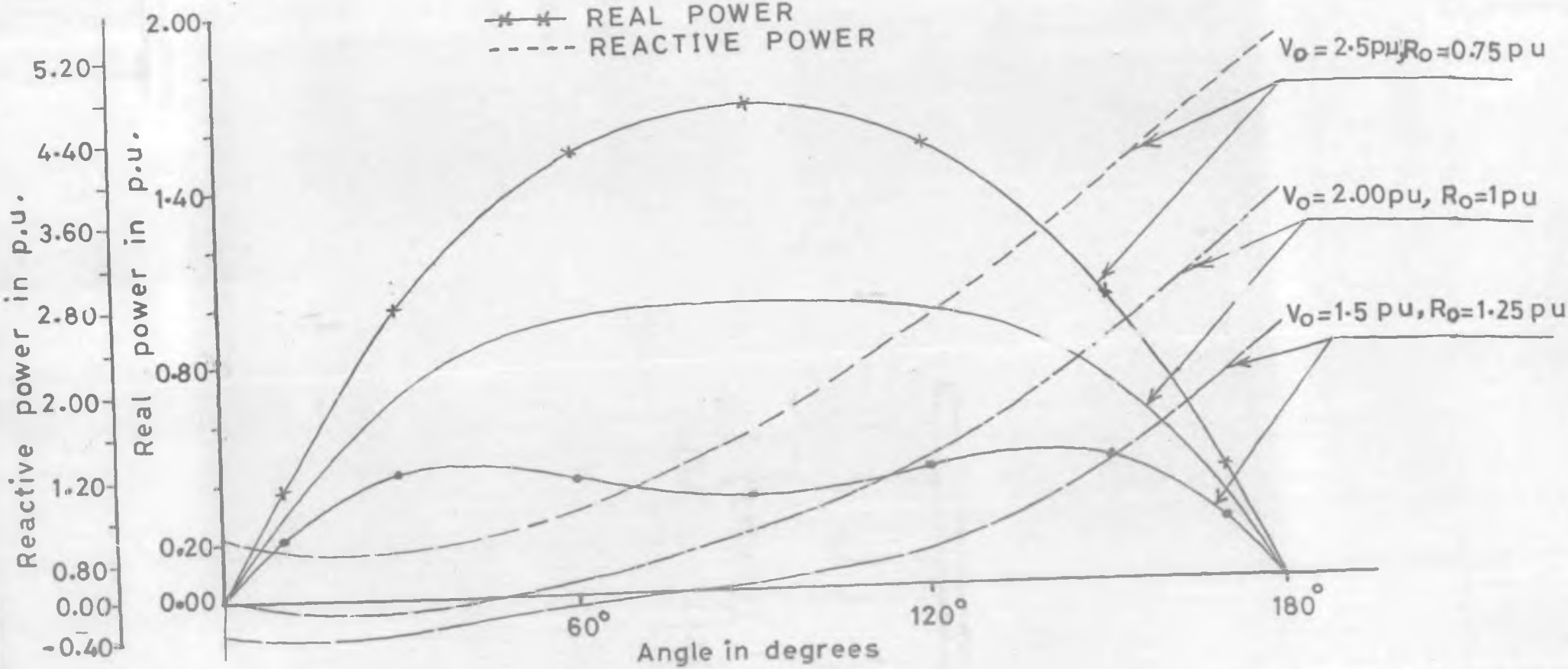

FIG. 2.9. VARIATION OF REAL AND REACTIVE POWER WITH PHASE SHIFT.

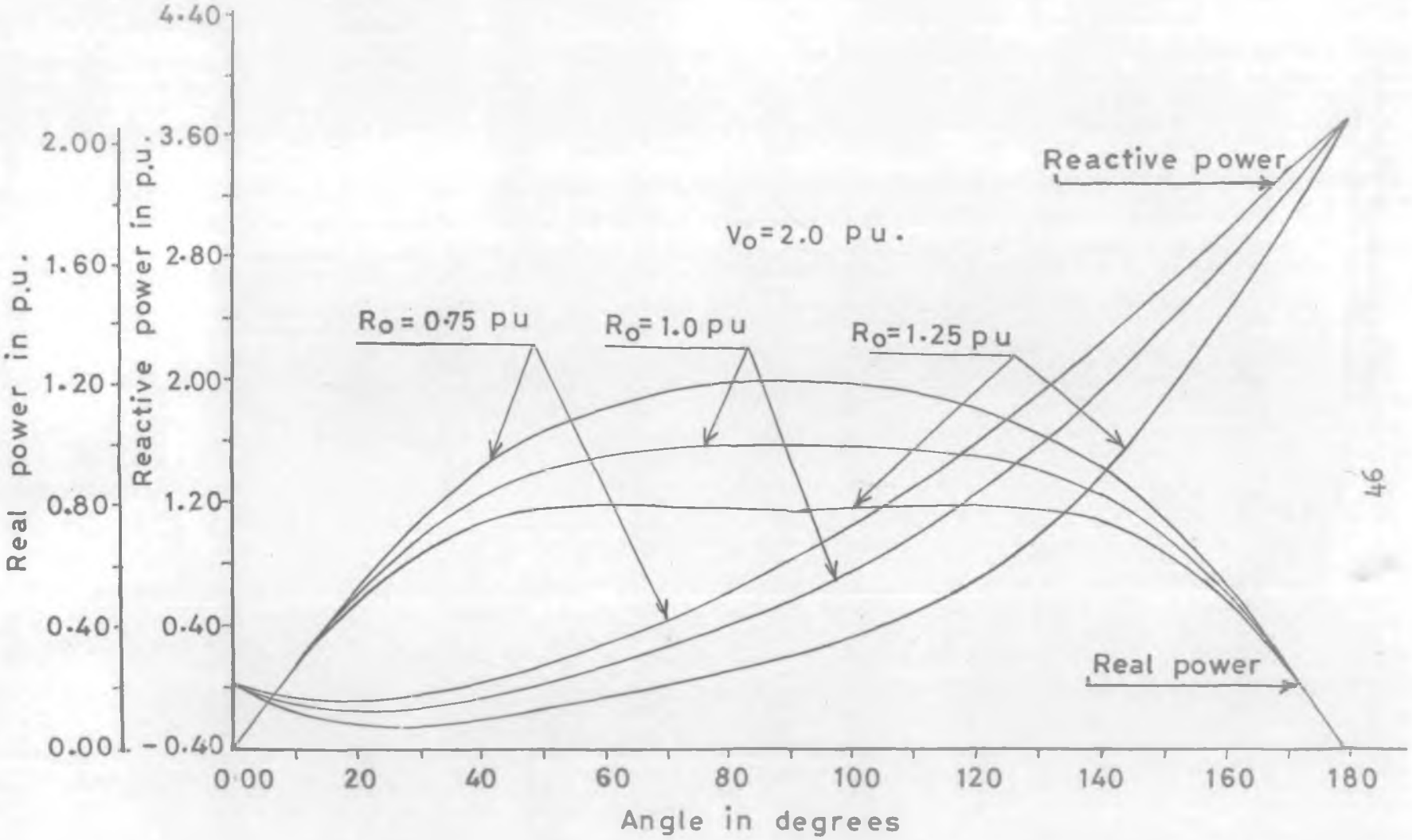

FIG. 2.10. VARIATION OF REAL AND REACTIVE POWER WITH PHASE SHIFT.

2.6.3 Variation of real and reactive power with MHD duct current

Real power remains unchanged for any phase shift between inverter output and a.c. bus voltage. It is zero at open and short circuit and maximum when current is 1 PU. Reactive power changes with different phase shift as shown in figure 2.11. It is lagging for large phase shift and is zero at a phase shift of 60° and 1 PU current.

2.6.4 Variation of real and reactive power with changes in internal resistance from operating point

To consider the quasistatic changes in fluid dynamic conditions ($M \neq N \neq 1$) as discussed in section 2.2.2, change in internal resistance is considered here for fixed values of duct voltages as shown in figure 2.12. The real and reactive power variation is shown for $\pm$ 25 percent change in internal resistance from the normal operating point. The negative sign means reduction in resistance from the designed value. List A-6 in appendix A shows the computer program and tables A-8 to A-10 show the computational results for different voltages and phase shifts.

2.6.5. Variation of real and reactive power with changes in duct voltage from operating point

As discussed above, change in duct voltage is considered

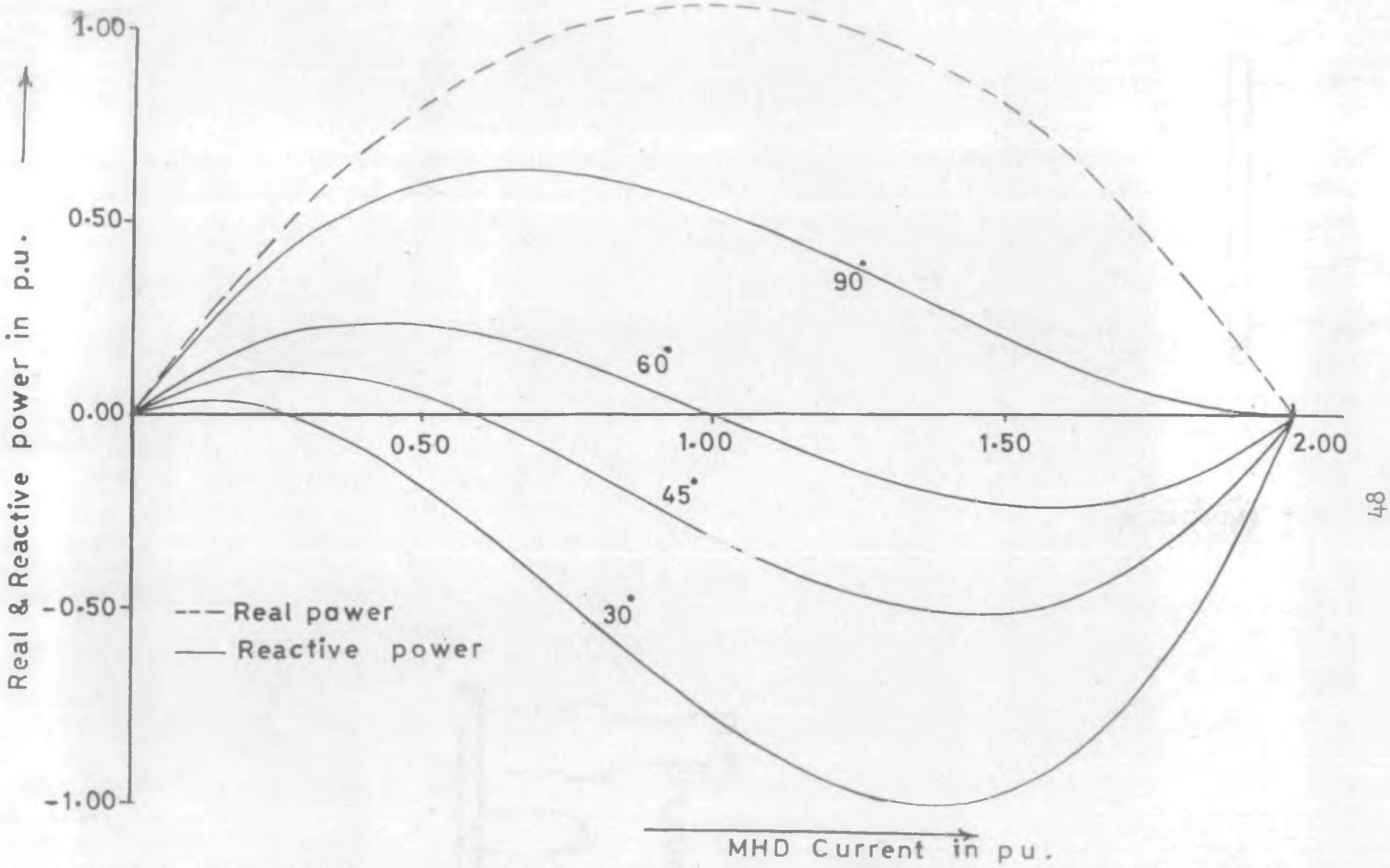

FIG.2.11. VARIATION OF REAL AND REACTIVE POWER WITH CURRENT FOR FIXED SHIFT.

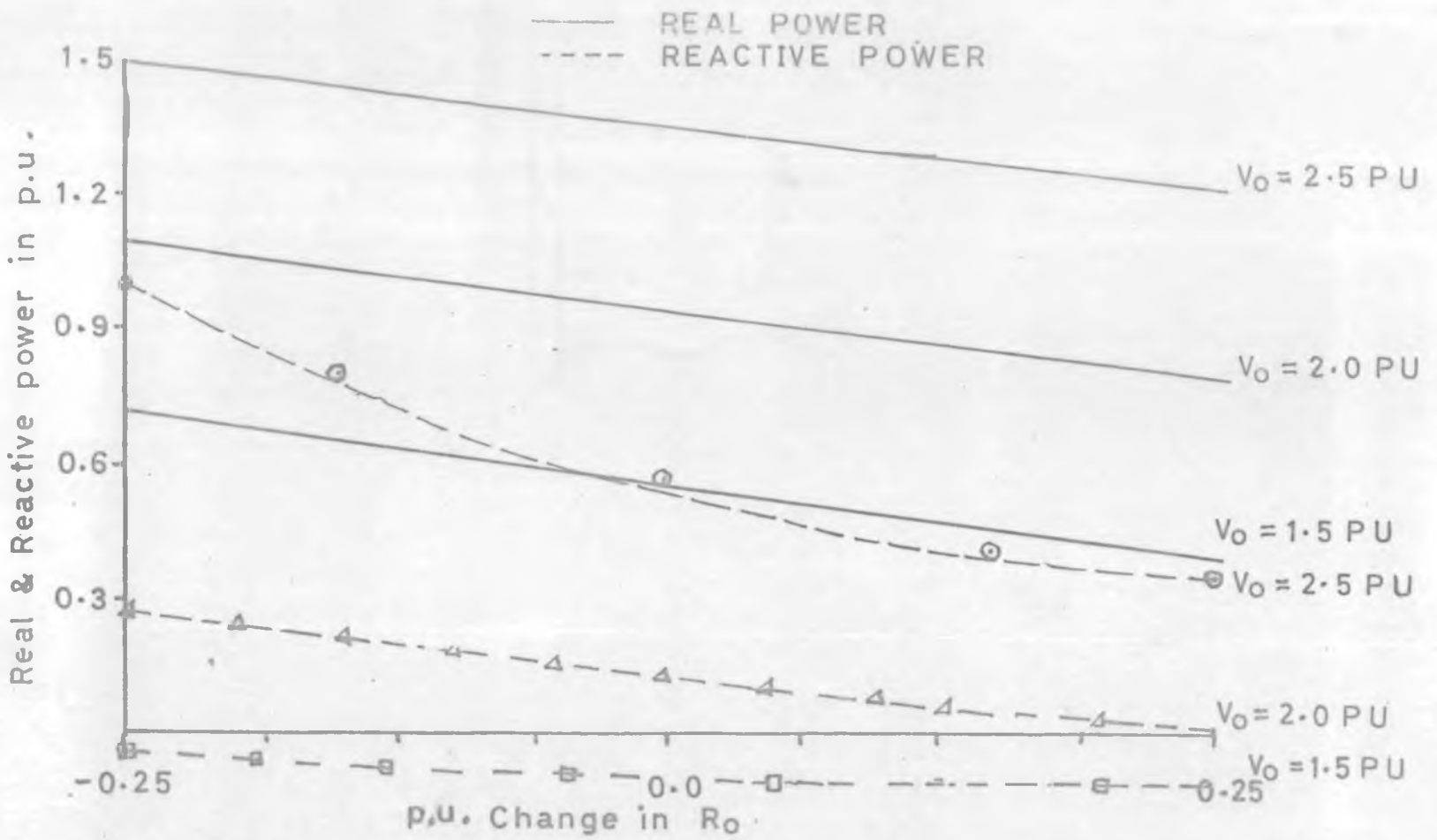

FIG.2.12.VARIATION OF REAL AND REACTIVE POWER WITHOUT PHASE SHIFT CONTROL.

here for fixed values of internal resistance as shown in figure 2.13. The real and reactive power variation is shown for ±25 percent change in duct voltage from the normal operating point value. The negative sign means a reduction in duct voltage from the operating value. Similar program and tables were prepared as mentioned in section 2.6.4, but omitted from the appendix A because of limitation in volume of appendix.

2.6.6 Control of power to a.c. system

The inversion scheme considered here converts d.c. power to a.c. power. Lower order harmonics are filtered in 5th and 7th harmonic filters and higher order harmonics in the series reactor connected in the scheme. It is clear from above study that such a scheme can transfer maximum power under unity power factor when the inverter output voltage and bus voltage have a phase difference of 60° and system reactance has a value of 0.45 PU. Quasi-static changes in fluid dynamic conditions of the duct may alter the maximum power transfer. Phase shift control is applied here to regulate this power transfer to reference value.

1. Power control for changes in internal resistance

Three cases are considered with change in resistance in the range of ± 25 percent. When the voltage is raised from

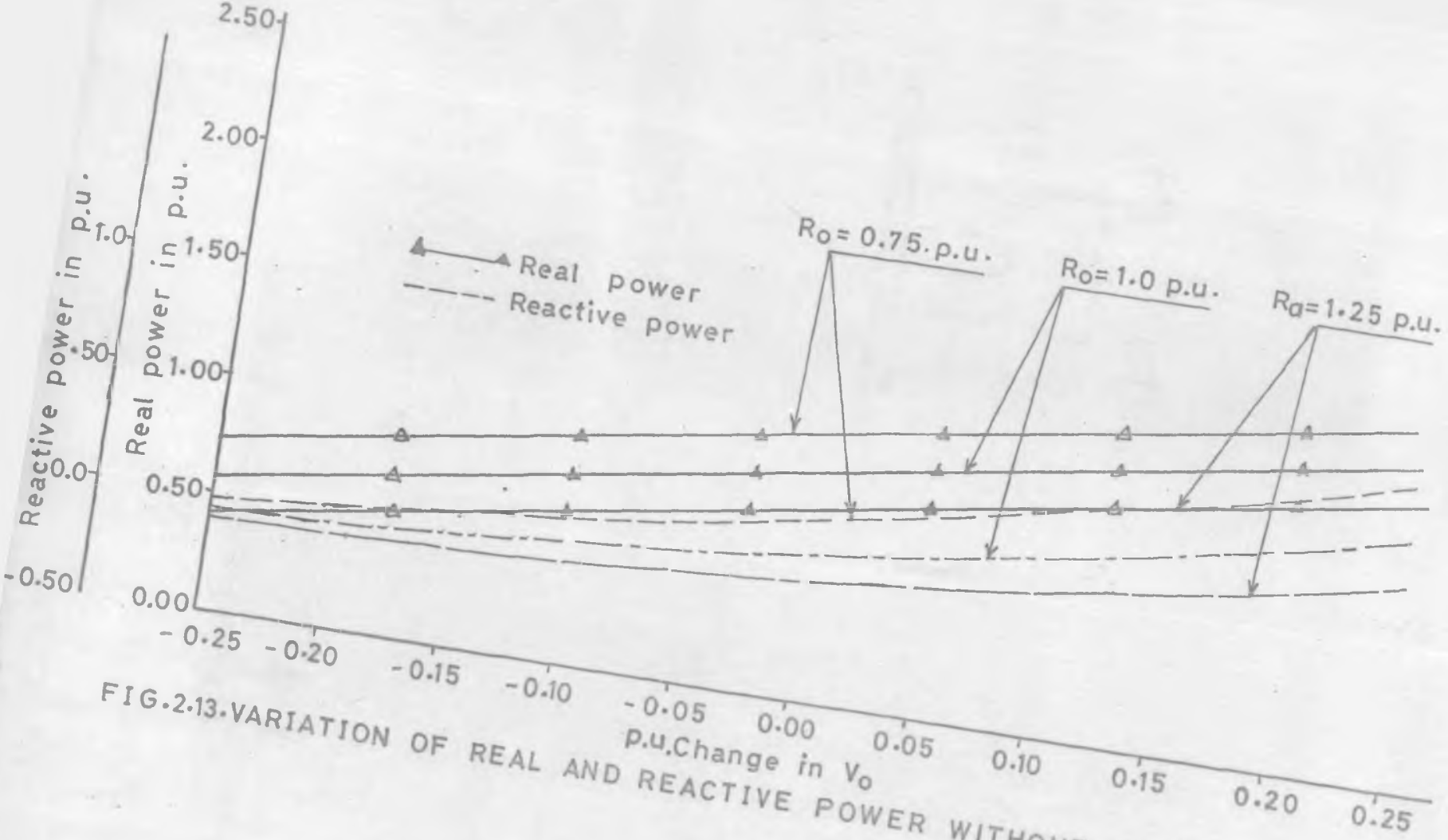

FIG.2.13. VARIATION OF REAL AND REACTIVE POWER WITHOUT-PHASE SHIFT CONTROL.

the designed value, phase shift control can easily maintain the reference power by reducing the phase shift. For a 2.5 PU voltage and 25 percent change in resistance the reference power is kept as 1 PU. Other cases are also plotted in figure 2.14. It can be concluded from figure 2.14 that with phase shift control the power flow to infinite bus can be increased whenever there is an increase in internal resistance or decrease in duct voltage. If the change is within 15 percent in either of the two quantities the reference power can be maintained to reference level. This is how power can be regulated to the desired level by phase shift control. Therefore unsteady MHD process may be controlled for supplying the desired power. The reactive power is within the reasonable limit and as such there is no need of its control. List A-11 in appendix A shows the program for control of power to a.c. system and table A-12 shows the computed results when phase shift control is applied.

2. Power control for changes in duct voltage

The change in voltage is taken as $\pm$ 25 percent with fixed values of resistances as shown in figure 2.15. The desired power is kept as 1 PU for any increase in voltage and decrease in resistance by applying the phase shift control. However if voltage reduces and resistance increases the phase shift control can increase the power but not to the reference value as 1 PU. A change of 15 percent in any of two

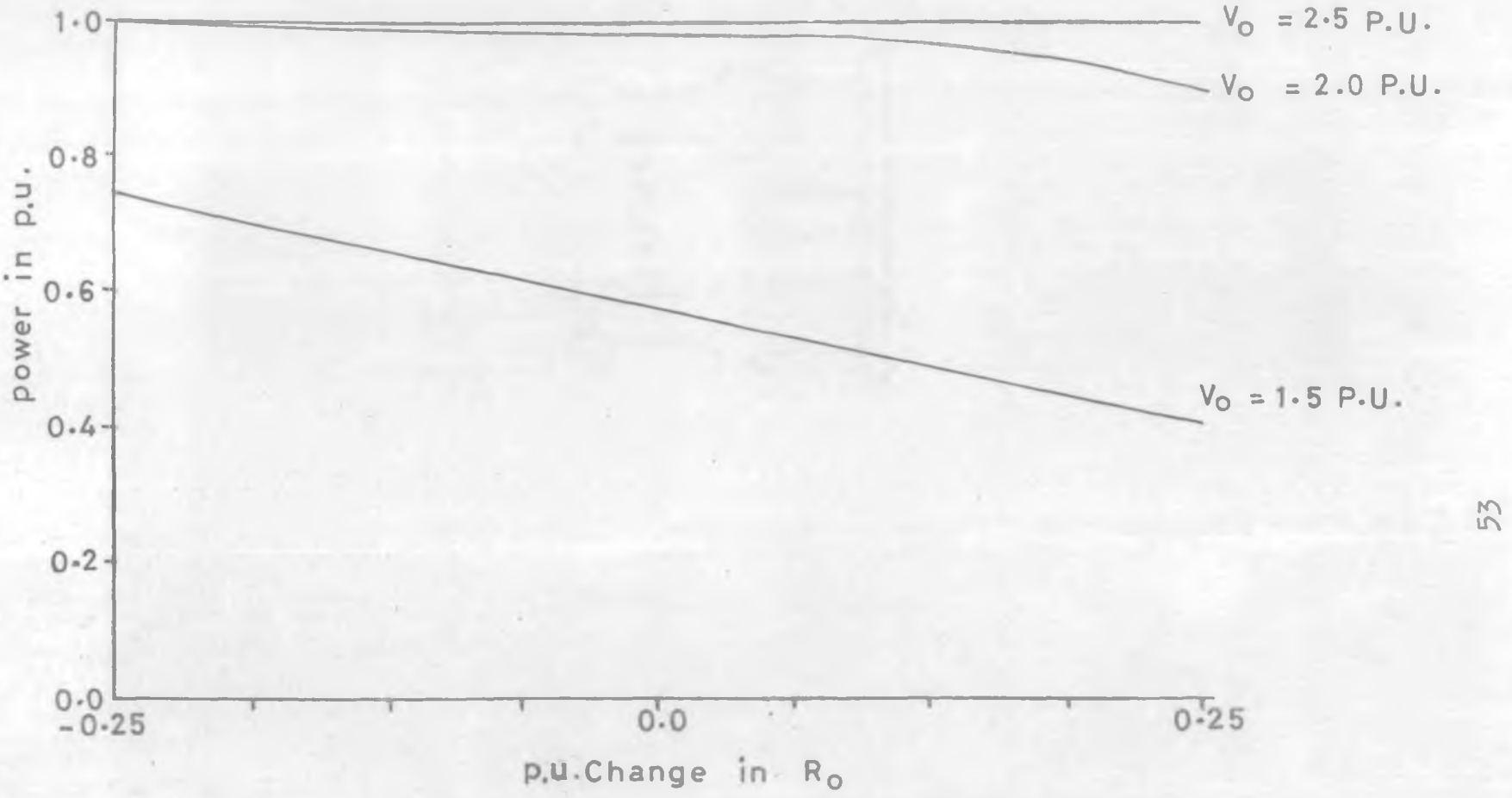

FIG·2·14·VARIATION OF REAL POWER WITH PHASE SHIFT CONTROL.

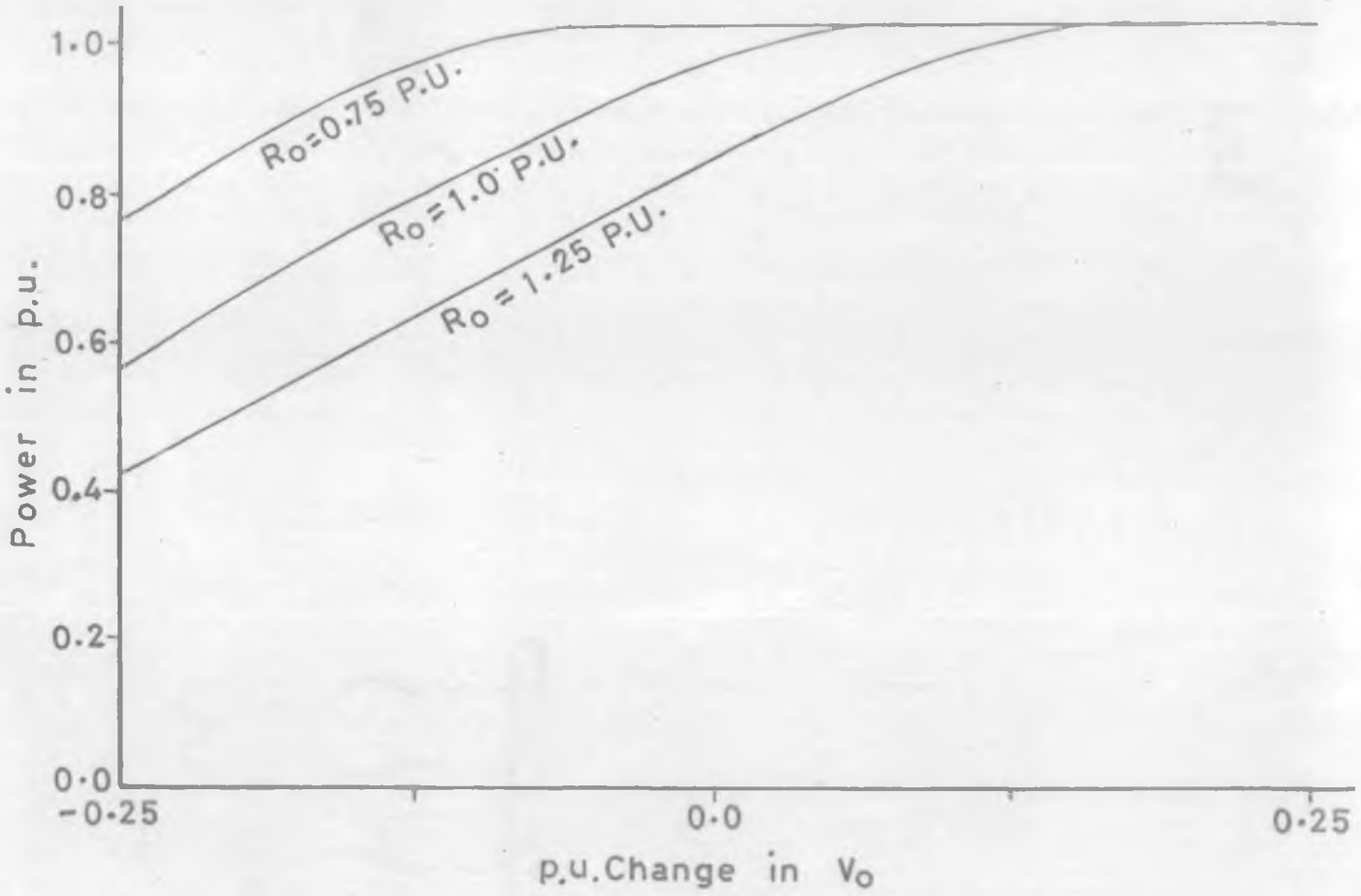

FIG. 2.15. VARIATION OF REAL POWER WITH PHASE SHIFT CONTROL.

parameters can be controlled. The reactive power in case of voltage variation is more compared to the resistance variation. This can be visualised from the power flow equations derived earlier. In this case also the reactive power does not need any compensation as the power factor remains within the desired limit.

2.6.7 Change in Electrical parameters with other fixed phase shifts

Digital computer study made above has been extended to take into account the phase shifts of 90, 45 and 30 degrees. As seen in figure 2.11, the reactive power will not be zero at the operating point and therefore for operation under unity power factor conditions power factor compensation will be required in the above cases. For smaller phase shifts the power control range increases but power transfer will not be maximum.

2.6.8 Power control with the output parameters

It can be seen from the power flow equations that the two parameters which can effect the power are the system reactance and the bus voltage. If any of these parameters changes the phase shift control can be applied to keep the power transfer maximum. However it is neither needed nor feasible in practice to control power flow on a.c. side. In

case of open circuit or short circuit the power variation has to be determined. This has been done with variable line reactor and results show that if line reactance is reduced power flow can be easily controlled to maximum. Table A-13 in appendix A shows the power control for changes in system reactance.

2.7 Summary and Conclusion

This chapter derives the general power flow equations for an MHD-Inverter link using force commutated inverter. A particular case of square wave inverter is considered because of advantages mentioned in the preceding sections. Power flow equations have been derived on per unit basis for ease of calculations. Per unit quantities are derived for a.c. and d.c. both. Digital simulation results are obtained with simple computer programs using step by step calculations. The results covering the following aspects have been obtained.

1. The input electrical parameters with phase shift.
2. The real and reactive power flow with changes in internal resistance and duct voltage.
3. Variation of real and reactive power as a function of MHD current for different phase shifts.
4. Variation of real and reactive power flow with quasi-static changes in fluid dynamic conditions.

5. Power control to the desired level by varying the phase shift between inverter output and a.c. bus voltage.

6. Power control on other phase shifts.

7. Power control with the output parameters.

From these computations it is concluded that :

1. A phase shift of 60° with a system reactance of 0.45 PU should be chosen as operating point for maximum power transfer under unity power factor conditions.

2. Power control to reference level can be achieved within ± 15 percent of the changes in the internal resistance or the voltage of the MHD duct.

3. The phase shift control is effective for any increase in duct voltage or decrease in internal resistance of the duct. The reference power is maintained in the above cases.

4. In case the internal resistance increases and duct voltage decreases from normal operating value, the control still helps to increase power flow to a.c. system but not to the reference value.

These results are verified in the next chapter where an experiment is set up to simulate MHD-inverter link. Other phase shifts are also considered but reactive power compensation is needed in those cases.

CHAPTER 3 : EXPERIMENTAL VERIFICATION AND DESIGN CONSIDERATIONS

CHAPTER 3

EXPERIMENTAL VERIFICATION AND DESIGN CONSIDERATIONS++

3.1 Introduction

Power flow equations have been derived for the MHD inverter link in the last chapter. Digital simulation results have been obtained using the power flow equations.

This chapter describe a simple scheme to simulate MHD-Inverter link in the laboratory. The experimental results are also obtained and compared with those of digital simulation in the last chapter.

Filters have been designed to suit the experimental setup specifications and results with filters have been obtained. An inverter has been designed to inter-connect the given 2 MW (thermal) linear MHD-Generator test facility to a.c. grid. At high frequencies in the range of 250 to 1000 Hz, the losses in the commutation circuit become important. The minimization of losses, skin effect and volume is important at high frequency operation for this purpose. Inductors with different design are compared for inverter commutation circuit. Due to changes in internal resistance

---

++ A portion of this chapter is based on the authors paper number 4 and part of paper number 1 mentioned in the list of publications.

and duct voltage, the peak current through the inverter changes. But for the safe inverter operation this current should always be less than the peak of the commutation pulse. Digital computer study is made to show the current variation under different operating conditions.

Semiconductor fuse is found most suitable for power semiconductors, its cost is a major obstacle in its adoption. Rewirable fuse link is economical and fast in comparison to all other protective devices. But its joule integral (I^2t) and the transient arching voltage are quite high. However an ordinary fuse wire when placed in water, carries a large current compared to that in air at reduced joule integral the tests has been carried to predict the approximate length for a given I^2t rating of a particular device.

3.2 Experimental setup

The results of digital simulation in chapter two are verified with the experimental setup in the laboratory as shown in figure 3.1. The d.c. voltage is taken from the d.c. variable supply bus and internal resistance from the resistance box. A small transistor inverter has been used to convert d.c. power to a.c. Over load protection is provided with c.t. to check any unbalance or over load. Line reactors are connected in each line as discussed in last chapter. Three phase delta/ star transformer is connected to an auto-

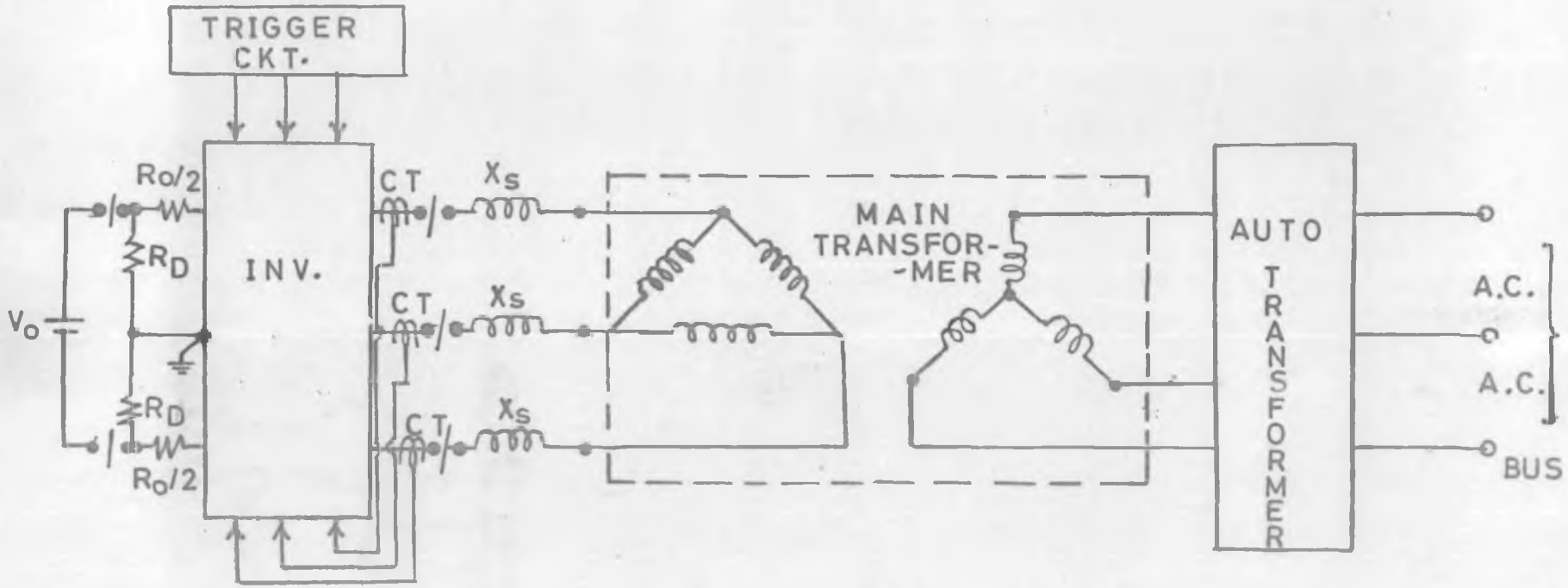

FIG.3.1. EXPERIMENTAL SETUP FOR MHD GENERATOR INVERTER LINK

transformer to connect with the infinite bus. Auto transformer is needed to adjust the bus voltage to match the operating point voltage at the MHD generator.

To get the required point of operation as discussed in last chapter, the MHD voltage was adjusted to 45 volts and resistance box were adjusted to 24 ohms and line reactance to 40 ohms (0.4 PU). The auto-transformer was adjusted to give on the secondary of the delta connected winding of the transformer about 35 volts which is the no load voltage of the inverter at zero phase shift. The above data were chosen such that the inverter is under safe operation. A phase shifting transformer to suit the above ratings is used to shift the inverter voltage phase with respect to a.c. bus. The measuring instruments have not been shown in the block diagram. The detailed diagram for the MHD-inverter link experimental setup with measuring instruments and protection provided is shown in figure B-1 in appendix B.

3.2.1 MHD-Generator-inverter link simulation data

1. D.C. supply (V_o) — 120/240 volt variable supply bus available in the laboratory

2. Resistance Box (R_o) — (i) 240 ohms and 1.25 A each and a group of 20 in one box. All in parallel with switch provided. Maximum dessipation is 2.6 KW.

	(ii) 20 ohms and 5.3 A each and a group of 20 in one box. All in parallel with switch provi-did. Maximum dissipation is 3.9 KW.
3. Inverter (INV)	Power transistor inverter input 80 volts d.c. with centre tapping and output a.c. 60 volts and 5 amps.
4. External inductance	240 V, 50 c/s, 20 Amps. max. current with ohmic values of 80,40,20 and 5 ohms.
5. Main transformer (delta/star)	Primary 415/240/207/120 volts, 5 KVA. Secondary 415/240 volts.
6. Three phase auxiliary transformer (star/ star)	415 Volts, 1.25 amps. primary 104 Volts, 5 amps. and Secondary with multiple sections in winding of 5,10,20,40 and 60 Volts.
7. Autotransformer	Input 415/240 Volts, 20 amps. and output 0-260 Volts.
8. Phase Shifter	Δ/λ, 0.6 KVA, 440/0-254 Volts, 3 Phase, 50 c/s, 1.36 amps.
9. Measuring Instruments	
(i) Ameters	0-5 Amps. 0-2.5/5 Amps., 1.5, 15 and 7.5 amps. (Moving iron and moving coil both).

(ii)	Voltmeters	0-30/60 Volts MI and MC (Moving coil and moving iron both)
(iii)	Wattmeters	0-125 W, current oil 1.25/2.5/5 amps. and pressure coil 62.5/125/250/500 Volts (Dynamometer type).
(iv)	Current transformers	Primary 5/10/20/50/100 amps. and Secondary 5 Amps.

3.2.2 Simulation of MHD generator

As described in section 2.2 and MHD generator between any electrode pair can be represented by an equivalent circuit with a d.c. voltage source in series with resistance.

The voltage and resistance of the duct are both variables and differ from their design volues. The MHD generator electrode pair is therefore simulated with resistance boxes and a d.c. variable supply as shown in figure 3.2. Because of the centre tapped supply two banks of 240 ohms resistance boxes are used to give 12.Ω in each line and 20 ohms resistance box is used to give 10 ohms across centre tapping as shown in figure B-1 in appendix B.

The variable supply and resistance boxes can be adjusted to chose desired point of operation for maximum power transfer.

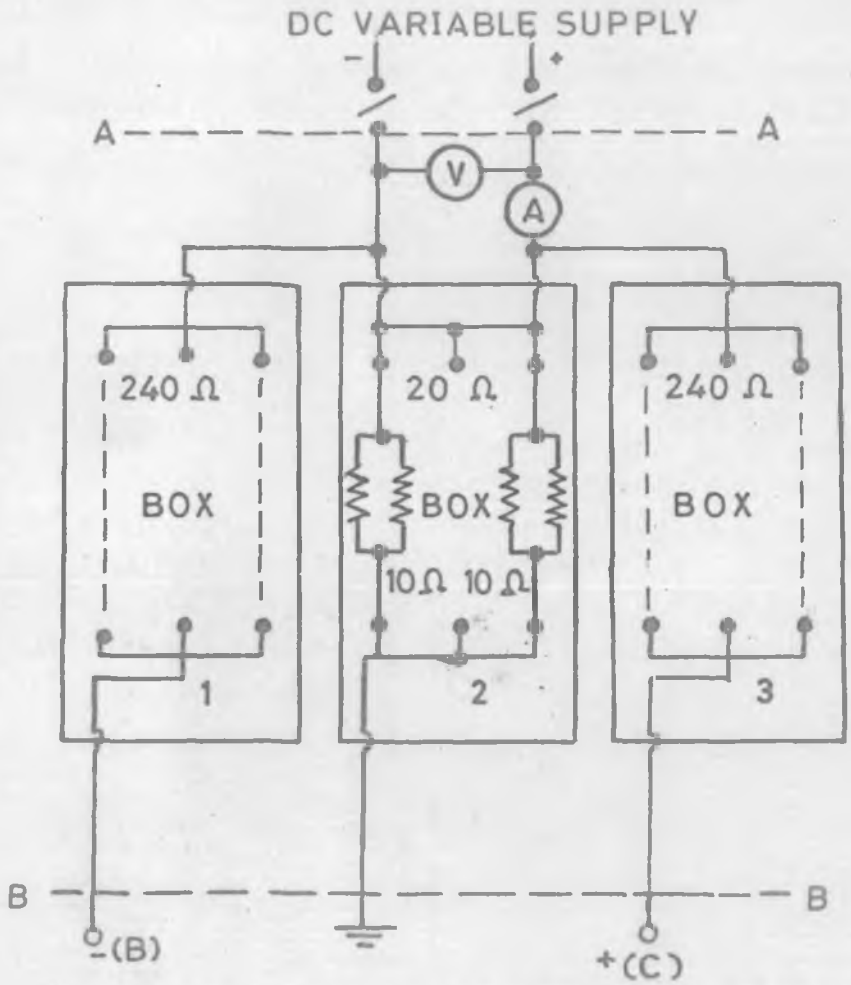

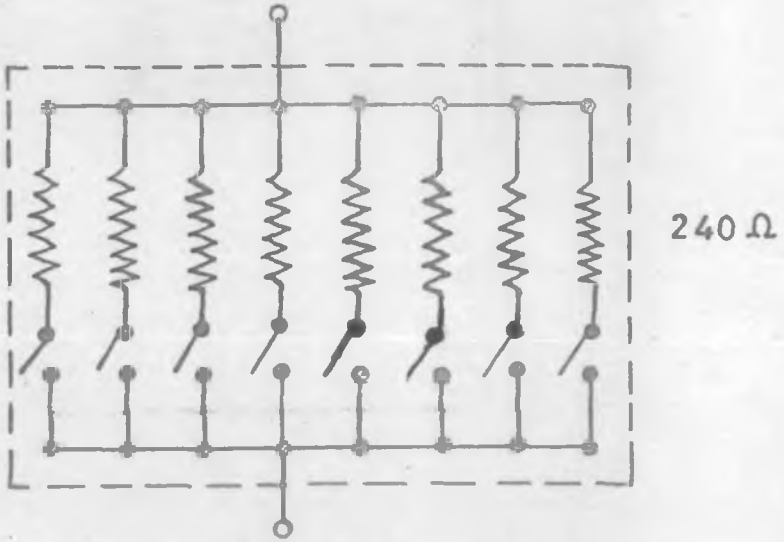

Resistor Box 20 Sections

FIG. 3.2. MHD GENERATOR SIMULATION.

3.2.3 Interconnection with infinite bus

MHD generator inverter link is a dual system. MHD-generator simulation gives d.c. which is inverted to three phase a.c. Infinite bus is connected to three phase variac and then to a three phase star/delta transformer and line reactor. This is shown at section C-C in figure B-1 in appendix B.

3.2.4 Phase shift control arrangement

In order to change the phase shift of the inverter output with respect to infinite bus, a three phase shifting transformer is used of the ratings mentioned in section 3.2.1. An auxiliary star/star transformer is connected to the output of the phase shifter which gives the desired phase shifted output at low voltage to control logic of the inverter. The phase shift control arrangement is shown in Figure 3.3.

3.2.5 Measurement of electrical quantities

The measurement of voltage, current and power has been made on both a.c. as well as d.c. side with instruments connected as shown in the diagram of figure B-1 of appendix B. These instruments are with the range and rating as described in section 3.2.1.

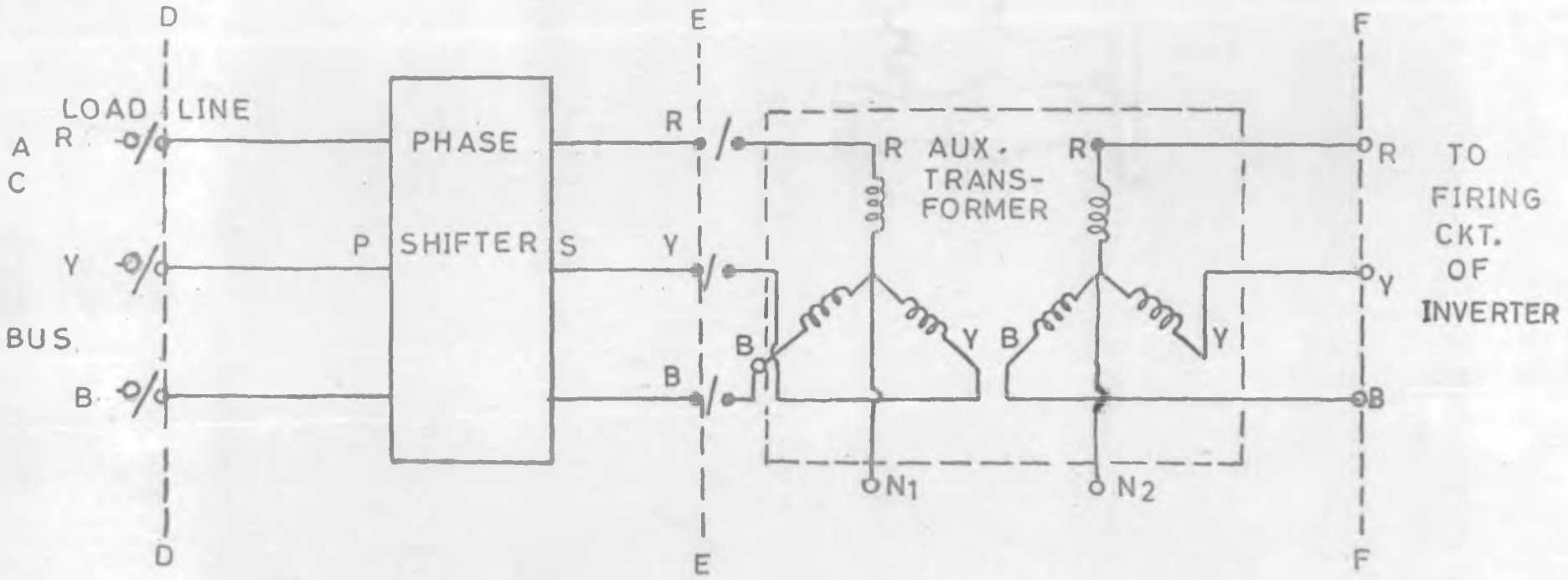

FIG. 3.3. PHASE SHIFT CONTROL ARRANGEMENTS.

3.3 Results of Experimental Study

The results of digital simulation study made in section 2.6 of the last chapter has been experimentally verified in this section with the experimental setup described in section 3.2.

3.3.1 Variation in Electrical parameters with phase shift

1. Variation of current and voltage with phase shift

The input d.c. variable supply is adjusted to 45 volts which gives 35 volts at no load on the output terminals of the inverter with zero phase shift. The variac is adjusted to give 35 volts. The inverter output was connected to infinite bus. The phase shifter control knob is adjusted to 15 degrees interval. Readings were noted on d.c. side using two voltmeters, two ammeters and a wattmeters at sections A-A and B-B in figure B-1 in appendix B. On a.c. side also the voltage, current and power were measured at two locations as a double check up. The results are converted to perunit quantities and tabulated in tables B-2 and B-3 in appendix B and graphed in figure 3.4 for added line reactance of 0.40 PU and 0.80 PU.

3. Variation of real and reactive power with phase shift

Real and reactive power is measured as a function of phase shift at the output terminals of the inverter and just

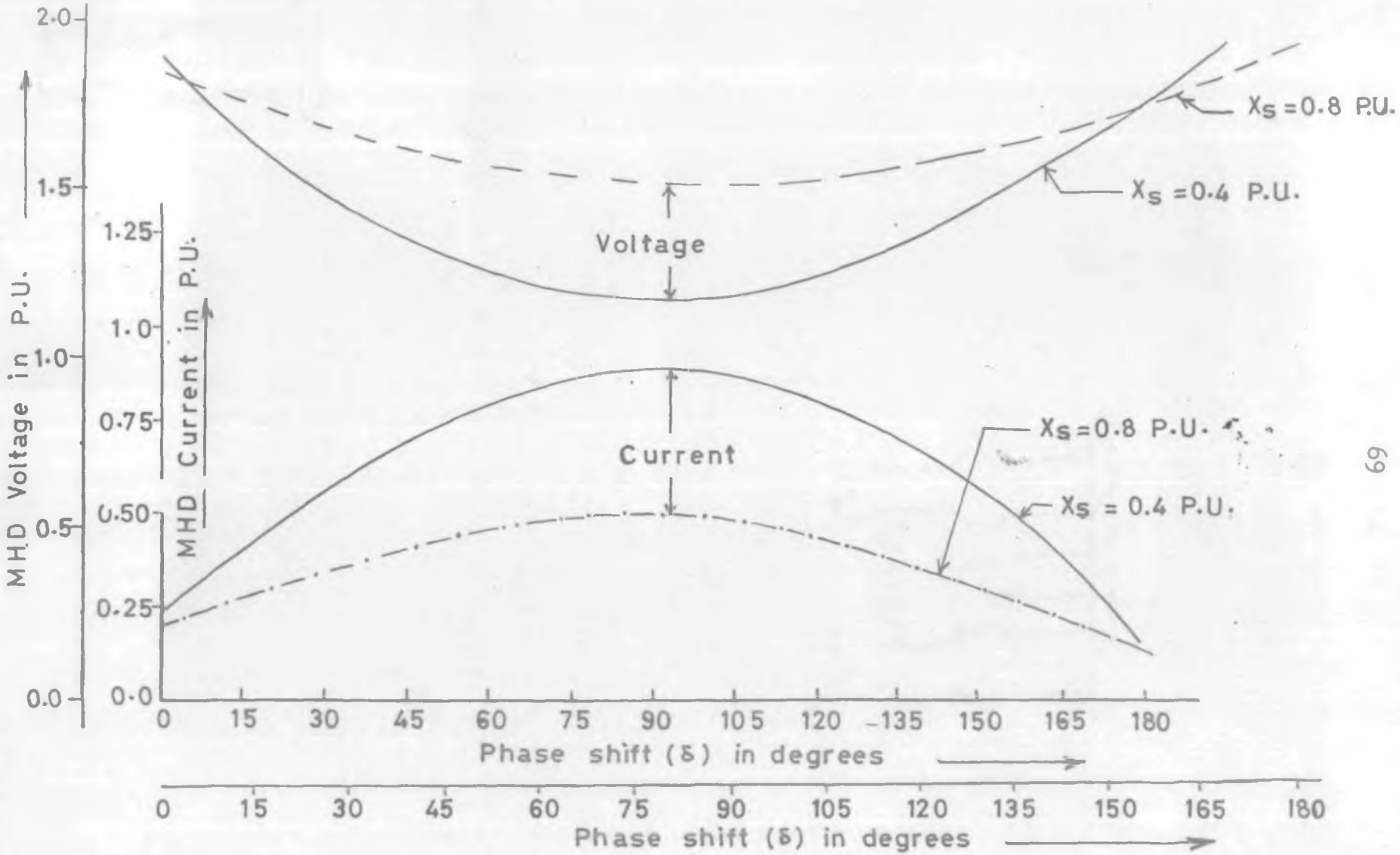

FIG. 3.4. VARIATION OF MHD VOLTAGE AND CURRENT WITH PHASE SHIFT.

after the line reactor. The two wattmeter method has been used for the measurement of power in a.c. circuit. Real power is almost constant between phase shift of 60 to 120 degrees for a line reactance of 0.40 PU and reactive power is zero at about 52 degrees. The variation of real and reactive power is tabulated in tables B-2 and B-3 in appendix B and graphed in figure 3.5. The other value of line reactance chosen is 0.80 PU. Lower values of the line reactance has not been chosen because of the limited range of over load protection of the inverter provided and also to save the inverter from being short circuited or over loaded.

5. Comments

The above experimental results obtained very well verify the theory stablished in the last chapter. The difference in the two cases is the power loss in the inverter and therefore the real power curve is shifted upward to include the inverter losses. The results of the digital simulation neglect any resistance in the system and also inverter losses are neglected. But in practice the small size power transistor inverter has considerable amount of loss and system is not purely reactive but there is resistance in actual system. Due to resistance the maximum power transfer is not at 90 degrees phase shift but it is shifted to 105 degrees. For maximum power transfer therefore occurs at 105° where reactive power is not zero. These variations may be possible

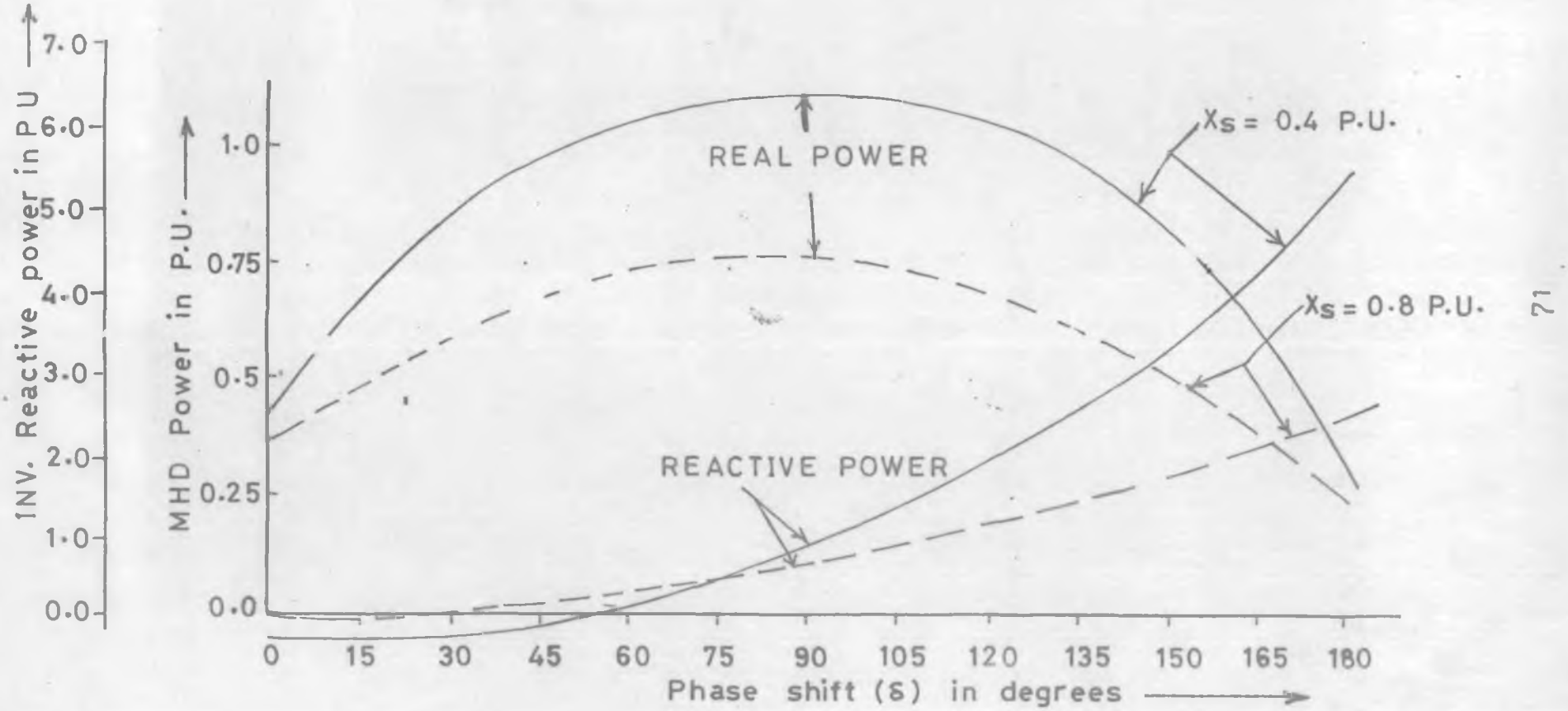

FIG. 3.5. VARIATION OF REAL AND REACTIVE POWER WITH PHASE SHIFT.

due to change in system reactance because of the practical difficulty to choose a reactor which gives exactly 0.45 PU reactance at the given base.

3.3.2 Variation of real and reactive power with changes in duct voltage and resistance as a function of phase shift

As discussed in section 2.6.2 of the last chapter that the MHD process being unsteady. The change in resistance and duct voltage affect the real and reactive power flow. The real and reactive power flow with change in resistance and duct voltage is plotted as a function of phase shift and shown in figure 3.6. 25 percent change in resistance and voltage is adjusted with resistance box and variable d.c. supply. The results are similar to that obtained in section 2.6.2 except that the curve obtained include inverter losses and resistance of the system.

3.3.3 Variation of real power with change in internal resistance from operating point

To consider the quasistatic changes in fluid dynamic conditions ($M \neq N \neq 1$) as discussed in section 2.2.2, resistance from the resistance box is changed for 2.0 PU and 1.5 PU of MHD duct ovoltage. Because of the limitations of the resistance box, the change in resistance is not in equal steps as considered in section 2.6.4 for digital computer

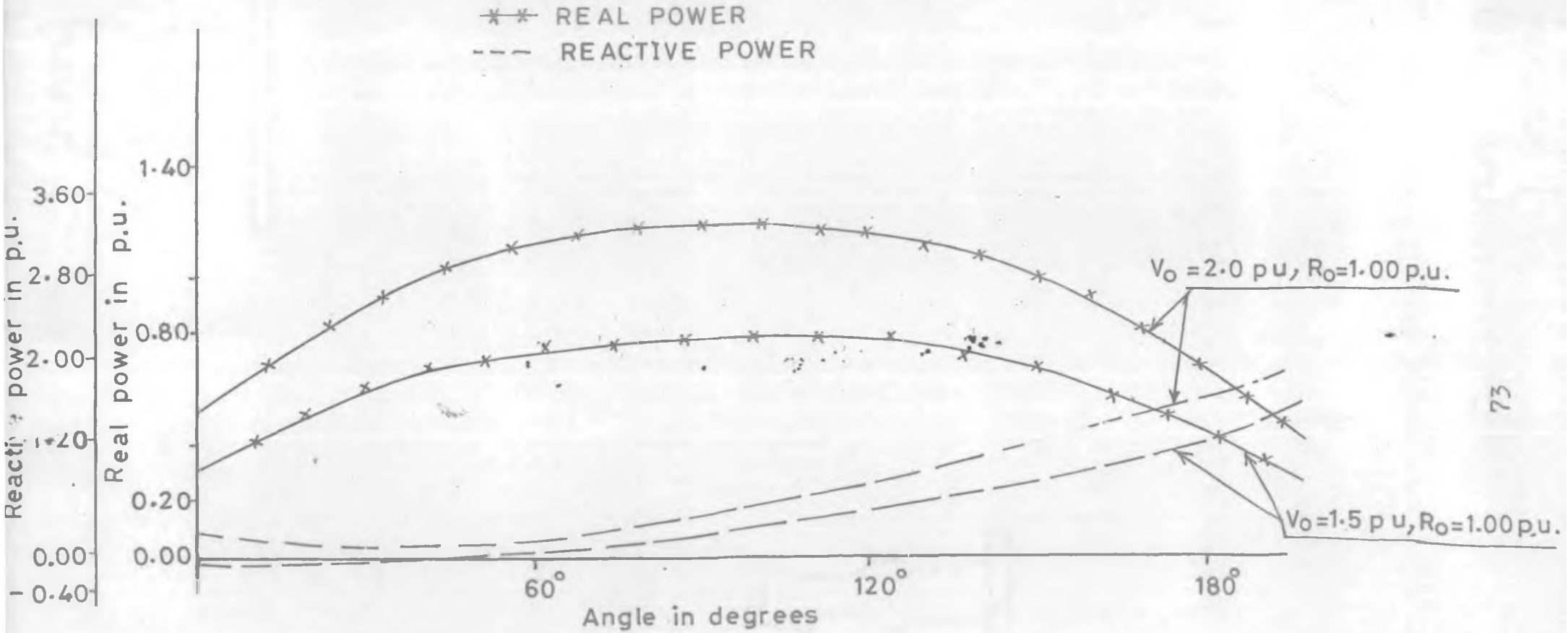

FIG.3.6. VARIATION OF REAL AND REACTIVE POWER WITH PHASE SHIFT.

study The variation for voltage 2.5 PU is not considered because of the inverter rating limitations. The variation of real power is plotted against change in internal resistance as shown in figure 3.7. The negative sign signifies a reduction in resistance from designed value. The variation of reactive power has been tabulated in tables B-4 and B-5 in appendix B only.

3.3.4 Variation of real power with change in duct voltage from operating point

Change in duct voltage is considered in this section for fixed values of internal resistances. The phase shift for operating point is taken as 30 degrees because at 60° phase shift, the increase in voltage exceeds the safe operation of inverter. The negative sign means reduction in duct voltage. Reactive power variation is small in this case also and wattmeter reading is such that currect values are difficult to measure. Figure 3.8 shows the variation of real power and the tabulated results are shown in tables B-6 and B-7 of appendix B.

3.3.5 Power control for changes in internal resistance

Two cases are considered with change in resistance of the duct with 30° and 60° phase shift. The resistance box is adjusted tin steps and then the phase shifter knob is turned till the wattmeter reads the reference power. Figure 3.9

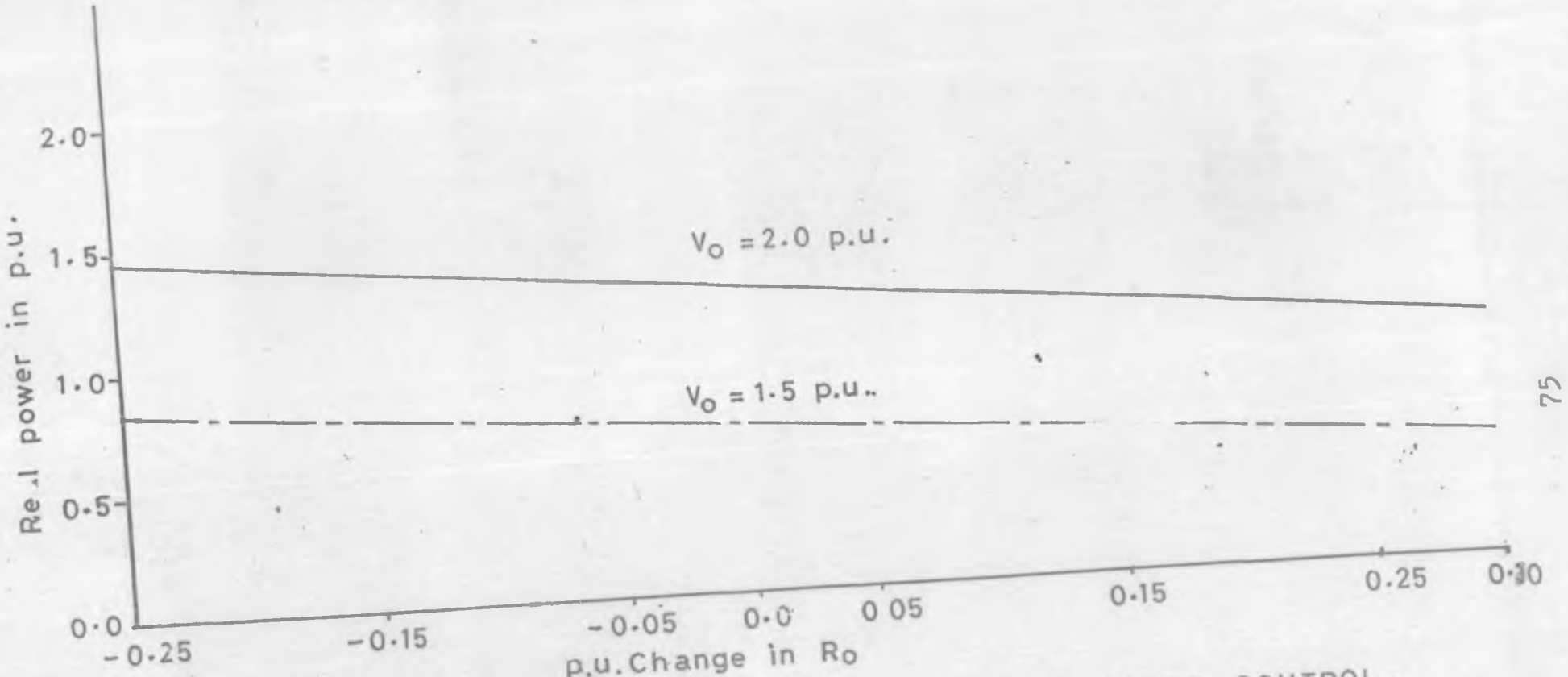

FIG. 3.7. VARIATION OF REAL POWER WITHOUT PHASE SHIFT CONTROL.

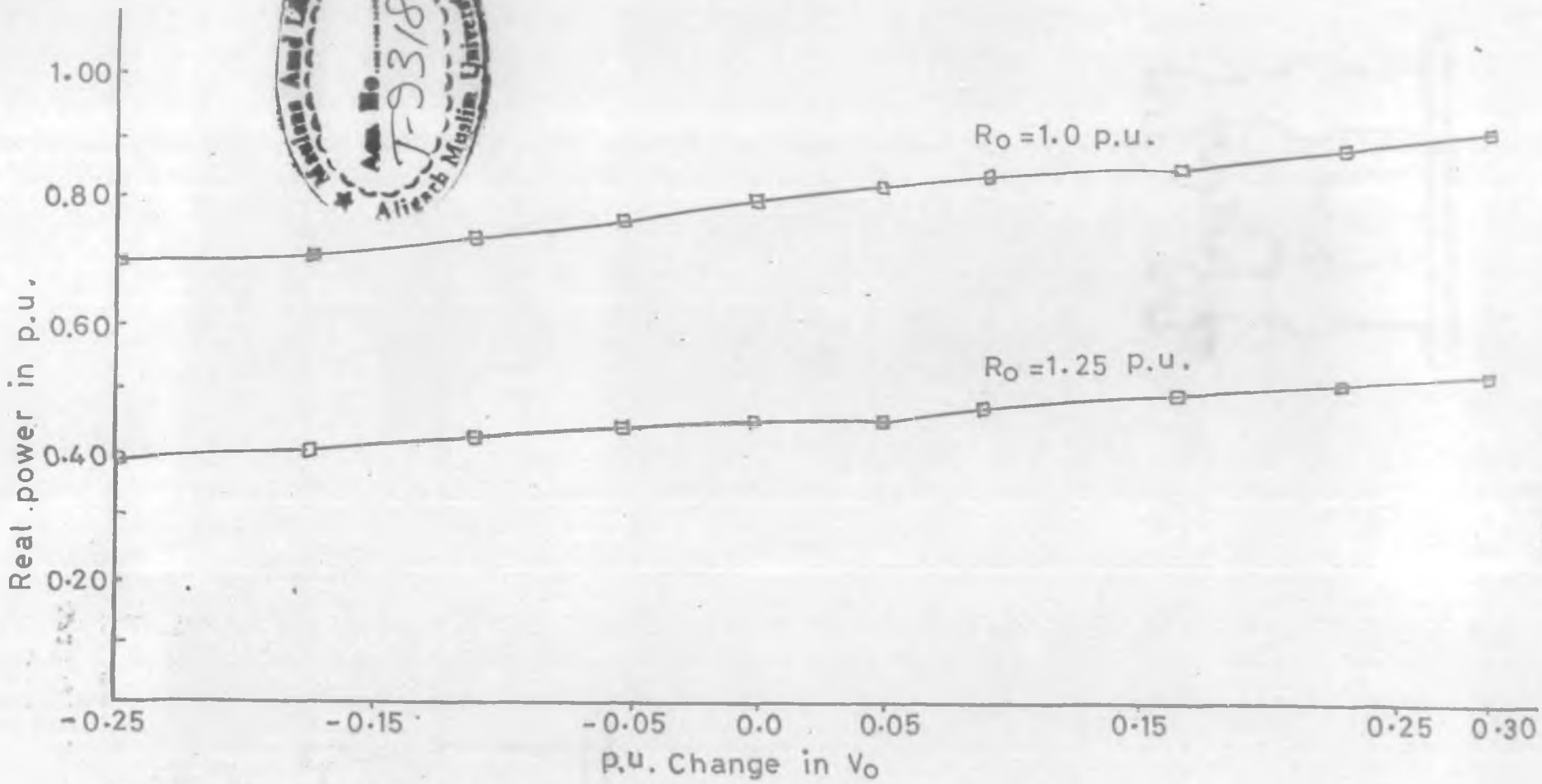

FIG. 3.8. VARIATION OF REAL POWER WITHOUT PHASE SHIFT CONTROL.

shows the power control for changes in internal resistance and the tabulated results are shown in tables B-8, B-9 and B-10 in appendix B. Due to slight error in measuring instrument and small setup the perunit base quantities and phase shift angle is different from the digital computer study made in section 2.6.6 of the last chapter.

3.3.6 Power control for changes in duct voltage

The reference power is fixed for a phase shift of 30 degrees. The voltage is varied from the variable d.c. supply. The phase shifter knob is turned to get the reference power. A change of 15 percent in any of the two parameters i.e. resistance and duct voltage can be controlled to reference power. The power to a.c. bus can always be increased with the phase shift control. This can be seen in column 4 and 5 in tables B-6 and B-7 of appendix B. Figure 3.10 shows the variation of real power with phase shift control. This can be compared with figure 3.8 without phase shift control. The reactive power for the reasons already specified has not been plotted. Moreover from the theoretical study it is clear that power factor remains within the desired limit.

3.3.7 Change in electrical parameters with other phase shifts

The operating point for other phase shifts has been chosen but as discussed earlier that for other than 60° phase

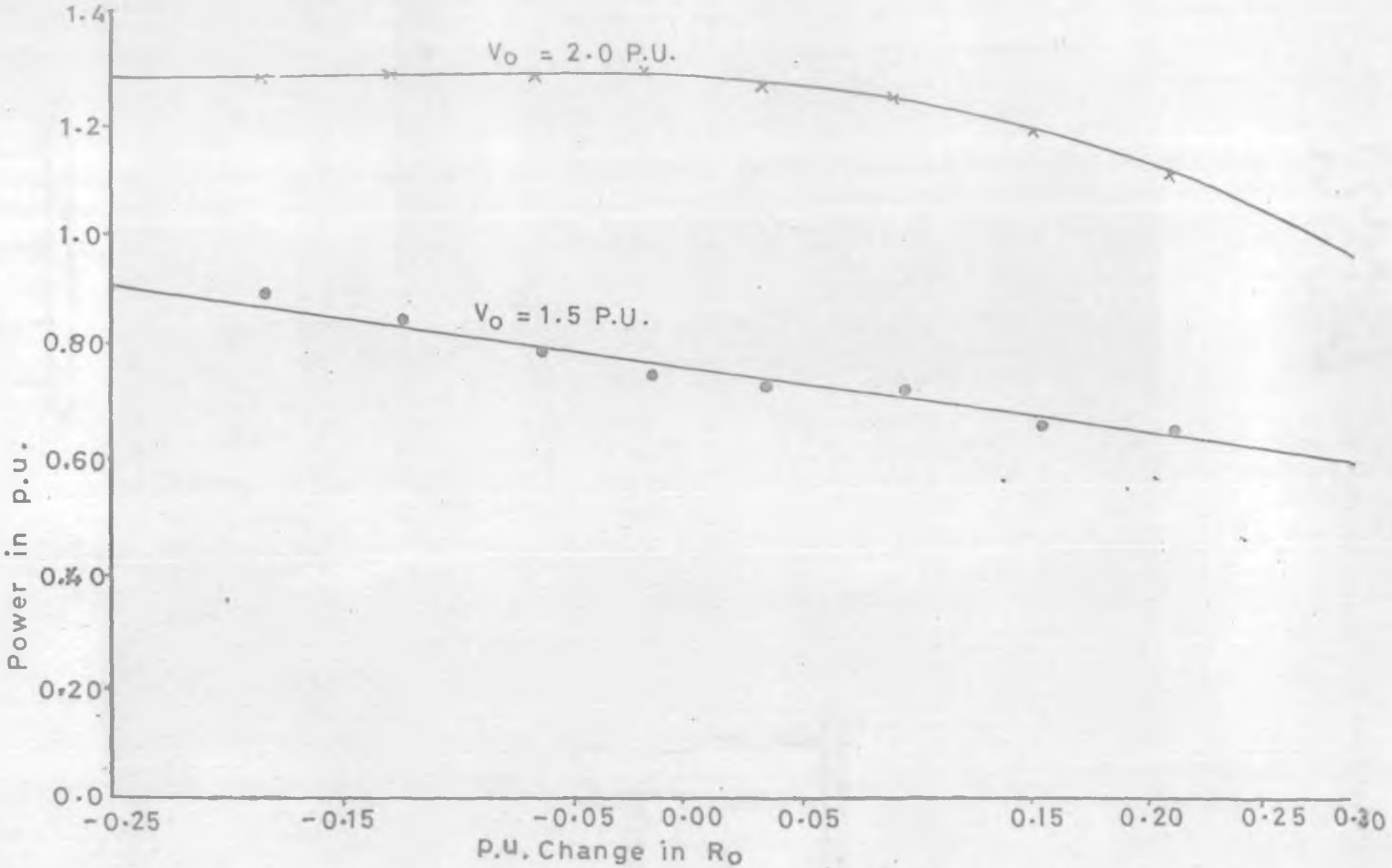

FIG. 3.9. VARIATION OF REAL POWER WITH PHASE SHIFT CONTROL.

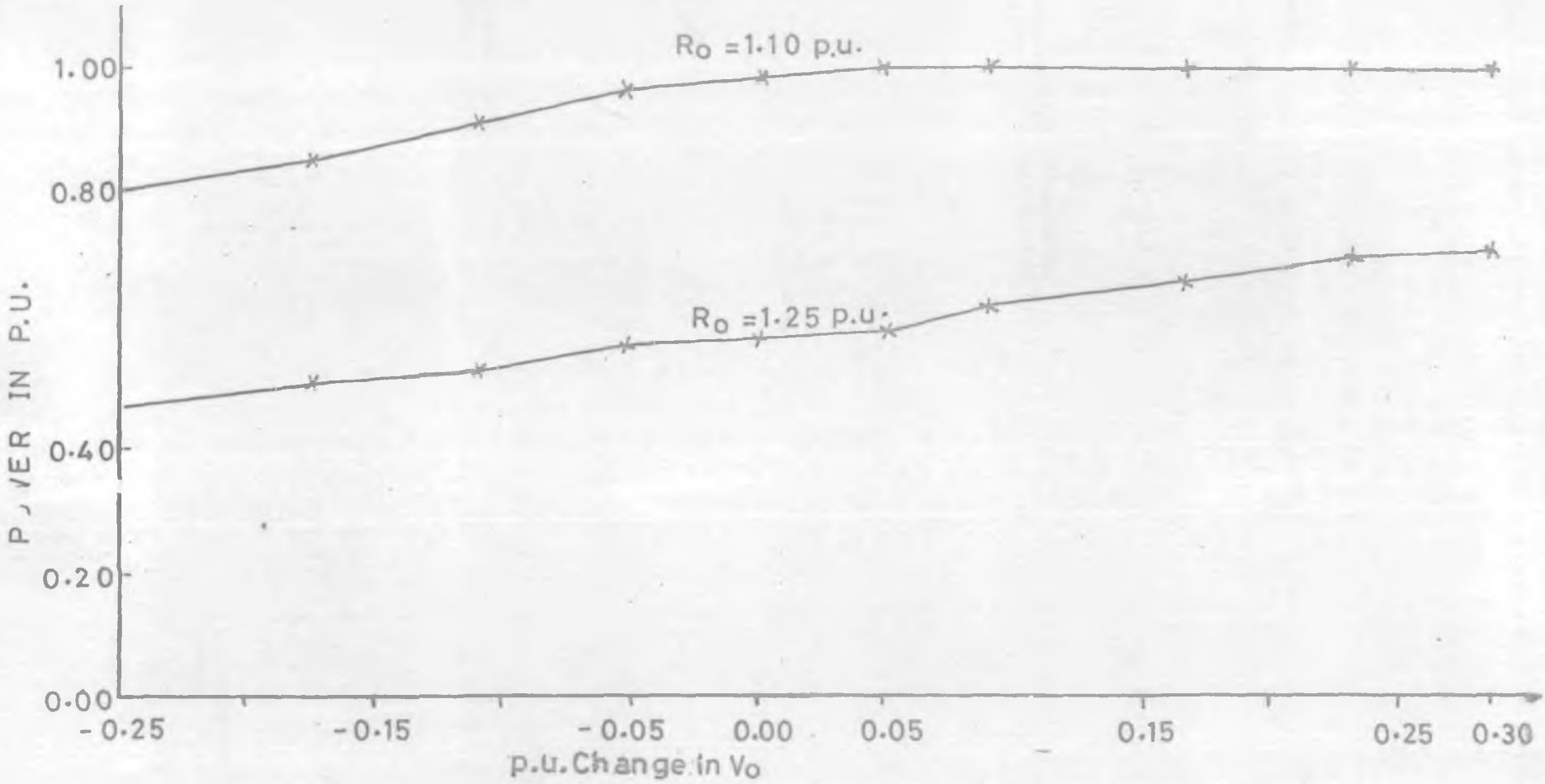

FIG. 3.10. VARIATION OF REAL POWER WITH PHASE SHIFT CONTROL.

shift the reactive power compensation will be required. The experimental study is also been extended to 90, 45 and 30 degrees fixed phase shifts. Only the voltage variation and control has been included at 30 degree phase shift because of the safe inverter operation as tabulated in B-6 and B-7 in appendix B.

3.3.8 Power control with the output parameters

As discussed in section 2.6.8, the output parameters taken are system reactance and bus voltage. This study is conducted because of the slight variation of bus voltage or a short circuit on the a.c. side to keep the power to reference level. Fixed resistances are changed in steps and the meter readings are recorded. The variation of electrical parameters are tabulated on perunit basis in table B-11 of appendix B. Phase shift control i.e. the phase shifter knob is adjusted for changes in PU system reactance and reference power is kept constant. Experimental varification for the power control with the change in system reactance is tabulated in table B-12 of the appendix B.

The second output parameter is bus voltage. Any change in bus voltage is not possible practically but it can be concluded by the digital computer study that changes in bus voltage can keep the power to reference level.

3.4 Design of Minimum cost filters [54]

A converter is the source of harmonic voltages and currents, as discussed in section 2.4. Filters are added to reduce as far as practicable the harmonic currents and voltages. A.C. filters serve two purpose simultaneously, supplying reactive power in addition to reducing harmonics. The part of the cost of filters is charged for reducing harmonics and the rest for supply of reactive power. Thus we are lead to the concept of minimum cost filters, which is required for harmonic reduction only in installations where reactive power required by the converter can be supplied by the a.c. system without reinforcing the latter.

For a shunt filter tuned at a particular harmonic frequency, the capacitive reactance equals inductive reactance. Now it remains to choose resistance. Following equations are therefore given for the choice of filter components at resonance :

$$W_n^2 \, L \, C = 1 \qquad (3.1)$$

$$Q = \frac{W_n \, L}{R} \qquad (3.2)$$

where $W_n = 2 \pi \times$ harmonic frequency. The filter presents its lowest impedance equal to the resistor R, when accurately tuned for this condition. In practice detuning effects exist due to errors in network frequency, change in capacitance and

inductance. It has been shown that a change of inductance or capacitance of say one percent near resonance is equivalent in detuning effect to a frequency change of 0.5 per cent near resonance which presents a higher impedance than R and is given as

$$Z_{f_n} = R\,(1 + j\,2\,Q\,\delta) \qquad (3.3)$$

where Z_{f_n} = filter impedance with frequency error

Q = quality factor

δ = effective frequency error

A.C. network impedance also varies with changes in load and disconnection or extension of lines and generators etc. The safest assumption is that the a.c. network impedance, Z_a, can adopt any complex value. The harmonic voltage magnitude for this impedance in parallel is given as

$$U_n = I_n\,[(G_a + G_{f_n})^2 + (B_a + B_{f_n})^2]^{-1/2} \qquad (3.4)$$

where U_n and I_n nth harmonic voltage and current

G_a and G_{f_n} conductances of filter and a.c. network

B_a and B_{f_n} suseptances of filter and a.c. network

It is shown that if G_a and B_a are unrestricted (except that G_a is positive) then maximum U_n is obtained when a.c. network is purely reactive i.e. $G_a = 0$ and $B_a = -B_f$ and on substitution

of G_f and B_f from equation (3.3) we get :

$$U_n = \frac{I_n W_n L}{Q} (1 + 4 Q^2 \delta^2) \qquad (3.5)$$

This has a maximum of harmonic voltage which is independent of the a.c. network impedance as

$$U_n = 2 I_n R \qquad (3.6)$$

$$\text{at} \quad Q = \frac{1}{2\delta} \qquad (3.7)$$

It has been shown that the presence of losses (a phase angle of Z_a of less than $\pm 90^\circ$) makes permissible a higher Q and lower U_n, but for a conservative design this will be ignored.

3.4.1 Filter Calculations [51,54,55]

The fifth and seventh harmonic filters have been designed for the experimental setup described in section 3.2. The line reactor takes into account all higher order harmonics. Equations (3.1), (3.2) and (3.6) are used to determine the components of the filters with the following assumptions.

1. Quality factor = 50
2. Pure reactive network
3. Harmonic voltage at the point of common coupling taken as 1 percent

Fifth harmonic filter components :

Capacitance (C_5) = 7.5 μF

Inductance (L_5) = 54 mH

Resistance (R_5) = 1.7 ohms

Seventh harmonic filter components

Capacitance (C_7) = 2.8 μF

Inductance (L_7) = 75 mH

Resistance (R_7) = 3.3 ohms

3.4.2 Results of digital simulation with filter

Modified equations with filters from (2.36) to (2.40) are now computed with above filter components on per unit basis. The above designed filters are the minimum cost filters therefore the only difference in results at power frequency values is the reduction of real and reactive power both as shown in figure 3.11 and list B-13 is attached in appendix B for the modified program. This can be compared with figure 2.8 for X_s = 0.45 PU. Real and reactive power flow are reduced compared to the case when filter components are not added. This is because filter behaves as a capacitive shunt branch at power frequency. The reactive power is being supplied by the capacitive branch to the system. Therefore the reduction in the reactive power from inverter results. The real power flow to infinite bus is also slighty reduced

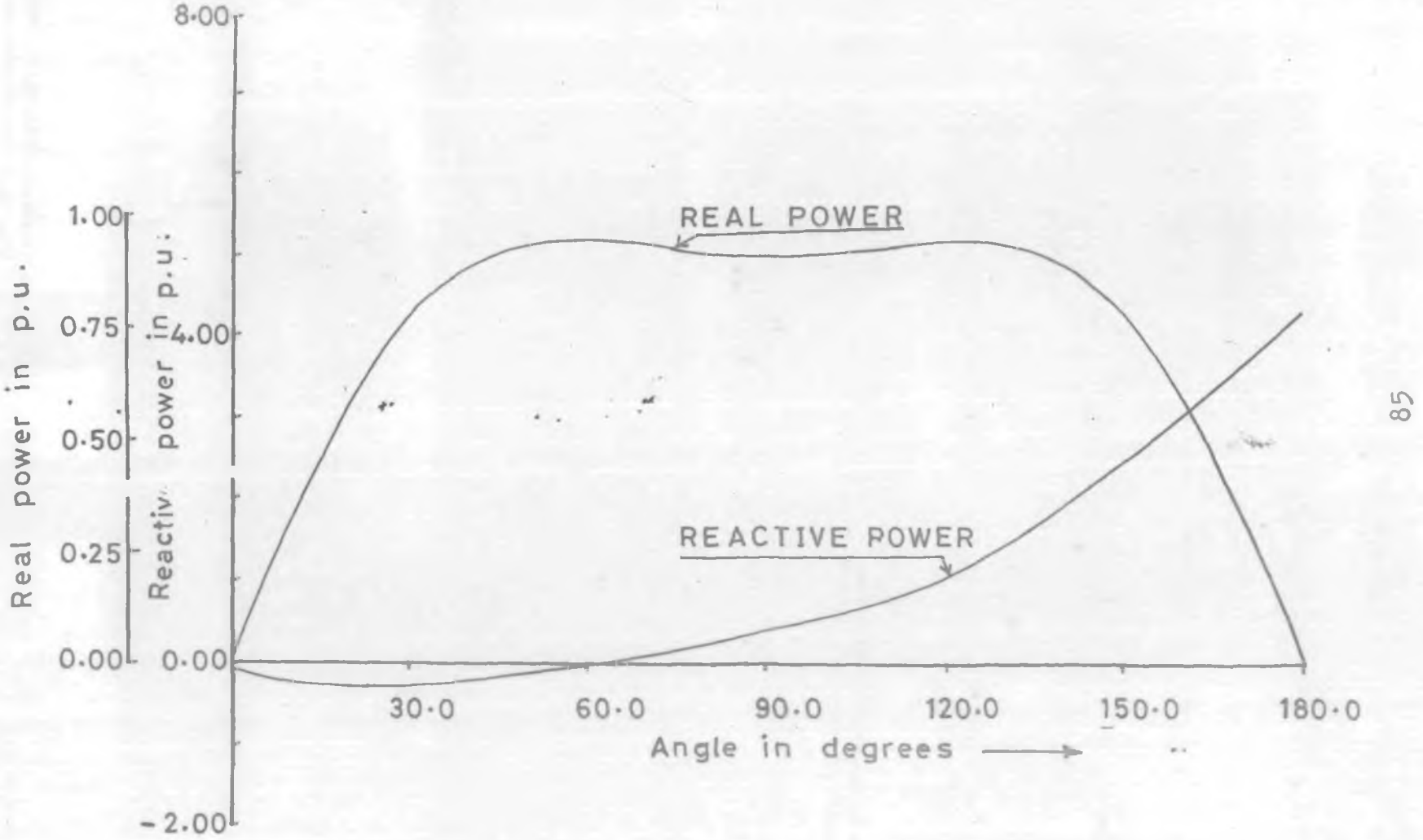

FIG. 3.11. VARIATION OF REAL AND REACTIVE POWER WITH PHASE SHIFT.

because of filter consuming power in resistance. Other results are also obtained but are not included as they are slighty different with those diseussed in section 2.6.

3.5 Design of three phase auxiliary commutated Mc Murray Inverter

The Mc Murray inverter, because of its excellent square waveform, its high efficiency, and capability of high frequency operation is used as the three phase power source for experimental investigations [56]. The inverter provides an interface between the MHD generator and infinite bus for the conversion and control of MHD power.

The Mc Marray inverter [57] is widely known and used and only the brief description, sufficient to define the inverter specification, is given here. A three phase inverter is shown in figure 3.12, where components of each phase are clearly defined by letters. Each phase comprises a pair of main thyristors T_{1M} and T_{2M}, a pair of auxiliary thyristors T_{1A} andTT_{2A}, a pair of feedback diodes D_{1F} and D_{2F}, a pair of clamping diodes D_{1C} and D_{2C}, a pair of line inductances damping resistors L_s and R_c, a filter capacitor C_{in}, a commutating inductor L_c and a commutating capacitor C_c. When T_{1M} is triggered, the output is connected to the positive d.c. bus. When T_{2M} is triggered, the output is connected to the negative d.c. bus. Thus the output is a square wave whose peak

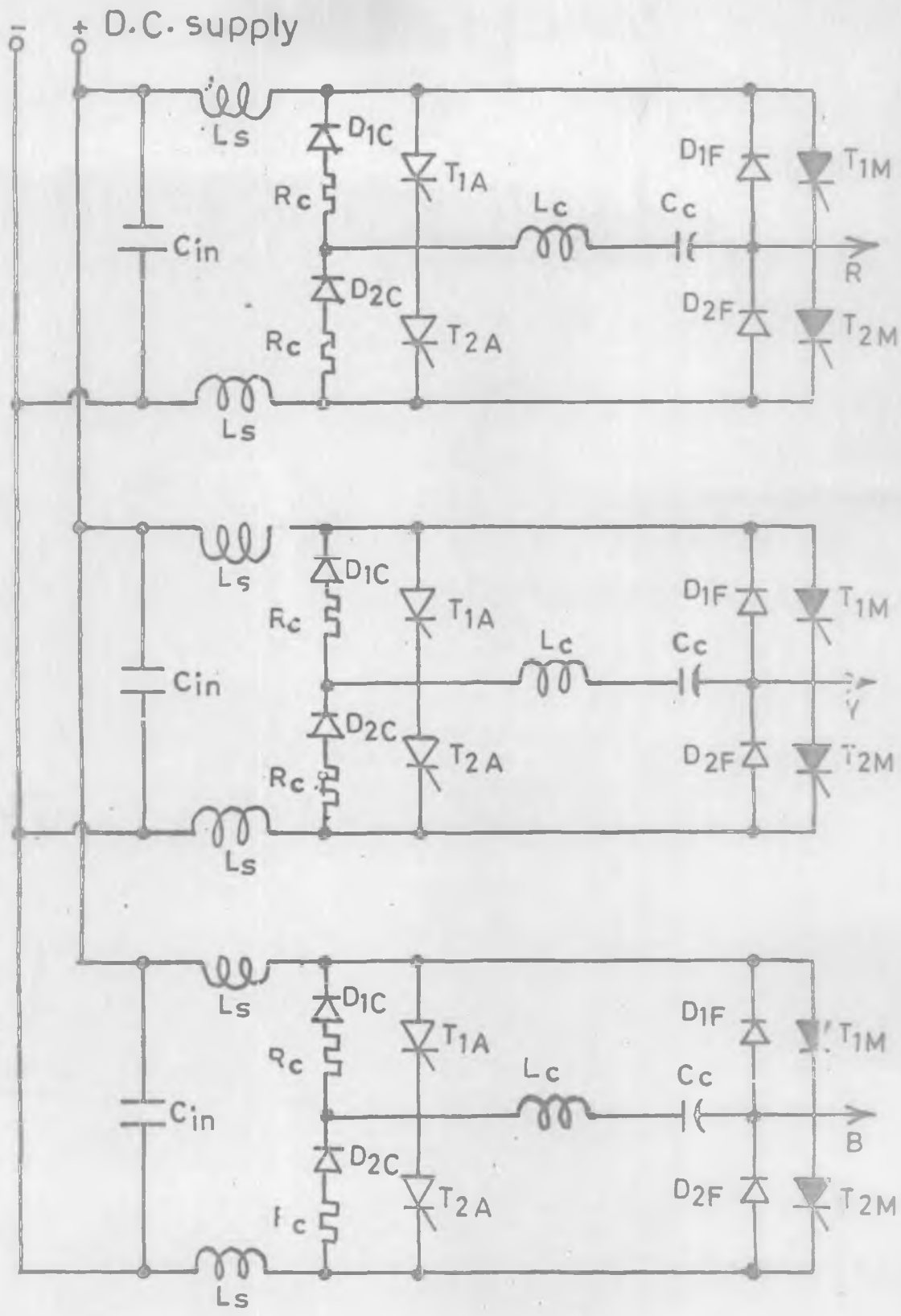

FIG. 3.12. THREE PHASE AUXILIARY COMMUTATED INVERTER.

to peak amplitude is V_{DC}. The three units will be operated sequentially so as to give output voltages mutually displaced by 120^{o}. Thus producing a three phase square wave output.

3.5.1 Design specifications

The above described inverter is designed with the aim of connecting the 2 MW (Thermal) MHD-generator test facility [21]. The output of generator can be connected to this inverter with or without consolidation circuits in segmented Farady, Hall or diagonal mode. The inverter has been designed for the following specifications.

(a) Nominal rating : 30 KVA or 30 amps rms per phase with

(i) overload capacity (short term) to 60 amps rms per phase.

(ii) Instantaneous peak current for commutation purpose - 100 A.

(iii) Design to be based on worst likely case.

(b) Supply from 415 V, 3 phase full wave bridge and capacitor giving about 560 Volts d.c.

(c) Normal commercial SCRS with about 20 μS turn off time are to be used.

3.5.2 Selection of optimum value of commutating capacitance and inductance (C_c and L_c)

The commutation pulse which commutates the SCR must exceed the load current for an interval longer than the turn of time of SCR. Also the optimum wave shape of the commutating pulse is decided which requires the least energy with higher Q' at its natural frequency [58] for the optimum commutating pulse as shown in figures B-17 in appendix B. Commutating capacitance is calculated (C_c) = 5 microfarad and commutating inductance is calculated (L_c) = 56 microfarad.

3.5.3 Selection of main device (T_{1M} and T_{2M})

The main load carrying SCRS are chosen from the semicron manufacturer data for the worst likely case as mentioned in section 3.5.1. The suitable SCR from table B-14 in appendix B is

No SKT 45 F12D

3.5.4 Selection of auxiliary device (T_{1A} and T_{2A})

Auxiliary SCRS are used to turn off main SCRS. These SCRS carry the commutation current with the peak amplitude of 100 amps. and duration given by half cycle of the ring around frequency of commutation circuit. The rms current is calculated as 24 amps. The suitable SCRS from table B-14 in appendix B is

No SKT 16 F12D

3.5.5 Selection of feedback diodes (D_{1F} and D_{2F})

Feed back diodes carry the commutation current but for reactive loads these diodes conduct during half of each cycle to return power from the load to the d.c. supply. The rms current rating is the same as the main device current. Transient current through these diodes are taken as peak of commutation current [58].

Based on the above ratings the suitable diode is chosen from table B-15 shown in appendix B.

No SKN2M 100/12

3.5.6 Selection of clamping diodes (D_{1C} and D_{2C})

Under inductive load conditions the commutation capacitance can overcharge twice the d.c. rail voltage. This extra stored energy must be removed through the damping circuit and it must be dissipated in the damping resistor [59]. The inverter circuit is analysed for the critical damping case and rms current through the diode is calculated [59]. The diode is selected from table B-15 shown in appendix B.

No SKN1M 20/12

This diode has rms current rating as 40 amps because no other diode is available for lower rating for safe operation.

3.5.7 Selection of line inductors and damping resistors (L_s and R_c)

Referring to figure 3.12 the line reactors have been included to limit the rate of rise of on state current. The worst possible case for rate of rise of current will be when the device is turned on without the gate signal. This is approximately 20 percent of the di/dt with gate signal. The di/dt for the main and auxiliary devices are 250 A/μS and 200 A/μS as shown in table B-14. With the d.c. rail voltage as 560 volts inductance needed for worst likely case comes as 14 μH. This could be distributed in both the rails as shown in figure 3.12. Apart from the worst likely case the inductance and resistance of supply line would also bring the rate of rise of current to below 40 A/μS. These line inductors must be air cored because of the high prospective currents during fire through.

The damping resistor is in series with the clamping diode to dissipate the excess stored energy in one of the resistor till the voltage across C_c becomes equal to d.c. rail voltage. The resistance is chosen such that the equivalent circuit containing C_c, L_c, D_{1F}, D_{1C} and L_s is critically damped. The calculated value is as [59].

R_c = 7.24 ohms and power dissipation of damping diode

= 629.15 Watts with rms current of 9.24 amps.

3.5.8 Selection of filter capacitor (C_{in})

The filter capacitor is chosen such that it can supply a current of 150 amps. during commutation period which is equal to width of the commutating pulse. A 10 percent voltage drop is assumed when capacitor is supplying load current. The calculated min. value comes as 170 μF. But usually a large capacitor is chosen for safe operation and continuous supply under commutation period.

3.5.9 Selection of snubber components [29,60,61]

Proper protection of thyristers from excessive dv/dt and di/dt is necessary for thyristers. The design of snubber circuit is considered here for SCRS selected in section 3.5. This snubber circuit design is for minimum voltage spikes with the following specifications [60].

$$\Psi_o = 1.3,\ \xi_o = 0.23 \text{ and } (dv/dt)_o/Ew_o = 1.3$$

The snubber components are

R = 10 Ohms.

C = 0.12 μF

L = 3.3 μH

3.6 Inductor Design [62,63,64]

The careful design of inductor is necessary because at high frequencies the inductor is only few microhenries. A

large current flows which means more losses. The high frequency operation means skin effect. To minimize these problems different designs are considered in this section.

3.6.1 Brooks coil design

The brooks coil in different designs for the same inductance has been obtained in single layer, double layers, 5 layers and 6 layers coils. The dimensions of the designed coils for the same inductance are given. The frequency response and quality factor is also experimentally determined. Single and double layer coil has been found suitable for variable frequency operation. It has constant inductance and improved quality factor as frequency is increasing. The dimensions are shown in figure 3.13 and design values are as follows :

(a) 6 layer coil

(i) Copper wire with six turns and six layer of 9 AWG

(ii) Former diameter = 3.48 cms

(iii) Inductance = 56.95 μH

(b) 5 layer coil

(i) Copper wire with five turns and five layers of 10 AWG.

(ii) Former diameter = 6.3 cms

(iii) Inductance = 59 μH

(c) 2 layer coil

(i) Copper with two layers and 15 turns of 10 AWG

(ii) Inductance = 54.35 μH.

3.6.2 Flat Spiral strip design

Strip designs for inductor are preferred because of minimization of its volume. These designs offer more uniform voltage distribution under surge or impulse conditions, better heat transfer, improved space factor and stronger coil structure. Strip conductors are used in many electromagnetic devices including transformers, clutches and choke coils. The design here has been adopted for the experimental work to compare the performance of strip coil with those discussed in section 3.6.1. The figure 3.13(d) shows the size of such a coil wound for the same inductance. For higher frequency the resistance of copper strip is lower than the resistance of a solid wire of the same cross section.

Copper strip dimensions

(i) Width = 2 cms

(ii) Thickness = 0.029 cms

(iii) Insulation thickness = 0.73 cm (paper glass)

(iv) Former diameter = 2.5 cms

(v) Inductance = 57.1 μF

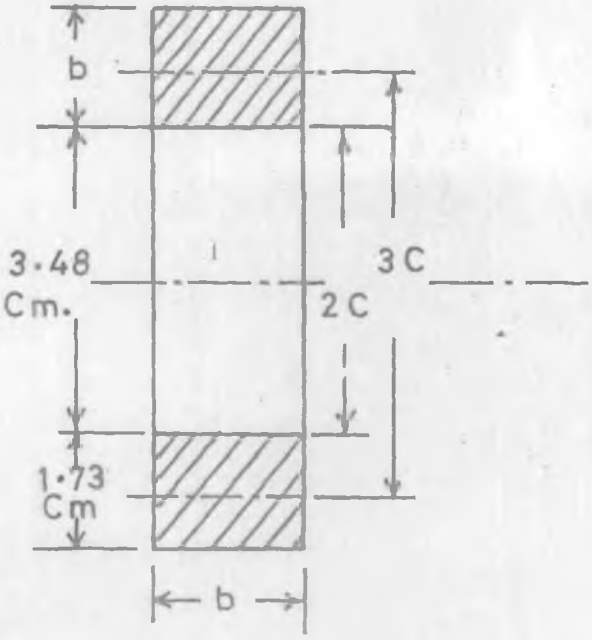

(a) 6 LAYER COIL

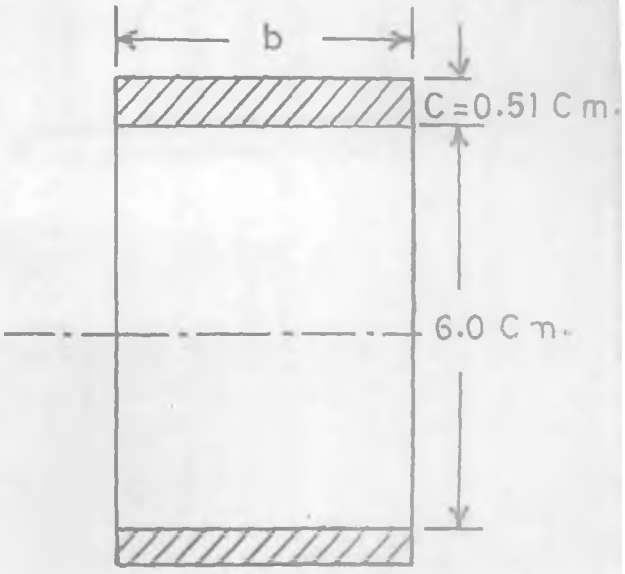

(c) 2 LAYER COIL.

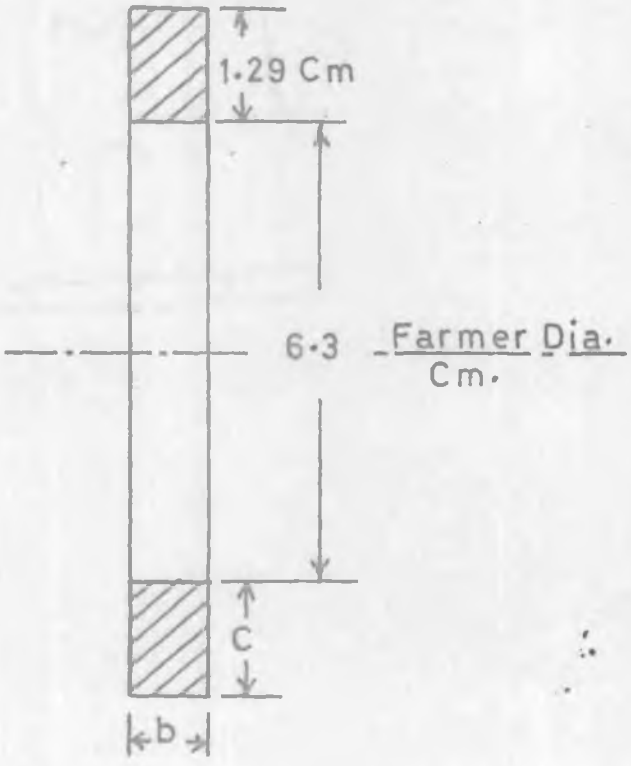

(b) 5 LAYER COIL

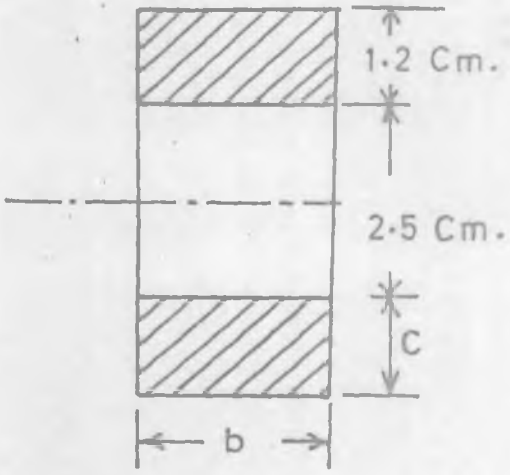

(d) MULTI LAYER STRIP.

FIG. 3.13. INDUCTOR DESIGN FOR $L_c = 56\,\mu H$.

3.7 Design consideration for safe Inverter Operation

For successful commutation of inverter SCRS, peak current of the inverter should not increase more than the commutation current. The ratio of load current peak and discharge current has a particular ratio already described in section 3.5. The load current due to changes in duct resistance and voltage will also affect the peak current through the inverter. Possible variation in peak current due to changes in various parameters is discussed in following subsections.

3.7.1 Variation in peak current with phase shift

In power control, the variation of phase shift is considered. Therefore the variation in peak current through the inverter is plotted with phase shift. Maximum changes in internal resistance and duct voltage are considered. Figure 3.14 (a) shows variation for 2.5 PU voltage and 0.75 PU resistance. It can be seen at more than 90 degrees phase shift,the peak current increases more than 2 PU. Figure 3.15 (a) also shows the other maximum possible variation in peak current with phase shift for two values fof system reactance.

3.7.2 Variation in peak current for changes in duct internal resistance

Due to change in internal resistance from the operating

point current variation is plotted for a 50 percent increase in voltage. The peak current remains within 1 PU. Therefore it can be concluded that due to change in internal resistance the current will be within safe limits for successful inverter operation as shown in figure 3.14 (b).

3.7.3 Increase in peak current for changes in duct voltage

The variation of duct voltage from operating point also affects the peak current through the inverter. A 25 percent change in voltage is plotted against peak current as shown in figure 3.15 (b). The variation of current due to change in voltage is more compared to change in resistance as can be seen from graphs. The current increase remains within 2 PU. Therefore the control of power due to changes will pose no problem for the inverter within the above variation in voltage.

3.8 Water fuse protection for power thyristor

Semiconductor fuse is found most suitable for power semi-conductors. However, its cost is a major issue. Rewirable fuse link is cheap and fast. But it is not suitable for power semi-conductors as its joule integral (I^2t) and the transient arching voltage are quite high. However an ordinary fuse wire when placed in water, carries a large current compared to that in air at reduced joule integral. A particular length

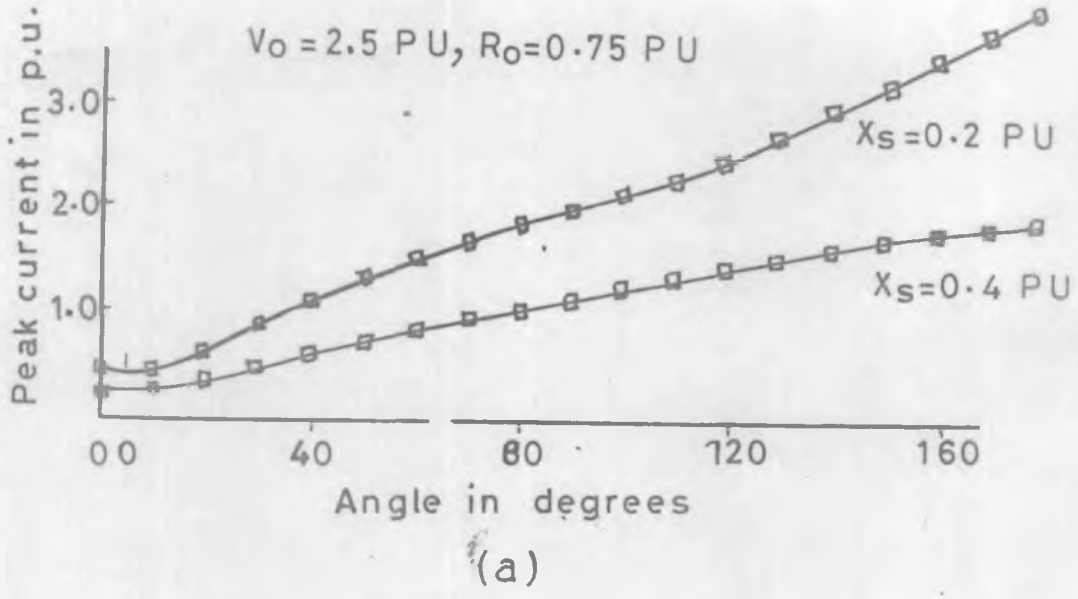

(a)

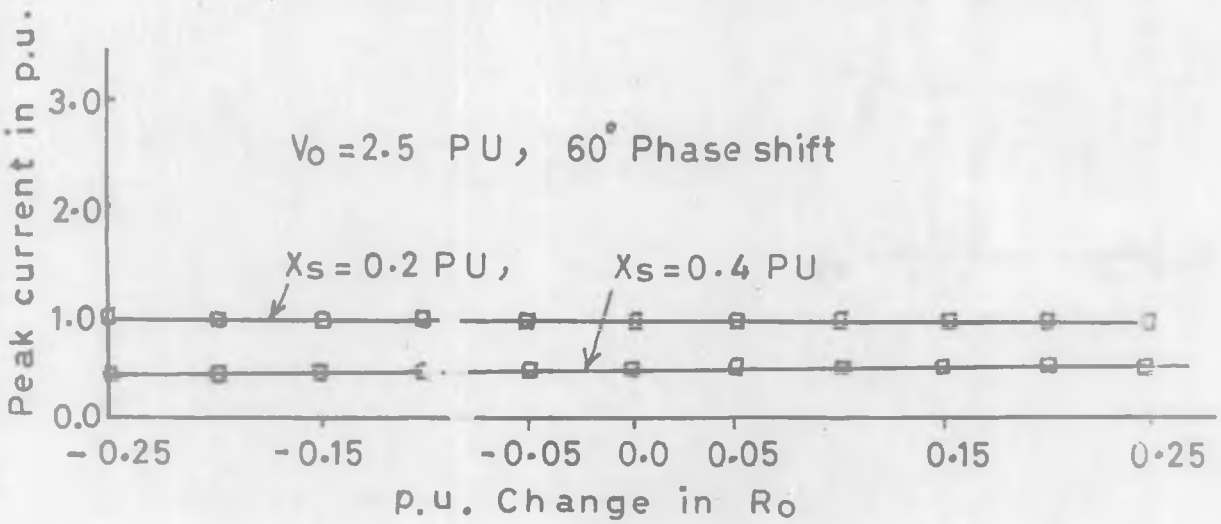

(b)

FIG. 3.14. VARIATION OF PEAK CURRENT WITH PHASE SHIFT AND Ro .

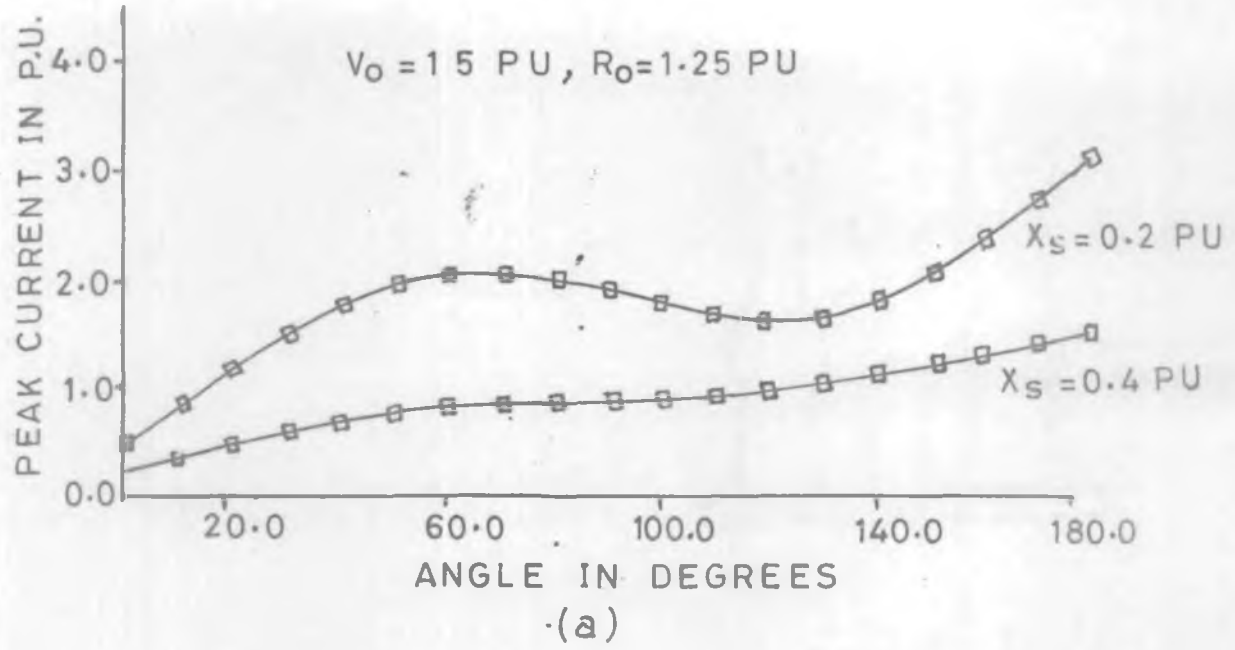

(a)

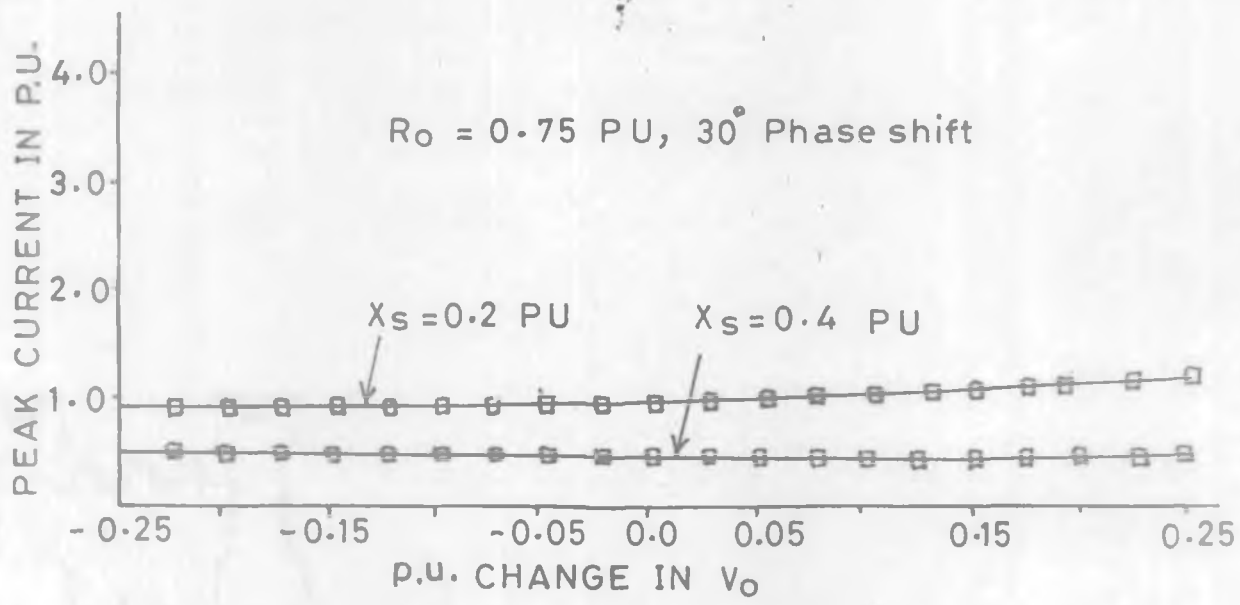

(b)

FIG. 3.15. VARIAT. N OF PEAK CURRENT WITH PHASE SHIFT AND Vo .

of rewrirable fuse wire has been used for overload protection in inverter circuits [29]. The behaviour of such a fuse is described in water and experiments are conducted to suggest suitable length of fuse wire to protect the device or circuits.

3.8.1 Fuse protection in inverter circuits

Current limiting fuses in an inverter circuit are usually connected in series with each thyristor to protect them from excessive surge currents. The purpose is to limit the fault current pulse in magnitude and duration to values below the point where permanent damage to the thyristor results. This, infact, means that junction temperature rise must be limited to safe value.

3.8.2 Behaviour of an ordinary fuse wire in water

An ordinary rewirable fuse is most economical. But it has high joule integral value and the transient arcing voltage. When the same wire is placed in water, the heat energy dissipation (due to convection currents in water) increases, compared to that in air. The water immersed fuse link exhibits a much higher steady state current rating than the same link in free air. Test conducted with different rewirable fuse wire show that jule integral and arcing voltage in water is reduced compared to in free air. However the clearing time is approximately the same once the rupture of the fuse link occurs.

3.8.3 Experimental varification and results

The test arrangement has been shown in figure 3.16. Different wires can be mounted between the connector terminals of the water tank (20 x 15 x 15 cms) as shown in 3.16(b). A large rating SCR is connected in series with a high frequency shunt and fuse wire. The SCR is triggered and the fuse is blown. The oscilloscope stores the arc voltage and current wave form. The firing angle can be varied with the help of firing circuit and length of the fuse wire can be varied with the help of connector leads. The fuse elements tested are

(i) Eureka 34 SWG

(ii) Copper wire 34 SWG

(iii) Fine copper wire 0.051 and 0.089 mm

(iv) Ordinary solder wire with different gauges.

The test was conducted with 240 volts ac and dc both. Batteries were also employed for 24 and 48 volts dc tests.

From the different tests conducted, the most suitable fuse wire is found to be Eureka 34 SWG. For large currents and high voltage, shorter lengths of the fuse wire can be used as the voltage drop across the fuse will be small. For low voltage and small current rating SCRS, long fuse wire can be used to limit the peak current and arc voltage. The approximate length of the wire needed for a particular SCR can be found out from graphs plotted for I^2t and arching voltage vs

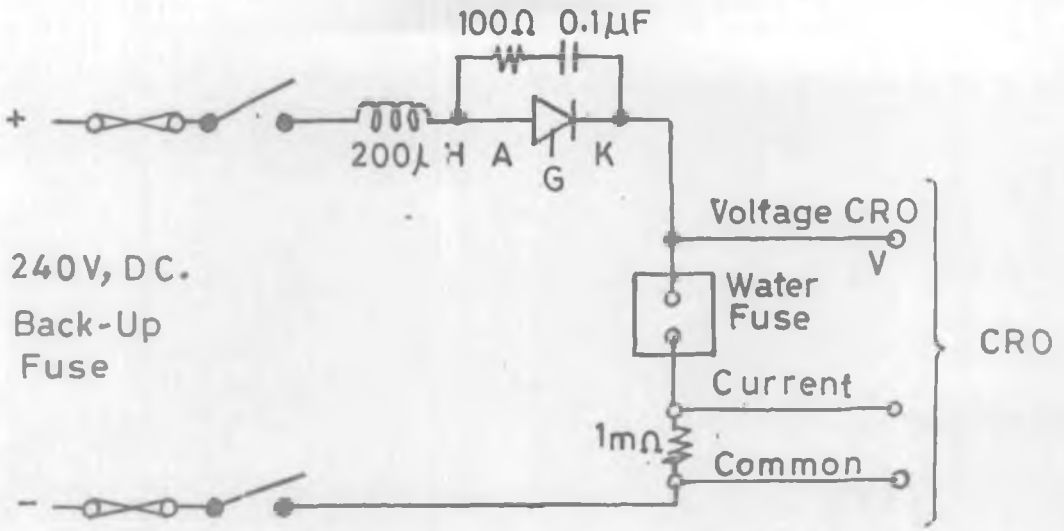

(a) SCR FIRING CIRCUIT

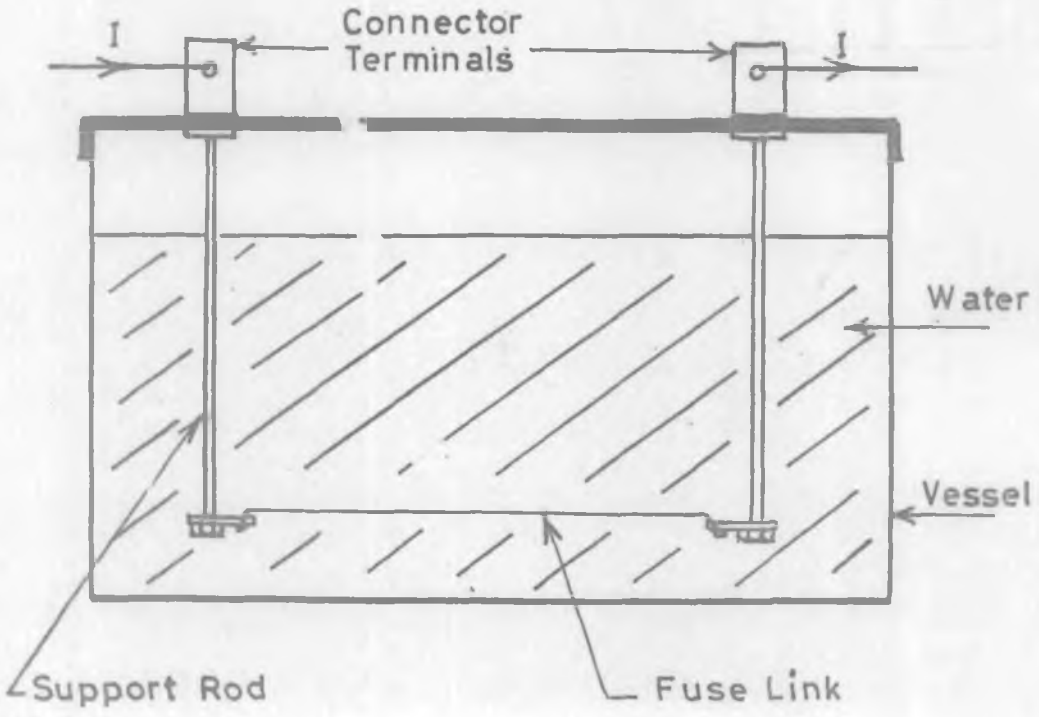

(b) WATER FUSE

FIG. 3.16. FUSE TEST ARRANGEMENT .

length of wire. The length l is taken as 2.5 cms. Figures 3.17 and 3.18 are the graphs plotted from which we can choose the approximate length of fuse wire for a particular SCR of known I^2t. Fine copper wire also give the reduced I^2t but large arc voltages. Therefore it has not been found suitable. Tests are also carried out with different firing angles for a.c. case. Arc voltage, peak current, I^2t and di/dt ratings are reduced as the firing angle is reduced from 90 degrees. Therefore the choice of fuse wire length from figure 3.17 will be safe for a.c. circuits. Stored waveforms of arc voltage and current for different length and materials are shown in figures 3.19, 3.20.

More details are still under investigation but beyond the scope of this thesis.

3.9 Summary and Conclusion

The results of digital simulation study of the last chapter has been verified by the experimental setup in the laboratory. The experimental results are in good agreement with the digital simulation study except that losses are included. Those results which overload the inverter has been omitted. Minimum cost filter has been designed for the simulated system and results of digital simulation obtained.

A three phase Mc Murray inverter has been designed

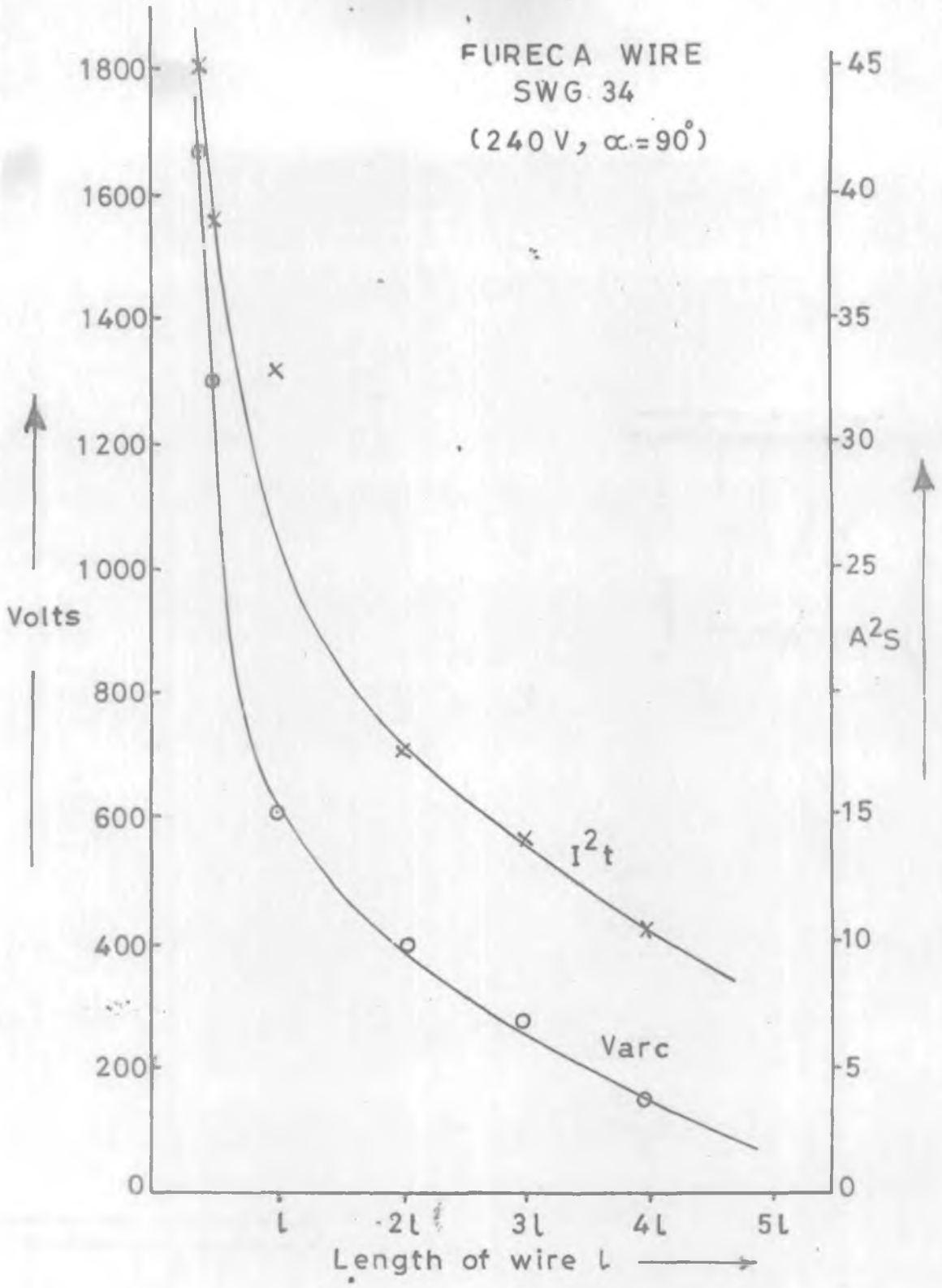

FIG. 3.17. VARIATION OF ARC VOLTAGE AND I^2t WITH LENGTH.

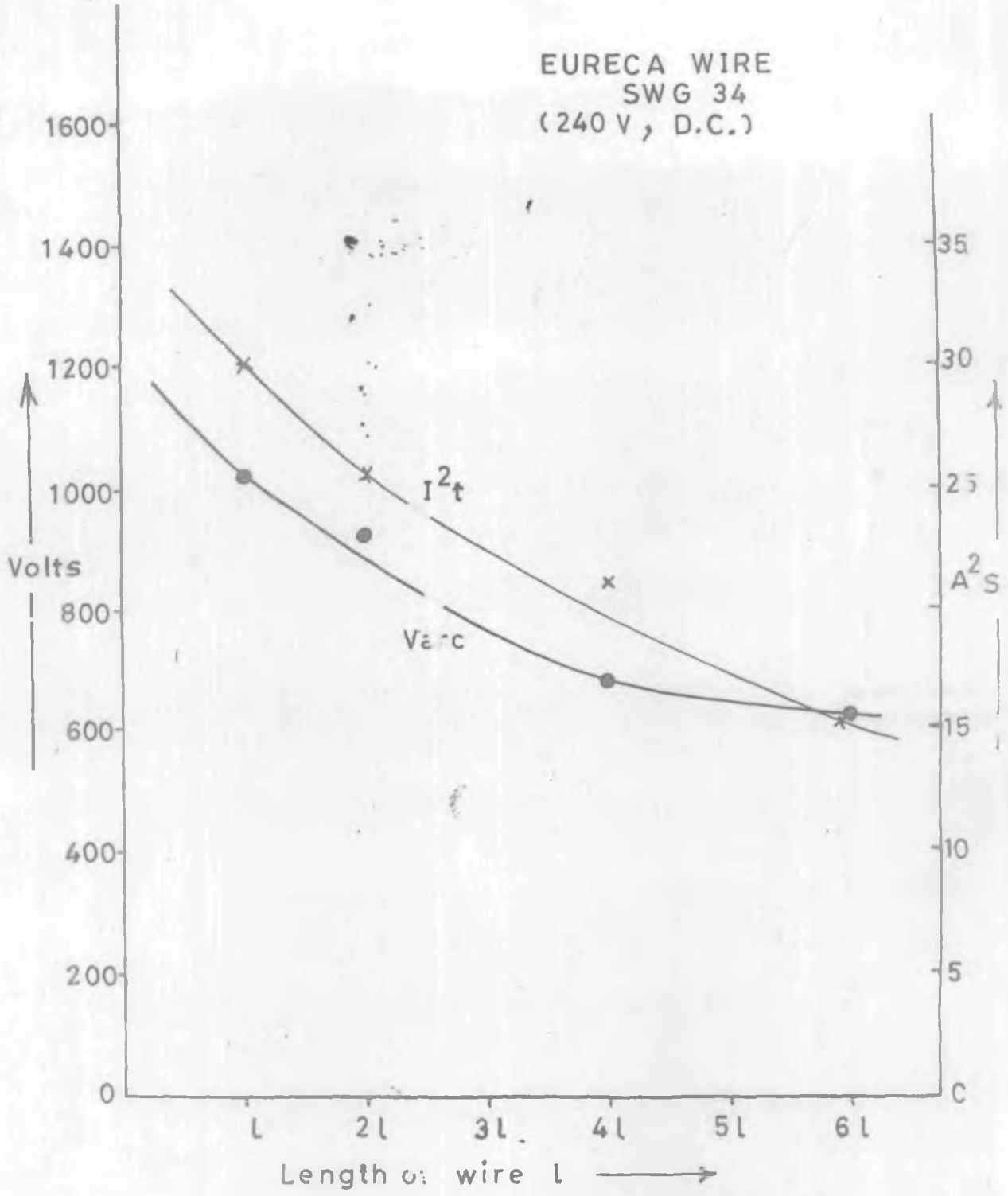

FIG. 3.18. VARIATION OF ARC VOLTAGE AND I^2t WITH LENGTH.

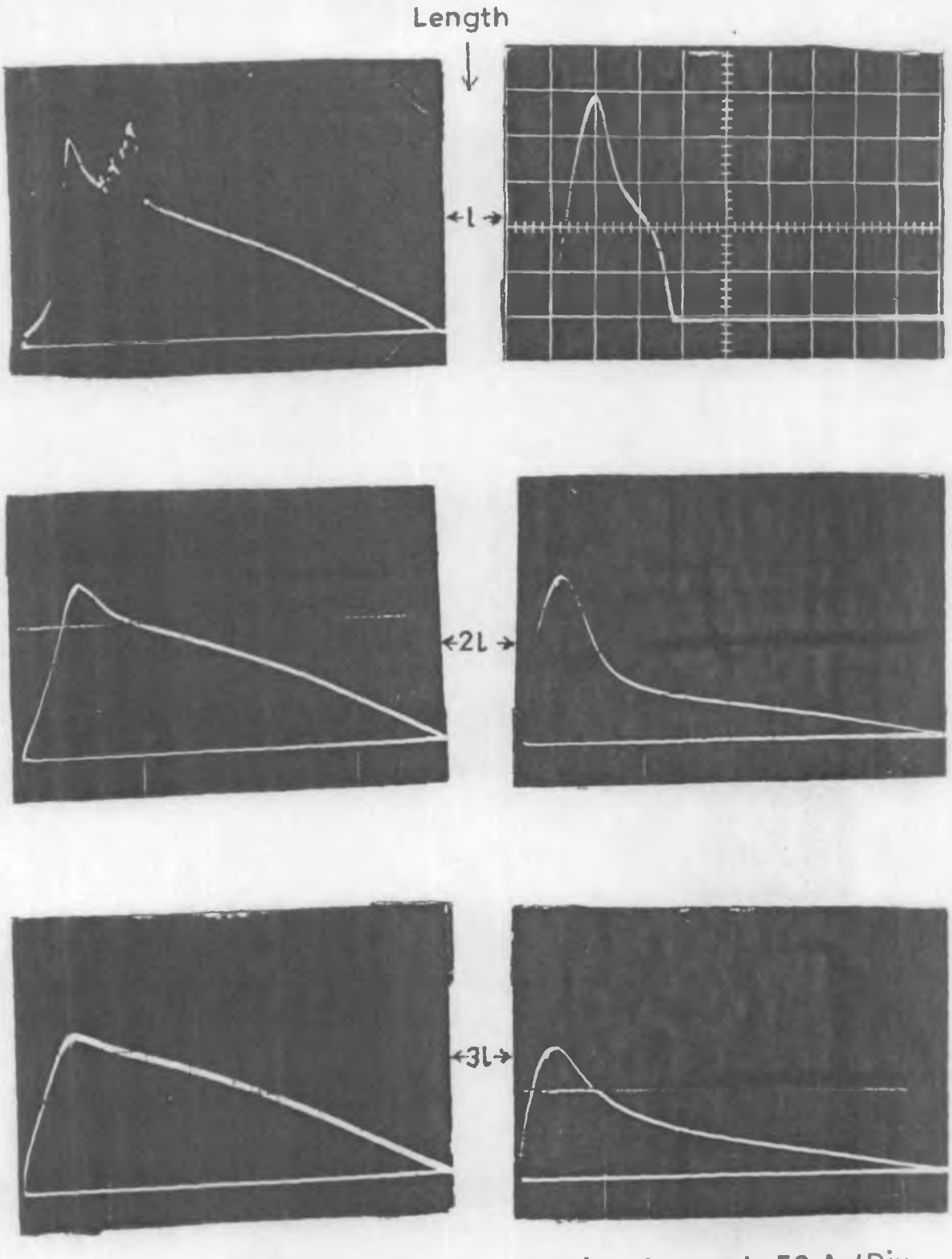

Arc voltage 100 V/Div. Fusing Current 50 A/Div.
Time base 0.5 ms/Div.

FIG. 3.19. STORED WAVEFORMS FOR EUREKA WIRE 34 SWG.

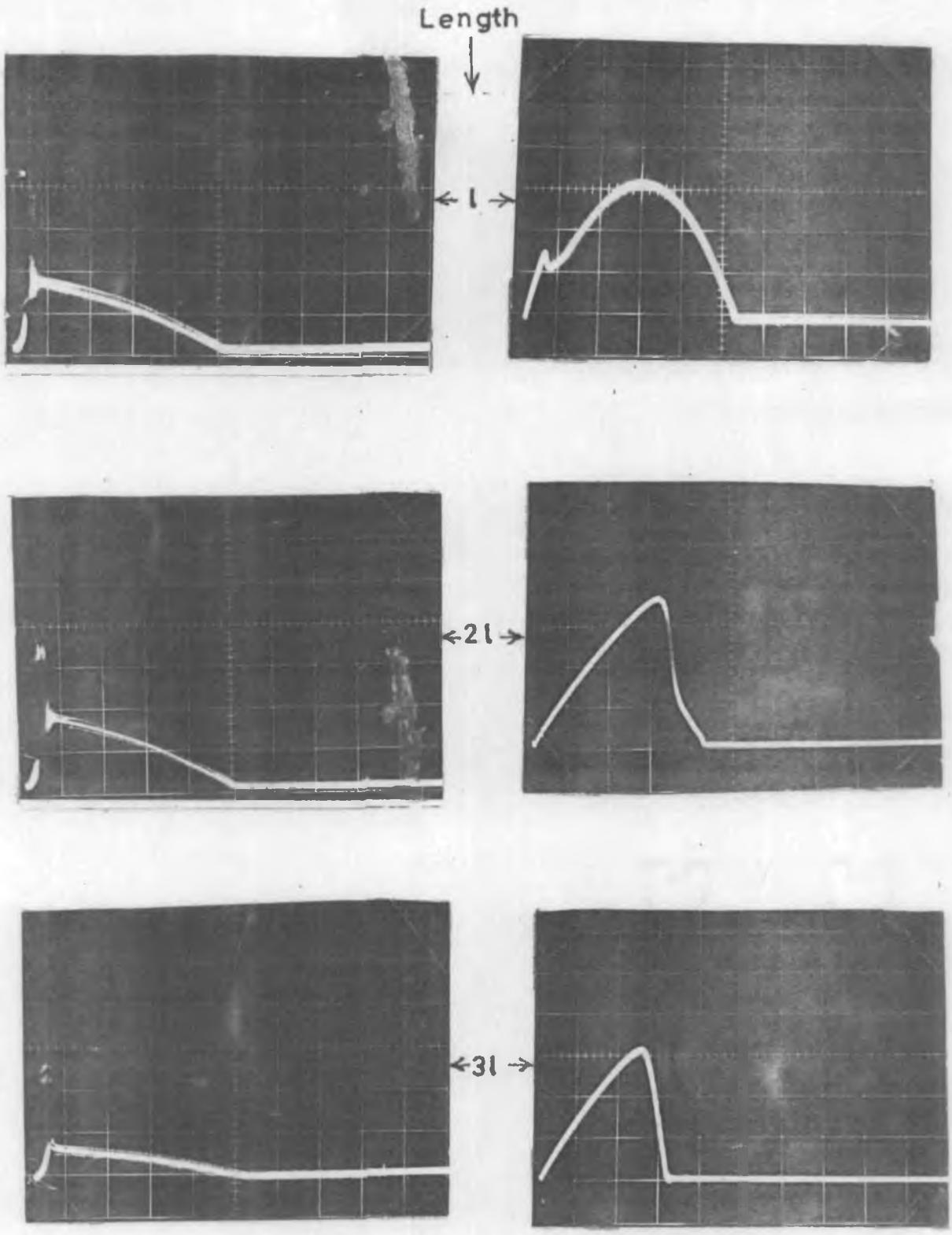

Arc voltage 200V/Div. Fusing Current 100 A/Div.
Time base 1 ms/Div.

FIG.3.20. STORED WAVEFORMS FOR COPPER WIRE 34 SWG.

to interconnect the 2 MW (thermal) generator in any mode of operation. Special attention has been given to commutating component design. Safe inverter operation is also discussed. Waterfuse tests has been conducted for an ordinary fuse wire to be used for the protection of thyristors.

CHAPTER 4 : FEED-BACK CONTROLLER DESIGN, FEBRICATION AND TESTING FOR MHD DUCT POWER CONTROL

4.1 Introduction

4.2 Description of the system

4.3 Digital simulation of the controller

4.4 Analogue simulation of the PI controller

4.5 Analogue simulation of the PID controller

4.6 Design of feedback controller

4.7 MHD duct power control

4.8 Discussion and comparison of the results

4.9 Summary and conclusion

CHAPTER 4

FEEDBACK CONTROLLER DESIGN, FABRICATION AND TESTING FOR MHD DUCT POWER CONTROL++

4.1 Introduction

An attempt has been made in this chapter to practically demonstrate the steady state and transient response of the simulated system described in Chapter 2.with a feedback controller. The experimental setup described in section 3.2 has been used to design the controller for the control of MHD duct power. The phase shifting transformer has been replaced in the experimental setup by the feedback controller.

Inorder to predict the behaviour of the chosen system the digital simulation of the feedback controller is done using 1st order controller in closed loop system. Because a closed loop system has the advantage of greater accuracy, improved dynamic response and reduced effects of disturbances. A proportional plus integral type of controller has been designed to achieve good dynamic and steady state responses and compensation is also provided to improve stability. First order estimates are made for stable operation of the controller. The time constants involved with the feedback loop are assumed

---

++ A major portion of publication number 2 is based on the theme of the material presented in this chapter.

small compared to that of controller. The mathematical model of the controller is obtained and then simulated on the digital computer. The approximate parameters of the controller are determined using step by step calculations as described in chapter 2. An analogue simulation has been done to evaluate exact parameters. With the exact parameters, the feedback controller is designed, fabricated and tested for the steady state and dynamic response of the system. The control logic has been designed with CMOS integrated circuits for low power consumption and high noise immunity.

4.2 Description of the system

The experimental setup chosen for automatic feedback control of MHD power to a.c. system is same as described in section 3.2. The block diagram of the control arrangement is shown in figure 4.1. The detailed diagram of the system is shown in figure B-1 of the appendix B. Model HM-3000 Hall-Pack multipliers are used as power transducer. The detailed specifications, circuit connections and characteristics are attached in table C-1 and figure C-2 in appendix C. The transfer function of this transducer is approximated as pure gain. Tests conducted have shown that this transducer has excellent performance under steady state but unreliable under transient conditions. Therefore a digital integrating type transducer [65] has been used for transient response. The transfer function of this transducer is approximated as

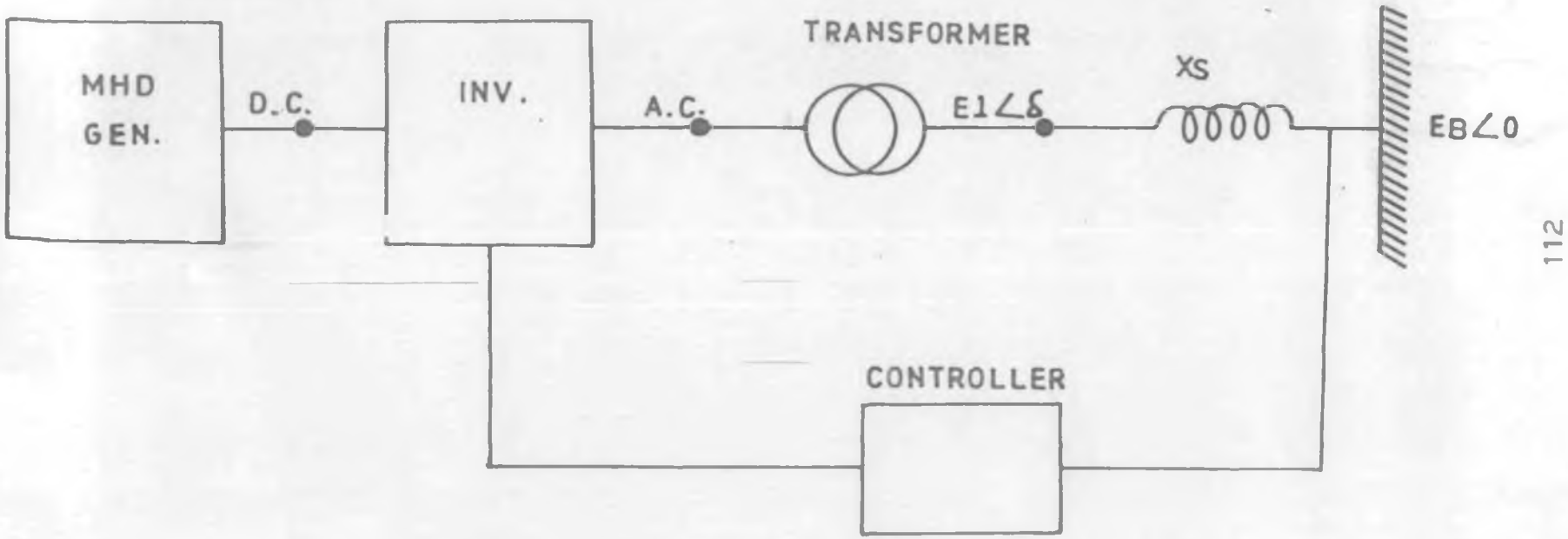

EIG. 4.1 BLOCK DIAGRAM OF MHD GENERATOR INVERTER LINK WITH FEED BACK CONTROLLER

$$G_p(s) = \frac{K_1}{(1 + T_1 s)} \qquad (4.1)$$

where

K_1 = Gain of transducer and realised as 10^{-3}

T_1 = Time constant of transducer and realised as 0.1 sec.

The controller compares the power flow to a.c. bus with set reference power and gives a voltage proportional to the difference power that controls the firing angle α. The transfer function of the PI controller is as under [66].

$$G_p(s) = \frac{dP}{d\delta} = K_2 (1 + T_c s)/ T_c s \qquad (4.2)$$

where

dP = change in power

$d\delta$ = a proportional change in phase shift

K_2 = gain of PI controller

T_c = Time constant of PI controller

The output of PI controller is given to firing circuit of the inverter whose transfer function is given as

$$G_F(s) = \frac{K_3}{1 + T_3 s} \qquad (4.3)$$

where

K_3 = gain of the firing circuit of SCR

T_3 = time constant of the firing circuit

The value of K_3 is realised as 0.131. Average gain of inverter firing circuit is calculated as 7.7 degrees/volt from the swing of PI controller as shown in figure C-5 in appendix C. The time constant T_3 is taken as 3.3 ms using transportation time delay model [67]. The inverter control system analysis has been subject of many studies [68,69,70] but at present none of the thyristor models are considered for theoretical analysis of the system because the exact parameters of the simulated system may be quite different from that of actual system. Therefore an analogue simulation has been carried out for the determination of steady state and transient response of the system.

4.3 Digital simulation of the controller

The usual procedure for simulating the controller on the digital computer is to obtain mathematical model of the controller and then to write the program for simulating this model. For such simulation program, the behaviour of the control system under normal and abnormal operating conditions must be known in advance to enable writing mathematical equations. The assumptions and approximations necessary to translate the actual system characteristics into the mathematical form always introduce inaccuracy. Since the approximate parameters of the controllers are determined with digital simulation, therefore, the unforseen conditions like harmonics

in the supply voltage, unbalance in the system etc. are left in mathematical formulation.

The proportional controller gives appreciable steady state error and an integral controller gives zero steady state error but adds a phase shift to the system and this decreases the stability. To overcome the above problems a PI controller is used which adjusts gain and phase both. For the present study the PI controller and analogue firing circuit is used. The mathematical model of the transfer function is written from equation 4.2 as

$$d\delta = (K_2 + 1/T_c)\, dP \qquad (4.4)$$

where the terms used are already defined earlier. In practice the control circuit is provided with compensation such that the transfer function has an extra term as

$$(1 + T_a s)/(1 - T_b s)$$

However, since the function of compensation circuit is to improve the stability limit of the control loop and the aim of the present analysis is to mapout the onset of instabilities for the worst possible case, the compensation term is ignored for the present analysis.

4.3.1 Computational procedure

Computation is carried out on the digital computer with the approximate analysis of the control system under consideration using an iterative solution [71]. The operating point is same as discussed in section 2.2. For the transient analysis, the step change in duct voltage and resistance is made from operating point. A computer programme has been developed for the calculation of dynamic response of the controller as described by equation 4.4. This programme neglects the resistances in the system and time constants involved in the firing circuit and power transducer. Generally the controller time constant is appreciably larger than the dead time involved in cascade loop. Therefore the effect of transducer and firing circuit dynamics is neglected for the initial design of feedback controller. Figure 4.2 shows the flow chart for the calculation of transient response of the system.

4.3.2 Transient response of the simulated system

The approximate value of the proportional and integral gain is determined following the iterative procedure [71]. First operating point is defined and reference power is chosen. Time step for calculations and controller gain are selected. A step change in operating voltage is made by switching the charged batteries. The power variation with time due to step

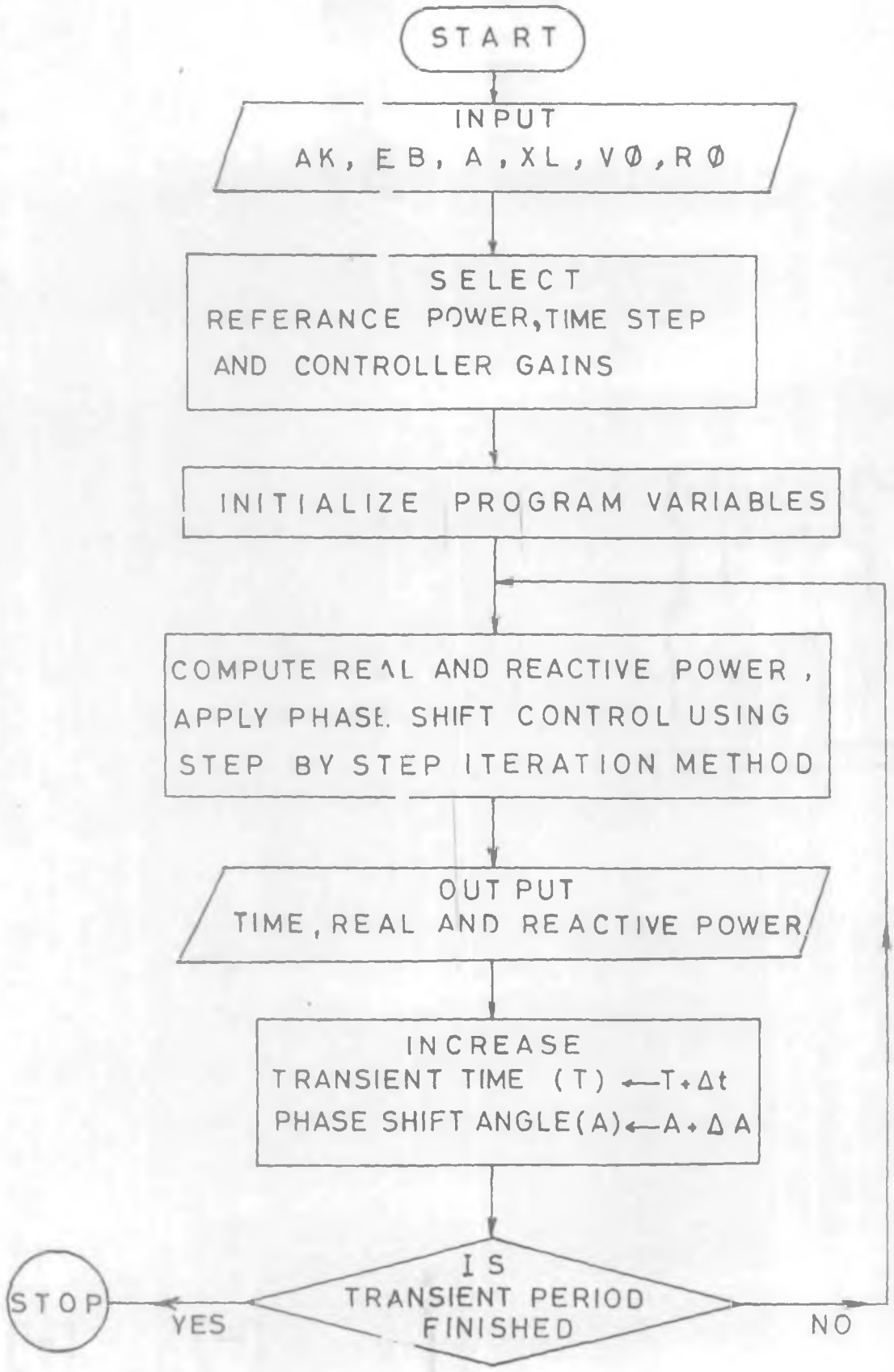

FIG. 4.2. FLOW CHART OF TRASIENT RESPONSE OF CONTROLLER

increase and decrease in operating voltage is shown in figure 4.3(a). The transients are oscillatory and continue for longer time for selected gains. Now the proportional gain is kept constant and the integral gain is varied as shown in figure 4.4(a). The overshoot and settling time both reduce and setting time is approximately calculated as 0.5 second.

Similarly the transient response due to setp change in resistance is calculated and the power variation for step decrease in resistance is plotted in figure 4.3(b). The proportional and integral gains were varied and the best response was calculated and potted as shown in figure 4.4(b). The transients due to voltage variation is more pronounced compared to resistance variation. This is obvious and can be realised from equation (2.29) of section 2.3.3.

4.4 Analogue simulation of PI controller

An important application of analogue computer is the simulation of control systems by employing computing modules, namely integrators, summers and potentiometers. The greatest asset of an analogue computer is that when setup, it resembles closely the system studied, a one to one correspondance between the variables of the physical problem and the analogue computer setup may be ensured with fast operation. The analogue computer works in real time and accepts continuous waveforms as

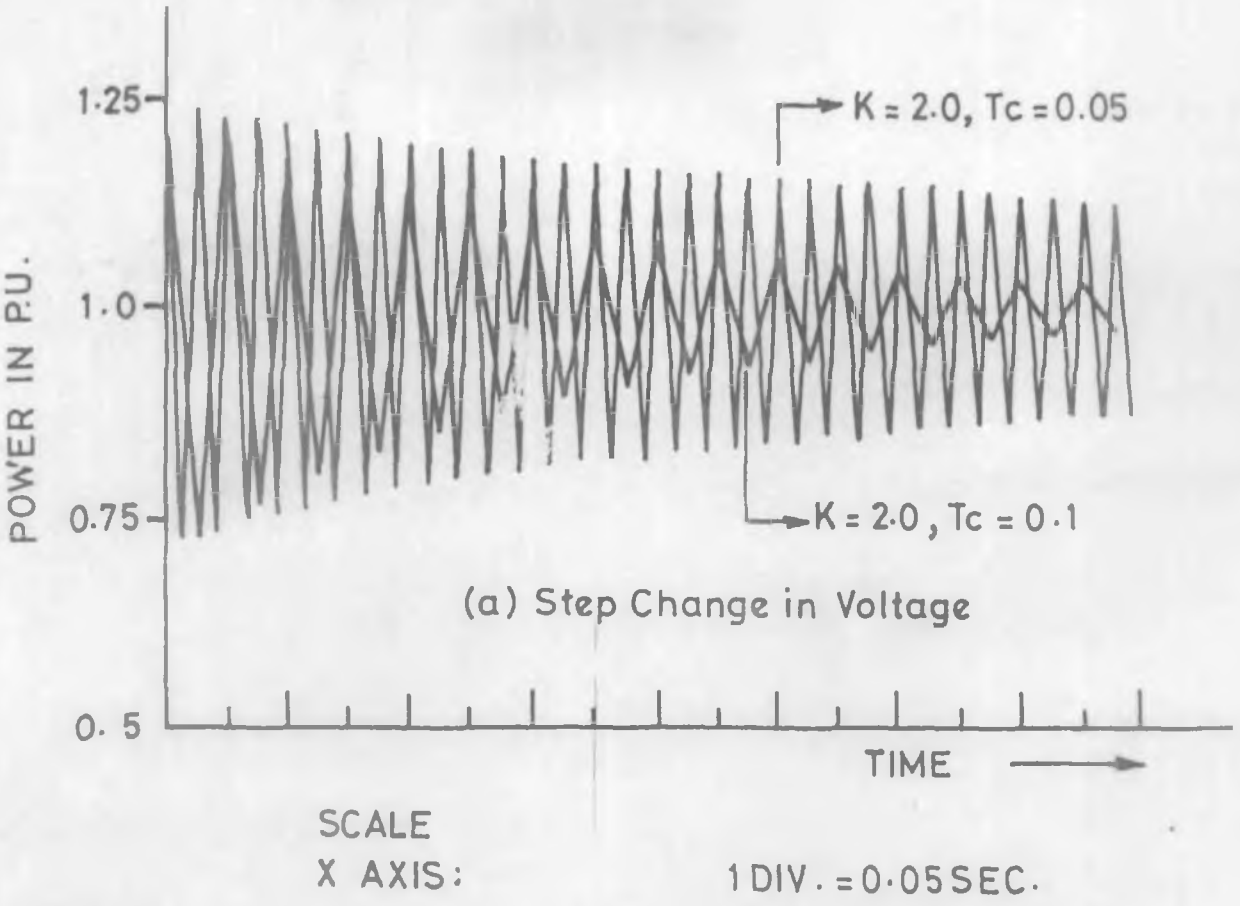

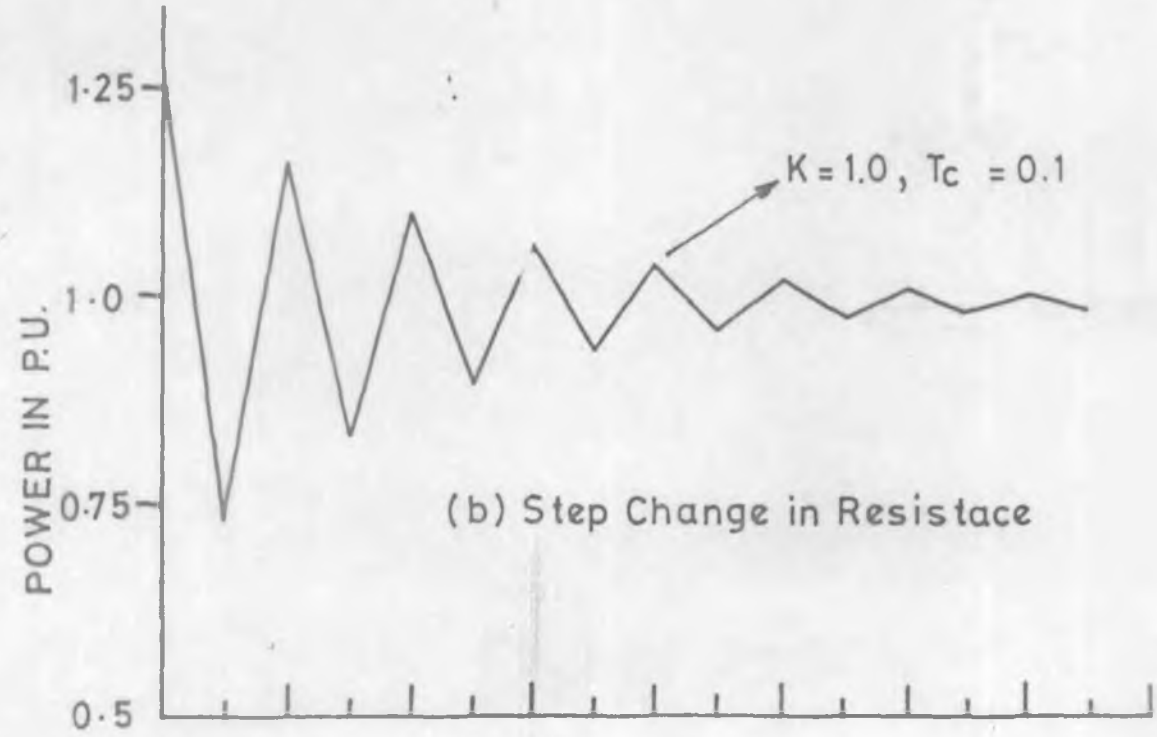

FIG. 4.3 TRANSIENT RESPONSE OF SIMULATED FEED BACK CONTROLLER.

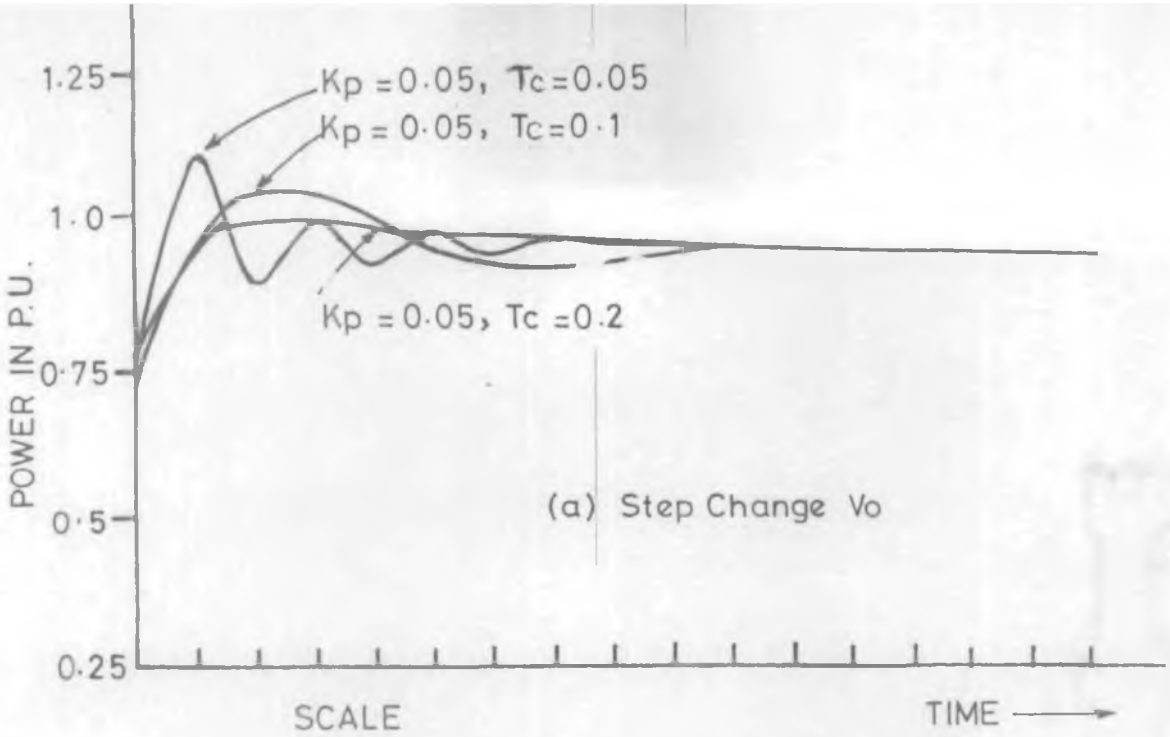

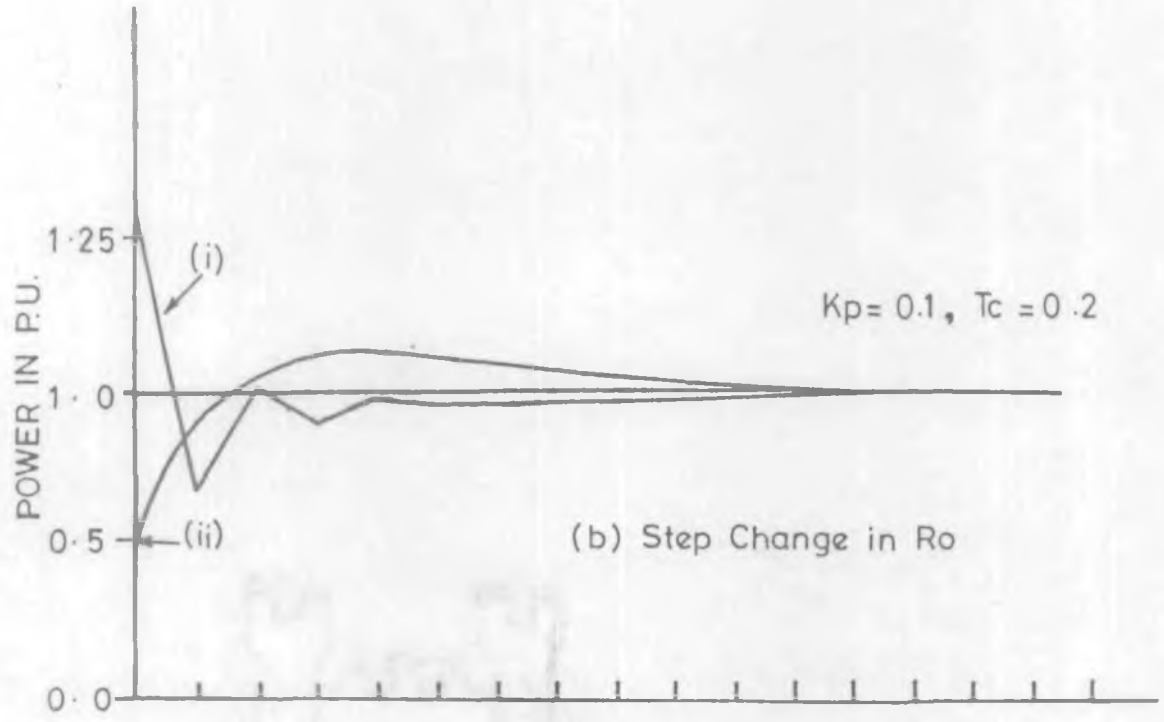

FIG. 4.4 TRANSIENT RESPONSE OF SIMULATED FEEDBACK CONTROLLER.

inputs. Thus use of analogue computers as compensators or controllers in feedback system is easily implemented. Therefore the PI controller is simulated on analogue computer type YEW 3316-11 and 3316-21 and YEW 3318-11 and 3318-21 series. Figure 4.5 shows the analogue computer simulation of PI controller. The power transducer described earlier gives a proportional voltage for the power flow to infinite bus from MHD duct. This is compared to a reference power available from preset potentiometer after necessary amplification. The error signal is fed to controller and gains are adjusted to get stable operation of the system for step change in duct resistance and voltage. The symbolic representation and use of above analogue computer components are shown in figures C-3 and C-4 in appendix C.

4.4.1 Transient response of the system with PI controller

The approximate values of the controller gains are already calculated from the digital simulation described in section 4.3. The power variation with time due to step increase and decrease in voltage is recorded on X-Y recorder for open loop system. The potentiometers are varied till best response is obtained. Figure 4.6(b) shows the open loop response to a step change in duct voltage. The best results are obtained for proportional gain (K_p) =10 and integral gain (K_I) = 10. Figure 4.6(a) shows similar response for step

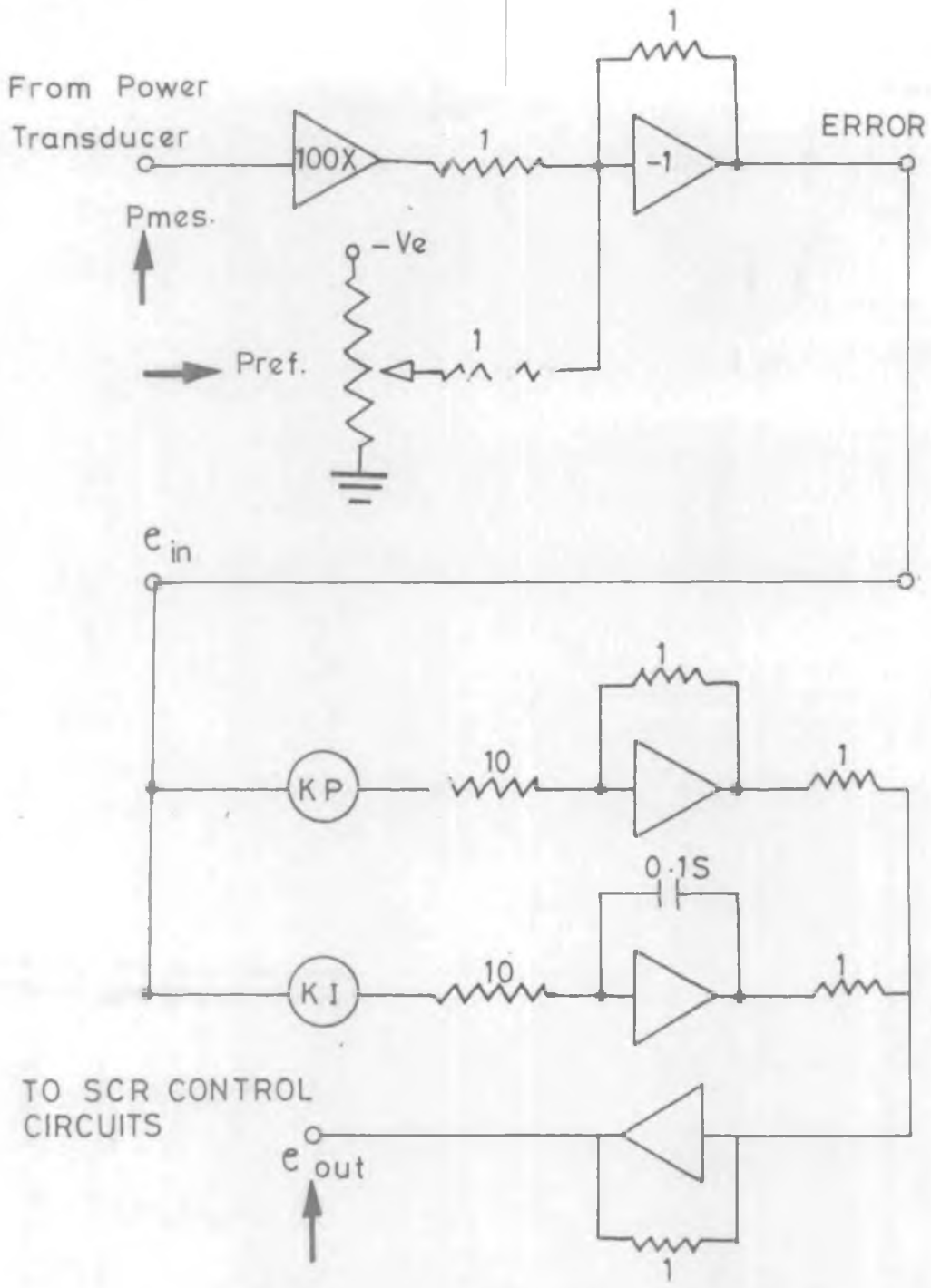

FIG. 4.5 ANALOGUE COMPUTER SIMULATION OF THE P I CONTROLLER.

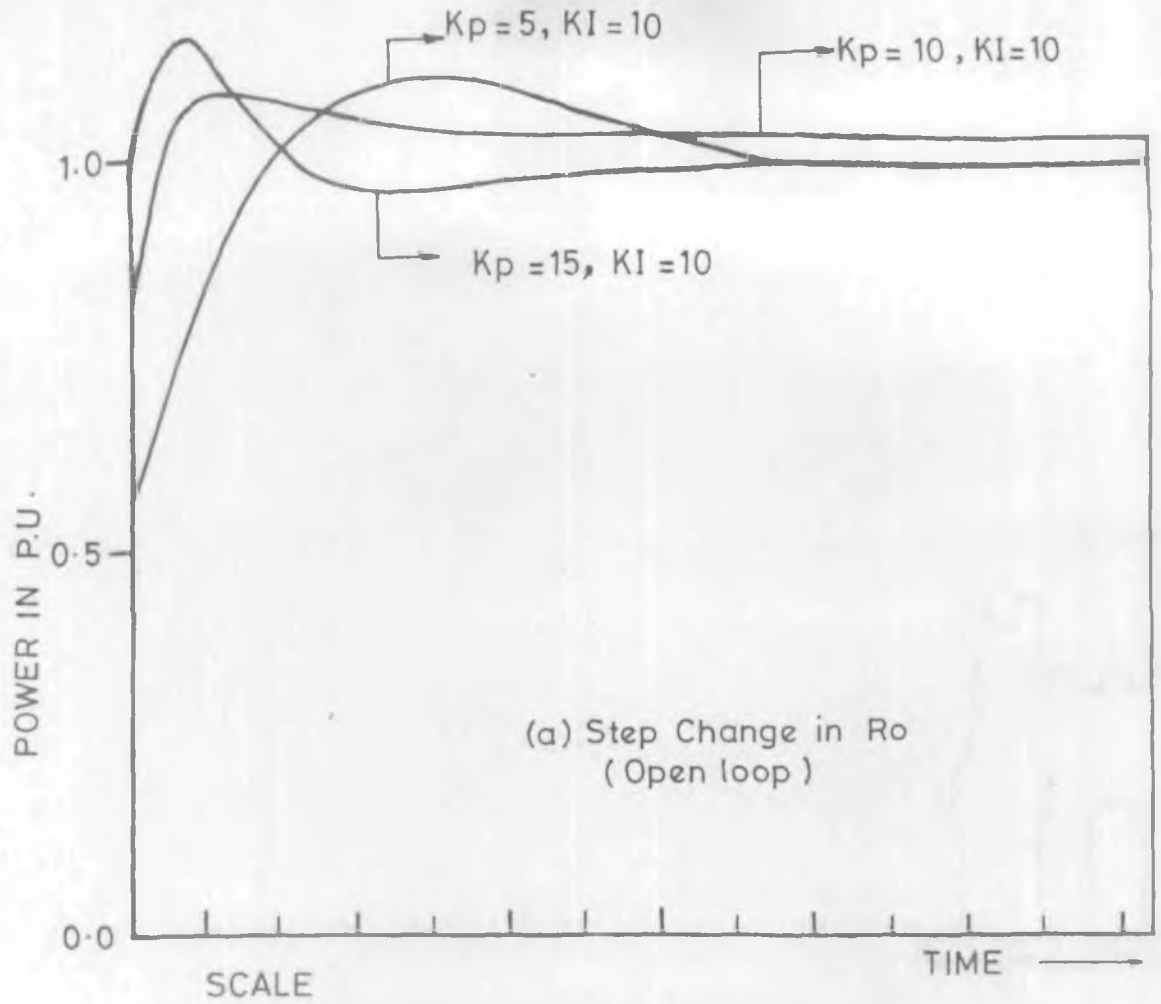

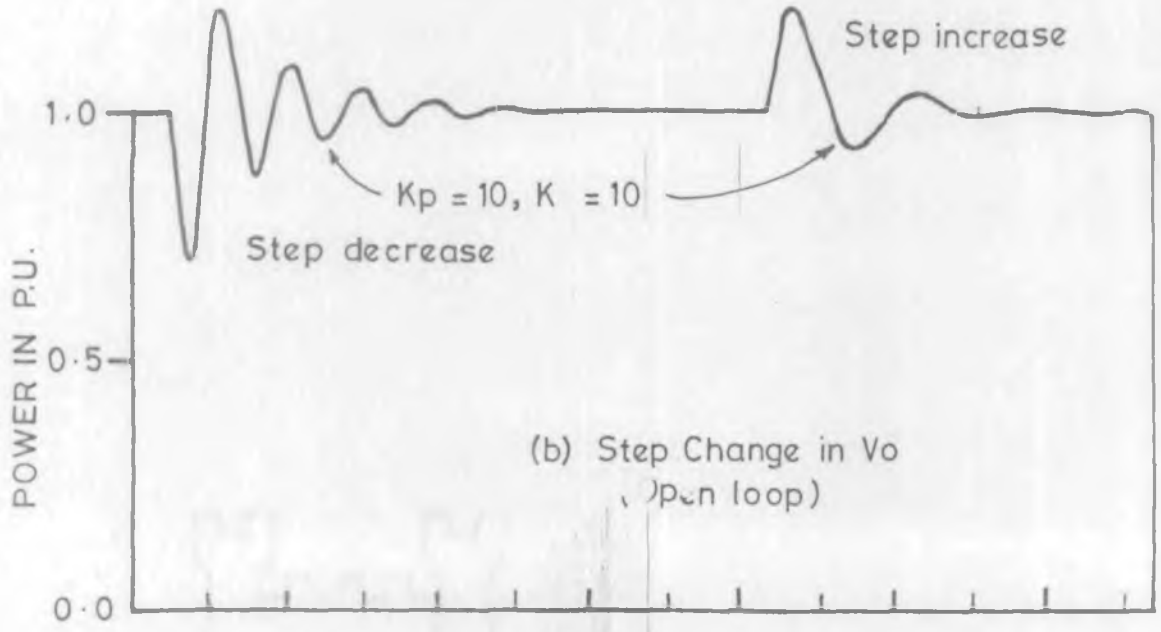

FIG. 4.6 TRANSIET RESPONSE OF ANALOGUE SIMULATION OF PI CONTROLLER.

change in resistance for different settings of K_p and K_I.

A closed loop system generally has the advantage of greater accuracy, improved transient response and reduced effects of disturbances. Therefore closed loop operation is preferred. Figure 4.7 is a plot for power versus time variation due to step change in resistance and voltage of the MHD duct in closed loop system. The best response is recorded for Kp = 7.5 and K_I = 8.9 in closed loop operation.

4.5 Analogue simulation of PID controller

The performance of a control system is measured by its stability, accuracy and speed of response. In general these items are specified when a system is being designed to satisfy a specific task. Quite often the simultaneous satisfaction of all these requirements cannot be achieved by using the basic eliments in the control system. The desired transient response as well as steady state behaviour of a system may be obtained by introducing the compensatory eliments into the control system. These compensatory eliments are designed so that they help achieve system performance i.e. bandwidth, phase margin, peak overshoot, steady state error etc. without modifying the entire system in a major way. Therefore a compensation is provided to the analogue simulation of figure 4.5. Figure 4.8 shows analogue simulation with compensation. The gains K_p, K_I and K_d are changed to get the best performance

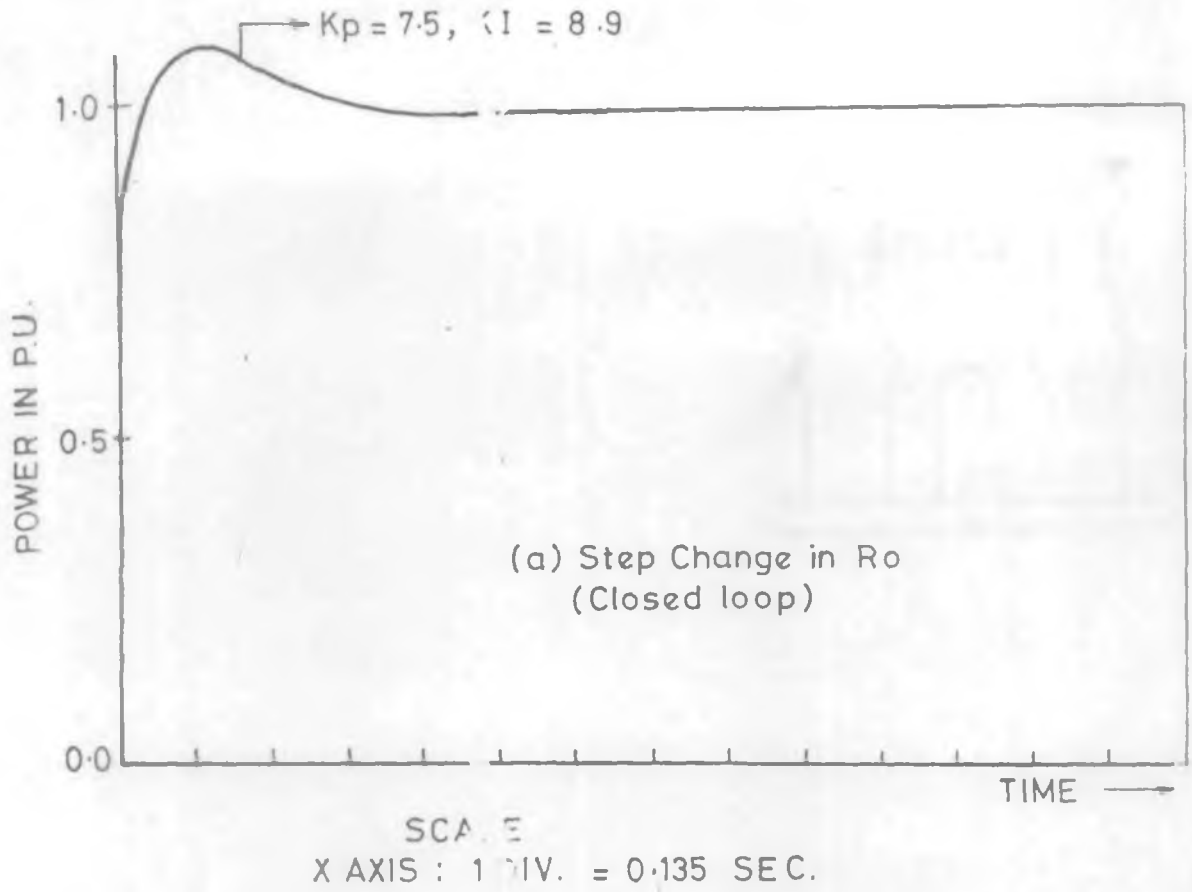

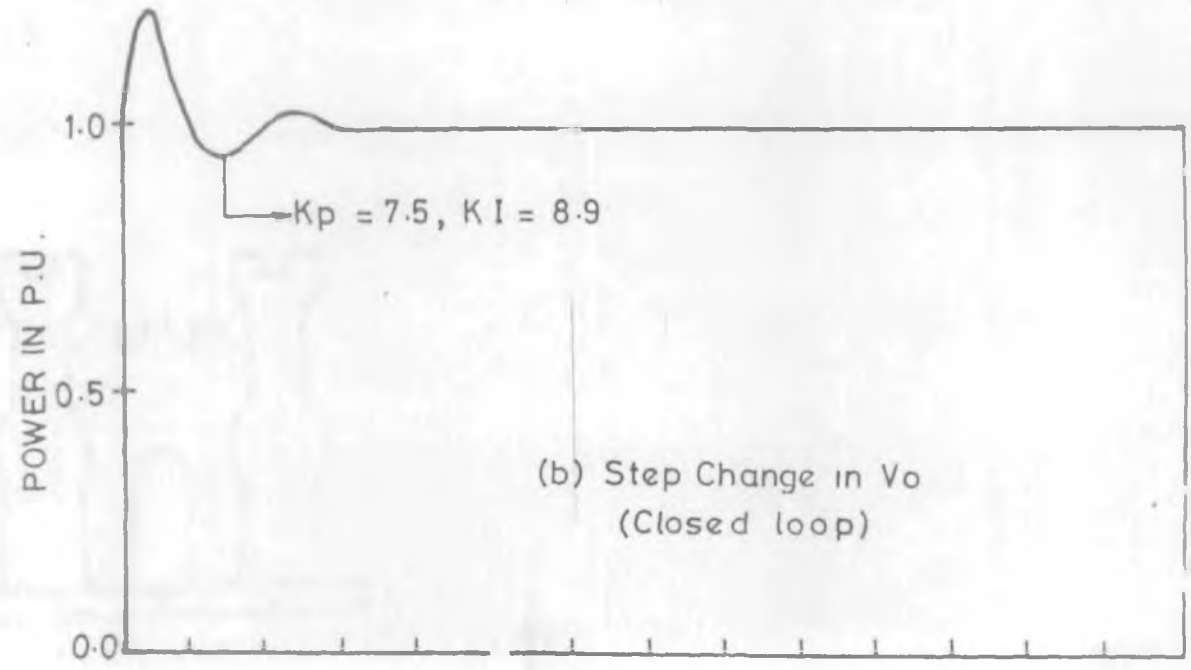

FIG. 4·7 TRANSIENT RESPONSE OF ANALOGUE SIMULATION OF PI CONTROLLER.

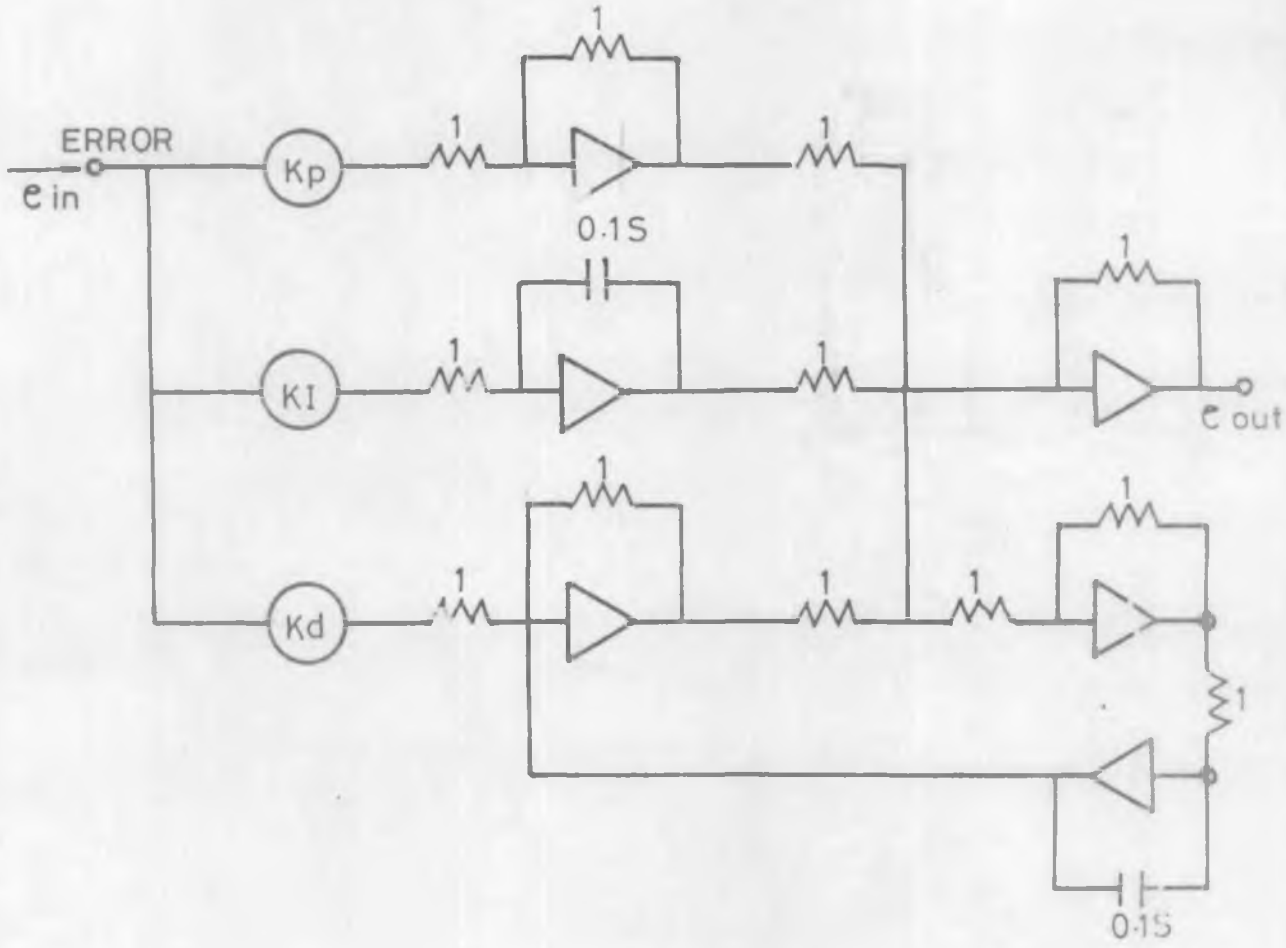

FIG. 4·8 ANALOGUE COMPUTER SIMULATION OF THE PID CONTROLLER

of the controller for step change in duct voltage and resistance.

4.5.1 Transient response of the system with PID controller

The controller gains determined in section 4.4.1 are set on potentiometer and a derivative gain is also added. The power variation with time due to step change in resistance and voltage is recorded. Figure 4.9 shows the power variation due to step change in voltage with and without compensation. It can be seen from above figure that with compensation the system response improves and time taken for the transients to die down is approximately half than that in the uncompensated case.

4.6 Design and fabrication of feedback controller

The analogue simulation of the controller in last section determines the gains for the best performance of the controller and possible swing of the controller. These two parameters are used to design the controller. For chosen operating point as discussed earlier, the reference power gives a proportional voltage of 6 volts after amplification. This voltage is taken as reference power. The swing of the PI controller is determined from this reference for 25 percent change in voltage and resistance of the duct as shown in figure C-5 in appendix C. The fixed time delay is adjusted

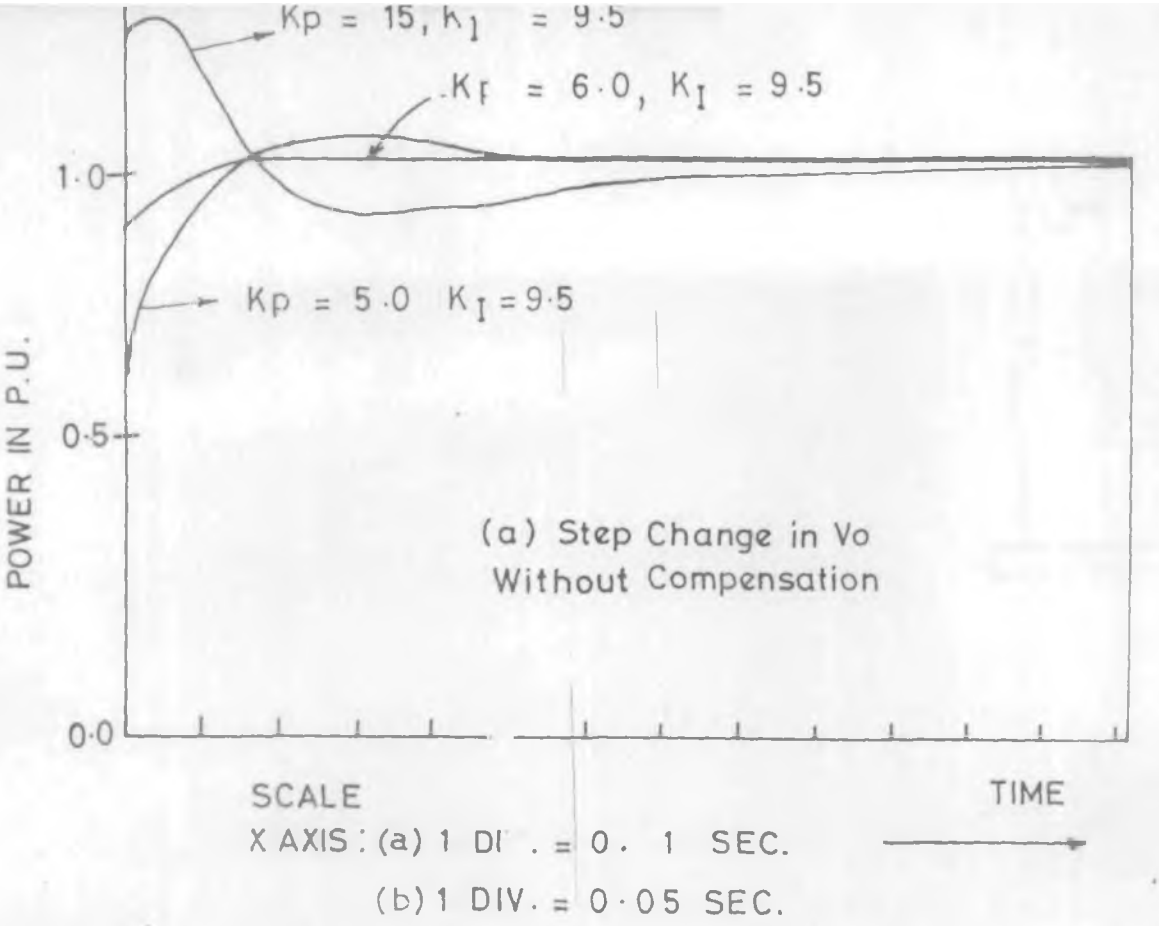

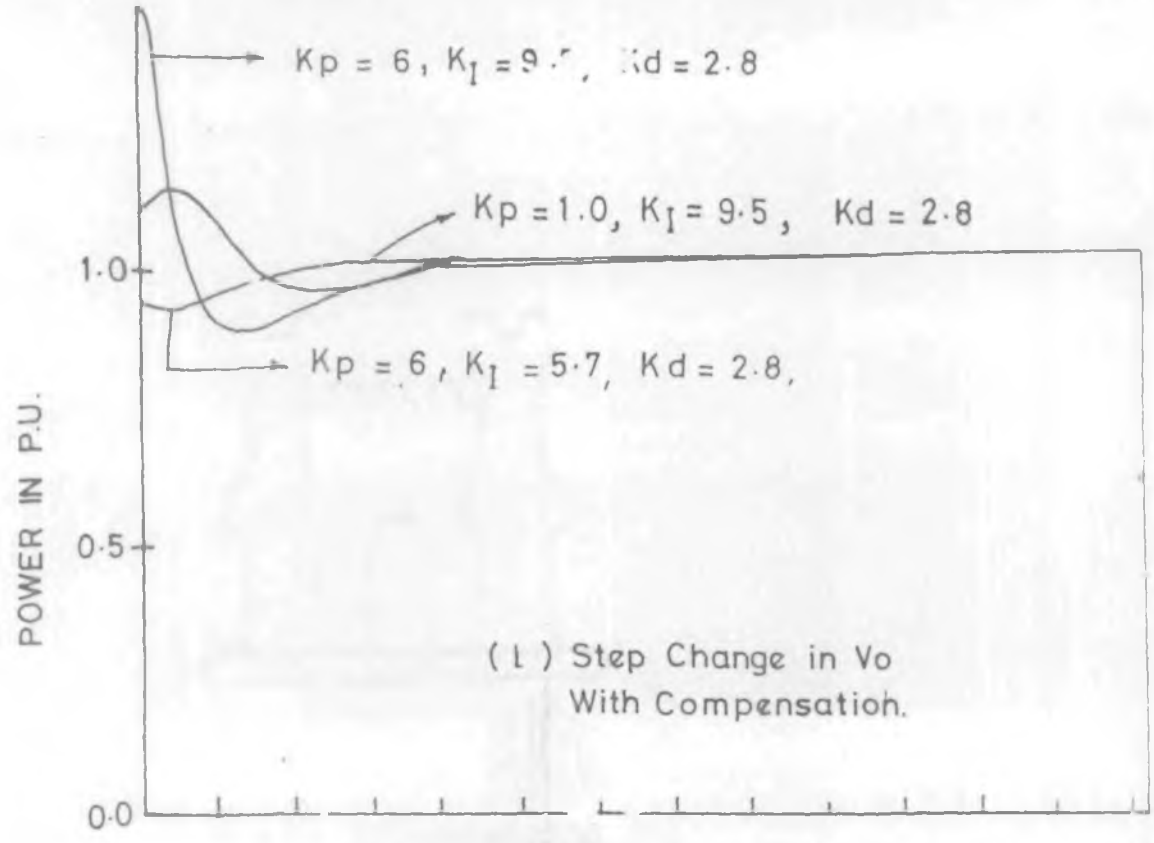

FIG. 4.9 TRANSIENT RESPONSE OF ANALOGE SIMULATION OF PID CONTROLLER

from the timing components of the dual monostable and variable time delay is adjusted so that the zero feedback gives a fixed time delay as 3 ms. The pulse to the input of the dual monostable is obtained from phase A,B and C with a 240/9.5 v volts transformer through a squaring and waveshaping circuit. The control logic uses dual pack type 747 C operational amplifier, dual pack MM 74C221 monostable and CD4013B type dual 'D' type flip-flop. The detailed specification of these devices are given in figures C-6 to C-11 in appendix C. The designed feedback controller is fabricated as shown in Figure 4.10.

4.6.1 Transient response of the system with fabricated feedback controller

The analogue controller is replaced by the above fabricated controller. The step changes in resistance and voltage are made as already discussed in section 4.4.1. The response is stored on a multichannel oscilloscope and photographed for the best performance of the controller with and without compensation. Figure 4.11 shows the oscillograms for transient, response of the controller with step change in R_o. Following cases are considered for stable operation of the controller.

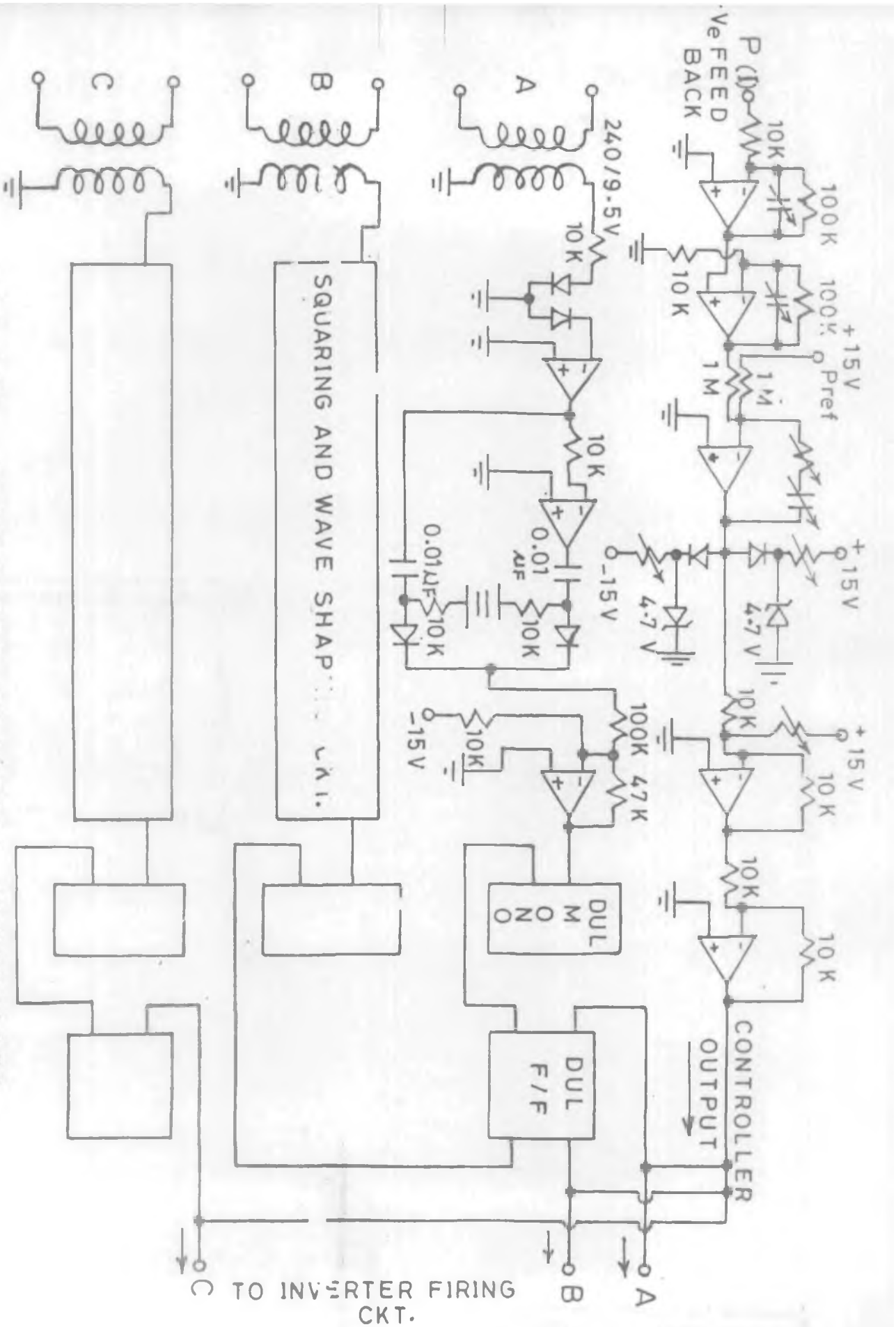

FIG. 4.10. FABRICATED FEEDBACK CONTROLLER.

Figure 4.11(a) Without compensation

(i) $K_p = 1.2$ and $K_I = 10$

(ii) $K_p = 2.4$ and $K_I = 10$

(iii) $K_p = 4.0$ and $K_I = 10$

Figure 4.11(b) With compensation

(i) $K_p = 10$, $K_I = 8.3$ and $K_d = 5.7$

(ii) $K_p = 10$, $K_I = 8.0$ and $K_d = 5.7$

(iii) $K_p = 10$, $K_I = 6.0$ and $K_d = 2.7$

Figure 4.12 shows the oscillograms for transient response of the controller with step change in V_o. Following cases are considered for stable operation of the controller.

Figure 4.12(a) Without compensation

(i) $K_p = 1.0$ and $K_I = 9.5$

(ii) $K_p = 5.0$ and $K_I = 9.5$

(iii) $K_p = 6.0$ and $K_I = 9.5$

Figure 4.12(b) With compensation

(i) $K_p = 1.0$, $K_I = 9.5$ and $K_d = 2.8$

(ii) $K_p = 5.0$, $K_I = 9.5$ and $K_d = 2.8$

(iii) $K_p = 6.0$, $K_I = 9.5$ and $K_d = 5.7$

Using these results, the control system performance was examined

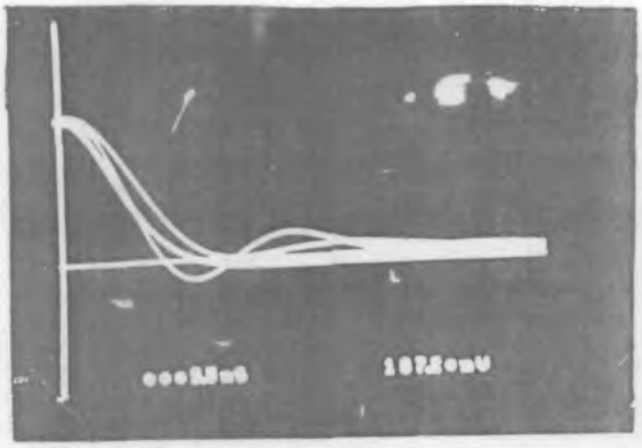

Scale:
X-Axis:~ 0·2 Sec/cm.
Y-Axis:~10 mV/cm.

(a) WITHOUT COMPENSATION

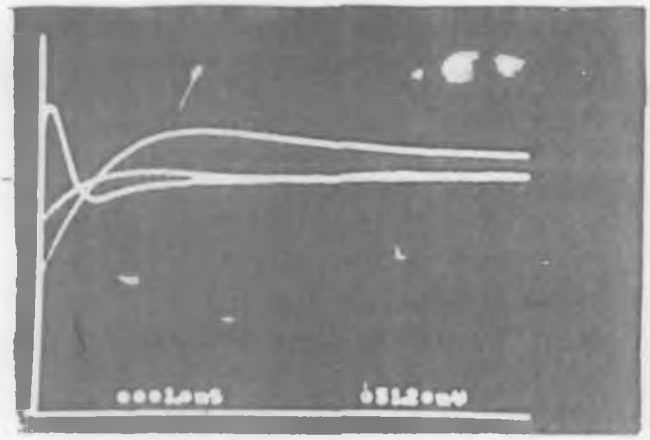

Scale:
X-Axis:~ 0.1 Sec/cm.
Y-Axis:~ 20 mV/cm.

(b) WITH COMPENSATION

FIG. 4.11. TRANSIENT RESPONSE OF CONTROLLER WITH STEP CHANGE IN R_o.

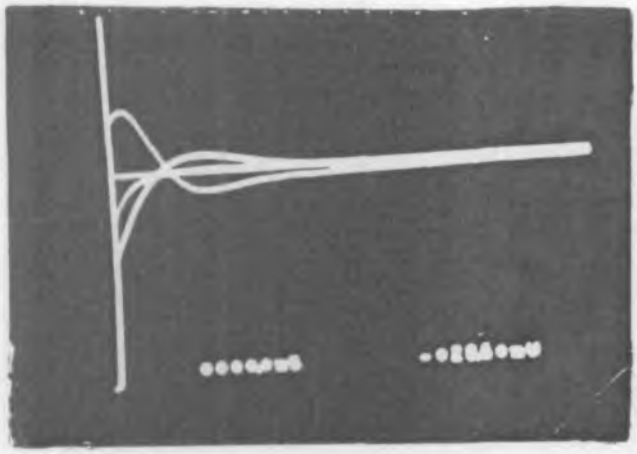

Scale:
X-Axis:~0.2 Sec/cm.
Y-Axis:~10 mV/cm.

(a) WITHOUT COMPENSATION

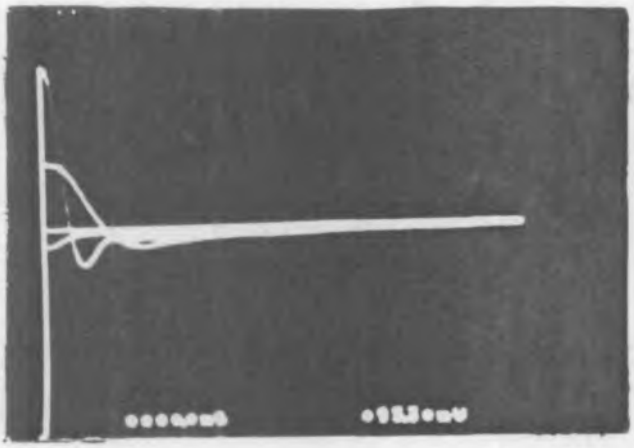

Scale:
X-Axis:~0.1 Sec/cm.
Y-Axis:~10 mV/cm.

(b) WITH COMPENSATION

FIG.4.12. TRANSIENT RESPONSE OF CONTROLLER WITH STEP CHANGE IN V_o.

for various combinations of K_p, K_I and K_d. The best performance was obtained with

$$K_p = 1.0,\ K_I = 9.5 \text{ and } K_d = 2.8$$

The feedback controller was finally designed and fabricated as photographed in figure 4.15.

4.7 MHD duct power control

The quasistatic changes in fluid-dynamic conditions ($M \neq N \neq 1$) has been discussed in section 2.2.2. In this section, the changes in resistance and voltage of the simulated duct are made for the automatic power control. The variation in resistance is made as discussed in section 3.3.3 for duct voltage of 2 PU. The variation in voltage is made as discussed in section 3.3.4 for 30 degrees phase shift for the safe inverter operation.

4.7.1 Power control for changes in internal resistance

The variation of resistance is considered from operating point as shown in figure 4.13. The negative sign signifies the reduction in resistance from operating point. The variation of power is shown in the above figure with and without phase shift control. Reference power is maintained for reduction in resistance but the system becomes unstable beyond an increase of 25 percent in resistance. The reactive

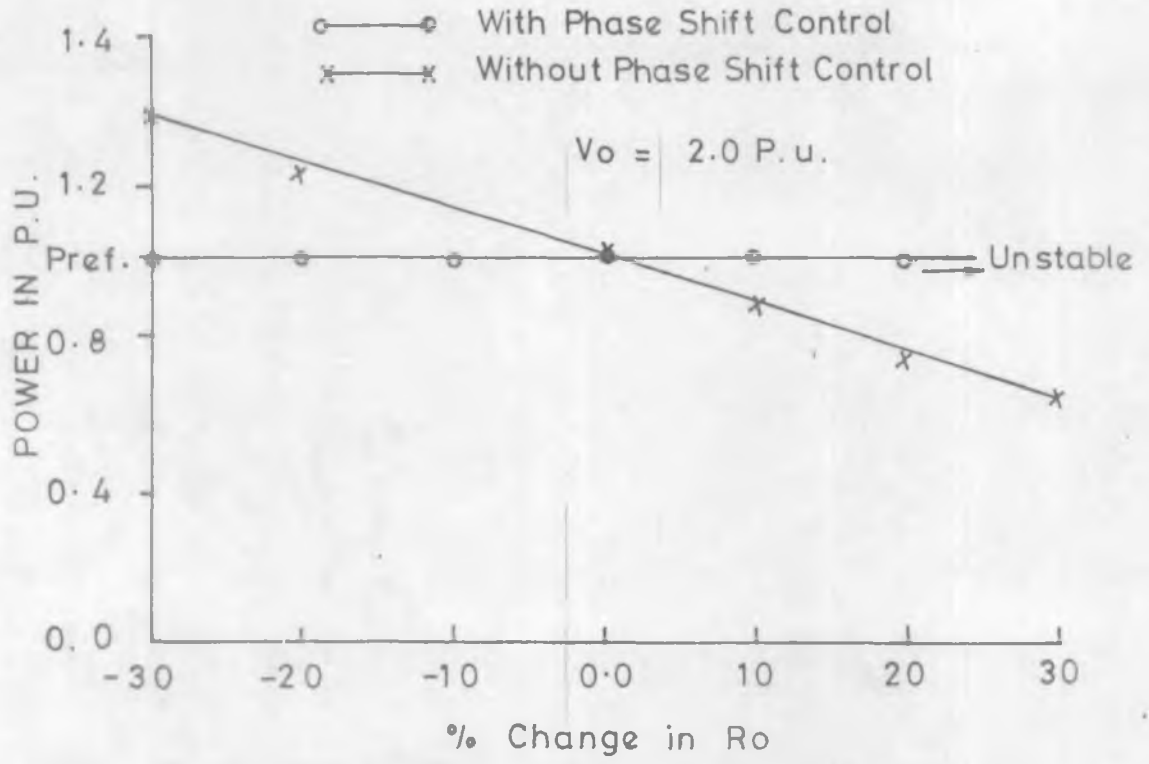

FIG. 4.13 VARIATION OF REAL POWER WITH Ro

power remains within the limit so that the desired power factor is maintained. The changes in resistance are made in steps as described in section 3.3.5.

4.7.2 Power control for changes in duct voltage

Variation in duct voltage is considered in this section for rated value of internal resistance. The negative sign signifies reduction in duct voltage. Figure 4.14 shows the variation of real power with and without phase shift control. The graph shows that the system becomes unstable for reduction in voltage beyond approximately 25 percent. The variation in voltage is made as described in section 3.3.2. The reactive power does not vary much and remains within the desired limit as discussed in section 2.6.6.

4.8 Discussion and comparison of the results

The feedback controller described in section 4.2 is used for automatic control of power for the simulated MHD duct. The controller for 2 MW (thermal) MHD test facility may be designed from the experience gained in this chapter. The digital simulation of the controller gives approximate parameters because of simplified analysis. However, higher order mathematical modelling can be made to account for the other time constants involved with the control loop. In this chapter the analogue simulation has been used to determine the

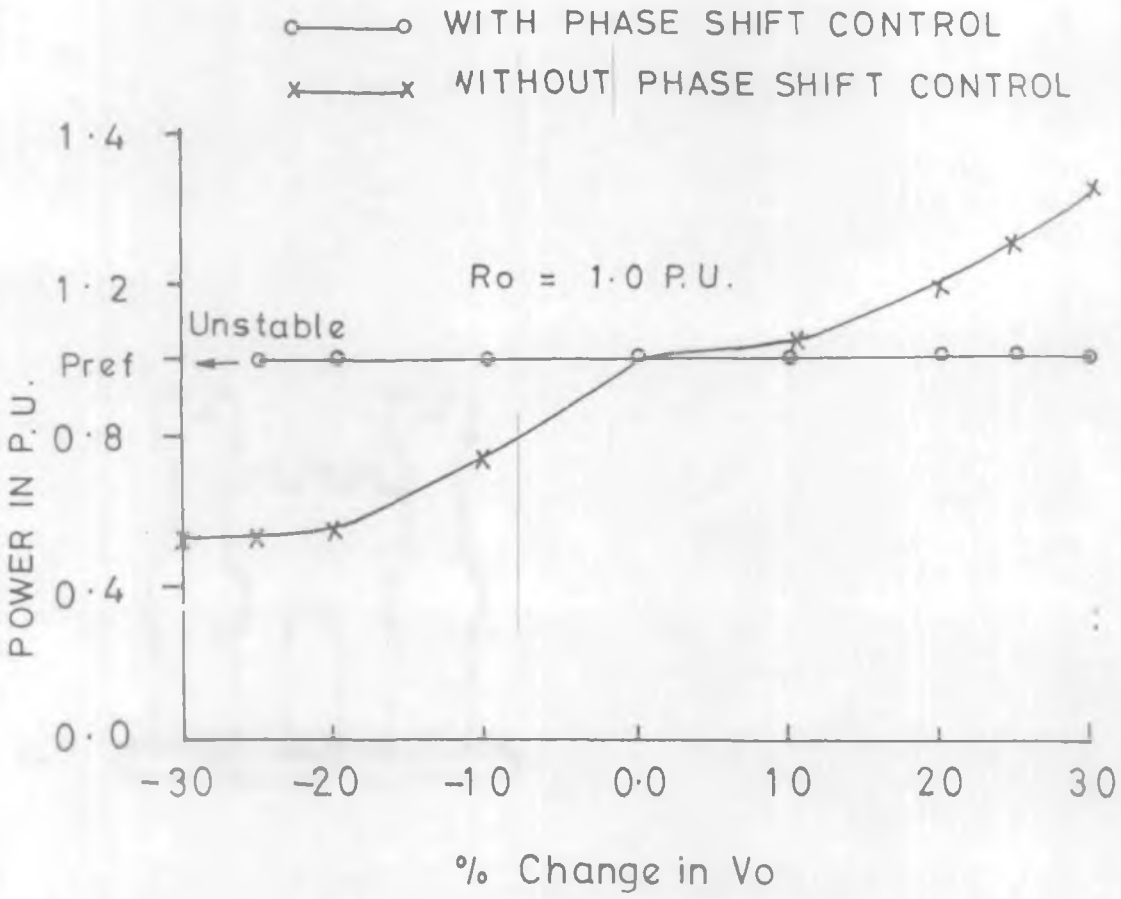

FIG. 4.14 VARIATIO'I OF REAL POWER WITH Vo.

behaviour of the simulated system instead of going to mathematical modelling. The transient response of the analogue simulation and fabricated feedback controller are found to be in reasonable agreement with each other.

4.9 Summary and Conclusion

This chapter is devoted to demonstrate the steady state and transient response of the MHD-inverter link with feedback controller. The manual control described in last chapter has been replaced by the feedback controller. The design of the controller is carried out first with digital simulation then with analogue simulation. The controller is designed, fabricated and tested on the MHD-inverter link in open loop and closed loop system. Transient response has been recorded on the X-Y recorder and oscillograms are also obtained Theoretical results of the transient response are compared with those of fabricated controller. The controller designed in this chapter may be utilised for power control of the 2 MW (thermal)MHD generator test facility.

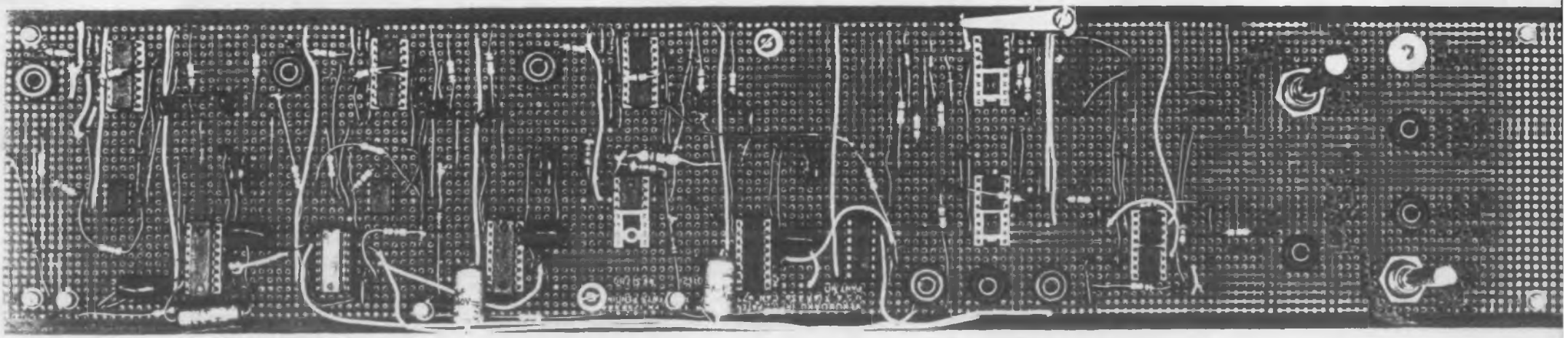

FIG. 4.15 FEEDBACK CONTROLLER

CHAPTER 5 : TIME DEPENDENT MODELLING OF MHD GENERATOR AND TRANSIENT RESPONSE OF THE MHD-GENERATOR INVERTER LINK

CHAPTER 5

TIME DEPENDENT MODELLING OF MHD GENERATOR AND TRANSIENT RESPONSE OF THE MHD GENERATOR INVERTER LINK++

5.1 Introduction

The V-I characteristics of the MHD duct has been assumed linear for all calculations in the previous chapters. In this chapter time dependent modelling of the duct yields actual characteristics. The V-I characteristics obtained in this chapter are for a 2 MW (thermal) MHD generator. The power control of the duct now utilizes these characteristics.

The transient operation of the MHD duct is complicated and has been receiving attention only in recent years [72-75]. The calculations made by Oliver [73] for a segmented Faraday generator show that when a sudden load is imposed on the generator, a strong shock development takes place. Such fast fluid dynamic transient for sudden load disturbances will have adverse effects on the power system as a whole. Therefore more details are needed for integration of MHD generator with power system under transient state. A voltage source inverter

---

++ The material presented in this chapter has led to the authors publication number 9, 10 and part of publication number 2.

(VSI) is used in this chapter for the transient analysis of the MHD-inverter link. A set of current and voltage equations are derived to predict the transient behaviour of the MHD duct with gas dynamic coupling.

5.2 MHD fluid flow equations

The equations describing particular flow conditions are usually these derived from the conservation quantities i.e. conservation of mass (equation of continuity), conservation of momentum (equation of motion) and energy conservation. For plasma flow in e.m. field these equations are derived by Sutton and Sherman [76]. They describe the motion of a compressible, viscous fluid using conservation principles and Maxwell's equations assuming nonrealistic motion.

Conservation of mass principles results in :

$$\frac{\partial \rho}{\partial t} + \nabla \cdot \rho \underline{V} = 0 \qquad (5.1)$$

where ρ = mass density of the plasma

$\underline{V}$ = velocity vector for the flow

Conservation of momentum :

$$\rho \frac{D\underline{V}}{Dt} + \nabla \cdot \tau + \nabla p = \rho_e \underline{E} + \underline{J} \times \underline{B} \qquad (5.2)$$

where τ = shear stress vector

P = hydrostatic pressure

ρ_e = charge density

$\underline{E}$ = electric field vector

$\underline{B}$ = Magnetic field vector

J = Electric current density

note $\frac{D}{Dt} = \frac{\partial}{\partial t} + \underline{V}$

Conservation of energy :

$$\rho \frac{D(e + \frac{V^2}{2})}{Dt} = -\nabla.q - \nabla.(P\underline{V}) - \nabla(\underline{V}.\tau) + \underline{E}.\underline{J} \qquad (5.3)$$

where e = internal energy of the plasma

q = heat flux vector

The general form of the fluid flow equations (5.1) to (5.3) are complex to solve. Therefore for ease of solution they are approximated and verified by the numerical analysis in section 8.3 of Sutton and Sherman [76]. With the above MHD approximations they can be written as

Conservation of Mass

$$\frac{\partial P}{\partial t} + \nabla.(\rho\underline{V}) = 0 \qquad (5.4)$$

Conservation of Momentum

$$\rho \frac{D\underline{V}}{Dt} = -\nabla P + \underline{\mathcal{F}} + \underline{J} \times \underline{B} \qquad (5.5)$$

where $\underline{\psi}$ = Viscus force vector

Conservation of Energy

$$\rho \frac{D(e+V^2/2)}{Dt} = \underline{J}.\underline{E} - \nabla\cdot\underline{q} - \nabla\cdot(P\underline{V}) + \phi \qquad (5.6)$$

where ϕ = viscus dissipation function

5.3 Quasi-one dimensional flow equations

MHD process for generating power is inherently three dimensional. The quasi one dimensional approximations permit the reduction of the three dimensional MHD equations to a simpler system of first order ordinary differential equations for the ease of numerical solution [77-80]. The following assumptions are made for the solution of quasi-one dimensional flow equations for linearly diverging segmented Faraday generator as shown in figure 5.1.

(i) The velocity vector, v, has only one component, u in the x direction and applied magnetic field is in z direction only. Due to fine segmentation, the electric field is only in Y direction.

(ii) Non uniformities at the exit and entrance to the duct caused by the end effects are neglected.

(iii) Fluid variables such as pressure, temperature, density, conductivity and velocity are considered to be

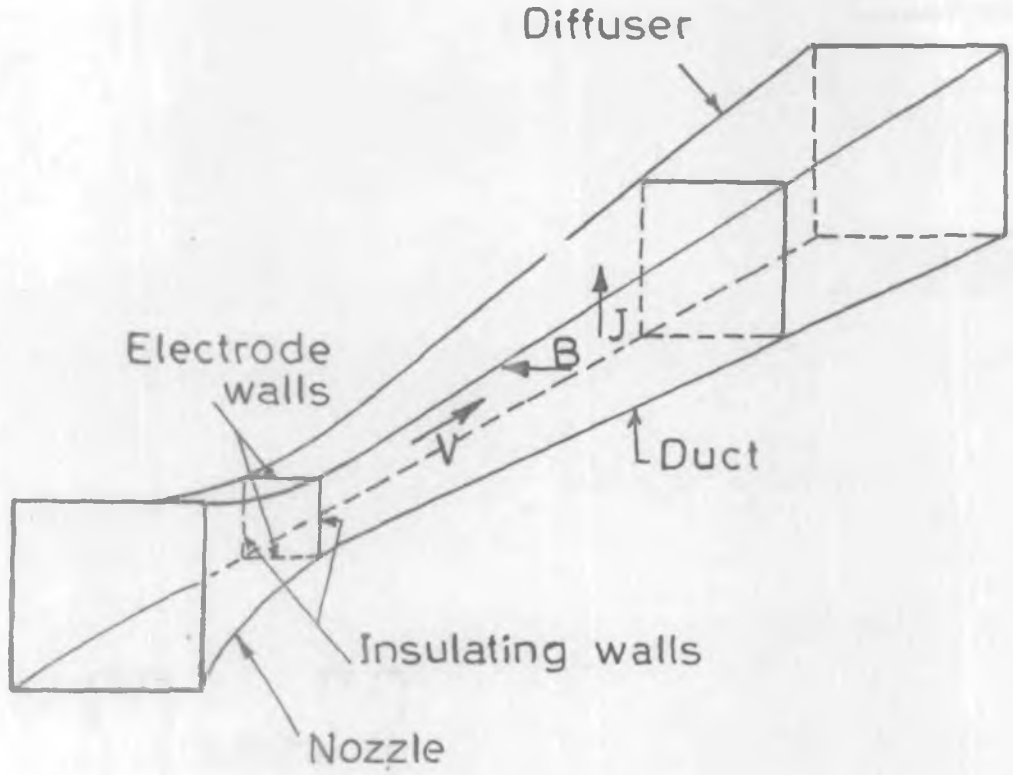

FIG. 5.1. LINEAR MHD GENERATOR .

reasonably constant over a transverse (Y-Z) cross section.

The quasi-one dimensional equations can now be derived on the basis of these assumptions [80-81]. From the third assumption many of the flow parameters are taken as constant over a cross section so that the constant value taken over the cross sectional area is the average value at any time. In this way such parameters vary only with axial position along the duct (i.e. in X direction) and with time.

Applying the approximations to equations (5.4), (5.5) and (5.6) the following quasi one dimensional relations are obtained.

Conservation of Mass :

$$\frac{\partial A\bar{\rho}}{\partial t} + \frac{\partial (A\overline{\rho u})}{\partial X} = 0 \qquad (5.7)$$

Conservation of Momentum :

$$\frac{\partial A\overline{\rho u}}{\partial t} + \frac{\partial A\overline{\rho u^2}}{\partial X} = -A\frac{\partial \bar{p}}{\partial X} + A\,\overline{J_y B_z} + A\bar{F}_b \qquad (5.8)$$

where F_b = Wall friction term due to shearing stress on the wall

Conservation of Energy :

$$\frac{\partial\{A\overline{\rho(u^2/2+e)}\}}{\partial t} + \frac{\partial\{A\overline{\rho(u^2/2+e)}\}}{\partial X} = -\frac{\partial A\overline{pu}}{\partial X} + AE_yJ_y + AQ_T \qquad (5.9)$$

where Q_T = heat transfer term due to viscous dissipations, heat loss by conduction and heat addition by chemical reaction

Droping the bar notation to denote average values and introducing the momentum density $m = \rho u$ and the total energy density $e_t = \rho (e + u^2/2)$ the equations (5.7), (5.8) and (5.9) take the form

$$\frac{\partial \rho}{\partial t} = - \frac{\partial m}{\partial X} - \frac{m}{A} \frac{\partial A}{\partial X} \tag{5.10}$$

$$\frac{\partial m}{\partial t} = - \frac{\partial (m^2/\rho + P)}{\partial X} - \frac{(m^2/\rho)}{A} \cdot \frac{\partial A}{\partial X} + J_y B_z - F_b \tag{5.11}$$

$$\frac{\partial e_t}{\partial t} = - \frac{\partial (e_t + P) m/\rho}{\partial X} - \frac{(e_t + P) m/\rho}{A} \cdot \frac{\partial A}{\partial x} + J_y E_y + Q_T \tag{5.12}$$

Expressions for F_b and Q_T are given in terms of the wall shear stress τ and heat flux [73].

$$F_b = 4 \tau_w / D_H$$

$$Q_T = 4 q_w / D_H$$

where D_H is a constant and τ_w and q_w are functions of the flow variables ρ, u and e related to boundary layer mechanics of the appropriate wall regions in the duct.

5.4 Theoretical model of the MHD generator [73]

In order to simplify the description of the flow in terms of mass, momentum and energy conservation equations for the quasi-one-dimensional equations (5.10), (5.11) and (5.12) may be rearranged and combined in vector notation to form a single vector equation. The vector functions $\underline{U}(x,t)$, $\underline{F}(\underline{U})$, $H(\underline{U},x)$, $\underline{S}(\underline{U},x,t)$ and $\underline{D}(\underline{U},x,t)$ are defined as in reference above.

$$\underline{U}(x,t) = (\varrho, m, e_t)^T \tag{5.13}$$

$$\underline{F}(\underline{U}) = \{m, (m^2/\varrho)+p, (e_t+p)m/\varrho\}^T \tag{5.14}$$

$$\underline{H}(\underline{U},x) = \frac{1}{A}\frac{dA}{\partial x}(m, m^2/\varrho, (e_t+p)m/\varrho)^T \tag{5.15}$$

$$\underline{S}(\underline{U},x,t) = (0, 0, J_y B, J_y E_y)^T \tag{5.16}$$

$$\underline{D}(\underline{U},x,t) = (0, 0, F_b, Q_T)^T \tag{5.17}$$

or, in the notation of Oliver [73]

$$\underline{D}(\underline{U},x,t) = (0, 0, 4\tau_w/D_H, 4q_w/D_H)^T \tag{5.18}$$

The equations (5.13) to (5.18) can be combined to form one single vector equation representing fluid state at any time t and position X.

$$\frac{\partial \underline{U}}{\partial t} = \frac{\partial \underline{F}}{\partial X} - \underline{H}-\underline{D}-\underline{S} \tag{5.19}$$

There are a number of different techniques that may be

employed to obtain numerical solutions for partial differential equations of the form (5.19). The methods used in this case must hold for subsonic, supersonic and transonic conditions between such flow states. Currently one of the most popular methods used for evaluating the compressible flow relationship of the type under consideration involves a class of finite difference techniques called Lax-Wendroff methods. The particular type used in reference [37] is based on two-step Lax-Wendroff method devised by Richtmyer and modified by MacCormack.

This method is based on the replacement of the non-linear partial differential operator in equation (5.19) by a non-linear finite difference operator. The equation can be rewritten in the form

$$\frac{\partial \underline{U}\,(x,t)}{\partial t} = \frac{-\partial(\underline{F}(\underline{U}))}{\partial x} - \underline{C}\,(\underline{U},x,t) \qquad (5.20)$$

where $\underline{C}(\underline{U},x,t) = \underline{H}(\underline{U},x) + \underline{S}(\underline{U},x,t) + \underline{D}(\underline{U},x,t)$

The space and time co-ordinates within the duct are considered to be discretized into finite difference Δx and Δt, where $x = i\Delta x$ and $t = n\Delta t$ where i and n are integers. In this way the fluid state $\underline{U}$ at a time t and position x can then be represented as $\underline{U}(x,t) = \underline{U}_i^n$. The state of the fluid at a time Δt later i.e. $\underline{U}_i^{n+1}$ can be calculated from $\underline{U}_i^n$ using

the Richtmyer-MacCormack method. There are two steps required in the process, the first of which involves the evaluation of an intermediate state $\underline{U}_i^{n+1}$ where

$$\underline{U}_i^{n+1} = \underline{U}_i^{n} - \frac{\Delta t}{\Delta x}\{F(\underline{U}_{i+1}^{n} - F(\underline{U}_i^{n})\} - \Delta t\, \underline{C}(\underline{U}_i^{n}, x, t) \quad (5.21)$$

The second step allows the state $\underline{U}_i^{n+1}$ to be determined from the intermediate state and the state $\underline{U}_i^{n}$.

$$\underline{U}_i^{n+1} = 1/2\,\{\underline{U}_i^{n} + \underline{U}_i^{n+1} - \frac{\Delta t}{\Delta x}(\underline{F}(\underline{U}_i^{n+1}) - F(\underline{U}_{i-1}^{n+1}))\} - \Delta t\, \underline{C}(\underline{U}_i^{n+1}, x, t) \quad (5.22)$$

In this way if an initial fluid state $\underline{U}_i^{o}$ is given, the subsequent fluid states may be computed forward in time through the full subsonic, transonic and supersonic range.

To ensure the numerical stability of the relations (5.21) and (5.22), it is necessary to satisfy the Courant condition at each point where the fluid state is evaluated. This criterion, described by Roache (82) requires that

$$C = \frac{(|u| + a)\,\Delta t}{\Delta x} \leq 1 \quad (5.23)$$

where C = Courant number.

u = local fluid velocity

a = local sonic speed

Rearranging this criterion the restriction is imposed on Δt that

$$\Delta t \leq \frac{\Delta x}{u + a} \tag{5.24}$$

Examination of equations (5.21) and (5.22) reveals that neither $\underline{U}_N^{n+1}$ (i.e. the stream boundary (exit) fluid state where (N-1) x = length of the channel) or $\underline{U}_1^{n+1}$ (i.e. the upstream boundary (inlet) fluid state) can be calculated using the two-step finite difference method directly.

For the upstream boundary both ρ_1^{n+1} and $e_{t_1}^{n+1}$ can be calculated from the pressure and temperature specified under inlet conditions but u_1^{n+1} is allowed to develop as part of the solution by using backward linear interpolation so that

$$u_1 = 2u_2 - u_3$$

and hence $m_1 = u_1 \rho_1$

At the downstream linear extrapolation enables both the density ρ_N and momentum density m_N to be calculated.

$$\rho_N = 2 \rho_{N-1} - \rho_{N-2} \tag{5.25}$$

$$m_N = 2 m_{N-1} - m_{N-2} \tag{5.26}$$

Then e_{t_N} is obtained from the imposed exit boundary conditions, ρ_N and m_N.

5.5 Electrical characteristics of the MHD generator

The numerical technique described in section 5.4 is applied to a constant height duct with a rectangular cross sectional area. An analysis programme developed by Matair [83] was modified to take into account the Hall effect and electrical characteristics were obtained for both Faraday and diogonal modes. The model includes the wall skin friction and heat transfer to the walls. The characteristics are obtained for a constant mass flow rate (0.3 Kg/s) of plasma in the duct. At the inlet of the MHD duct, the stagnation temperature of the plasma is assumed to be equal to the stagnation temperature at the combustor. The pressure at the duct exit is determined from the exit stagnation pressure of the diffuser with the assumed diffuser efficiency of 0.7. The electrical loading of the generator is taken tinto account by computing the current density J from the specified current or the voltage of an electrode pair [37]. The equations described in last section are solved by a two step time marching, finite difference Mac-Cormack algorithim which can handle subsonic, supersonic and transonic flows [73,84].

5.5.1 Data for the calculation of electrical characteristics

The specification for the simulation procedure are as follows :

Duct : Linearly diverging from 3.2 cms to 4.2 cms. in width

Length = 1 meter

Nozzle : Width = 3.3 cms to 3.2.cms

Length = 0.1 meter

Diffuser : Width = 4.2 cms

Length = 0.4 meter

The hight of nozzle, duct and diffuser is constant at 0.1 meter.

Magnetic field	: 3 Tesla
Diffuser Efficiency	: 0.7
Electrode voltage drop	: 40 volts
Electrodes	: 20 pairs, pitch = 5 cm
Fuel	: Coal seeded with KOH
Inlet temperature	: 2800° K
Exit stagnation pressure	: 1.1×10^5 pa
Mass flow rate	: 0.3 Kg/s
Loading Parameter	: varied between open circuit and short circuit

Finite difference increments

$$= \Delta x = \frac{Z}{N-1} = 5 \text{ cms}$$

$$\Delta t = \frac{0.6\ \Delta x}{|u_{max}| + C_{max}}$$

Δt was set so as to obey the courant condition for the numerical stability of the Lax-Wendroff algorithm. The terms u_{max} and C_{max} are the values of the maximum gas velocity and maximum sonic velocity in the duct at any time.

With the above data the modified computer programme [83] was used to calculate the V-I characteristics of the generator. Figure 5.2 shows the V-I curves of the MHD generator for Faraday and diagonal mode. The programme MHD_4 and sample out put are listed in list D-1, table D-2 and D-3 in appendix D. The programme takes into account cross sectional area at N points when the duct is devided into (N-1) equal subsection of width Δx. The initial distribution of fluid state is specified for each point i Δx with i ranging from 2 to N. The gas used for the simulation of real gas magnetohydrodynamic generator flows consists of the products of the combustion of coal with a stoichiometric amount of oxygen, equal amount of nitrogen and 1.5 percent by weight of potassium hydroxide (KOH) which is used as seed material. The coal data is calculated by a subroutine incorporated in programme MHD_4. Rankin [85] has given the constants obtained from curve fits for the various equilibrium gas properties which were developed from the theory of an ideal gas and Saha's equation. These constants allow various properties of the gas to be calculated from the temperature and pressure. These constants are given in table D-4 of the appendix D.

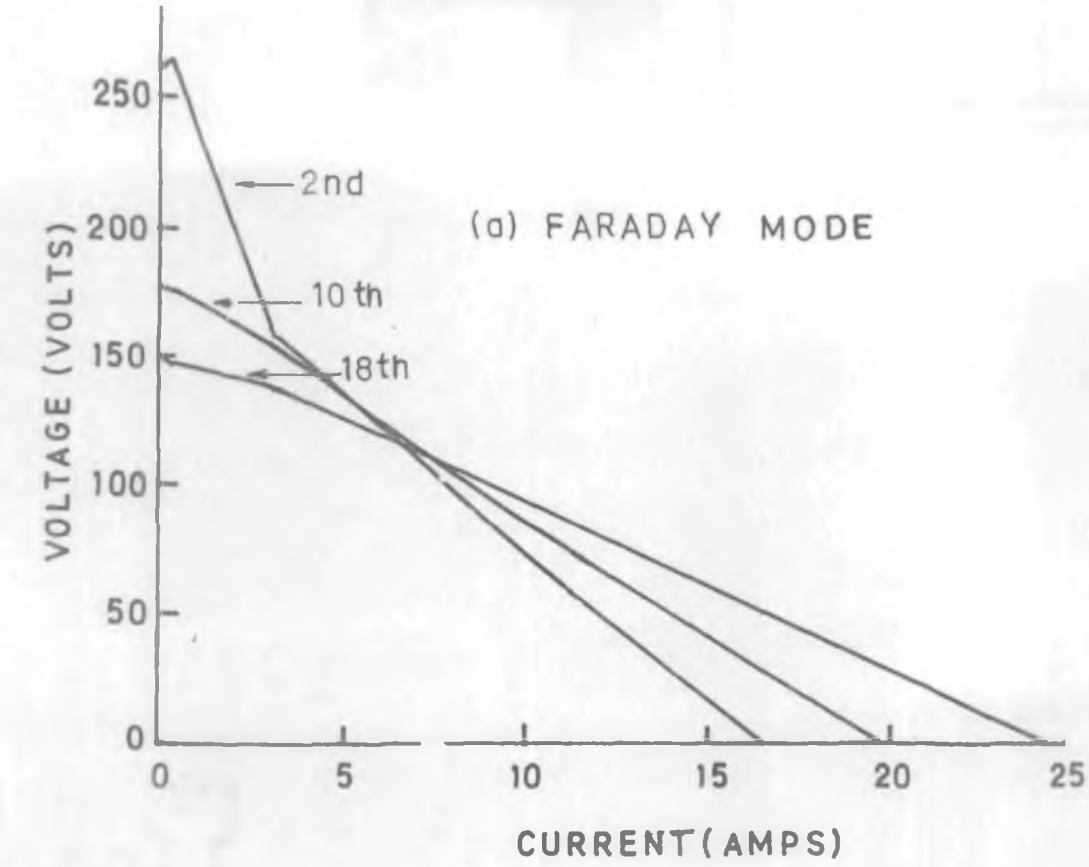

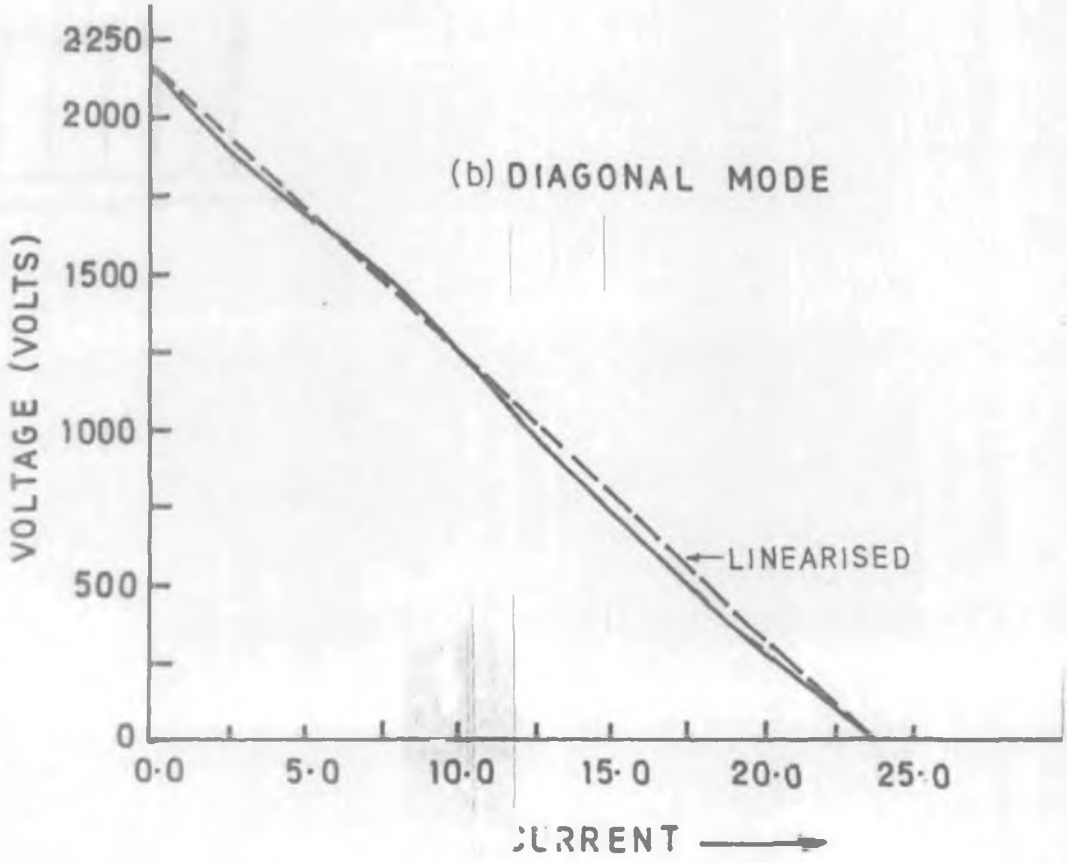

FIG 5.2 V-I CURVES OF MHD GENERATOR

5.6 Control of power to a.c. system

The V-I curves shown in figure 5.2 are linear except for the end electrodes where there is sharp change in slope of the curve due to change in velocity from subsonic to supersonic. For the reference power the operating point chosen is same as discussed in chapter two. The 10th electrode V-I curves for the Faraday mode are taken for the analysis. The base quantities are chosen as discussed in section 2.2.3 of chapter two. The computer programme PHSPLT7 shown in table A-1 is incarporated with the programme MHD_4 for the control of power to a.c. system. The mass flow rate is varied to get variation in duct voltage and resistance. Power control due to change in voltage is shown in figure 5.3. Similar programme was run for diagonal mode where linearised characteristics were used for power control. The change in duct voltage is only considered because resistance is also function of mass flow rate for fixed geometry of the MHD duct. Therefore for any change in duct voltage resistance automatically varies. The desired power is controlled within 10 percent of the voltage variation from the operating point which is less than the cases considered in section 2.6.6 and 3.3.6. This is because of the reason that in computer model of the MHD generator, the internal resistance is variable quantity with mass flow rate.

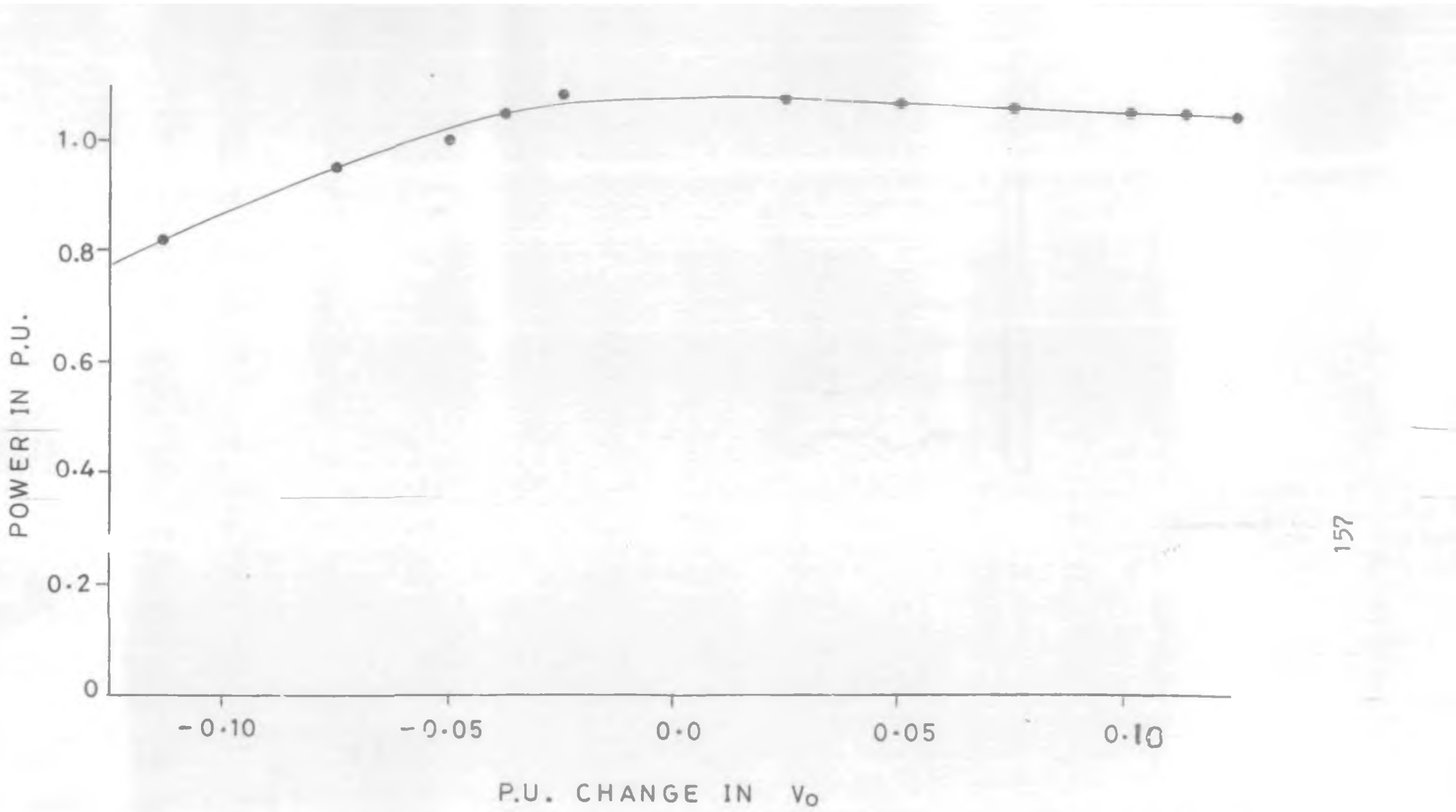

FIG. 5.3. VARIATION OF REAL POWER WITH PHASE SHIFT CONTROL.

5.7 Transient response of the MHD generator-inverter link

The transient response of an MHD generator to load fluctuations is an important study, particularly with a force commutated inverter. This study will lead to better design of inverter and control systems. Also this gives idea as to whether fluctuations due to load will be damped or cause instabilities.

In this section the same duct is used for transient analysis as described in section 5.5.1. The generator model discussed in section 5.5 is linked with the force commutated inverter interface for the transient analysis of the system. The system is subjected to sudden load changes from operating point to near open circuit and short circuit. The results are obtained for space and time variations for voltage, current, temperature, pressure and Mach number.

5.7.1 Derivation of equations for transient analysis

The energy source is constrained by shunt capacitors to act as a good approximation to an ideal voltage source. A d.c. input filter is added to limit the inverter ripple injection to MHD channel and the influence of the channel's voltage ripple on the inverter [41,86]. Figure 5.4 shows the block diagram of the MHD generator-inverter link with d.c. input filter.

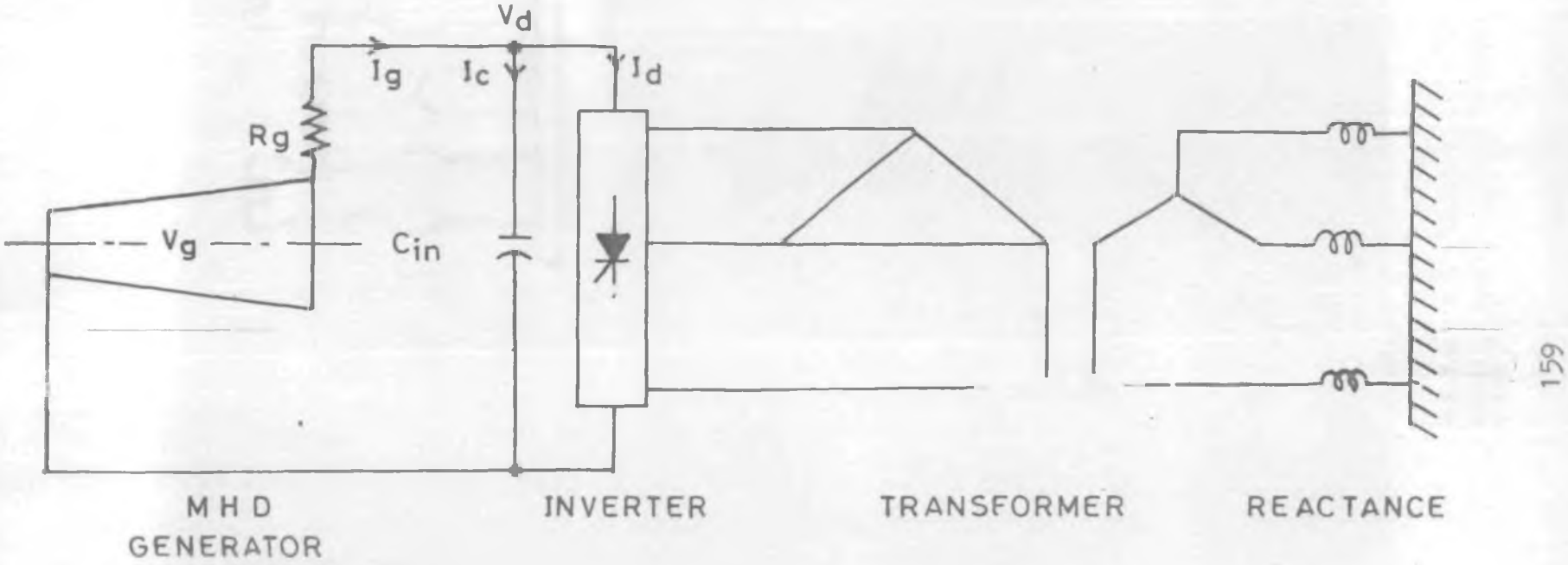

FIG. 5.4. BLOCK DIAGRAM OF MHD GENERATOR-INVERTER LINK.

Initially the generator is assumed under steady state working at operating point and giving reference power. The d.c. input filter (C_{in}) is fully charged. We can write the following equations under this condition.

$$I_g - I_d = I_c = 0 \tag{5.27}$$

where I_g = generator current under steady state

I_d = inverter current

I_c = current through capacitor. The current through the capacitor (C_{in}) is zero because under steady state it is fully charged

The differential equation may be written at t = 0

$$I_c = C_{in} \frac{dV_d}{dt} \tag{5.28}$$

using equation (5.27) we can express equation (5.28) in difference equation as

$$\Delta V_d = (I_g - I_d) \frac{\Delta t}{C_{in}} = 0 \tag{5.29}$$

At time $t^+ = 0$ a sudden change in load occurs. This current is to be supplied by the capacitor C_{in} as current I_g from MHD duct cannot change instantaneously because of fluid dynamic coupling of all the electrodes. The capacitor will discharge instantly leading to change in current (I_g) from generator.

Fluid dynamic conditions in the MHD channel will change now and V-I characteristics of all the electrodes will change. Iterative procedure is followed to predict the transient behaviour of the generator-inverter link. The following equations are written for Jth electrode and nth iteration for computerised solution of the transients :

$$i_{c_j}^{n} = I_{g_j}^{n} - I_{d_j}^{n} \tag{5.30}$$

$$\Delta V_{d_j}^{n} = \Delta t \, . \, i_c^{n} / C_{in} \tag{5.31}$$

$$V_{d_j}^{n+1} = V_{d_j}^{n} + \Delta V_{d_j}^{n} \tag{5.32}$$

$$I_{g_j}^{n+1} = (V_{g_j}^{n+1} - V_{d_j}^{n+1}) / R_{g_j}^{n+1} \tag{5.33}$$

$$K_j^{n+1} = f(I_{g_j}^{n+1}) \tag{5.34}$$

$$i_{c_j}^{n+1} = I_{g_j}^{n+1} - I_{d_j}^{n+1} \tag{5.35}$$

$$t^{n+1} = t^{n} + \Delta t \tag{5.36}$$

K_j^{n+1} is the new load factor which is a function of current as shown in equation (5.34). The above equations are linked with programme MHD_4 for the transient behaviour of the MHD generator.

The calculations are carried for step changes in load from operating point. The data needed for calculations is same as described in section 5.5.1.

5.7.2 Transient response due to step increase in load

The operating point is chosen for a load factor of 0.5. The load is suddenly increased. The transient response due to increase in load is recorded by the computer plotter as shown in figure 5.5. Three different electrode pairs are chosen for simplicity. The one near inlet, the other in the middle and the 3rd at the exit of the duct. Voltages and currents are plotted against time. The internal resistance is different for different electrodes as this depends upon the geometry of the duct and conductivity. For this geometry, the internal resistance reduces towards the out of the duct. Therefore rate of rise of current for different electrodes is different. The difference in the rate of rise of current is asmall because the variation in internal resistance of the electrodes is small. The rate of change of current gives rise to large rate of change of Lorentz force. The voltage oscillations die down in 3 to 4 milliseconds and electrode.pair voltages attain steady state value i.e. the operating value. The variation of pressure, temperature and Mach number along the duct is also plotted at different time intervals. At t = o, the distribution of pressure, temp. and Mach number is shown in

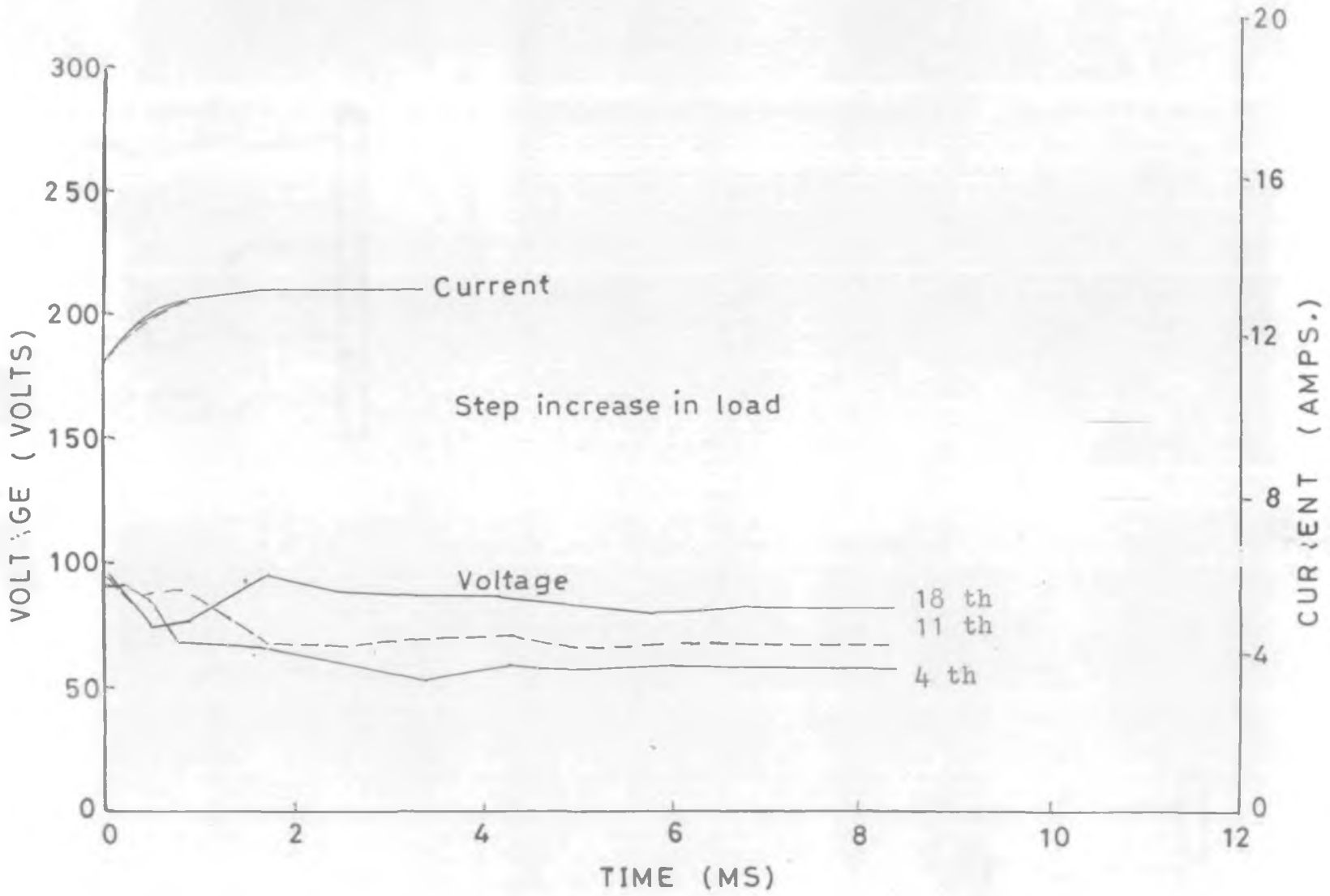

FIG.5.5. TRANSIENT RESPONSE TO LOAD CHANGE.

figure D-5 in appendix D. From the polts it can be seen that pressure is increasing slightly from inlet to outlet of the duct and temperature is decreasing from inlet to outlet of the duct. The Mach number is increasing from inlet to outlet but the flow remains subsonic ($M < 1$). Figures D-6 and D-7 in appendix D show the computer plots of temperature, pressure and Mach number at different time intervals. It is observed from the above figures that after the steady state is attained, the distribution of these parameters have the uniform gradient and flow remains still subsonic.

5.7.3 Transient response due to step decrease in load

In this section a step decrease in load is considered from operating point. The voltage and current variation is plotted against time as shown in figure 5.6. The time response is plotted for 4th, 11th and 18th electrode pairs. The current decrease is almost exponential which characterises the nature of the circuit as R-C. The voltage oscillations in this case is more due to less retarding force compared to step increase in load. The voltage oscillations are settled in little less time compared to previous case. The variation of temperature, pressure and Mach number is also plotted along the duct at different time intervals. Figures D-8 to D-10 in appendix D show the variation of temperature, pressure and Mach number at different time intervals. The distribution of

FIG. 5.6. TRANSIENT RESPONSE TO LOAD CHANGE.

these parameters becomes uniform after the transient is over and flow remains subsonic.

5.7.4 Transient response due to short circuit

In this section the generator is suddenly loaded near to short circuit from operating point. The actual short circuit (K = 0) is not considered because of the numerical instability of the programme developed. Therefore the inlet electrode is taken as working at 0.05 load factor. The transient response is calculated and time variations of voltage and current are shown in figure 5.7. The response is similar to that discussed in section 5.7.2. The currents rise exponentially and attain thes teady state with the same rate as discussed in section 5.7.2. The voltage oscillations are more pronounced and take more time to settle down to steady state. The space variation of temperature, pressure and Mach number is also plotted at different time intervals as shown in figures D-11 to D-13 in appendix D. The variation in temperature and pressure is more in this case compared to step increase in load. The Mach number is reduced from inlet to outlet of the duct. The flow along the duct still remains subsonic.

5.7.5 Transient response due to open circuit

In this section the transients due to sudden change in

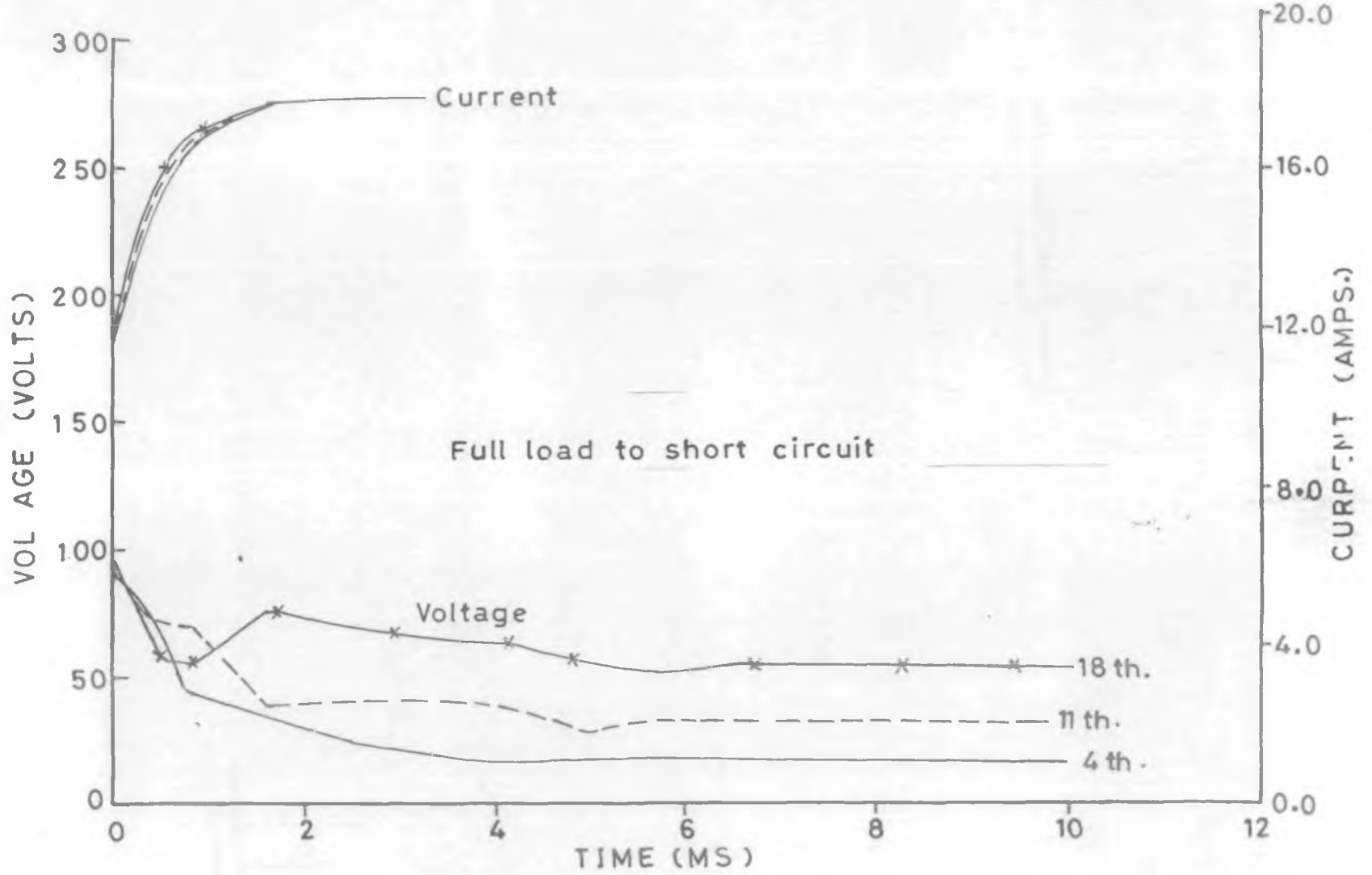

FIG. 5.7. TRANSIENT RESPONSE TO LOAD CHANGE.

load from operating point to open circuit are considered. The load factor increases from 0.5 to near unity. The current and voltage transients are plotted in figure 5.8. The currents of different electrode configuration decrease to zero but voltages rise exponentially and about 2 ms seconds latter become oscillatory. The flow inside the generator becomes unstable and voltage oscillations increase in magnitude and frequency both. This case is most interesting because with the decrease in velocity at any electrode from previous value, changes the direction of current flow to electrode. The d.c. input filter has more charged voltage than the particular electrode pair when the velocity is decreased. Now the current is supplied from the filter to the generator electrode pairs, giving rise to negative retarding Lorentz force ($J_y XB$). The fluid flow pattern is completely disturbed giving rise to instability inside the duct. The capacitor works as a source and sink both in open circuit case. The fluid velocity changes from subsonic to transonic. Therefore the capacitor should be disconnected in case of sudden open circuits. Figures D-14 ato D-17 in appendix D, show the space variation of temperature, pressure and Mach number. More pronounced variation, are observed in temperature and pressure along the duct and about 7 ms, the flow pattern changes from subsonic to transonic as shown in figure D-16.

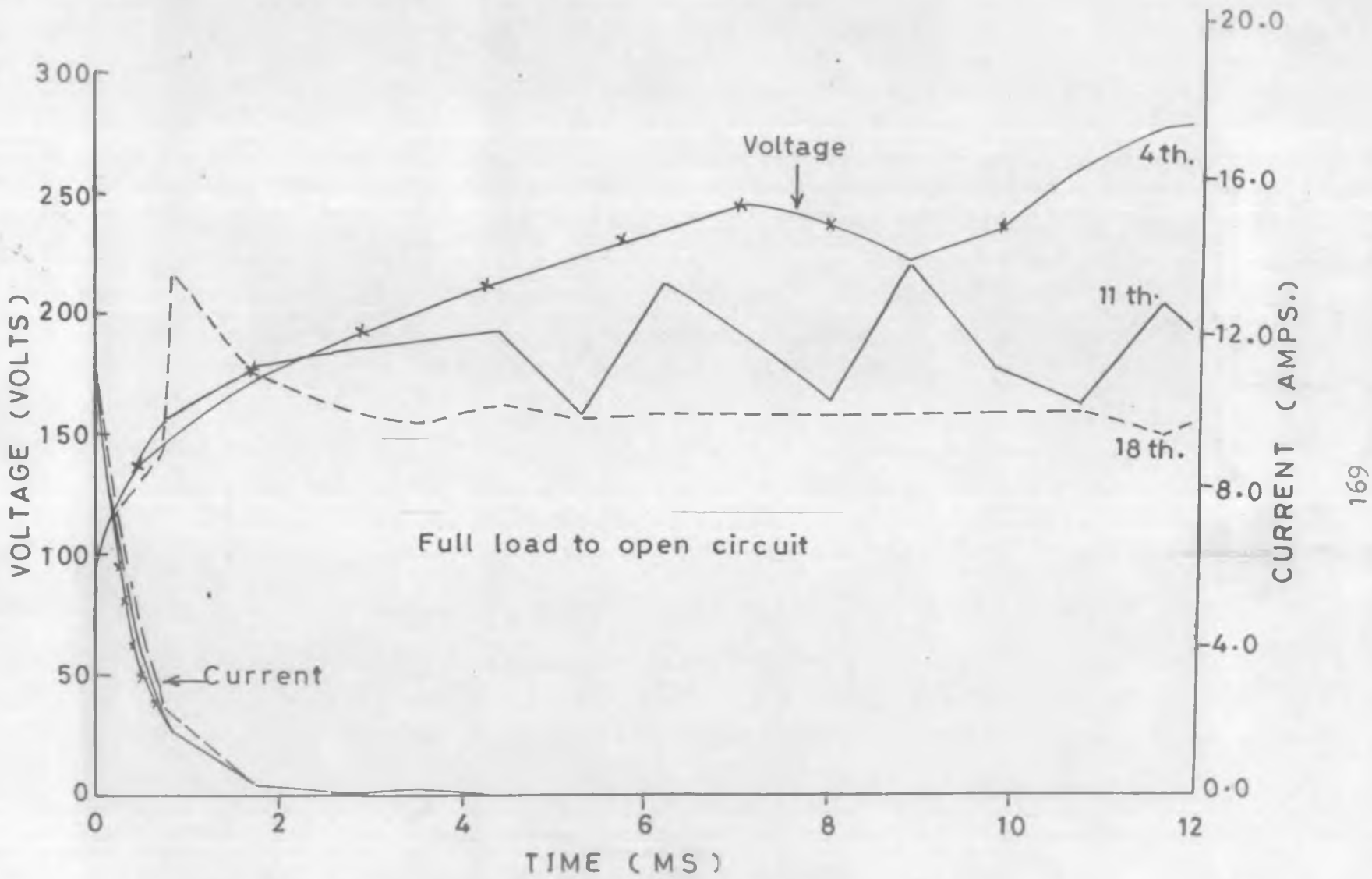

FIG. 5-8. TRANSIENT RESPONSE TO LOAD CHANGE.

5.7.6 Transient response due to d.c. input filter

The size of the d.c. input filter is an important consideration for the determination of transient behaviour of the MHD generator. This acts as source when the electrode pair voltage is less than capacitor voltage (V_d) and sink when the electrode pair voltage is more than the capacitor voltage. For large size of capacitor, the Lorentz force ($J_y x\ B$) is more and for small size of the capacitor, the control action will be slow. Therefore the size of the capacitor was varied for the calculation of the transient behaviour. An optimum size of 0.1 μF/VA is suggested for better performance of the generator under transient conditions.

5.8 Summary and conclusion

In this chapter a time dependent computer model is considered for the calculation of electrical characteristics. These characteristics are used for the power control to a.c. system in different modes of loading of the MHD generator. A voltage source inverter (VSI) interface is taken for the transient analysis of the MHD-generator inverter link. A set of current and voltage equations are derived for the system. Digital simulation is carried out with these equations.

The duct is subjected to sudden load changes from operating point chosen for various.cases. The computer plots

have been obtained for transients in voltage and current for the cases considered. The variation of temperature, pressure and Mach number along the duct is also plotted for the transient conditions. An optimum size of the input filter capacitor is also suggested for the better performance of the control system under transient conditions.

CHAPTER 6 : SUMMARY AND RECOMMENDATIONS

6.1 Summary of the main findings of the thesis

6.2 Recommended further studies

C H A P T E R 6

SUMMARY AND RECOMMENDATIONS

6.1 Summary of the main findings of the thesis

The work carried out in previous chapters pertains to the problems of most economic and useful application of MHD generator for the interconnection with electrical supply utility for bulk power transmission. The force commutated inverter link is used in this study because of major advantages already mentioned in section 1.2. The MHD generator inverter link is treated as a single machine connected to infinite bus with simplifying assumptions and approximations.

The findings described in this thesis can be summerised in the following main points :

1. The feasibility of using a simple square wave inverter has been illustrated for the conversion and control of MHD duct feeding into a power system. The salient features of the feasibility study are :

(a) A computer programme has been prepared which simulates the connection of either a square wave or PWM inverter to the MHD duct.

(b) A modified computer programme has been prepared for the satisfactory harmonic reduction by using 5th and 7th

harmonic filters.

(c) Quasi static changes in fluid dynamic conditions have been allowed for, by considering variations in MHD duct voltage and internal resistance.

(d) It has been investigated that power transfer from MHD duct is maximum for a system reactance (X_s) of 0.45 P.U. and phase difference between inverter and infinite bus voltage as 60 degrees. The reactive power flow to infinite bus for this condition is zero and therefore power factor is unity.

(e) A simple and single controller has been used for power control compared to complex control arrangements described earlier [39,42].

(f) Maximum power has been transferred from MHD inverter link to infinite bus at any desired power factor without any power factor correction needed.

2. A simple scheme has been presented for the simulation of MHD inverter link in the laboratory. The results of the digital simulation are verified with the experimental setup.

3. The detailed design of the force commutated inverter is presented for the interconnection of the 2 MW MHD test facility. Special attention has been paid for the design of

commutating components. The minimization of commutation losses, skin effect and size of the component is considered. The different designs of inductor is presented for this purpose.

4. Safe inverter operation is investigated under various operating conditions.

5. A simple rewirable fuse wire is suggested for the protection of semiconductor devices. An experiment has been conducted to suggest an approximate length of the fusewire for the protection of a semiconductor device of known I^2t rating. The graphs are plotted for different lengths of the fusewire versus I^2t rating. These graphs can be used to predict the approximate length of the fuse wire for the protection of any power electronic device of known I^2t rating.

6. A feedback controller has been designed for the automatic control of power from MHD duct to infinite bus. A good steady state and dynamic response is demonstrated by the controller in open loop and closed loop system.

7. Time dependent computer model of the generator has been used for the determination of V-I characteristics of a 2 MW, 20 electrode pair MHD generator in Faraday and diagonal mode. These curves then are utilized for power control to infinite bus.

8. The transient studies are carried out on the above model with a voltage source inverter (VSI) interface. Sudden load changes has been considered from operating point. The time variations of voltage and current for different electrode pairs have been plotted. The variation of temperature, pressure and Mach No. along the duct is also plotted. The important conclusions have been drawn as discussed in Chapter 5. These conclusions will form the basis of further transient stability studies of the MHD-inverter link. Results were also obtained with different values of filter capacitor. An optimum size of 0.1 μF/VA is suggested for fast control action and better system stability.

6.2 Recommended further studies

Because of the simplifying assumptions adopted in some of the investigations described in this thesis, some of the results obtained can be regarded as first order approximations. Therefore, as a possible improvement on the present study more realistic approach can be made on the following points :

1. The representation of the generator model should be more accurate and resistance should be added for the MHD-generator inverter link analysis as discussed in section 2.3.

2. The present study assumes velocity $\bar{v}$, magnetic field $\bar{B}$ and electric field $\bar{E}$ in one direction only. Also

temperature, pressure, mass density and conductivity are taken constant over Y-Z plane. In practice these quantities vary significantly in the channel. The calculations with variations in these quantities will lead to more accurate results of the proposed inverter.link.

3. The work should be extented to commercial size MHD generator connected to a multimachine power system rather than single machine connected to infinite bus bars.

4. Two independent 3 phase square wave inverters combined via a single transformer should be analysed with the variation of phase relative to a.c. bus.

5. So far time dependent quasi one dimensional equations are considered for the solution of MHD flow in the duct as discussed in section 5.3. The present analysis should be extended with accurate time dependent two and three dimensional equations. These approaches in numerical analysis can be made so that a comparison on the results is obtained. These calculations should include effect of varying magnetic field, dynamic coupling of electrodes, end effects and electrode effects as mentioned in section 2.2.1.

6. Analogue models of the MHD generator are very useful [31] for many types of study which cannot be conveniently carried out.with digital technique. Therefore the MHD

xL

simulation in the laboratory shall be replaced by analogue model for better results.

7. The study presented is related with a single electrode pair analysis. Therefore more inverters will be needed for the power transfer to infite bus. For the reduction of inverters the voltage consolidation circuits be included for the analysis.

The above recommended work would significantly increase the under standing of the operational characteristics and stability of large MHD-inverter utility interactive power system. These proposed investigations are only a few of the many possible direct extension of the study presented in this thesis. Since the integration of an MHD generator into a conventional a.c. network is a very new and challenging engineering problem, the number of areas that still require much study are innumerable.

REFERENCES

1. J.B. Heywood and G.J. Womack, Open Cycle MHD Power Generation, Pergamon Press, London, 1969.

2. Marsha Freeman, Doubling energy efficiency by direct conversion. Fusion, April 1980, Fusion Energy Foundation, NY, USA.

3. R.J. Rosa, Magnetohydrodynamic energy conversion. Mc Graw Hill, New York, 1968.

4. R.J. Rosa, Experimental Magnetohydrodynamic Power Generator. Journal of Applied Physics, 31 : 735-736, April 1960.

5. R.J. Rosa, Physical Principles of Magnetohydrodynamic Power Generator. Physics of Fluids, 4 : 182-194, February, 1961.

6. 1981 Status Report, MHD Electrical Power Generation (UNESCO International Liaision Group)

7. Mohibullah, M. Salman Beg, M.S. Jamil Asghar and M.A. Jani, MHD Generation for Better Environmental Control and Cheaper Electrical Power. Indian Congress on Engineering and Environment, November 10, 1985, New Delhi.

8. G.R. Seikel, R.J. Sovie, R.K. Burns, G.J. Barna, J.A. Burkhart, J.J. Nainiger and J.M. Smith. A summary of the ECAS performance and cost results from MHD systems. Proceedings 15th Symposium on Engg. Aspects of MHD, Philadelphia, 1976.

9. J.W. Griswold, J.W. Moyer and M.C. Wehrey. The retrofit approach to MHD demonstration and commertialization. Proc. 18th Symposium on Engg. Aspects of MHD, Butte, Montana, 1979.

10. F.M. Shelkov, S.I. Pishchikov, M.S. Pinkhasik and Yu.A. Zakharko. Some Results of Researching the Application of Magnitohydrodynamics in Power Engineering. Magneto-hydrodynamics, Vol. 13, No. 4, 1977.

11. W.D. Jackson and E. Levi Magnetohydrodynamic Power Generation : Programme, Planning and Status. IEEE Trans. on Power Apparatus and Systems, Vol. PAS-98, No. 6, 1979.

12. H.K. Messerle, Magnetohydrodynamics or electricity from hot gas jets. Report, University of Sydney, Australia, July 1981.

13. K. Okazaki, A. Yuki, M. Uemura and K. Ohtake, Experimental study on combustion and NOx formation Mechanisms of pulverised coal. Specialists Meeting on Coal-Fired MHD Power Generation, Sydney, 1981.

14. T.P. Lynch, J.A. Cooper, J.L. Casey and J.A. Winkleman. Environmental studies for the low mass flow test series (1982-83) at the DOE coal fired flow facility. Proceedings 22nd Symposium on Engg. aspects of MHD, Mississippi, USA, 1984.

15. M. Petrick and Ya, Shumatsky. Open-cycle MHD Electric Power Generation. Argonne National Laboratory, Argonne, 1978.

16. V.A. Kirillin, A.E. Sheindlin, E.M. Shelkov, S.I. Pischikov, B. Ya. Shumiatsky and Yu. N. Sokolov. Principle Directions of Investigations and Development works on Elaboration of a coal fired MHD power plant in the USSR. Specialists Meeting on Coal-Fired MHD Power Generation, Sydney, 1981.

17. K. Takano, K. Ohtake, Y. Aiyama and H. Kaminosono. Conceptual Design of 2000 MWt Coal Fired MHD Plant. Specialists Meeting on Coal-Fired MHD power Generation, Sydney, 1981.

18. Zhang Mingyao, Wei Qidong, Yao Weiwen Xu Yigian, Li Fuan and Cai Ruihong. A Direct Coal Fired MHD Test Facility Specialists Meeting on Coal-Fired MHD Power Generation, Sydney, 1981.

19. S. Cervenka and R.A. Van der Laken. Results from study of a 500 MWe Coal fired closed cycle MHD plant. Eight International Conference on MHD Electrical Power Generation, Volume 1, Moscow, 1983.

20. Yan Changgi, Zu Zi-Xiang, Li Gang, Chou Kua, Chong Xi-ing, Chen Yuan-Li, Yang Ai-hua, Dong Cheng-Kang, Huang Li, Sha Ci-Wen, Wang Shi-Ying, Zhong Xing, Liang Chui-fang and He Xue-qiu. The Preliminary Investigations of the coal fired MHD Power Generation. Eight International Conference on MHD Electrical Power Generation, Volume 1, Moscow, 1983.

21. H.K. Messerle, S.W. Simpson, B. Campbell, S. Ramakrishnan, S. Marty, M. Rados, R.R. Rankin and J.D. Scott. MHD Studies in Australia, Eighth International Conference on MHD Electrical Power Generation, Volume 1, Moscow, 1983.

22. R.L. Lawit, M.L.R. Murthy, J.C. Cutting, W.R. Owens and P.R. Sheth. Recent Studies on MHD systems : Baseline plant and part load performance. Proceedings 22nd Symposium on Engg. Aspects of MHD, Mississippi, 1984.

23. V.R. Rama Prasad. Design and development of a conceptual MHD/steam power plant for western India. Proceedings 22nd Symposium on Engg. Aspects of MHD, Mississippi, 1984.

24. S. Sridharan. Pilot Plant for MHD power generation. Research Programme of Bharat Heavy Electricals Limited (India). Proceedings 22nd Symposium on Engg. Aspects of MHD, Mississippi, 1984.

25. Y. Kusaka, K. Takano, K. Kato, Y. Kaga, Y. Aiyama, T. Imatake, Y. Fukaya and I. Osada. Experiments of ETL Mark VII MHD Facility. Proceedings 22nd Symposium on Engg. Aspects of MHD, Mississippi, 1984.

26. H. Yamasaki, S. Kabashima, Y. Yoshikawa, N. Harada, Y. Okuno, T. Okamura, Y. Hasegawa, T. Yokota, Ishimura, K. Matsutani, and T. Sasaki. Recent results of power Generation Experiments with the Fuji - 1 Facility Proceedings 22nd Symposium on Engg. Aspects. of MHD, Mississippi, 1984.

27. C. St. J. Lamb, S. Ramakrishnan and H.K. Misserle. A. Rotary Inverter system for a Multiple Electrode MHD Generator. Proceedings 18th Symposium on Engg. Aspects of MHD, Butte, Montana, 1979.

28. D.T. Trung, H.K. Messerle, S. Ramakrishnan and S. Marty. Operating Regions for MHD Generator Inverter Links. 7th International Conference on MHD electrical power generation MIT, Cambridge, 1980.

29. S. Ramakrishnan, V.J. Gosbell and T. Kearney. Inverter Systems for MHD Generator. Report EEC 82.5, School of Electrical Engineering University of Sydney, Dec. 1982.

30. A. Valfells. Conceptual design of an MHD Motor. Proceedings of 22nd Symposium on Engg. Aspects of MHD, Mississippi State University, Starkville, Mississippi, 1984.

31. D.T. Trung. System Analysis of the Integration of a Segmented MHD Generator into an A.C. Power Network. Ph.D. Thesis, University of Sydney, 1981.

32. B.M. Antonov, A.D. Iserov, V.A. Labuntsov, G.I. Mal'tsev, C.I. Pishchikov. A Study of an Inverter with series capacitive Compensation for Operation in Conjunction with MHD Generator. Proceedings of 7th International Conference on MHD Electrical Power Generation, Vol. 1, Massachusetts, 1980.

33. Xu Yi-Qian, Zhao Yi-Yu, Fang Yi-Lin, Yao Wei-Wen, Wan Cai-Chun, Fang Qiu-Hua. JS-1 MHD power generation experimental installation and the investigation of its inverter system for a segmented Faraday Channel. Proceedings of 7th International Conf. on MHD Elect. Power generation, Vol. 1, Massachusetts, 1980.

34. D.T. Trung, Prof. H.K. Messerle, Electrical operating and stability region for MHD generator/inverter link. Proceedings IEE, Vol. 128 Pt C No. 1, January 1981.

35. S. Matair, S. Ramakrishnan, V.J. Goskell, T. Kearney and H.K. Messerle, Performance of a line commutated Inverter system for a multiple electrode MHD generator. 8th International Conference on MHD Electrical Power Generation, Moscow, 1983.

36. J.K. Koester, P. Wood, L.C. Farrar and R.J. Ferraro, Integrated MHD generator inverter system test results at CDIF. Proceedings of 21st symposium on Engg. Aspects of MHD, Argonne National Laboratory Argonne, Illinois, 1983.

37. S. Matair and S. Ramakrishnan, Stability Study of an Inverter Controller for an MHD Generator. Proceedings of 22nd Symposium on Engg. Aspects of MHD, Mississippi, Starkville, 1984.

38. C.K. Peterson, L. Barnett, L. Stephenson, M.H. Scott, Inverter development at UTSI. Proceedings of 17th Symposium on Engg. Aspects of MHD, Stanford, California, 1978.

39. AVCO Everett Research Laboratory Inc., Open-Cycle MHD Generator Inverter Interaction Test. EPRI Contract Research Report RP 642-1, Palo Alto, California, 1978.

40. A. Chaffee, I. Quijano, A. Solbes, A. Humphrey and J. Manalakas, Design, Construction and Initial operation of an MHD inverter System for the mark VI Generator. Proceedings of 18th Symposium on Engg. Aspects of MHD, Butte, Montana, 1979.

41. Emerson R. Ray and Dr. Robert Schainker, Inverter System Development for MHD Application. 7th International Conference on MHD Electrical power generation, MIT, Cambridge, 1980.

42. AVCO Everett Research Laboratory Inc., Open Cycle MHD Power Conditioning and Control Requirements Definition EPRI Research Report, AP-1345, Palo Alto, California, 1980.

43. S. Petty and K. Williams, Magnetohydrodynamic Bulk Power Inverter and Control System Part II Description of the Mark VI Inverter. Power Conversion International March 1981, pp. 67-70.

44. M. Sundgren and I. Ruohonew, Force Commutated MHD-Inverter. 8th International Conference on MHD Electrical Power Generation, Moscow, 1983.

45. S. Petty and K. Williams, Magnetohydrodynamic Bulk Power Inverter and Control System. Power Conversion International, Feb. 1981, pp 36-47.

46. K. Crisafulli, K. Morcotte, R. Johnson, and B. Jordon, A computer controlled electrode consolidation force commutated three phase inverter system for MHD power generation. Proceedings of 19th Symposium on Engg.. Aspects of MHD, UTSI, Tallahoma, N.J. 15-17, 1981.

47. Z.N. Celisnki, Electrical Equivalent Circuits of D.C. MHD Generators. Advance Energy conversion, Vol. 7, pp. 67-75, Pergaman Press, 1967, U.K.

48. W.D. Stevenson, Eliments of Power System Analysis. Mc Graw Hill, Kogakusha Ltd. Third Edition, 1970.

49. E.W. Kimbark, Power System Stability, Vol. 1, John Wiley and Sons Inc., New York, 1956.

50. M. Ramamorty, An Introduction to Thysistors and their Applications. Affiliated East-West Press, Pvt. Ltd. New Delhi, 1977.

51. E.W. Kimbark, Direct Current Transmission. Volume 1, Wiley Interscience, New York, 1971.

52. E. Barnitz, Harmonics in Electrical Circuits and their Reduction Through Filter Circuits. C.I.G.R.E. Vol. III, 1958.

53. Mohibullah and K.P. Basu, Computerised Evaluation of the Magnetising Inrush Current in Transformers. Electric Power Research Journal, Vol. 2, No. 3, November 1979, Swtizerland.

54. J.D. Ainsworth and F.G. Goodrich, Design of Harmonic filter for H.V.D.C. Transmission systems. International Conference on large Electric Systems, 20th Meeting, C.I.G.R.E. Vol. III, 1964, pp 14-25.

55. Engineering recommendation G 5/2, Supplies to converter Equipment, 39th Chief Engineers Conference REQ 23 Aug. 1971, Electricity Councils (Australia).

56. F. Rodrigues and T.H. Barton, A Mc Murray Inverter Controller, IEEE Trans. On Industrial Electronics and Control Instrumentation, Vol. IECI-26, No. 3, August,1976.

57. W. Mc Murray, SCR Inverter Commutated by an auxiliary impulse, IEEE Trans. Communication Electronics, Vol. 83, pp, 824-829,1981.

58. B.D. Bedford and R.G. Hoft, Principles of Inverter Circuits, John Wiley and Sons, New York, 1964.

59. L.J. Penkowski and K.E. Pruzinsky, Fundamentals of a pulse width modulated power circuits, fifth annual

meeting of Industry and general applications group, pp. 669-678, 1970.

60. W. Mc Murray, Optimum snubbers for power semiconductors, IEEE Conference Record of Sixth Annual Meeting of Industry and applications Group, pp. 885-893, 1971.

61. L.M. Faulkenberry, How to snub thyristors, Power Conversion International, Feb., 1983, pp. 11-13.

62. H.B. Dwight, Electrical Coils and Conductors, McGraw Hill.

63. Terman, Radio Engineers Handbook, McGraw Hill.

64. P.N. Murgatroyd, Frequency dependent inductance and resistance of foil conductor loops, Proc. IEE, Vol. 124, No. 5, May 1977.

65. T. Kearney, Professional Officer, School of Electrical Engineering, University of Sydney, Private Communication.

66. T. Krishnan and B. Ramaswami, A Fast Response DC Motor Speed Control System, IEEE Trans. on Industry Applications, Volume IA-10, September/October 1974.

67. R. Hernandez Millan, J.P. Sucena Paiva and L.L. Freris, Modelling of controlled rectifiers in feedback systems, IEEE Trans. Power Apparatus and systems, Vol. PAS-93, No. 1, 1974.

68. N.A. Bjaresten. The static converter as a high speed power rectifier, Direct current, Vol. 8, No. 6, 1963.

69. F. Fallside and A.F. Farmer. Ripple instability on closed loop control systems with thyristor amplifiers, Proc. IEE, Vol. 114, No. 1, 1967.

70. P.A. Hazell and J.O. Flower. Stability properties of certain thyristor bridge control system, Part I, Proc. IEE, Vol. 117, No. 7, 1970.

71. M. Ramamoorty, Visting Fellow, School of Electrical Engineering, University of Sydney, Private Communication.

72. W.D. Jackson, W.E. Feero, W. Gish and G.R. Seikel. Integration of MHD Plants into electric Utility Systems, 22nd Symposium on Engineering Aspects of MHD, June 26-28, 1984, Mississippi, USA, pp. 9.1.1 to 9.1.24.

73. D.A. Oliver, The Time Dependent MHD Generator. Proc. 14th Symposium on Engineering Aspects of MHD, Tullahoma, Tennessee, pp. V 5.1-V 5.9, 1974.

74. D.R. Wilson, and C.S. Stewart, Analysis of Transient MHD Channel Flows by a Hybrid Lax-Wendroff Method of Characteristics Computer Code. Proc. 20th Symposium on Engineering Aspects of MHD, University of California, Irvine, pp. 14.5.1-14.5.5, 1982.

75. R. Johnson, P. Mackin, and B. Jordon. Step Response of a Globally Controlled Faraday Connected MHD Generator System. Proc. 20th Symposium on Engineering Aspects of MHD, University of California, Irvine, pp. 12.9.1-12.9.5, 1982.

76. G.W. Shutton and A. Sherman, Engineering Magneto hydrodynamics, Mc Graw Hill Book Company, New York, 1965.

77. J.F. Louis, J. Lothrop and T.R. Brogan. Fluid Dynamic Studies with a Magnetohydrodynamic Generator. Physics of Fluids, Vol. 7, No. 3, 1964.

78. K. Fushimi, T. Homma, S. Ikeda, K. Onda, K. Takano, Y. Kusaka, H. Hosaka, M. Furuyama, Y. Kaga, K. Kato and M. Amano. Experimental Study on an MHD Generator with ETL Mark II. Electrical Engineering in Japan, Vol. 95, No. 2, 1975.

79. Y. Kusako, T. Masuda, S. Ideda and T. Honda. Experiment on MHD Generator with a large-scale superconducting magnet (ETL Mark V) Proc. 16th Symposium on Engineering Aspects of MHD, Pennsylvania, 1977.

80. V.A. Bityurin, A.D. Iserov, V.I. Kovbasynk, S.A. Medin, D.S. Pinkhasik and B. Ya. Shumyatskii. Some Results on Gasdynamics and Electrodynamics Investigation of U-25 Faraday MHD Generator. Proc. 6th Int. Conference on MHD Electrical Power Generation, Vol. II, Washington, DC, 1975.

81. V.A. Bilyurin, V.A. Zhelnin, G.A. Yubimov and S.A. Medin. Comparison of Results of Calculation of Flow in an MHD Generator with Experimental data obtained on the U-25 device. High Temperature, Vol. 16, No. 4, 1978.

82. P.J. Roache. Computational Fluid Dynamics. Hermosa Publishers, Albuquerque, New Mexico, 1972.

83. S. Matair, School of Electrical Engineering, University of Sydney, Private Communication.

84. G.N. Vinogradova and V.P. Panchenko, Numerical study of Unsteady Processes in a Faraday MHD Generator. High Temperature, Vol. 19, No. 1, pp. 127-133, 1981.

85. R.R. Rankin, Insulating Wall boundary Layers in MHD Generators. Topical Report Standford University, Stanford, California, 1978.

86. P. Wood, Switching Power Converters. Van Nostrand Reinhold Company, New York, 1969.

A P P E N D I C E S

APPENDIX - A

Simple programs are developed directly from the equations derived in sections 2.3.3 and 2.4.2. The computational technique adopted for these programs have been described in section 2.5 and also a sample flow chart is prepared.

A record of all such computer program is listed below.

In order to keep the length of this thesis to a reasonable limit, only few of these programs are listed.

Table A-1 List of stored program

```
catlist,
 CATALOG OF 7977735          FM/DINGO   83/04/28. 13.51.24.

 INDIRECT ACCESS FILE($)

 ABC       MHD4      SHNLT     (MHDCNP4) (MO7)     (PHPLT22) (PLTPHS7)
 AUTOCN1   MINIT     SUB       (MMP)     (MO8)     (PHSPLT8) (PLT1)
 BABC      MLT       SUB1      (MOHB)    (MO9)     (PHSPLT9) (PLT2)
 BMHD1     PHPLT23   THESIS    (MOMIB10) (MPH)     (PHSPL10) (PL1)
 BMHD4     PHSLT7    (CNTB)    (MOHIB2)  (M)       (PHSPL11) (PMH)
 BMINIT    PHSPLT7   (CNTD1)   (MOHIB3)  (MP2)     (PHSPL12) (PUVALUE)
 IDATA     PHS7      (CURNT3)  (MOHIB6)  (MP3)     (PLOTIT)  (PUM1CN)
 JOB       POPLOT    (FPLOT9)  (MOHIB7)  (MP4)     (PLOTIT1) (PUM1CN1)
 MDATA     POPLOTT   (HPLT29)  (MOHIB8)  (MT3)     (PLOTIT2) (PUM1CN2)
 MDATA3    POPLOT1   (LINPLT1) (MOHIB9)  (OPL)     (PLTPHS1) (PUM1CN3)
 MDATA4    POPLOT2   (LOP)     (MO1)     (OPT)     (PLTPHS2) (PUM1CN4)
 MHDCNP    POPLOT3   (M)       (MO10)    (PANTO1)  (PLTPHS3) (SHFPLT3)
 MHD1      PUN       (MHDCNP1) (MO2)     (PHPLT20) (PLTPHS5) (SHFPLT4)
 MHD2      PUM1      (MHDCNP2) (MO6)     (PHPLT21) (PLTPHS6) (SHFTCN2)
 MHD3      SHFPLT2   (MHDCNP3)

   INDIRECT FILES :        34 ON-LINE,        67 ARCHIVED.
      TOTAL PRUS :       451 ON-LINE,       163 ARCHIVED.
```

List A-2 Program for variation in Electrical Parameters with phase shift.

```
PROGRAM   PHSPLT1

00100 PROGRAM PHSPLT(OUTPUT,TAPE6=OUTPUT)
00110 DIMENSION D(99),DM(99),AID(99),VD(99),E1(99),PD(99),P(99),QS(99)
00120 PB=(V0**2)/(4.0*R0)
00130 VB=V0/(2.0)
00140 AIB=V0/(2.0*R0)
00150 DATA EB,V0,XL,R0/20.21,45.0,27.135,24.0/
00160 PAI=4.0*ATAN(1.0)
00170 WRITE(6,3)
00180 3 FORMAT(29X,62("="))
00190 WRITE(6,4)
00200 4 FORMAT(32X,"PHASE",4X,"MHD",6X,"MHD",7X,"INV.",5X,"MHD",
00210+ 6X,"INV.",6X,"INV.")
00220 WRITE(6,5)
00230 5 FORMAT((32X,"SHIFT",2X,"CURRENT",3X,"VOLTAGE",3X,"VOLTAGE",
00240+2X,"POWER",4X,"POWER",6X,"REP")/)
00250 DO 10 I=1,19
00260 WRITE(6,13)
00270 13 FORMAT(29X,62("-"))
00280 D(I)=(I-1)*PAI/18.0
00290 AID(I)=(3.0*SQRT(2.0)/PAI)*(EB/XL)*SIN(D(I))
00300 VD(I)=(V0-AID(I)*R0)
00310 E1(I)=(SQRT(2.0)/PAI)*VB(I)
00320 PD(I)=VD(I)*AID(I)
00330 PD(I)=PD(I)/PB
00340 P(I)=(3.0/XL)*E1(I)*EB*SIN(D(I))
00350 P(I)=P(I)/PB
00360 QS(I)=1.0/XL*((E1(I)**2)-(E1(I)*EB*COS(D(I))))
00370 QS(I)=QS(I)/PB
00380  QS(I)=QS(I)*3.0
00390 AID(I)=AID(I)/AIB
00400 VD(I)=VD(I)/VB
00410 E1(I)=E1(I)/VB
00420 DM(I)=D(I)*180.0/PAI
00430 WRITE(6,20)DM(I),AID(I),VD(I),E1(I),PD(I),P(I),QS(I)
00440 20 FORMAT(30X,F5.1,6(3X,F6.2))
00450 10 CONTINUE
00460 WRITE(6,15)
00470 15 FORMAT(29X,62("-"))
00480 STOP
00490 END
READY.
```

Table A-3 Computation of Electrical parameters with phase shift.

$X_S = 0.225$ PU

PHASE SHIFT	MHD CURRENT	MHD VOLTAGE	INV. VOLTAGE	MHD POWER	INV. POWER	INV. REP
0.0	0.00	2.00	.90	0.00	0.00	.01
10.0	.37	1.63	.73	.61	.61	-.59
20.0	.73	1.27	.57	.93	.93	-.83
30.0	1.07	.93	.42	.99	.99	-.80
40.0	1.38	.62	.28	.86	.86	-.61
50.0	1.64	.36	.16	.59	.59	-.35
60.0	1.86	.14	.06	.26	.26	-.13
70.0	2.02	-.02	-.01	-.03	-.03	.01
80.0	2.11	-.11	-.05	-.24	-.24	.06
90.0	2.15	-.15	-.07	-.31	-.31	.02
100.0	2.11	-.11	-.05	-.24	-.24	-.03
110.0	2.02	-.02	-.01	-.03	-.03	-.01
120.0	1.86	.14	.06	.26	.26	.17
130.0	1.64	.36	.16	.59	.59	.63
140.0	1.38	.62	.28	.86	.86	1.43
150.0	1.07	.93	.42	.99	.99	2.65
160.0	.73	1.27	.57	.93	.93	4.28
170.0	.37	1.63	.73	.61	.61	6.29
180.0	.00	2.00	.90	.00	.00	8.59

Table A-4 Computation of Electrical parameters with phase shift.

X_s = 0.45 PU.

PHASE SHIFT	MHD CURRENT	MHD VOLTAGE	INV. VOLTAGE	MHD POWER	INV. POWER	INV. REP
0.0	0.00	2.00	.90	0.00	0.00	.01
10.0	.19	1.81	.82	.34	.34	-.15
20.0	.37	1.63	.74	.60	.60	-.21
30.0	.54	1.46	.66	.79	.79	-.21
40.0	.69	1.31	.59	.90	.90	-.15
50.0	.82	1.18	.53	.97	.97	-.07
60.0	.93	1.07	.48	.99	.99	.04
70.0	1.01	.99	.45	1.00	1.00	.16
80.0	1.06	.94	.42	1.00	1.00	.30
90.0	1.07	.93	.42	.99	.99	.46
100.0	1.06	.94	.42	1.00	1.00	.65
110.0	1.01	.99	.45	1.00	1.00	.89
120.0	.93	1.07	.48	.99	.99	1.19
130.0	.82	1.18	.53	.97	.97	1.56
140.0	.69	1.31	.59	.90	.90	2.00
150.0	.54	1.46	.66	.79	.79	2.51
160.0	.37	1.63	.74	.60	.60	3.08
170.0	.19	1.81	.82	.34	.34	3.69
180.0	.00	2.00	.90	.00	.00	4.30

Table A-5 Computation of Electrical parameters with phase shift.

X_s = 0.90 PU.

PHASE SHIFT	MHD CURRENT	MHD VOLTAGE	INV. VOLTAGE	MHD POWER	INV. POWER	INV. REP
0.0	0.00	2.00	.90	0.00	0.00	.00
10.0	.09	1.91	.86	.18	.18	-.03
20.0	.18	1.82	.82	.33	.33	-.03
30.0	.27	1.73	.78	.46	.46	.00
40.0	.34	1.66	.75	.57	.57	.06
50.0	.41	1.59	.72	.65	.65	.13
60.0	.46	1.54	.69	.71	.71	.22
70.0	.50	1.50	.67	.75	.75	.33
80.0	.53	1.47	.66	.78	.78	.45
90.0	.54	1.46	.66	.79	.79	.58
100.0	.53	1.47	.66	.78	.78	.72
110.0	.50	1.50	.67	.75	.75	.88
120.0	.46	1.54	.69	.71	.71	1.05
130.0	.41	1.59	.72	.65	.65	1.23
140.0	.34	1.66	.75	.57	.57	1.42
150.0	.27	1.73	.78	.46	.46	1.61
160.0	.18	1.82	.82	.33	.33	1.80
170.0	.09	1.91	.86	.18	.18	1.98
180.0	.00	2.00	.90	.00	.00	2.15

List A-6 Program for variation in real and reactive power with change internal resistance from operating point.

```
PROGRAM   PHPLT17

00100 PROGRAM PHSPLT(OUTPUT,TAPE6=OUTPUT)
00110 DIMENSION D(99),DM(99),AID(99),VD(99),E1(99),PD(99),P(99),QS(99)
00120+,DR(99),DP(99),DQ(99),R(99),V(99)
00130 PB=28.10524
00140 AIB=1.0821
00150 VB=25.97
00160 DATA EB,XL/23.38,31.575/
00170 R0=18.0
00180 V0=38.96
00182 DV=12.985
00190 DO 31 J=1,3
00200 V(J)=V0+(J-1)*DV
00210 WRITE(6,26)V(J)
00220 26 FORMAT(40X,"V0=",F6.2,2X,"VOLTS")
00230 WRITE(6,2)
00240 2 FORMAT(29X,36("=")/)
00250 WRITE(6,4)
00260 4 FORMAT(32X,"S.NO.",3X,"DR",6X,"DP",8X,"DQ")
00270 WRITE(6,5)
00280 5 FORMAT(29X,36("-"))
00290 AK=0.45
00300 PAI=4.0*ATAN(1.0)
00310 DO 10 I=1,21
00320 D(I)=PAI/3.0
00330 R(I)=R0+(I-1)*0.6
00340 AID(I)=3.0*AK*EB*SIN(D(I))/XL
00350 VD(I)=(V(J)-AID(I)*R(I))
00360 E1(I)=AK*VD(I)
00370 PD(I)=VD(I)*AID(I)
00380 P(I)=(3.0/XL)*E1(I)*EB*SIN(D(I))
00390 QS(I)=1.0/XL*((E1(I)**2)-(E1(I)*EB*COS(D(I))))
00400 PD(I)=PD(I)/PB
00410 P(I)=P(I)/PB
00420 QS(I)=QS(I)*3.0
00430 QS(I)=QS(I)/PB
00440 AID(I)=AID(I)/AIB
00450 VD(I)=VD(I)/VB
00460 E1(I)=E1(I)/VB
00470 DA(I)=D(I)*180.0/PAI
00480 10 CONTINUE
00490 DO 30 I=1,21
00500 DR(I)=(R(11)-R(I))/R(11)
00510 DP(I)=(P(11)-P(I))/P(11)
00520 DQ(I)=(QS(11)-QS(I))/QS(11)
00530 WRITE(6,40) I,DR(I),DP(I),DQ(I)
00540 40 FORMAT(30X,I4,3(3X,F5.3))
00550 WRITE(6,28)
00560 28 FORMAT(29X,36("-"))
00570 30 CONTINUE
00580 31 CONTINUE
00590 STOP
00600 END
READY.
```

Table A-7 Computation of real and reactive power for ± 25% change in internal resistance.

V_o = 2.0 PU, 60° phase shift

PHASE SHIFT	MHD CURRENT	MHD VOLTAGE	INV. VOLTAGE	MHD POWER	INV. POWER	INV. REP	p. Change in R_o
60.0	.80	1.40	.63	1.12	1.12	.26	0.25
60.0	.80	1.38	.62	1.10	1.10	.24	0.23
60.0	.80	1.36	.61	1.09	1.09	.23	0.20
60.0	.80	1.34	.60	1.07	1.07	.21	0.18
60.0	.80	1.32	.59	1.06	1.06	.20	0.15
60.0	.80	1.30	.59	1.04	1.04	.18	0.13
60.0	.80	1.28	.58	1.02	1.02	.17	0.10
60.0	.80	1.26	.57	1.01	1.01	.15	0.08
60.0	.80	1.24	.56	.99	.99	.14	0.05
60.0	.80	1.22	.55	.98	.98	.12	0.03
60.0	.80	1.20	.54	.96	.96	.11	0.00
60.0	.80	1.18	.53	.94	.94	.10	0.02
60.0	.80	1.16	.52	.93	.93	.09	0.05
60.0	.80	1.14	.51	.91	.91	.07	0.07
60.0	.80	1.12	.50	.90	.90	.06	0.10
60.0	.80	1.10	.50	.89	.89	.05	0.12
60.0	.80	1.08	.49	.86	.86	.04	0.15
60.0	.80	1.06	.48	.85	.85	.03	0.17
60.0	.80	1.04	.47	.83	.83	.02	0.20
60.0	.80	1.02	.46	.82	.82	.01	0.22
60.0	.80	1.00	.45	.80	.80	.00	0.25

Table A-8 Computation of real and reactive power for ± 25% change in internal resistance

V_o = 2.5 PU , 60° phase shift

PHASE SHIFT	MHD CURRENT	MHD VOLTAGE	INV. VOLTAGE	MHD POWER	INV. POWER	INV. REP
60.0	.80	1.90	.86	1.52	1.52	.79
60.0	.80	1.88	.85	1.50	1.50	.77
60.0	.80	1.86	.84	1.49	1.49	.74
60.0	.80	1.84	.83	1.47	1.47	.71
60.0	.80	1.82	.82	1.46	1.46	.69
60.0	.80	1.80	.81	1.44	1.44	.67
60.0	.80	1.78	.80	1.42	1.42	.64
60.0	.80	1.76	.79	1.41	1.41	.62
60.0	.80	1.74	.78	1.39	1.39	.60
60.0	.80	1.72	.77	1.38	1.38	.57
60.0	.80	1.70	.77	1.36	1.36	.55
60.0	.80	1.68	.76	1.34	1.34	.53
60.0	.80	1.66	.75	1.33	1.33	.51
60.0	.80	1.64	.74	1.31	1.31	.49
60.0	.80	1.62	.73	1.30	1.30	.46
60.0	.80	1.60	.72	1.28	1.28	.44
60.0	.80	1.58	.71	1.26	1.26	.42
60.0	.80	1.56	.70	1.25	1.25	.40
60.0	.80	1.54	.69	1.23	1.23	.38
60.0	.80	1.52	.68	1.22	1.22	.37
60.0	.80	1.50	.68	1.20	1.20	.35

Table A-9 Computation of real and reactive power for ± 25% change in internal resistance

V_o = 2.0 PU, 30° phase shift

PHASE SHIFT	MHD CURRENT	MHD VOLTAGE	INV. VOLTAGE	MHD POWER	INV. POWER	INV. REP
30.0	.46	1.65	.74	.76	.76	-.06
30.0	.46	1.64	.74	.76	.76	-.07
30.0	.46	1.63	.73	.75	.75	-.08
30.0	.46	1.62	.73	.75	.75	-.08
30.0	.46	1.61	.72	.74	.74	-.09
30.0	.46	1.60	.72	.74	.74	-.10
30.0	.46	1.59	.71	.73	.73	-.11
30.0	.46	1.57	.71	.73	.73	-.12
30.0	.46	1.56	.70	.72	.72	-.12
30.0	.46	1.55	.70	.72	.72	-.13
30.0	.46	1.54	.69	.71	.71	-.14
30.0	.46	1.53	.69	.71	.71	-.14
30.0	.46	1.52	.68	.70	.70	-.15
30.0	.46	1.50	.68	.69	.69	-.16
30.0	.46	1.49	.67	.69	.69	-.17
30.0	.46	1.48	.67	.68	.68	-.17
30.0	.46	1.47	.66	.68	.68	-.18
30.0	.46	1.46	.66	.67	.67	-.18
30.0	.46	1.45	.65	.67	.67	-.19
30.0	.46	1.44	.65	.66	.66	-.20
30.0	.46	1.42	.64	.66	.66	-.20

Table A-10 Computation of real and reactive power for ± 25% change in internal resistance.

V_o = 2.0 PU, 30° phase shift.

PHASE SHIFT	MHD CURRENT	MHD VOLTAGE	INV. VOLTAGE	MHD POWER	INV. POWER	INV REP
30.0	.46	2.15	.97	1.00	1.00	.42
30.0	.46	2.14	.96	.99	.99	.41
30.0	.46	2.13	.96	.98	.98	.39
30.0	.46	2.12	.95	.98	.98	.38
30.0	.46	2.11	.95	.97	.97	.37
30.0	.46	2.10	.94	.97	.97	.35
30.0	.46	2.09	.94	.96	.96	.34
30.0	.46	2.07	.93	.96	.96	.33
30.0	.46	2.06	.93	.95	.95	.31
30.0	.46	2.05	.92	.95	.95	.30
30.0	.46	2.04	.92	.94	.94	.29
30.0	.46	2.03	.91	.94	.94	.28
30.0	.46	2.02	.91	.93	.93	.26
30.0	.46	2.00	.90	.93	.93	.25
30.0	.46	1.99	.90	.92	.92	.24
30.0	.46	1.98	.89	.92	.92	.23
30.0	.46	1.97	.89	.91	.91	.22
30.0	.46	1.96	.88	.90	.90	.20
30.0	.46	1.95	.88	.90	.90	.19
30.0	.46	1.94	.87	.89	.89	.18
30.0	.46	1.92	.87	.89	.89	.17

```
 82/02/10. 15.37.04.
PROGRAM   PHPLT25

00100 PROGRAM PHSPLT(OUTPUT,TAPE6=OUTPUT)
00110 DIMENSION D(99),DM(99),AID(99),VD(99),E1(99),PD(99),P(99),QS(99)
00120+,R(99),V(99),DR(99),PP(99)
00130 DATA PB,AIB,VB,AK,PREF/28.10524,1.0821,25.97,0.45,1.0/
00140 RB=VB/AIB
00150 DATA EB,XL/23.38,31.575/
00160 DATA V0,R0/38.93,18.0/
00170 PAI=4.0*ATAN(1.0)
00180 DO 39 J=1,3
00190 V(J)=V0+(J-1)*12.9925
00200 WRITE(6,3)
00210 3 FORMAT(29X,62("="))
00220 WRITE(6,4)
00230 4 FORMAT(32X,"PHASE",5X,"MHD",6X,"MHD",6X,"INV.",5X,"MHD"
00240+,6X,"INV.",6X,"INV.")
00250 WRITE(6,5)
00260 5 FORMAT((32X,"SHIFT",2X,"CURRENT",3X,"VOLTAGE",3X,"VOLTAGE"
00270+,2X,"POWER",4X,"POWER",6X,"REP")/)
00280 DO 10 I=1,21
00290 ITER=0
00300 WRITE(6,12)
00310 12 FORMAT (29X,62("-"))
00320 D(I)=PAI/3.0
00330 R(I)=R0+(I-1)*.6
00340 GOTO 25
00350 15 D(I)=D(I)+PAI/180.0
00360 GOTO 25
00370 21 D(I)=D(I)-PAI/180.0
00380 25 AID(I)=3.0*AK*EB*SIN(D(I))/XL
00390 VD(I)=(V(J)-AID(I)*R(I))
00400 E1(I)=AK*VD(I)
00410 PD(I)=VD(I)*AID(I)
00420 PD(I)=PD(I)/PB
00430 P(I)=(3.0/XL)*E1(I)*EB*SIN(D(I))
00440 P(I)=P(I)/PB
00450 QS(I)=1.0/XL*((E1(I)**2)-(E1(I)*EB*COS(D(I))))
00460 QS(I)=QS(I)*3.0
00462 IF(J-2)89,89,99
00470 89 IF(I-5)99,99,91
00480 91 ITER=ITER+1
00490 PP(ITER)=P(I)
00500 IF(ITER.EQ.1) GOTO 99
00510 IF(PP(ITER).LE.PP(ITER-1)) GOTO 31
00520 99 IF(VB(I)) 31,31,33
00530 33 IF(D(I))31,31,32
00540 32 IF(D(I)-PAI/2.0)35,31,31
00550 35 IF(ABS(P(I)-PREF)-.04)31,31,34
00560 34 IF(P(I)-PREF)15,31,21
00570 31 QS(I)=QS(I)/PB
00580 AID(I)=AID(I)/AIB
00590 VD(I)=VD(I)/VB
00600 E1(I)=E1(I)/VB
00610 DR(I)=(R(I)-R0)/RB
00620 DM(I)=D(I)*180.0/PAI
00630 WRITE(6,20)DM(I),AID(I),VD(I),E1(I),PD(I),P(I),QS(I)
00640+,DR(I)
00650 20 FORMAT(30X,F5.1,7(3X,F6.2))
00660 10 CONTINUE
00670 WRITE(6,13)
00680 13 FORMAT(29X,62("-"))
00690 30 CONTINUE
00700 STOP
00710 END
00720 $
```

List A-11 Program for control power to A.C. System.

Table A-12 Computation of power control for ± 25% change in internal resistance.

V_o = 2.5 PU, 60° phase shift.

PHASE SHIFT	MHD CURRENT	MHD VOLTAGE	INV. VOLTAGE	MHD POWER	INV. POWER	INV. REP
31.0	.48	2.14	.96	1.02	1.02	.42
32.0	.49	2.12	.95	1.04	1.04	.41
32.0	.49	2.11	.95	1.03	1.03	.40
32.0	.49	2.10	.94	1.03	1.03	.39
32.0	.49	2.08	.94	1.02	1.02	.37
33.0	.50	2.06	.93	1.04	1.04	.36
33.0	.50	2.05	.92	1.03	1.03	.35
33.0	.50	2.03	.92	1.02	1.02	.33
34.0	.52	2.01	.90	1.04	1.04	.32
34.0	.52	2.00	.90	1.03	1.03	.31
34.0	.52	1.98	.89	1.02	1.02	.30
35.0	.53	1.96	.88	1.04	1.04	.29
35.0	.53	1.94	.87	1.03	1.03	.27
35.0	.53	1.93	.87	1.02	1.02	.26
36.0	.54	1.90	.86	1.03	1.03	.25
36.0	.54	1.87	.85	1.03	1.03	.24
37.0	.56	1.86	.84	1.03	1.03	.23
37.0	.56	1.85	.83	1.03	1.03	.21
38.0	.57	1.82	.82	1.03	1.03	.20
37.0	.56	1.79	.80	1.04	1.04	.19
39.0	.58	1.77	.80	1.03	1.03	.18

Table A-13 Computation of Power Control for ± 25% change in system reactance.

V_0 = 2.0 PU, 60° phase shift.

PHASE SHIFT	MHD CURRENT	MHD VOLTAGE	INV. VOLTAGE	MHD POWER	INV. POWER	INV. REP
90.00	.00	2.00	.90	.00	.00	.00
90.00	.12	1.88	.85	.22	.22	.21
90.00	.23	1.77	.80	.41	.41	.36
90.00	.35	1.65	.74	.57	.57	.47
90.00	.46	1.54	.69	.71	.71	.55
90.00	.58	1.42	.64	.82	.82	.58
90.00	.69	1.31	.59	.91	.91	.59
90.00	.81	1.19	.54	.96	.96	.57
60.00	.80	1.20	.54	.96	.96	.11
60.00	.90	1.10	.49	.99	.99	.06
60.00	1.00	1.00	.45	1.00	1.00	-.00
60.00	1.10	.90	.40	.99	.99	-.06
57.50	1.17	.83	.37	.97	.97	-.14
52.50	1.19	.81	.36	.96	.96	-.25
47.50	1.19	.81	.36	.96	.96	-.36
42.50	1.17	.83	.37	.97	.97	-.46
40.00	1.19	.81	.37	.96	.96	-.54
37.50	1.20	.80	.36	.96	.96	-.62
35.00	1.19	.81	.36	.96	.96	-.70
32.50	1.18	.82	.37	.97	.97	-.78
30.00	1.16	.84	.38	.98	.98	-.87

A P P E N D I X - B

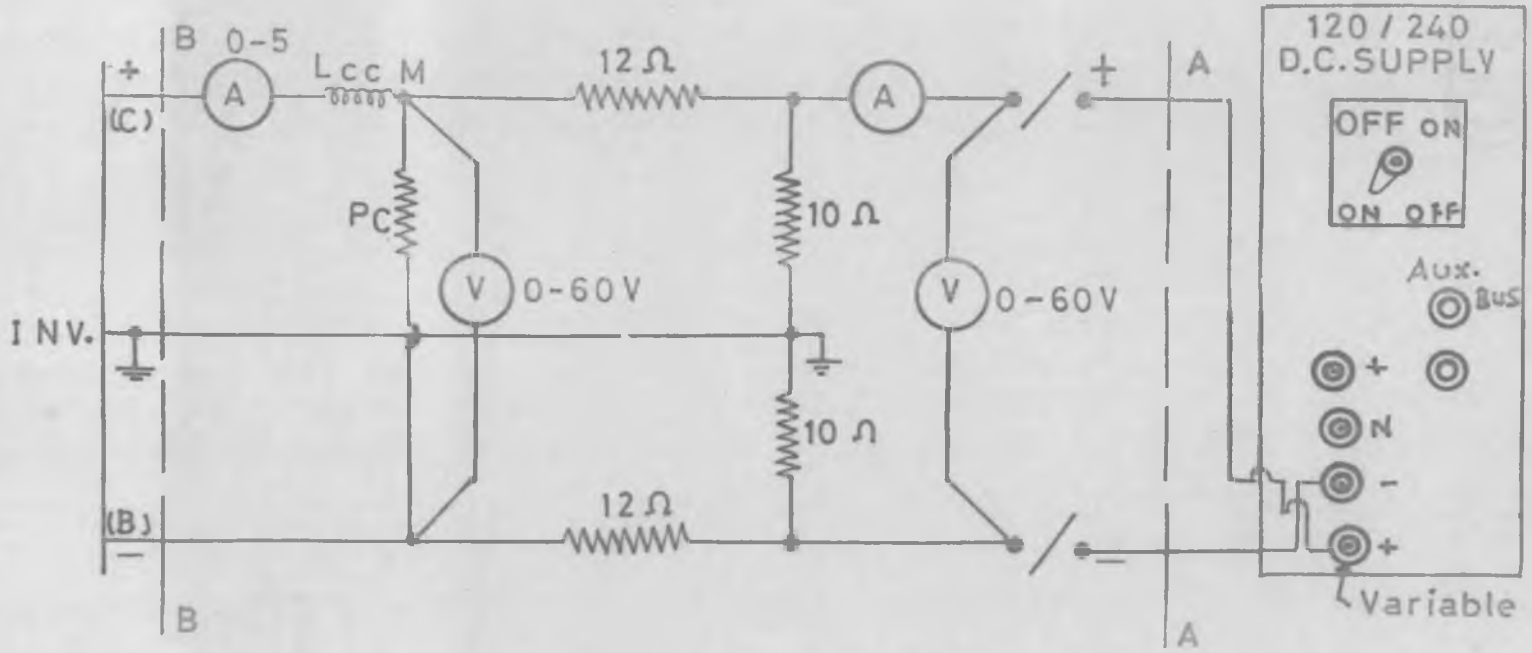

FIG.B.1. DETAILED DIAGRAM FOR EXPERIMENTAL SETUP.

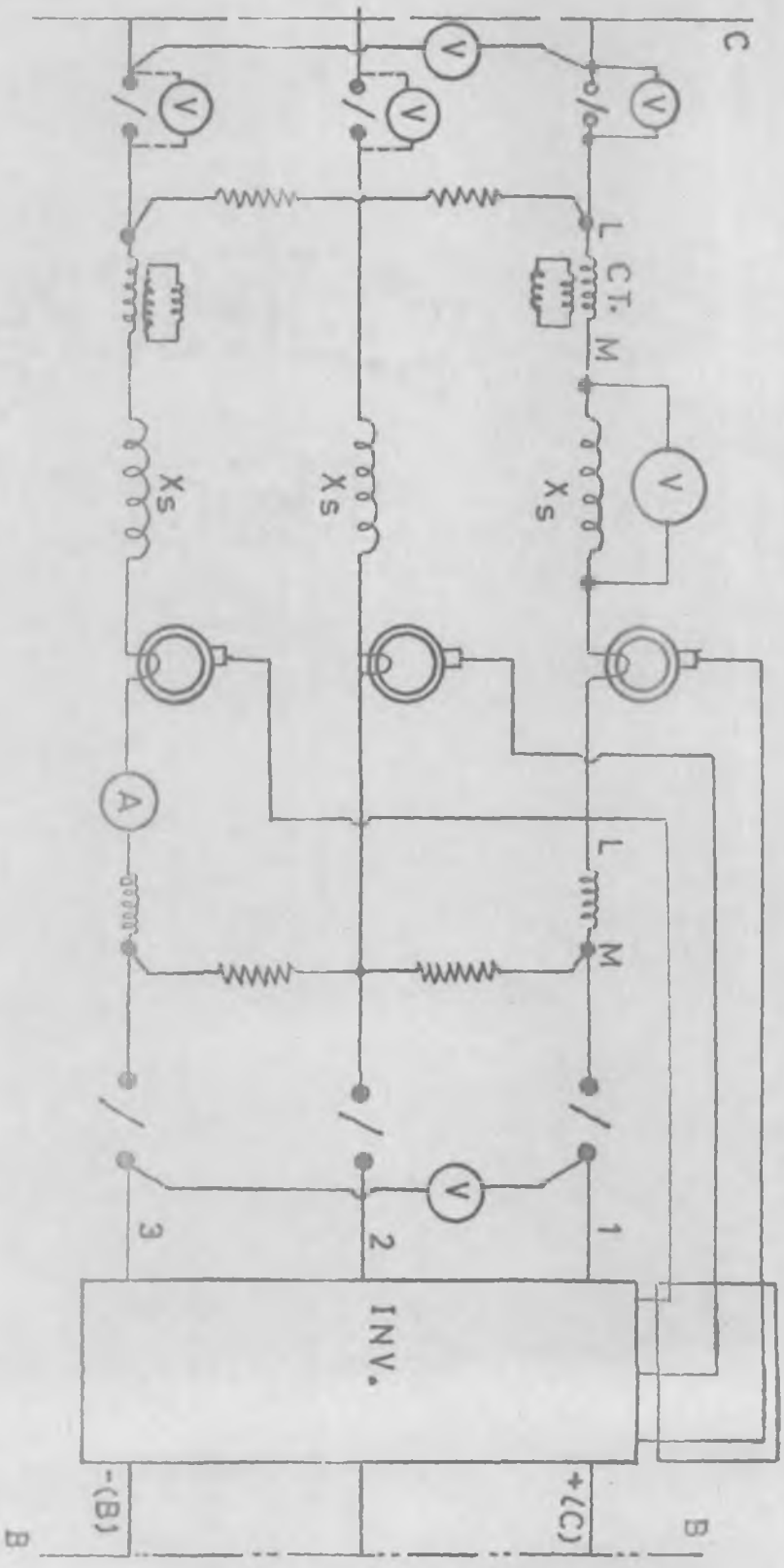

FIG. B-1. CONTINUED.

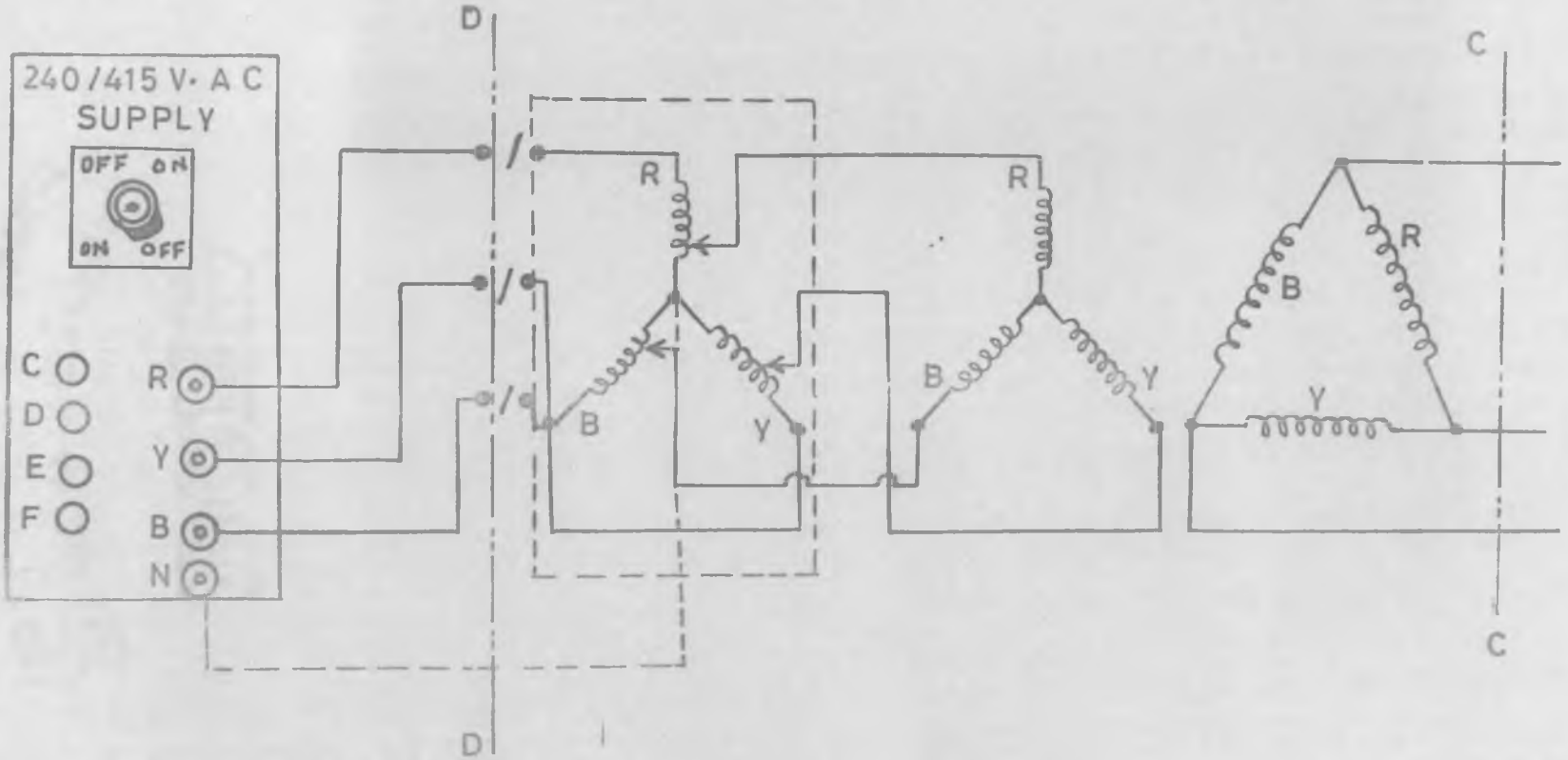

FIG. B-1 CONTINUED -

Table B-2 Variation of Electrical parameters with phase shift.

X_1 = 0.4 PU

Phase Shift	MHD current	MHD voltage	INV voltage	MHD power	INV power	INV REP
0.00	0.234	1.86	0.82	0.435	.022	-0.196
15.0	0.409	1.67	0.73	0.675	.405	-0.310
30.0	0.565	1.51	0.64	0.854	0.53	-0.27
45.0	0.693	1.37	0.58	0.955	0.62	-0.10
60.0	0.790	1.29	0.53	1.017	0.69	0.15
75.0	0.850	1.24	0.52	1.060	0.796	0.45
90.0	0.864	1.22	0.50	1.078	0.815	0.78
105.0	0.832	1.24	0.52	1.03	.845	1.18
120.0	0.757	1.33	0.53	1.048	.757	1.66
135.0	0.629	1.40	0.64	0.88	.736	2.55
150.0	0.490	1.60	0.70	0.785	0.57	3.263
165.0	0.340	1.75	0.76	0.599	0.32	3.93
180.0	0.160	1.91	0.87	0.306	0.00	4.86

Table B-3 Variation of Electrical parameters with phase shift.

X_1 = 0.80 PU

Phase shift	MHD Current	MHD Voltage	INV Voltage	MHD Power	INV Power	INV REP
0.0	0.20	1.82	0.82	0.37	0.37	-0.10
15.0	0.28	1.73	0.76	0.28	0.48	-0.13
30.0	0.35	1.64	0.72	0.50	0.57	-0.07
45.0	0.42	1.58	0.70	0.69	0.67	-0.06
60.0	0.46	1.53	0.67	0.81	0.70	0.23
75.0	0.48	1.51	0.65	0.88	0.73	0.43
90.0	0.50	1.49	0.64	0.90	0.75	0.64
105.0	0.48	1.52	0.65	0.88	0.73	0.90
120.0	0.44	1.56	0.68	0.82	0.69	1.20
135.0	0.37	1.62	0.72	0.71	0.60	1.52
150.0	0.30	1.69	0.74	0.53	0.51	1.81
165.0	0.22	1.78	0.80	0.29	0.39	2.06
180.0	0.14	1.88	0.85	0.0	0.26	2.30

Table B-4 Variation of Real and Reactive power for pu change in internal resistance.

V_o = 2.0 PU, 60^o phase shift.

S. No.	Phase Shift	MHD Power	INV. Power	INV. REP	pu Change in Ro
1.	60	1.48	1.01	+ 0.08	- 0.250
2.	60	1.41	0.98	+ 0.07	- 0.175
3.	60	1.36	0.94	+ 0.045	- 0.110
4.	60	1.30	0.92	0.027	- 0.0525
5.	60	1.27	0.88	0.027	0.000
6.	60	1.20	0.86	+ 0.027	0.050
7.	60	1.15	0.84	0.018	0.090
8.	60	1.11	0.77	0.009	0.166
9.	60	1.05	0.75	0.009	0.230
10.	60	1.01	0.75	0.018	0.286

Table B-5 Variation of Real and Reactive power for PU change in internal resistance.

V_o = 1.5 PU, 60° phase shift.

S. No.	Phase Shift	MHD Power	INV. Power	INV. REP.	PU Change in Ro
1	60	0.78	0.54	0.0	- 0.250
2	60	0.75	0.51	+ 0.018	- 0.175
3	60	0.73	0.51	+ 0.018	- 0.110
4	60	0.68	0.49	+ 0.018	- 0.052
5	60	0.65	0.45	0.0	0.00
6.	60	0.64	0.45	- 0.36	0.050
7	60	0.63	0.43	- 0.45	0.090
8	60	0.61	0.41	- 0.45	0.166
9	60	0.56	0.40	- 0.45	0.230
10	60	0.55	0.40	- 0.54	0.286

Table B-6 Variation of real power for

PU change in duct voltage.

R_o = 1.0 PU, 30^o phase shift.

S. No.	Const. Phase Shift in DEG.	Control Phase Shift in DEG.	MHD Power without control	MHD Power with Control	PU (DV) Change in Vo
1.	30.0	93.0	0.70	0.80	- 0.250
2.	30.0	93.0	0.71	0.85	- 0.175
3.	30.0	93.0	0.74	0.91	- 0.110
4.	30.0	92.0	0.76	0.96	- 0.052
5.	30.0	92.0	0.80	0.97	+ 0.000
6.	30.0	76.0	0.82	1.00	0.050
7.	30.0	62.0	0.84	1.00	0.090
8.	30.0	52.0	0.85	1.00	0.166
9.	30.0	44.8	0.87	1.00	0.230
10.	30.0	40.5	0.90	1.00	0.286

Table B-7 Variation of real power for

PU change in duct voltage.

R_o = 1.25, 30^o phase shift.

S. No.	Const. Phase Shift in DEG.	Control Phase Shift in DEG.	MHD Power without Control	MHD Power with Control	PU Change in Vo
1.	30.0	90.0	0.385	0.464	- 0.250
2.	30.0	90.0	0.400	0.500	- 0.175
3.	30.0	90.0	0.420	0.514	- 0.110
4.	30.0	90.0	0.436	0.557	- 0.052
5.	30.0	90.0	0.446	0.571	+ 0.0
6.	30.0	90.0	0.443	0.579	0.05
7.	30.0	90.0	0.460	0.621	.0.09
8.	30.0	90.0	0.490	0.657	0.166
9.	30.0	90.0	0.500	0.700	0.230
10.	30.0	90.0	0.514	0.710	0.286

Table B-8 Power Control for change in internal resistance.

V_o = 2.0 PU, 60° phase shift.

S. No.	Phase shift	MHD Power	INV Power	INV REP	PU Change in R_o
1.	30°	1.28	0.73	-0.18	- 0.25
2.	40.1	1.28	0.82	-0.09	- 0.175
3.	46.0	1.28	0.84	-0.07	- 0.110
4.	54.0	1.28	0.89	-0.018	- 0.052
5.	66.0	1.28	0.93	+0.018	0.0
6.	96.0	1.28	0.91	0.228	0.05
7.	96.0	1.22	0.89	0.20	0.09
8.	96.0	1.17	0.89	0.20	0.166
9.	96.0	1.11	0.85	0.21	0.23
10.	96.0	1.11	0.76	0.18	0.286

Table B-9 Power Control for change in internal resistance.

V_o = 2.0 PU, 30^o phase shift.

S. No.	Phase shift	MHD power	INV. power	INV. REP	PU change in R_o
1.	40.5	1.28	0.97	0.027	- 0.25
2.	44.8	1.28	0.94	0.06	- 0.175
3.	52.0	1.28	0.89	0.0	- 0.11
4.	62.0	1.28	0.92	0.009	- 0.052
5.	76.0	1.28	1.0	0.09	0.0
6.	92.0	1.25	0.94	0.25	0.05
7.	92.0	1.23	0.88	0.24	0.09
8.	93.0	1.17	0.86	0.22	0.166
9.	93.0	1.09	0.82	0.23	0.23
10.	98.0	1.02	0.78	0.21	0.286

Table B-10 Power Control for change in internal resistance.

V_o = 1.5 PU, 30° phase shift.

S. No.	Phase shift	MHD Power	INV. Power	INV. REP	PU change in R_o
1.	90°	0.91	0.68	0.22	-0.25
2.	90	0.89	0.66	0.21	-0.175
3.	90	0.84	0.64	0.18	-0.110
4.	90	0.79	0.59	0.13	-0.052
5.	90	0.74	0.56	0.16	0.0
6.	90	0.73	0.54	0.15	0.05
7.	90	0.71	0.53	0.146	0.09
8.	90	0.65	0.50	0.13	0.166
9.	90	0.64	0.41	0.13	0.23
10.	90	0.59	0.45	0.09	0.286

Table B-11 Variation of Real and reactive power for P.U. change in System reactance.

V_o = 2.0 PU, 60^o phase shift.

S. No.	System Reactance P.U.	MHD current P.U.	MHD power P.U.	INV. Power PU.	INV. REP
1.	6.5	0.4	0.67	0.28	0.0135
2.	5.6	0.431	0.7	0.317	0.020
3.	4.78	0.47	0.776	0.40	0.027
4.	3.9	0.51	0.843	0.51	0.0337
5.	3.28	0.62	0.945	0.64	0.0337
6.	2.27	0.78	1.11	0.776	0.100
7.	1.45	1.20	1.07	0.91	-0.100
8.	1.27	1.52	1.012	0.96	-0.155

Table B-12 Power Control for PU change in system reactance.

V_o = 2.0 PU, 60^o phase shift.

S. No.	System reactance PU.	MHD current	MHD power	MHD power	INV. REP.
1.	6.5	0.44	0.73	0.347	0.05
2.	5.6	0.47	0.76	0.446	0.11
3.	4.78	0.515	0.83	0.486	0.11
4.	3.9	0.58	0.9	0.566	0.116
5.	3.28	0.716	1.0	0.70	0.30
6.	2.27	0.80	1.10	0.776	0.10
7.	1.45	0.80	1.03	0.80	- 0.26
8.	1.27	0.80	1.05	0.78	- 0.35

List B-13 Program for variation in Electrical parameters with filters.

```
 81/06/12. 17.14.22.
PROGRAM   PF12

00100 PROGRAM FPLOT(OUTPUT,TAPE6=OUTPUT)
00110 DIMENSION D(99),DM(99),AID(99),VD(99),E1(99),PD(99),P(99),QS(99)
00120 PB=(V0**2)/(4.0*R0)
00130 VB=V0/2.0
00140 AIB=V0/(2.0*R0)
00150 WRITE(6,3)
00160 3 FORMAT(12X,62("="))
00170 WRITE(6,4)
00180 4 FORMAT(13X,"PHASE",4X,"MHD",6X,"MHD",7X,"INV.",5X,"MHD",
00190+6X,"INV.",6X,"INV.")
00200 DATA V0,EB,R0/45.0,20.21,24.0/
00210 X=16.82
00220 XC=371.547
00230 WRITE(6,5)
00240 5 FORMAT((13X,"SHIFT",2X,"CURRENT",3X,"VOLTAGE",3X,"VOLTAGE",
00250+2X,"POWER",4X,"POWER",6X,"RcP")/)
00260 PAI=4.0*ATAN(1.0)
00270 DO 10 I=1,19
00280 WRITE(6,13)
00290 13 FORMAT(12X,62("-"))
00300 D(I)=(I-1)*PAI/18
00310 XLL=(2.0*X-X**2/XC)
00320 AID(I)=1.35*(EB/XLL)*SIN(D(I))
00330 VD(I)=(V0-AID(I)*R0)
00340 E1(I)=(SQRT(2.0)/PAI)*VD(I)
00350 PD(I)=VD(I)*AID(I)
00360 PD(I)=PD(I)/PB
00370 P(I)=(3.0/XLL)*E1(I)*EB*SIN(D(I))
00380 P(I)=P(I)/PB
00390 QS(I)=(E1(I)**2)/((X*(X-2.0*XC))/(X-XC))-E1(I)*EB*COS(D(I))/XLL
00400 QS(I)=3.0*QS(I)/PB
00410 AID(I)=AID(I)/AIB
00420 VD(I)=VD(I)/VB
00430 E1(I)=E1(I)/VB
00440 DM(I)=D(I)*180.0/PAI
00450 WRITE(6,20) DM(I),AID(I),VD(I),E1(I),PD(I),P(I),QS(I)
00460 20 FORMAT(13X,F5.1,6(3X,F6.2))
00470 10 CONTINUE
00480 WRITE(6,15)
00490 15 FORMAT(12X,62("-"))
00500 STOP
00510 END
READY.
```

Table B-14. Semikron fast thyristors.

Types [1]	V_{DRM} V_{RRM} V	V_{DSM} V_{RSM} V	I_{TRMS} A	I_{TAV} T_{case} = 85 °C A	I_{TSM} 10 ms A	i^2t $t_{g(max)}$ A²s	$\left(\frac{di}{dt}\right)_{cr}$ A/µs	$\left(\frac{di}{dt}\right)_{cr}$ A/µs	$\left(\frac{dv}{dt}\right)_{cr}$ V/µs	t_g [2] µs	I_{GT} max. mA	I_H max. mA	V_{GT} min. V	I_{GT} min. mA	$V_{T(TO)}$ V	r_t mΩ	T_{vj} max. °C	R_{thjc} cont. °C/W	R_{thch} °C/W		I_{TAV} sint 180 A	I_{TAV} rec 120 A
SKT 12	F02D	300	200	23	12	210	220	-	200	500	R, S	300	1000	3	100	1,6	24	125	1,2	0,5	K9	4,2	4
	F04D	500	400		T_{case} = 80 °C						R, S										K5	6	5,8
	F06D	700	600								R, S										K3	8	7,7
	F08D	900	800								S, T												
	F10D	1100	1000								S, T												
	F12D	1300	1200								S, T												
SKT 18	F02D	300	200	30	18	330	550	-	200	500	R, S	300	1000	3	100	1,4	20	125	1,2	0,5	K9	5,5	5,4
	F04D	500	400								R, S										K5	7,8	7,3
	F06D	700	600								R, S										K3	10	9,2
	F08D	900	800								S, T, U												
	F10D	1100	1000								S, T, U												
	F12D	1300	1200								S, T, U												
SKT 45	F02D	300	200	110	54	1100	6000	800	250	500	S, T	300	1000	5	150	1,5	6	125	0,25	0,08	K 1,1	24	23
	F04D	500	400								S, T										K 0,55	37	34
	F06D	700	600								T, U										K 1,1 F	50	47
	F08D	900	800								T, U										P 1/120	38	33
	F10D	1100	1000								T, U												
	F12D	1300	1200								T, U												
SKT 70	F02D	300	200	135	70	1450	10500	800	250	500	T, U	300	1000	5	150	1,5	3	125	0,25	0,08	K 1,1	31	29
	F04D	500	400								T, U										K 0,55	47	43
	F06D	700	600								T, U										K 1,1 F	65	60
	F08D	900	800								T, U, V										K 0,55 F	88	81
	F10D	1100	1000								T, U, V										P 1/120	44	40
	F12D	1300	1200								T, U, V												
SKT 110	F02D	300	200	220	110	2500	31000	800	250	500	T, V	300	1500	5	200	1,8	2	125	0,16	0,03	K 1,1	35	33
	F04D	500	400								T, V										K 0,55	60	57
	F06D	700	600								T, V										K 1,1 F	85	81
	F08D	900	800								U, V										K 0,55 F	115	108
	F10D	1100	1000								U, V										P 1/120	65	52
	F12D	1300	1200								U, V												
SKT 140	F02D	300	200	270	140	3200	50000	800	250	500	T, V	800	1500	5	200	1,2	1,6	125	0,16	0,03	K 1,1	45	43
	F04D	500	400								T, V										K 0,55	75	70
	F06D	700	600								T, V										K 1,1 F	105	100
	F08D	900	800								U, V										K 0,55 F	145	132
	F10D	1100	1000								U, V										P 1/120	70	64
	F12D	1300	1200								U, V												
SKT 170	/02C	300	200	375	170	5000	125000	-	125	200	T, U	300	1500	3	250	1,3	1,1	125	0,11	0,015	K 0,55	80	78
	/04C	500	400								T, U										K 0,55 F	175	170
	/06C	700	600								T, U										P 1/120	75	73
	/08C	900	800								V										P 1/200	90	83
	/10C	1100	1000								V, X												
	/12C	1300	1200		T_{case} = 90 °C						V, X [4]												
SKT 220	/02C	300	200	450	220	6000	180000	-	125	200	U	300	1500	3	250	1,1	0,75	125	0,11	0,015	K 0,55	95	91
	/04C	500	400								U										K 0,55 F	205	195
	/06C	700	600								U										P 1/120	85	82
	/08C	900	800								V										P 1/200	110	105
	/10C	1100	1000								V, X												
	/12C	1300	1200		T_{case} = 85 °C						V, X [4]												
SKT 400	F04C	500	400	850	400	8750	230000	1000	500	800	V, X	-	-	5	250	0,4	0,6	125	0,06	0,007	2xP8/180	140	130
	F06C	700	600								V, X										2xP8/150F	360	330
	F08C	900	800								V, X										2xP8/210F	400	370
	F10C	1100	1000								V, X										(2-pole)		
	F12C	1300	1200								V, X												
	F14C	1500	1400		T_{case} = 75 °C						V, X												
SKT 550	F04D	500	400	1000	550	9000	400000	800	500	500	U, X	-	-	3	200	1,7	0,4	125	0,04	0,007	2xP8/180	120	120
	F06D	700	600								U, X										2xP8/150F	400	370
	F08D	900	800								U, X										2xP8/210F	450	420
	F10D	1100	1000								U, X												
	F12D	1300	1200		T_{case} = 75 °C						U, X												

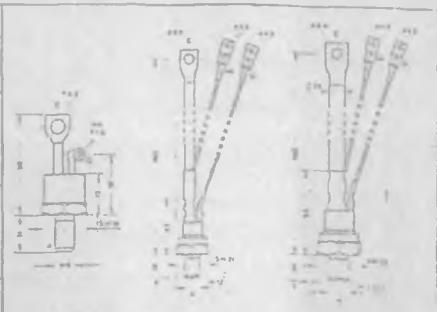

SKT 12 F, SKT 18 F
w = 35 g
M = 2,5 Nm
~TO-48

SKT 45 F, SKT 70 F
w = 80 g
M = 10 Nm
~TO-94

SKT 110 F, SKT 140 F
w = 270 g
M = 30 Nm
~TO-93

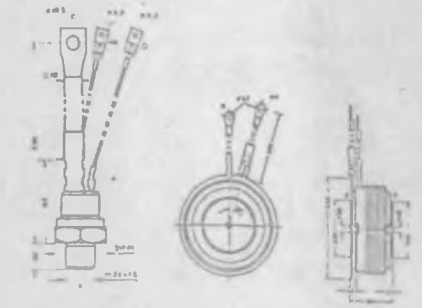

SKT 170, SKT 220
w = 450 g
M = 60 Nm
~TO-118

SKT 400 F, SKT 550 F
w = 130 g
F = 9000 N, F = 14 000 N

Q: $t_q \leq 5$ µs
R: $t_q \leq 10$ µs
M: $t_q \leq 12$ µs
S: $t_q \leq 15$ µs
N: $t_q \leq 18$ µs
T: $t_q \leq 20$ µs
U: $t_q \leq 25$ µs
V: $t_q \leq 30$ µs
W: $t_q \leq 35$ µs
X: $t_q \leq 40$ µs

Table B-15 Semikron Fast recovery silicon Rectifier Diode.

Table B-16 General Electric inverter grade capacitor

26F6700/6900 Series

STANDARD RATINGS

Capacitance μF TOL.: ±10%	Catalog Number	Case Style	Case Height "c" Inches	Case Height "c" MM	RMS Current 55°C (Amperes)
500 VOLTS PEAK					
2	26F6905FC	A	2.62	66.5	9
3	26F6906FC	A	3.50	88.9	12
5	26F6907FC	A	4.25	107.9	20
10	26F6908FC	C	4.25	107.9	32
20	26F6909FC	C	6.25	158.8	59
30	26F6910FC	D	7.25	184.2	8[illegible]
40	26F6911FC	G	5.88	149.4	100
50	26F6912FC	G	6.25	158.8	121
600 VOLTS PEAK					
1	26F6913FC	A	2.62	66.5	6
2	26F6914FC	A	2.62	66.5	10
5	26F6915FC	A	4.75	120.6	21
10	26F6916FC	C	4.75	120.6	35
20	26F6917FC	D	6.25	158.8	59
30	26F6918FC	G	6.25	158.8	92
40	26F6919FC	G	7.25	184.2	119
50	26F6920FC	G	9.00	228.6	145

Capacitance μF TOL.: ±10%	Catalog Number	Case Style	Case Height "c" Inches	Case Height "c" MM	RMS Current 55°C (Amperes)
800 VOLTS PEAK					
1	26F6921FC	A	2.62	66.5	7
2	26F6922FC	A	3.50	88.9	12
5	26F6923FC	C	4.50	114.3	24
10	26F6924FC	C	7.25	184.2	43
20	26F6925FC	G	6.25	158.8	75
25	26F6926FC	G	7.25	184.2	89
30	26F6927FC	G	8.00	203.2	106
1000 VOLTS PEAK					
1	26F6769FC	A	3.50	88.9	7
2	26F6732FC	A	4.25	107.9	13
5	26F6734FC	C	4.75	120.6	25
10	26F6735FC	D	6.25	158.8	45
20	26F6770FC	G	7.25	184.2	79
1500 VOLTS PEAK					
.5	26F6771FC	A	3.50	88.9	5
1	26F6742FC	A	4.25	107.9	9
2	26F6743FC	C	4.25	107.9	15
* 5	26F6745FC	D	7.25	184.2	34
10	26F6746FC	G	7.25	184.2	58

CASE STYLES C & D

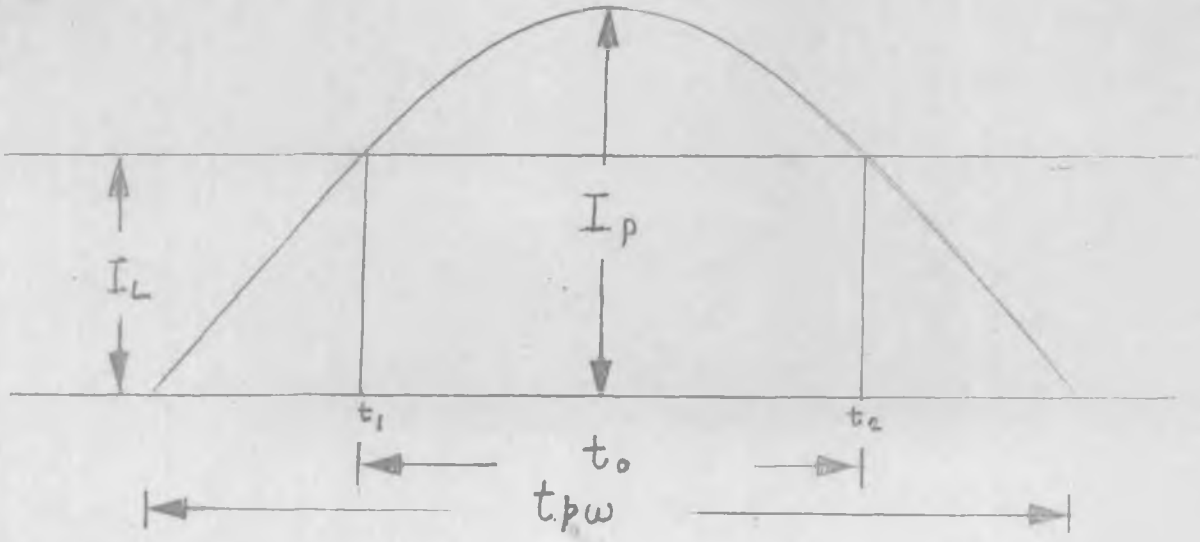

Fig. B-17 Commutating current pulse.

A P P E N D I X - C

Table C-1

Specifications

Model HM-3000 Series

Hall-Pak Multipliers

Specifications [1]	HM-3010	HM-3030	HM-3050	Units [2]	See Note Factor [3]
		Parallel Coils			
Magnetic Field Current Input I_f					
Resistance	.25	5	500	Ω	4
Inductance	.60	60	6000	mH	4
Rated Dissipation	.45	.45	45	w	
Rated Input dc	.15	1.5	15	V	2
	3000	300	30	mA	5
Rated Input 60 cps	.75	7.5	75	V	2
	3000	300	30	mA	5
Current derating at higher frequencies	3	3	3	%/kc	
Self resonant frequency, approx.	300	28	2.4	kc	5
Hall Current Input I_c					
Resistance, approx.	2.5	2.5	2.5	Ω	
Rated Dissipation	20	.20	.20	w	
Rated Current	250	250	250	mA	
Frequency Range	0 to 500	0 to 500	0 to 500	kc	
Hall Voltage Output V_H					
Resistance, approx.	10	10	10	Ω	
Load resistance [4]	50	50	50	Ω	
Transfer Constant [5] [6]	> .20	> 2.0	> 20	V/mA^2	2
Maximum Output	> 150	> 150	> 150	mV	
Linearity					
Multiplication Error	< ± 1	< ± 1	< ± 1	%F.S.	
Distortion					
T.H.D. in Output [6] [7]	< 1	< 1	< 1	%	
Temperature Influence					
On Field Input Resistance	+ .39	+ .39	+ .39	%/°C	
On Hall Input Resistance, approx.	+ .15	+ .15	+ .15	%/°C	
On Hall Output, [6] [8]					
over ambient range +15°C to +35°C	< ±.5	< ±.5	< ±.5	%	
over ambient range −25°C to +75°C	< ± 1	< ± 1	< ± 1	%	
Residual Output					
Inductive (caused by field current)	< .05	< .5	< 5	μV/mA-kc	2
Resistive (caused by Hall current)	< 1	< 1	< 1	μV/mA	
Common Mode Coupling					
Equiv. capacitance					
Field Input/Hall Output [9]	< 3	< 3	< 3	pF	
Mutual Resistance					
Hall Input/Hall Output [10]	< 1.5	< 1.5	< 1.5	Ω	
Environment					
Storage and Operating Range	−55 to +85	−55 to +85	−55 to +85	°C	
Polarity Relation					See Schematic Diagram

Packaging

Silicon rubber potted in hermetically sealed steel can 2⅞" x 1¾" x 1¾".
Plug-in type Naval header with two 4-40 UNF x ⅜" mounting inserts.

Weight — 8 oz.

Notes:

1. At 25°C ambient.
2. A-C values are r.m.s.
3. Factor by which values are multiplied when coils are series connected.
4. Matching resistance for specified output, linearity and temperature compensation.
5. Factor by which product of input currents must be multiplied to obtain output voltage.
6. With linearizing load resistance.
7. For input signals with T.H.D. < .1%.
8. At constant input currents.
9. Between shorted terminals 1, 2, 3, 4 and shorted terminals 8, 9.
10. Between shorted terminals 6, 7 and shorted terminals 8, 9.

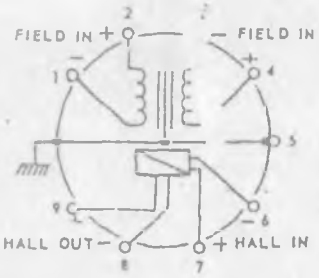

SCHEMATIC DIAGRAM

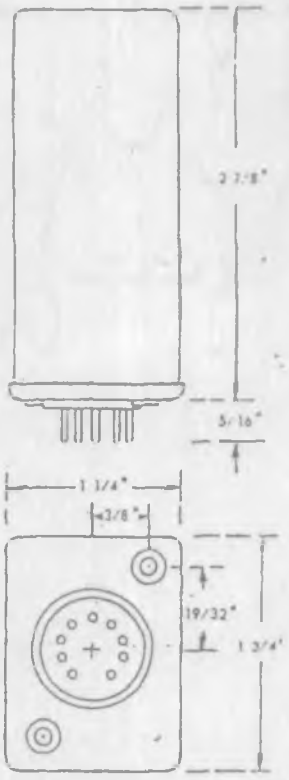

CHARACTERISTICS

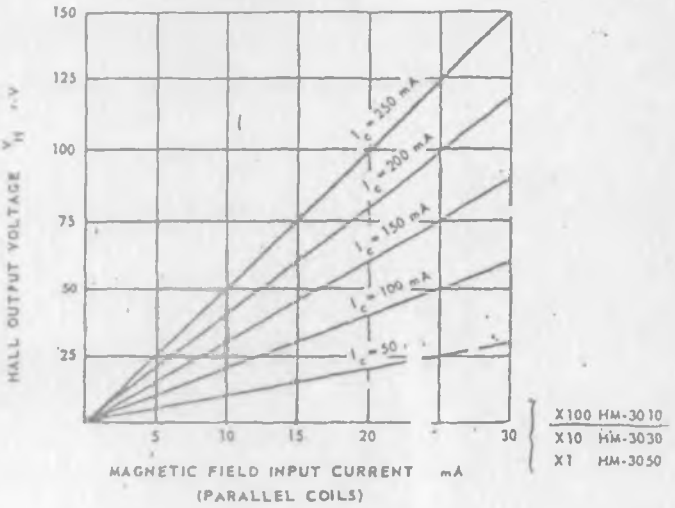

X100 HM-3010
X10 HM-3030
X1 HM-3050

Output voltage as function of field input currents for various values of the Hall input current.

Modifications on Special Order:

- Mumetal can (improved shielding from environmental magnetic fields).
- Different header, other terminal arrangement.
- Temperature compensation to smaller tolerances.
- Reduced non-linearity.
- Reduced residual output.
- Reduced equivalent capacitance.
- Extended field frequency range.
- Different coil combinations.
- Special customer designs.

ELECTRONIC DESIGN
DEVELOPMENT • MANUFACTURING

BELL INC.
1356 NORTON AVE.
COLUMBUS 12, OHIO
PHONE AX 4-4906

Fig. C-2 Hall Pak Multiplier Specifications Cont.

a) Symbols and Use of Dual Summing Amplifier, Types 3316-11 and 3316-21

Patch Block Connection		
Symbol Dual Summing Amplifier	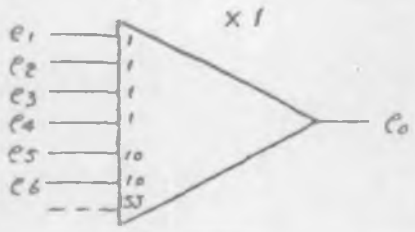	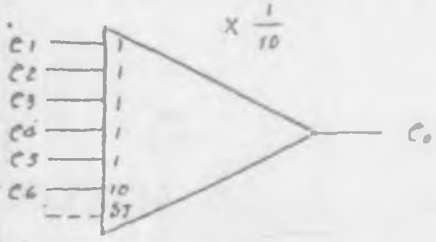
Circuit Dual Summing Amplifier	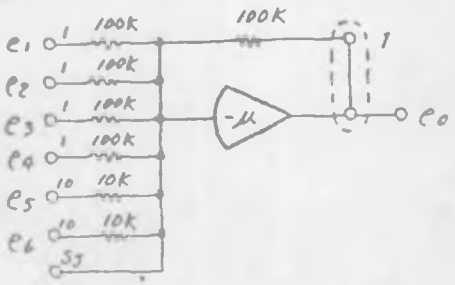	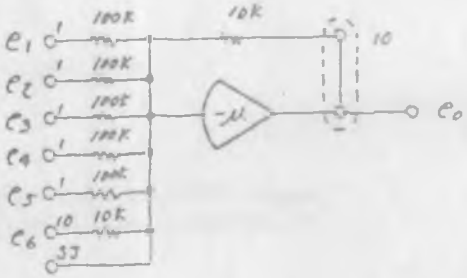
Sign Changer	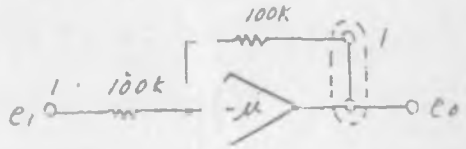	

1. Selection of Coefficient

Fig. 7-3-3 shows coefficients to be selected according to feedback resistors (1 and 10) in relation with input terminals.

Feedback	1 (100K)	10 (10K)
Input 1 (100K)	1	0.1
Input 10 (10K)	10	1

Fig. C-3 Analogue Computer Details

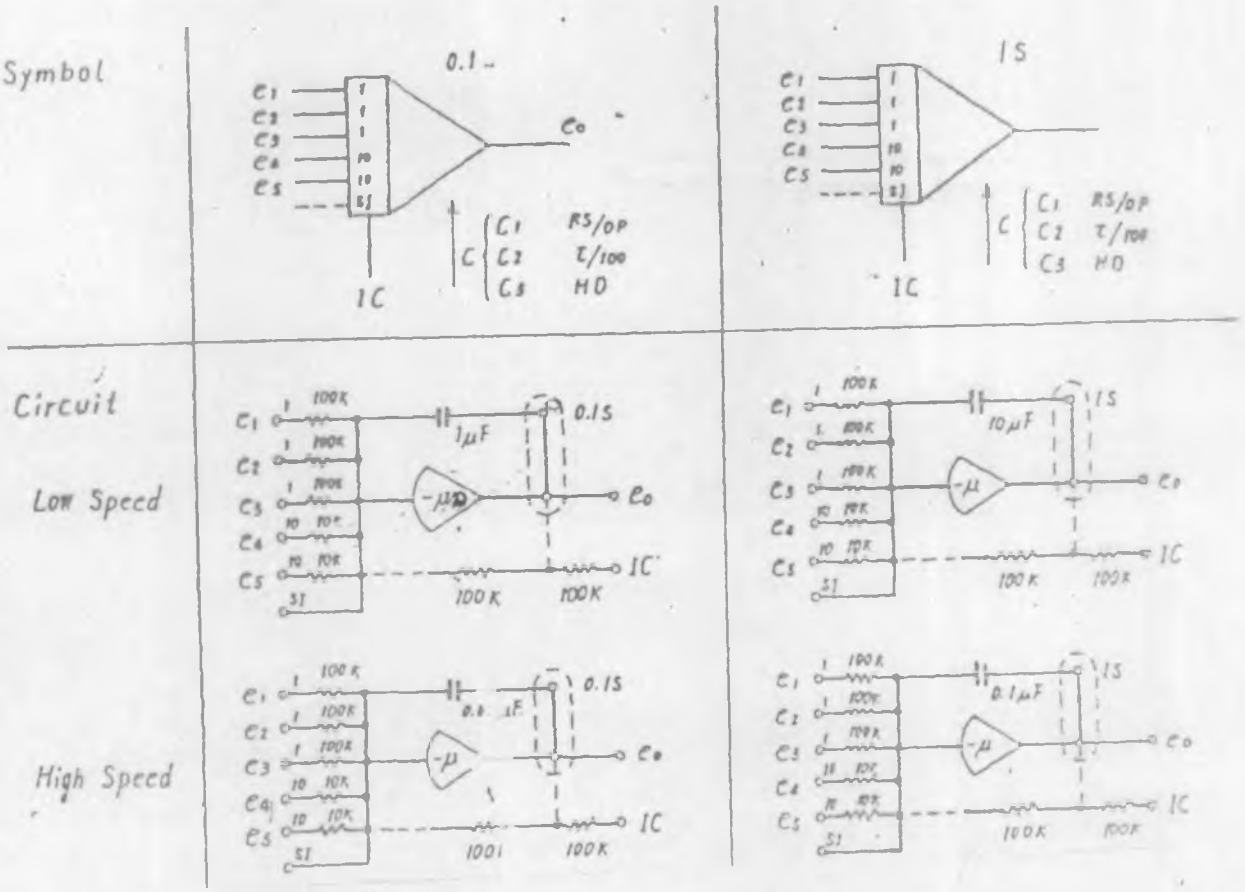

1. Selection of Time Constant

The time constant can be varied 100 times according to selection of high or low speed. This is available automatically by the use of control signal C_2. The constants are shown below.

Input	C	High Speed Computation		Low Speed Computation	
		0.1S	1S	0.1S	1S
		0.01μF	0.1μF	1μF	10μF
1	100K	10^{-3} sec	10^{-2} sec	10^{-1} sec	1 sec
10	10K	10^{-4} sec	10^{-3} sec	10^{-2} sec	10^{-1} sec

Fig. C-4 Analogue Coputer Details-Cont.

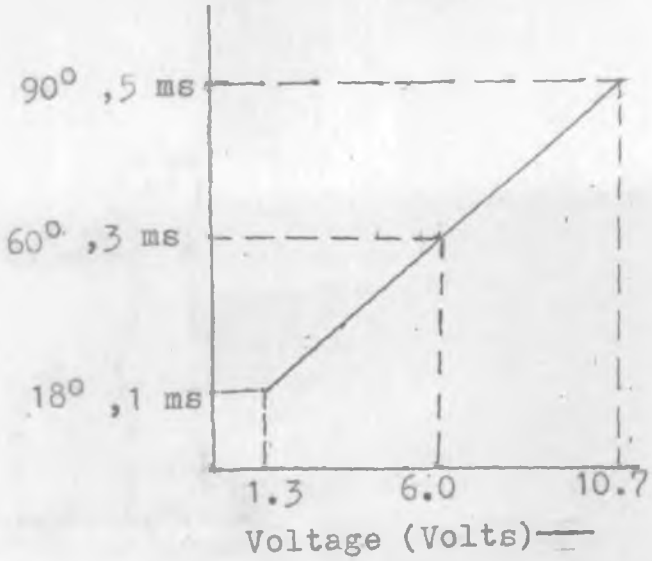

Fig. C-5 Swing of PI Controller

DUAL OPERATIONAL AMPLIFIER μA747/747C/SA747C

ABSOLUTE MAXIMUM RATINGS

PARAMETER	RATING	UNIT
Supply voltage		
μA747	±22	V
μA747C	±18	V
SA747C	±18	V
Internal power dissipation		
Metal can	500	mW
DIP	670	mW
Differential input voltage	±30	V
Input voltage	±15	V
Voltage between offset null and V-	±0.5	V
Storage temperature range	-65 to +155	°C
Operating temperature range		
μA747	-55 to +125	°C
μA747C	0 to +70	°C
SA747C	-40 to +85	°C
Lead temperature (soldering, 60 sec)	300	°C
Output short-circuit duration	indefinite	

PIN CONFIGURATIONS

F/N PACKAGE

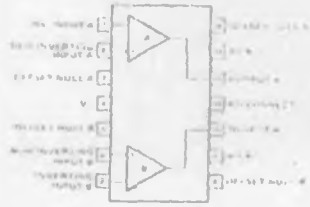

ORDER PART NO.
μA747CN, μA747CF, μA747N, μA747F, SA747CN, SA747CF

DESCRIPTION

The 747 is a pair of high performance monolithic operational amplifiers constructed on a single silicon chip. High common mode voltage range and absence of "latch-up" make the 747 ideal for use as a voltage follower. The high gain and wide range of operating voltage provides superior performance in integrator, summing amplifier, and general feedback applications. The 747 is short-circuit protected and requires no external components for frequency compensation. The internal 6dB/octave roll-off insures stability in closed loop applications. For single amplifier performance, see μA741 data sheet.

FEATURES

- No frequency compensation required
- Short-circuit protection
- Offset voltage null capability
- Large common-mode and differential voltage ranges
- Low power consumption
- No latch-up
- μA747, SA747C Mil std 883A,B,C available

Fig. C-6 Operational Amplifier Ratings and Characteristics

DC ELECTRICAL CHARACTERISTICS $T_A = 25°C$, $V_S = \pm 15V$ unless otherwise specified

PARAMETER		TEST CONDITIONS	SA747C			UNIT
			Min	Typ	Max	
V_{OS}	Offset voltage	$R_S \leq 10k\Omega$,		2.0	6.0	mV
V_{OS}	Offset voltage	$R_S \leq 10k\Omega$, over temp		3.0	7.5	mV
I_{OS}	Offset current			20	200	nA
I_{OS}	Offset current	Over temp			500	nA
I_{BIAS}	Input current				1500	nA
I_{BIAS}	Input current	Over temp			500	nA
V_{OUT}	Output voltage swing	$R_L \geq 2k\Omega$, over temp	±10	±13		V
		$R_L \geq 10k\Omega$, over temp	±12	±14		V
I_{CC}	Supply current			1.7	2.8	mA
		Over temp		2.0	3.3	mA
	Power consumption			50	85	mW
		Over temp		60	100	mW
	Input capacitance			1.4		pF
	Offset voltage adjustment range			±15		V
	Output resistance			75		Ω
	Channel separation			120		dB
P_{SRR}	Supply voltage rejection ratio	$R_S \leq 10k\Omega$, over temp		30	150	μV/V
	Large signal voltage gain (DC)	$R_L \geq 2k\Omega$ $V_{OUT} = \pm 10V$	25,000			V/V

AC ELECTRICAL CHARACTERISTICS $T_A = 25°C$, $V_S = \pm 15V$ unless otherwise specified.

PARAMETER	TEST CONDITIONS	μA747/μA747C/SA747C			UNIT
		Min	Typ	Max	
Transient response	$V_{IN} = 20mV$, $R_1 = 2k\Omega$, $C_1 < 100pf$				
Risetime	Unity gain CL ≤ 100pf		0.3		μs
Overshoot	Unity gain CL ≤ 100pf		5.0		%
Slew rate	RL > 2kΩ		0.5		V/μs

Fig. C-7 Operational Amplifier Details-Cont.

MM54C221/MM74C221 dual monostable multivibrator

general description

The MM54C221/MM74C221 dual monostable multivibrator is monolithic complementary MOS integrated circuit. Each multivibrator features a negative-transition-triggered input and a positive-transition-triggered input either of which can be used as an inhibit input, and a clear input.

Once fired, the output pulses are independent of further transitions of the A and B inputs and are a function of the external timing components C_{EXT} and R_{EXT}. The pulse width is stable over a wide range of temperature and V_{CC}. Pulse stability will be limited by the accuracy of external timing components. The pulse width is approximately defined by the relationship $t_{W(OUT)} \approx C_{EXT} R_{EXT}$. For further information and applications, see AN-138.

features

■ Wide supply voltage range	4.5V to 15V
■ Guaranteed noise margin	1.0V
■ High noise immunity	0.45 V_{CC} typ
■ Low power TTL compatibility	fan out of 2 driving 74L

connection diagrams

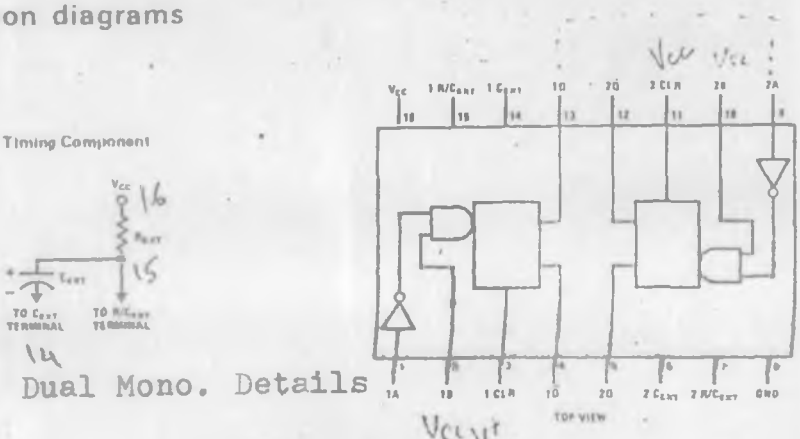

Fig.C-8 Dual Mono. Details

absolute maximum ratings (Note 1) MM54C221/MM74C221

Voltage at Any Pin	−0.3V to V_{CC} + 0.3V	Package Dissipation	500 mW
Operating Temperature Range		Operating V_{CC} Range	4.5V to 15V
MM54C221	−55°C to +125°C	Absolute Maximum V_{CC}	16V
MM74C221	−40°C to +85°C	$R_{EXT} \geq 80\ V_{CC}$ (Ω)	
Storage Temperature Range	−65°C to +150°C	Lead Temperature (Soldering, 10 seconds)	300°C

dc electrical characteristics Min/max limits apply across temperature range, unless otherwise noted.

PARAMETER	CONDITIONS	MIN	TYP	MAX	UNITS
CMOS TO CMOS					
Logical "1" Input Voltage ($V_{IN(1)}$)	V_{CC} = 5.0V	3.5			V
	V_{CC} = 10V	8.0			V
Logical "0" Input Voltage ($V_{IN(0)}$)	V_{CC} = 5.0V			1.5	V
	V_{CC} = 10V			2.0	V
Logical "1" Output Voltage ($V_{OUT(1)}$)	V_{CC} = 5.0V, I_O = −10μA	4.5			V
	V_{CC} = 10V, I_O = −10μA	9.0			V
Logical "0" Output Voltage ($V_{OUT(0)}$)	V_{CC} = 5.0V, I_O = 10μA			0.5	V
	V_{CC} = 10V, I_O = 10μA			1.0	V
Logical "1" Input Current ($I_{IN(1)}$)	V_{CC} = 15V, V_{IN} = 15V		0.005	1.0	μA
Logical "0" Input Current ($I_{IN(0)}$)	V_{CC} = 15V, V_{IN} = 0V	−1.0	−0.005		μA
Supply Current (I_{CC})	V_{CC} = 15V, R_{EXT} = ∞, Q1, Q2 = Logic 0 (Note 3)		0.05	300	μA
	V_{CC} = 15V, Q1 = Logic 1, Q2 = Logic 0		15		mA
	V_{CC} = 5.0V, Q1 = Logic 1, Q2 = Logic 0		2		mA
Leakage Current at R/C_{EXT} Pin	V_{CC} = 15V, V_{CEXT} = 5.0V		0.01	3	μA
CMOS/LPTTL INTERFACE					
Logical "1" Input Voltage ($V_{IN(1)}$)					
MM54C221	V_{CC} = 4.5V	V_{CC}−1.5			V
MM74C221	V_{CC} = 4.75V	V_{CC}−1.5			V
Logical "0" Input Voltage ($V_{IN(0)}$)					
MM54C221	V_{CC} = 4.5V			0.8	V
MM74C221	V_{CC} = 4.75V			0.8	V
Logical "1" Output Voltage ($V_{OUT(1)}$)					
MM54C221	V_{CC} = 4.5V, I_O = −360μA	2.4			V
MM74C221	V_{CC} = 4.75V, I_O = −360μA	2.4			V
Logical "0" Output Voltage ($V_{OUT(0)}$)					
MM54C221	V_{CC} = 4.5V, I_O = 360μA			0.4	V
MM74C221	V_{CC} = 4.75V, I_O = 360μA			0.4	V
OUTPUT DRIVE (See 54C/74C Family Characteristics Data Sheet)					
Output Source Current (I_{SOURCE}) (P-Channel)	V_{CC} = 5.0V, V_{OUT} = 0V, T_A = 25°C	−1.75	−3.3		mA
Output Source Current (I_{SOURCE}) (P-Channel)	V_{CC} = 10V, V_{OUT} = 0V, T_A = 25°C	8.0	15		mA
Output Sink Current (I_{SINK}) (N-Channel)	V_{CC} = 5.0V, V_{OUT} = V_{CC}, T_A = 25°C	1.75	3.6		mA
Output Sink Current (I_{SINK}) (N-Channel)	V_{CC} = 10V, V_{OUT} = V_{CC}, T_A = 25°C	8.0	15		mA

Fig. C-9 Dual Mono. Details-Cont.

COS/MOS Dual 'D'-Type Flip-Flop

High-Voltage Types (20-Volt Rating)

The RCA CD4013B consists of two identical, independent data-type flip-flops. Each flip-flop has independent data, set, reset, and clock inputs and Q and $\overline{Q}$ outputs. These devices can be used for shift register applications, and, by connecting $\overline{Q}$ output to the data input, for counter and toggle applications. The logic level present at the D input is transferred to the Q output during the positive-going transition of the clock pulse. Setting or resetting is independent of the clock and is accomplished by a high level on the set or reset line, respectively.

The CD4013B types are supplied in 14-lead hermetic dual in-line ceramic packages (D and F suffixes), 14-lead dual-in-line plastic packages (E suffix), and in chip form (H suffix).

Features:

- Set-reset capability
- Static flip-flop operation — retains state indefinitely with clock level either "high" or "low"
- Medium-speed operation — 16 MHz (typ.) clock toggle rate at 10V
- Standardized symmetrical output characteristics
- 100% tested for quiescent current at 20 V
- Maximum input current of 1 μA at 18 V over full package temperature range; 100 nA at 18 V and 25°C
- Noise margin (over full package temperature range): 1 V at V_{DD}=5 V; 2 V at V_{DD}=10 V; 2.5 V at V_{DD}=15 V
- 5-V, 10-V, and 15-V parametric ratings
- Meets all requirements of JEDEC Tentative Standard No. 13A, "Standard Specifications for Description of 'B' Series CMOS Devices"

Applications:

- Registers, counters, control circuits

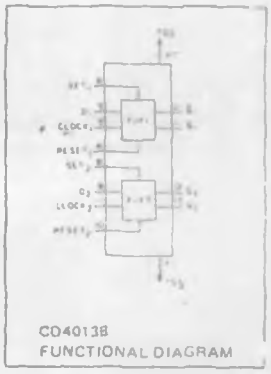

CD4013B
FUNCTIONAL DIAGRAM

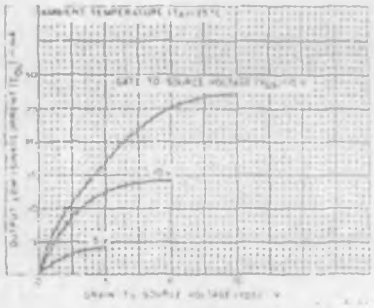

Fig. 1 — Typical output low (sink) current characteristics.

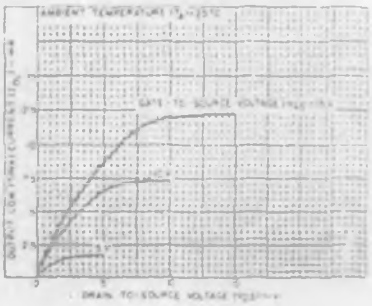

Fig. 2 — Minimum output low (sink) current characteristics.

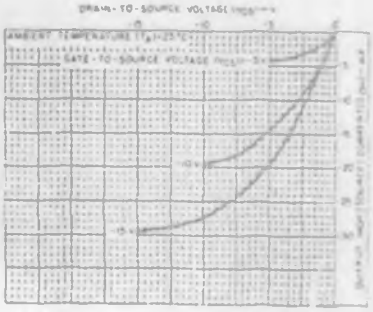

Fig. 3 — Typical output high (source) current characteristics.

RECOMMENDED OPERATING CONDITIONS

At T_A = 25°C, Except as Noted. For maximum reliability, nominal operating conditions should be selected so that operation is always within the following ranges

CHARACTERISTIC	V_{DD} (V)	LIMITS		UNITS
		MIN.	MAX.	
Supply-Voltage Range (For T_A = Full Package Temperature Range)	–		18	V
Data Setup Time t_S	5	40	–	ns
	10	20	–	
	15	15	–	
Clock Pulse Width t_W	5	140	–	ns
	10	60	–	
	15	40	–	
Clock Input Frequency f_{CL}	5	dc	3.5	MHz
	10		8	
	15		12	
Clock Rise or Fall Time t_rCL,* t_fCL	5	–	15	μs
	10	–	4	
	15	–	1	
Set or Reset Pulse Width t_W	5	180	–	ns
	10	80	–	
	15	50	–	

*If more than one unit is cascaded in a parallel clocked operation, t_rCL should be made less than or equal to the sum of the fixed propagation delay time at 15 pF and the transition time of the output driving stage for the estimated capacitive load.

Fig. C-10 DEtails of Dual Flip-Flop

MAXIMUM RATINGS, *Absolute-Maximum Values:*

DC SUPPLY-VOLTAGE RANGE, (V_{DD})
(Voltages referenced to V_{SS} Terminal) . . . . . −0.5 to +20 V
INPUT VOLTAGE RANGE, ALL INPUTS . . . . . −0.5 to V_{DD} +0.5 V
DC INPUT CURRENT, ANY ONE INPUT . . . . . ±10 mA
POWER DISSIPATION PER PACKAGE (P_D):
For T_A = −40 to +60°C (PACKAGE TYPE E) . . . . . 500 mW
For T_A = +60 to +85°C (PACKAGE TYPE E) . . . . Derate Linearly at 12 mW/°C to 200 mW
For T_A = −55 to +100°C (PACKAGE TYPES D, F) . . . . . 500 mW
For T_A = +100 to +125°C (PACKAGE TYPES D, F) . . . Derate Linearly at 12 mW/°C to 200 mW
DEVICE DISSIPATION PER OUTPUT TRANSISTOR
FOR T_A = FULL PACKAGE-TEMPERATURE RANGE (All Package Types) . . . . . 100 mW
OPERATING-TEMPERATURE RANGE (T_A):
PACKAGE TYPES D, F, H . . . . . −55 to +125°C
PACKAGE TYPE E . . . . . −40 to +85°C
STORAGE TEMPERATURE RANGE (T_{stg}) . . . . . −65 to +150°C
LEAD TEMPERATURE (DURING SOLDERING):
At distance 1/16 ± 1/32 inch (1.59 ± 0.79 mm) from case for 10 s max. . . . . +265°C

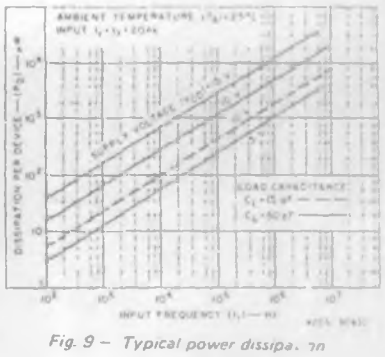

Fig. 9 – Typical power dissipation vs. frequency.

DYNAMIC ELECTRICAL CHARACTERISTICS

At T_A = 25°C; Input t_r, t_f = 20 ns, C_L = 50 pF, R_L = 200 kΩ

CHARACTERISTIC	TEST CONDITIONS V_{DD} (V)	LIMITS MIN.	TYP.	MAX.	UNITS
Propagation Delay Time: Clock to Q or $\overline{Q}$ Outputs t_{PHL}, t_{PLH}	5	–	150	300	ns
	10	–	65	130	
	15	–	45	90	
Set to Q or Reset to $\overline{Q}$ t_{PLH}	5	–	150	300	ns
	10	–	65	130	
	15	–	45	90	
Set to $\overline{Q}$ or Reset to Q t_{PHL}	5	–	200	400	ns
	10	–	85	170	
	15	–	60	120	
Transition Time t_{THL}, t_{TLH}	5	–	100	200	ns
	10	–	50	100	
	15	–	40	80	
Maximum Clock Input Frequency Frequency # f_{CL}	5	3.5	7	–	MHz
	10	8	16	–	
	15	12	24	–	
Minimum Clock Pulse Width t_W	5	–	70	140	ns
	10	–	30	60	
	15	–	20	40	
Minimum Set or Reset Pulse Width t_W	5	–	90	180	ns
	10	–	40	80	
	15	–	25	50	
Minimum Data Setup Time t_S	5	–	20	40	ns
	10		10	20	
	15	–	7	15	
Clock Input Rise or Fall Time t_{rCL}, t_{fCL}	5	–	–	15	μs
	10	–	–	4	
	15	–	–	1	
Input Capacitance C_{IN}	Any Input	–	5	7.5	pF

#Input t_r, t_f = 5 ns

TEST CIRCUITS

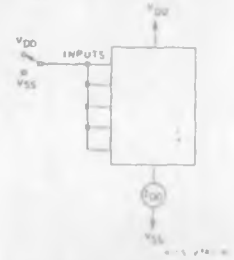

Fig. 10 – Quiescent device current.

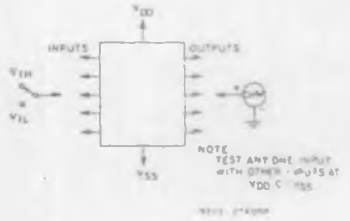

Fig. 11 – Input voltage.

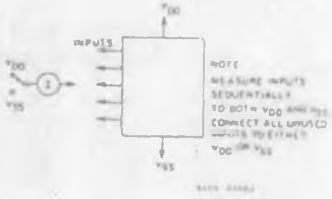

Fig. 12 – Input current.

Fig. C-11 Details of Dual Flip-Flop -Cont.

A P P E N D I X - D

APPENDIX - D

List D-1 Program MHD4 for time dependent flow calculations in the MHD duct

```
      PROGRAM MHD4 (INPUT,OUTPUT,TAPE5=INPUT,TAPE6=OUTPUT,
     + TAPE7=MHD4,TAPE8=IDATA)
      DIMENSION U(60),P(60),U(60),EP(60),APD(60),E(60),P(60),
     +A(60),AA(60),T(60),XM(60),A(60),XLAM(60),UI(60),EPI(60),
     -AEA(60),AAA(60),EI(60),PI(60),TI(60),XMI(60),SOUND(60),W(60),
     -SIS(60),DAREA(60),RR(60),SIGM(60),S2(60),S3(60),AX(60),APAD(60)
     +,VISC(60),W1(60),H1(60),A1(60),SA(10,25,14)
      COMMON EE(61,71),RHOO(61,71),PB,PT,DP,TB,TTP,DTT,ITER
C     THIS PROGRAM CAL. FLOW USING TIME DEPEND.2 ND. ORDER.
C
C     READ MATERIAL FUNCTION
C
      READ(5,*) G,CV,H,S,TTA,APC,AMUR,AAN,AAM,DEFF,VDR
      GAM=1.4
      GAM1=GAM - 1.
      EXPGAM=1/GAM
      PSTAR=1. E-05
C
C     READ INPUT DATA AND CALCULATE REQUIRED PARAMETERS
C
      READ(5,*)N,Z,DELT,NITER,NSTEP
      READ(5,*)PIN,TIN,PEXIT,FACTOR
      READ(5,*)PB,PT,DP,TB,TTP,DTT
      READ(5,*)XMASS
      DELY=Z/(N-1)
      DO 2 NAS=1,N
      READ(5,*)A(NAS)
    2 CONTINUE
      A(N+1)=A(N)
      DO 3 ID=1,N
      AVE=(A(ID)+A(ID+1))/2
      DAE=E-05*A(ID)*W(ID)
  22  FORMAT(2X,2F10.5)
    3 CONTINUE
C
C     READ INITIAL DIST.OF TEMP,PRES AND VELOCITY
C
      DO 4 IR=1,N
      READ(7,100)T(IR),P(IR),U(IR)
  100 FORMAT(1X,3E12.4)
    4 CONTINUE
      P(N)=PEXIT
      NP=(PT-PB)/DP+1
      NT=(TTP-TB)/DTT+1
      DO 600 NRT=1,NT
      DO 600 NRP=1,NP
      READ(21,*)RHOO(NRP,NRT),EE(NRP,NRT)
  600 CONTINUE
C
C     CONVERT INIT.DIST. TO CONSV. FORM FOR I=2 ,N-1
```

```
C
      NC=N-1
      DO 10 IC=2,NC
      TT=T(IC)
      PO=P(IC)
      CALL ABC(PO,TT,ENT,RH,SIG,VISC,K,R1)
      IF(IC.EQ.2)RI=R1
      IF(IC.EQ.NC)RE=R1
      RHO(IC)=RH
      XM(IC)=RHO(IC)*U(IC)
      E(IC)=RHO(IC)*(ENT+U(IC)*U(IC)/2.)-P(IC)
      SIGM(IC)=SIG
      VISC(IC)=VISC
   10  CONTINUE
C
C     CALCULATE BONDARY VALUES
C
C     INLET CONDITION
C
      U(1)=2.*U(2)-U(3)
      T(1)=TIN-(GAM1*U(1)*U(1))/(2.*GAM*RI)
      XMACH=U(1)/SQRT(GAM*RI*T(1))
      GAMX=1.+(GAM1*XMACH*XMACH/2.)
      P(1)=PIN/(GAMX**EX)
      IF(NW.EQ.0)GO TO 710
        RHO(1)=XMASS/(A(1)*U(1))
      P(1)=RHO(1)*(RI*T(1))
  710  TT=T(1)
      PO=P(1)
      CALL ABC(PO,TT,ENT,RH,SIG,VISC,K,R1)
      RHO(1)=RH
      XM(1)=RHO(1)*U(1)
      E(1)=RHO(1)*(ENT+U(1)*U(1)/2.)-P(1)
      SIGM(1)=SIG
      VISC(1)=VISC
C
C     EXIT CONDITION
C
      RHO(N)=2.*(RHO(N-1))-RHO(N-2)
      T(N)=P(N)/(RHO(N)*RE)
      XM(N)=2.*XM(N-1)-XM(N-2)
       PO=P(N)
      TT=T(N)
      CALL ABC(PO,TT,ENT,RH,SIG,VISC,K,R1)
      U(N)=XM(N)/RHO(N)
      E(N)=RHO(N)*(ENT+U(N)*U(N)/2.)-P(N)
      SIGM(N)=SIG
      VISC(N)=VISC
C
C     WRITE INITIAL DISTRIBUTION
C
```

```
      DO 13 NZ=1,N

      WRITE(6,101)T(NZ),P(NZ),U(NZ),RHO(NZ),XM(NZ),E(NZ),SIGM(NZ),VIS
     +C(NZ)
  101 FORMAT(2X,8E12.4)
   13 CONTINUE
      TIME=0.0
      DO 511 M=1,11
      AKH=(M-1)/10.0
       DO 50 ITER=1,NITER
      DO 580 IH=1,N
      TX=FLOAT(IH-1)*DELX+DELX
      REX=XM(IH)*TX/VISC(IH)
      DELTA1=0.0477*TX/REX**0.2
      W1(IH)=W(IH)-2.0*DELTA1
      H1(IH)=H-2.0*DELTA1
      A1(IH)=W1(IH)*H1(IH)
  580 CONTINUE

          INTERMEDIATE STEP

        TOW=DELT/DELX
      DO 20 I=2,NC
      DAREA(I)=A1(I+1)-A1(I)
      XLAM(I)=DAREA(I)/(A1(I)*DELX)
      APM=P(I)/APC
      AMUE=AMUR*(T(I)**AAN)*(APM**AAM)
      BTA=AMUE*B
      EDR=VDR/H1(I)
      S3(I)=AKH*(1.0-AKH)*SIGM(I)*((U(I)*B-EDR)**2)*(BTA**2)/(1.0+BTA
     +**2)
      S2(I)=(1.0+(BTA**2)*AKH)*SIGM(I)*(U(I)*B-EDR)*B/(1.0+BTA**2)
      RHOI(I)=RHO(I)-TOW*(XM(I+1)-XM(I))-DELT*XLAM(I)*XM(I)
      XMI(I)=XM(I)-TOW*(((XM(I+1)*XM(I+1)/RHO(I+1))+P(I+1))-
     +    ((XM(I)*XM(I)/RHO(I))+P(I)))-(DELT*XLAM(I)*XM(I)*
     +    XM(I)/RHO(I))-(DELT*S2(I))
      EI(I)=E(I)-TOW*(((E(I+1)+P(I+1))*XM(I+1)/RHO(I+1))
     +  -((E(I)+P(I))*XM(I)/RHO(I)))-(DELT*XLAM(I)*((
     +   E(I)+P(I))*XM(I)/RHO(I)))-(DELT*S3(I))
      UI(I)=XMI(I)/RHOI(I)
      CM=(EI(I)/RHOI(I))-UI(I)*UI(I)/2.
      HM=GM*P(I)/RHOI(I)
      HOI=RHOI(I)
      PO=P(I)
      TT=T(I)
  550 CALL INVES(HM,HOI,PO,TT)
      CALL SBI(PO,TT,ENT,RH,SIG,VISC,K,R1)
      IF(I.EQ.2)R1=R1
  582 IF(I.EQ.2)R1=R1
      PI(I)=PO
      TI(I)=TT
```

```
      $WRITE(6,8)
      VISC(1)=VISC
   20 CONTINUE
      IF(NUMBER.EQ.700) GOTO 38
      GO TO 37
   38 WRITE(6,105)
  105 FORMAT(//(*LORENTZ FORCE*))
       DO 3 J=1,5
      K=2+5*(J-1)
      WRITE(6,106)K,S2(K),S3(K),RHOI(K),XMI(K),SIGM(K),UI(K),EI(K),HM
  106 FORMAT(I4,2E17.6,6E15.6)
      WRITE(6,202)A1(K),XLAM(K),DAREA(K),H1(K),W1(K)
    3 CONTINUE
  202 FORMAT(2X,5F10.6)

      INTERMEDIATE BOUNDARY VALUES

      INLET CONDITION

   37 UI(1)=2.*UI(2)-UI(3)
      TI(1)=TIN-(GAM1*UI(1)*UI(1))/(2.*GAM*RI)
      XMACHI=UI(1)/SQRT(GAM*RI*TI(1))
      GAMXI=1.+(GAM1*XMACHI*XMACHI/2.)
      PI(1)=PIN/(GAMXI**EX)
      IF(NU.EQ.0)GO TO 720
      RHO(1)=XMASS/(P(1)*UI(1))
      PI(1)=RHO(1)-RI*TI(1))
  720 PO=P(1)
      TT=TI(1)
      CALL ABC(PO,TT,ENT,RH,SIG,VISC,K,R1)
      RHOI(1)=RH
      XMI(1)=RHOI(1)*UI(1)
      EI(1)=RHOI(1)*(ENT+UI(1)*UI(1)/2.)-PI(1)
      SIGM(1)=SIG
      VISC(1)=VISC

      EXIT VALUES

      PI(N)=2.*PI(N-1)-PI(N-2)
      UI(N)=2.*UI(N-1)-UI(N-2)
      PI(N)=PSTAS/(1.0-DEFF+DEFF*(1.0+GAM1*UI(N)*UI(N)/
     +(2.0*GAM*RE*TI(N)))**EX)
      PO=PI(N)
      TT=TI(N)
      CALL ABC(PO,TT,ENT,RHS,SIG,VISC,K,R1)
      XMI(N)=UI(N)*RH
      RHOI(N)=RH
      EI(N)=RHOI(N)*(ENT+UI(N)*UI(N)/2.0)-PI(N)
      SIGM(N)=SIG
      VISC(N)=VISC
```

```
      SECOND STEP

      DO 30 K=2,NC
      APL=P(K)/APC
      AMUS=AMUR*(T(K)**AAN)*(APL**AAM)
      BTA=AMUS*B
      EDR=VDR/H1(K)
      S3(K)=AKH+(1.0-AKH)*SIGM(K)*((U(K)*B-EDR)**2)*(BTA**2)/(1.0+BTA
     **2)
      S2(K)=(1.0+(BTA**2)*AKH)*SIGM(K)*(U(K)*B-EDR)*B/(1.0+BTA**2)
      RHO(K)=0.5*(RHO(K)+RHOI(K)-TOW*(XMI(K)-XMI(K-1))-DELT*
     +    XLAM(K)*XMI(K))
      XM(K)=0.5*((XM(K)+XMI(K)-TOW*(((XMI(K)*XMI(K)/RHOI(K))+PI(K))-
     +   ((XMI(K-1)*XMI(K-1)/RHOI(K-1))+PI(K-1)))-(DELT*XLAM(K)*
     +    XMI(K)*XMI(K)/RHOI(K))-(DELT*S2(K)))
      E(K)=0.5*(E(K)+EI(K)-TOW*((EI(K)+PI(K))*XMI(K)/RHOI(K))-
     +   ((EI(K-1)+PI(K-1))*XMI(K-1)/RHOI(K-1)))-(DELT*XLAM(K)*
     +    (EI(K)+PI(K))*XMI(K)/RHOI(K))-(DELT*S3(K)))
      U(K)=XM(K)/RHO(K)
      EM=(E(K)/RHO(K))-U(K)*U(K)/2.
      AM=EM*P(K)/RHO(K)
      RO=RHO(K)
      PO=P(K)
      TT=T(K)
      CALL INVEST(AM,RO,PO,TT)
      CALL ABC(PO,TT,ENT,RH,SIG,VISC,K,R1)
      IF(K.EQ.2)RI=R1
      IF(K.EQ.NC)RE=R1
      SIGM(K)=SIG
      VISC(K)=VISC
      SOUND(K)=SQRT(GAM*P*T)
   30 CONTINUE
      IF(ITER.EQ.ITDO) GO TO 26
      ITER=2
      DO 25 J=1,5
      JJ=5+(J-1)
      WRITE(6,102) J,S2(J),S3(J),RHO(J),XM(J),SIGM(J),U(J),E(J),HM
      FORMAT(I2,I3,2E7.6,6E15.6)
   25 CONTINUE

      SECOND STEP BOUNDARY VALUES


      BOUNDARY VALUES

      INLET CONDITIONS
      U(1)=2.*U(2)-U(3)
      T(1)=(1.-(GAM-1.)*U(1)*U(1))/(2.*GAM*RI)
      SOUND(1)=SQRT(GAM*RI*T(1))
```

```
      GAM1=1.+(GAM*XMACH*XMACH/2.)
      PSTAG=PIN/(GAM1**EX)
      IF(NU.EQ.0)GO TO 730
      RHO(1)=XMASS/(A(1)*U(1))
      P(1)=RHO(1)*(RI*T(1))
  730 PO=P(1)
      TT=T(1)
      CALL ABC(PO,TT,ENT,RH,SIG,VISC,K,R1)
      RHO(1)=RH
      XM(1)=RHO(1)*U(1)
      E(1)=RHO(1)*(ENT+U(1)*U(1)/2)-P(1)
      SIGM(1)=SIG
      VISC(1)=VISC

      EXIT VALUES

      T(N)=2.0*T(N-1)-T(N-2)
      U(N)=2.*U(N-1)-U(N-2)
      P(N)=PSTAG/(1.0-DEFF+DEFF*(1.0+GAM1*U(N)*U(N)/
     *(2.0*GAM*RE*T(N)))**EX)
      PO=P(N)
      TT=T(N)
      CALL ABC(PO,TT,ENT,RH,SIG,VISC,K,R1)
      RHO(N)=RH
      XM(N)=U(N)*RHO(N)
      E(N)=RHO(N)*(ENT+U(N)*U(N)/2.)-P(N)
      SIGM(N)=SIG
      VISC(N)=VISC
      SOUND(N)=SQRT(GAM*R*T(N))
C
C     CALCULATE TIME AND WRITE
C
      TIME=TIME +DELT
      ZAP=NSTEP
      WA=ITER/ZAP
      IW=WA
      IF((WA-IW).EQ.0.) GO TO 31
      GO TO 45
   31 WRITE(6,200)ITER,TIME
  200 FORMAT(2X,I10,2X,E12.6/)
      GO TO 45
      DO 32 IWR=1,N
      WRITE(6,10)T(IWR),P(IWR),U(IWR),RHO(IWR),
     *  XM(IWR),E(IWR)
   32 CONTINUE

      CALCULATE TIME STEP

      VEL=ABS(U(1))
      SVEL=ABS(SOUND(1))
```

```
      DO 40 IT=2,N
      AU1=ABS(U(IT))
      NITT=IT-1
      AU2=ABS(U(NITT))
      IF(AU1.GE.AU2)GO TO 41
      GO TO 42
   41 VEL=AU1
   42 ASO1=ABS(SOUND(IT))
      ASO2=ABS(SOUND(NITT))
      IF(ASO1.GE.ASO2)GO TO 43
      GO TO 40
   43 SVEL=ASO1
   40  CONTINUE
      DELT=DELX/(VEL+SVEL)
      DELT=FACTOR*DELT
   50 CONTINUE
      WRITE(6,340)
  340 FORMAT(15X,*FINAL OUTPUT*//)
      DO 34 IR2=1,N
      XMA=U(IR2)/SQRT(GAM*R*T(IR2))
      AST=1.+GAM1*XMA*XMA/2.
      TST=T(IR2)*AST
      PST=P(IR2)*(AST**EX)
      PRATIO=P(IR2)/PIN
      XFLOW=XM(IR2)*A1(IR2)
      WRITE(6,102)TST,T(IR2),PST,P(IR2),U(IR2)
     +    ,XMA,XFLOW
  102 FORMAT(7E11.4)
   34  CONTINUE
      REWIND 7
      DO 33 IR1=1,N
      WRITE(7,100)T(IR1),P(IR1),U(IR1)
   33 CONTINUE
      SAEX=0.0
      SAJAX=0.0
      SAPD=0.0
      SAJX=0.0
      DO 810 I=1,N
      AKP=P(I)/APC
      AMUE=AMUR*(T(I)**AAN)*(AKP**AAM)
      BTA=AMUE*B
      EDR=VDR/H1(I)
      APD(I)=(AKH*(1.0-AKH)*SIGM(I)*((U(I)*B-EDR)**2)*(BTA**2)/(1.0+BTA
     +**2))*(A1(I)*DELX)
      AEX(I)=AKH*BTA*(U(I)*B-EDR)*DELX
      IF(AKH.EQ.0)GOTO 66
      AJX(I)=APD(I)/AEX(I)
      GO TO 67
   66 AJX(I)=0.0
   67 AJY(I)=(1.0+(BTA**2)*AKH)*SIGM(I)*(U(I)*B-EDR)/(1.0+BTA**2)
      AX(I)=AEX(I)/DELX
```

```
      AJAX(I)=(SIGM(I)*(BTA*(U(I)*B-EDR)-AX(I))/(1.0+BTA**2))*A1(I)
      APAD(I)=AJAX(I)*AEX(I)
      SAEX=SAEX+AEX(I)
      SA(K,N,1)=I
      SA(K,N,2)=APD(I)
      SA(K,N,3)=APAD(I)
      SA(K,N,4)=AEX(I)
      SA(K,N,5)=AJX(I)
      SA(K,N,6)=AJY(I)
      SA(K,N,7)=AJAX(I)
      SA(K,N,8)=BTA
      SAPD=SAPD+APD(I)
      SAJX=SAJX+AJX(I)
      SAJAX=SAJAX+AJAX(I)
  810 CONTINUE
      AAJX=SAJX/25.0
      AAJAX=SAJAX/25.0
      SA(K,N,9)=SAPD
      SA(K,N,10)=SAEX
      SA(K,N,11)=AAJX
      SA(K,N,12)=AAJAX
      SA(K,N,13)=XMASS
      SA(K,N,14)=AKH
  811 CONTINUE
      DO 903 K=1,10
      DO 902 N=1,25
      WRITE(6,861)SA(K,N,1),SA(K,N,2),SA(K,N,3),SA(K,N,4),SA(K,N,5),
     +SA(K,N,6),SA(K,N,7),SA(K,N,8)
  861 FORMAT(I4,7E13.4)
      WRITE(6,870)SA(K,N,9),SA(K,N,10),SA(K,N,11),SA(K,N,12),
     +SA(K,N,13),SA(K,N,14)
  870 FORMAT(2X,*POWER=*,E14.6,2X,*VOLTAGE=*,F10.4,2X,*CURRENT=*,F6.3
     +,2X,*HALL CURRENT=*,F6.3,2X,*MASS FLOW RATE=*,F5.3,2X,*K=*,F5.3)
  902 CONTINUE
  903 CONTINUE
      STOP
      END
      SUBROUTINE INVEST(ES,RHOS,PS,TS)
      COMMON EE(61,71),RHOO(61,71),PB,PT,DP,TB,TTP,DTT,ITER
      EINT=0.0
      RHOINT=0.0
      DO 500 I=1,200
      IF(PS.LT.PB)GO TO 501
      IF(PS.GT.PT)GO TO 501
      IF(TS.LT.TB)GO TO 501
      IF(TS.GT.TTP)GO TO 501
      SI=((PS-PB)/DP)+1.
      IS=SI
      IS1=IS+1
      SJ=((TS-TB)/DTT)+1.
```

```
      JS=JJ
      JS1=JS+1
      EE1=(EE(IS1,JS1)-EE(IS1,JS))*(SJ-JS)+EE(IS1,JS)
      EE2=(EE(IS,JS1)-EE(IS,JS))*(SJ-JS)+EE(IS,JS)
      EE3=(EE(IS1,JS)-EE(IS,JS))*(SI-IS)+EE(IS,JS)
      EE4=(EE(IS1,JS1)-EE(IS,JS1))*(SI-IS)+EE(IS,JS1)
      RHOO1=(RHOO(IS1,JS1)-RHOO(IS1,JS))*(SJ-JS)+RHOO(IS1,JS)
      RHOO2=(RHOO(IS,JS1)-RHOO(IS,JS))*(SJ-JS)+RHOO(IS,JS)
      RHOO3=(RHOO(IS1,JS)-RHOO(IS,JS))*(SI-IS)+RHOO(IS,JS)
      RHOO4=(RHOO(IS1,JS1)-RHOO(IS,JS1))*(SI-IS)+RHOO(IS,JS1)
      EINT=(EE1-EE2)*(SI-IS)+EE2
      RHOINT=(RHOO1-RHOO2)*(SI-IS)+RHOO2
      FP=(EE1-EE2)/DP
      FT=(EE4-EE3)/DTT
      GP=(RHOO1-RHOO2)/DP
      GT=(RHOO4-RHOO3)/DTT
      DETER=FP*GT-FT*GP
      DH=(GT*(ES-EINT)-FT*(RHOS-RHOINT))/DETER
      DK=(-GP*(ES-EINT)+FP*(RHOS-RHOINT))/DETER
      ERRORH=ABS(DH/PS)
      ERRORK=ABS(DK/TS)
      IF(ERRORH.LT.1.E-5.AND.ERRORK.LT.1.E-5)GO TO 502
      PS=PS+DH
      TS=TS+DK
  500 CONTINUE
  501 WRITE(6,1001)I,PS,TS
      WRITE(6,1002)ERRORH,ERRORK,ITER
 1002 FORMAT(2E10.4,I5)
 1001 FORMAT(I2,2F8.2,2E10.3,2X,'VALUES FALL OUTSIDE RANGE')
      STOP
  502 RETURN
      END
C     THIS SUBROUTINE CALCULATE THE COAL DATA
      SUBROUTINE ABC(P0,T0,ENT,RHO,SIGM,VISC,K,R1)
      C1=0.2239
      C2=-671.6
      T0=TT
      C3=-5849000.
      R0=245.7
      THETA=24030.
      C4=-0.4038
      C5=11.22
      PN=P0/101300.
      PNPN=PN**C4
      ALP=C5*SQRT(T0)*EXP(-THETA/T0)
      R1=R0*(1-ALP*PNPN)
      C19=-0.4625
      PN2=PN**C19
      ENT=T0+T0+C2*T0+C3+(R0*PN2*ALP*(T0+2*THETA))
      RHO=P0/(R1*T0)
      ENT=H-(P0/RHO)
```

```
      C20=5.793
      C21=-0.2396
      C22=9.38
      C23=0.1014
      C24=22.8
      C25=-0.6663
      C26=2.0
      C27=2930.
      TB=(C27/T0)-1.
      TEX=(C20+C21*PN)*TB*TB+(C22*PN**C23*TB)
      SIGM=C24*PN**C25*(T0/C27)**2.*EXP(-TEX)
      C6=-3.64E-12
      C7=5.522E-08
      C8=-1.22E-05
      C9=-0.1437
      VISC=(C6*(T0**2)+C7*T0+C8)*(1.0+ALP*(PN**C9))
      RETURN
      END
```

```
 UN=7932736  LOG OFF  18.54.09.
JEN=A50A     Sku-S       1.001
```

TABLE D-2 SAMPLE OUTPUT OF PROGRAM MHD_4 (Faraday Mode)

ELECTRODE (No.)	POWER (Watts)	CURRENT (Amps.)	VOLTAGE (Volt.)	INTER RESIST (ohms.)	LOAD FACTOR (K)
1	470.44	10.37	45.33	4.37	.50
2	497.98	10.57	46.19	4.37	.50
3	503.12	10.70	47.02	4.39	.50
4	490.32	10.66	46.01	4.32	.50
5	497.09	10.80	46.02	4.26	.50
6	462.31	10.48	44.11	4.21	.50
7	429.76	10.61	40.50	3.82	.50
8	310.93	11.15	45.92	4.11	.50
9	439.68	10.50	41.88	3.99	.50
10	503.84	11.27	44.69	3.96	.50
11	514.06	11.04	46.57	4.22	.50
12	430.60	10.61	40.57	3.82	.50
13	485.95	11.24	43.22	3.84	.50
14	450.91	10.97	41.09	3.74	.50
15	443.55	10.91	40.66	3.73	.50
16	414.30	11.02	37.61	3.41	.50
17	491.42	11.58	42.42	3.66	.50
18	443.31	11.17	39.67	3.55	.50
19	475.19	11.54	41.18	3.57	.50
20	462.37	11.51	40.16	3.48	.50

Table D-3 Sample output of Program MH4 (Diagonal Mode)

ELECTODE (No.)	POWER (Watts.)	CURRENT (Amps.)	VOLTAGE (Volts)	INTER. RESIST (Ohms.)	LOAD FACTOR (K)	UHALL (Volts)	BETA (B)
1	627.91	10.68	58.79	5.50	.50	39.23	1.29
2	662.86	10.76	61.61	5.73	.50	41.24	1.29
3	705.82	10.95	64.43	5.88	.50	44.43	1.32
4	684.42	10.88	62.88	5.78	.50	43.37	1.32
5	721.09	11.15	64.69	5.80	.50	45.73	1.34
6	709.81	11.14	63.71	5.72	.50	45.24	1.35
7	738.19	11.35	65.02	5.73	.50	47.16	1.37
8	735.95	11.40	64.57	5.67	.50	47.23	1.38
9	757.85	11.58	65.46	5.65	.50	48.76	1.40
10	760.30	11.65	65.27	5.60	.50	49.43	1.41
11	779.93	11.82	65.99	5.58	.50	50.54	1.43
12	785.73	11.91	65.99	5.54	.50	51.14	1.44
13	802.95	12.06	66.56	5.52	.50	52.43	1.46
14	811.94	12.17	66.71	5.48	.50	53.25	1.48
15	830.19	12.35	67.23	5.44	.50	54.55	1.50
16	841.01	12.46	67.50	5.42	.50	55.56	1.52
17.	861.94	12.67	68.04	5.37	.50	56.96	1.54
18	870.97	12.73	68.42	5.37	.50	58.11	1.56
19.	894.93	12.98	68.95	5.31	.50	59.63	1.58
20	999.32	12.94	69.48	5.37	.50	60.93	1.60

TABLE D-4 Gas Property Curve Fits (85)

The constants below allow the gas properties specified to be calculated as functions of temperature, T , and pressure, P. They apply to a gas consisting of the products of the combustion of coal with a stoichiometric amount of oxygen, equal weight of nitrogen and 1.5 per cent by weight as KOH. The constants are considered valid over the temperature range 1800-2850K and the pressure range 0.5 - 6 atmospheres (5×10^4 - 6.1×10^5 pa.) MKS units are used in all cases.

Density $\rho = R/RT$ $\qquad R = R_o(1 + P_o^n)$

$\qquad\qquad\qquad\qquad \alpha = C\,T\,EXP(-\theta/T)$

$\qquad\qquad\qquad\qquad P_o = P/1.013 \times 10^5$

Where

$R_o = 245.7$

$\theta = 2.403 \times 10^4$

$C = 11.22$

$n = -0.4038$

Enthalpy $h = aT^2 + bT + c + R_o P_o^n (T+20)$

Where $a = 0.2255$

$b = -671.8$

$c = -5.849 \times 10^6$

$n = -0.4625$

The internal energy, e, can be calculated from the relation,

$h = e - RT.$

Thermal Conductivity $k = (aT^2 + bT + c)(1 + P_o^n)$

Where $a = -1.520 \times 10^{-8}$

$b = 1.026 \times 10^{-4}$

$c = -3.358 \times 10^{-2}$

$n = -0.1729$

Viscosity $\mu = (aT^2 + bT + c)(1 + P_o^n)$

Where $a = -8.64 \times 10^{-12}$
$b = 5.522 \times 10^{-8}$
$c = -1.221 \times 10^{-5}$
$n = -0.1437$

Prandit Number $P_r = aT^2 + bT - c)(1 - P_o^n/4)$

Where $a = 9.036 \times 10^{-9}$
$b = -2.921 \times 10^{-5}$
$c = 0.8456$
$n = -0.2424$

Electrical Conductivity $\sigma = eP_o^f \left(\frac{T}{h}\right)^g EXP(-T_{EX})$

$T_{EX} = (a+bP_o) T_B^2 + cP_o^d T_B$

$T_B = \frac{h}{T} - 1$

Where $a = 3.793$
$b = -0.2396$
$c = 9.380$
$d = 0.1014$
$e = 22$
$f = -0.6663$
$g = 2.0$
$h = 2850$

Electron Mobility $\mu e = \mu r \; T^n \; P_o^m$

Where $\mu r = 1.557 \times 10^{-5}$
$m = 1.330$
$n = -1.011$

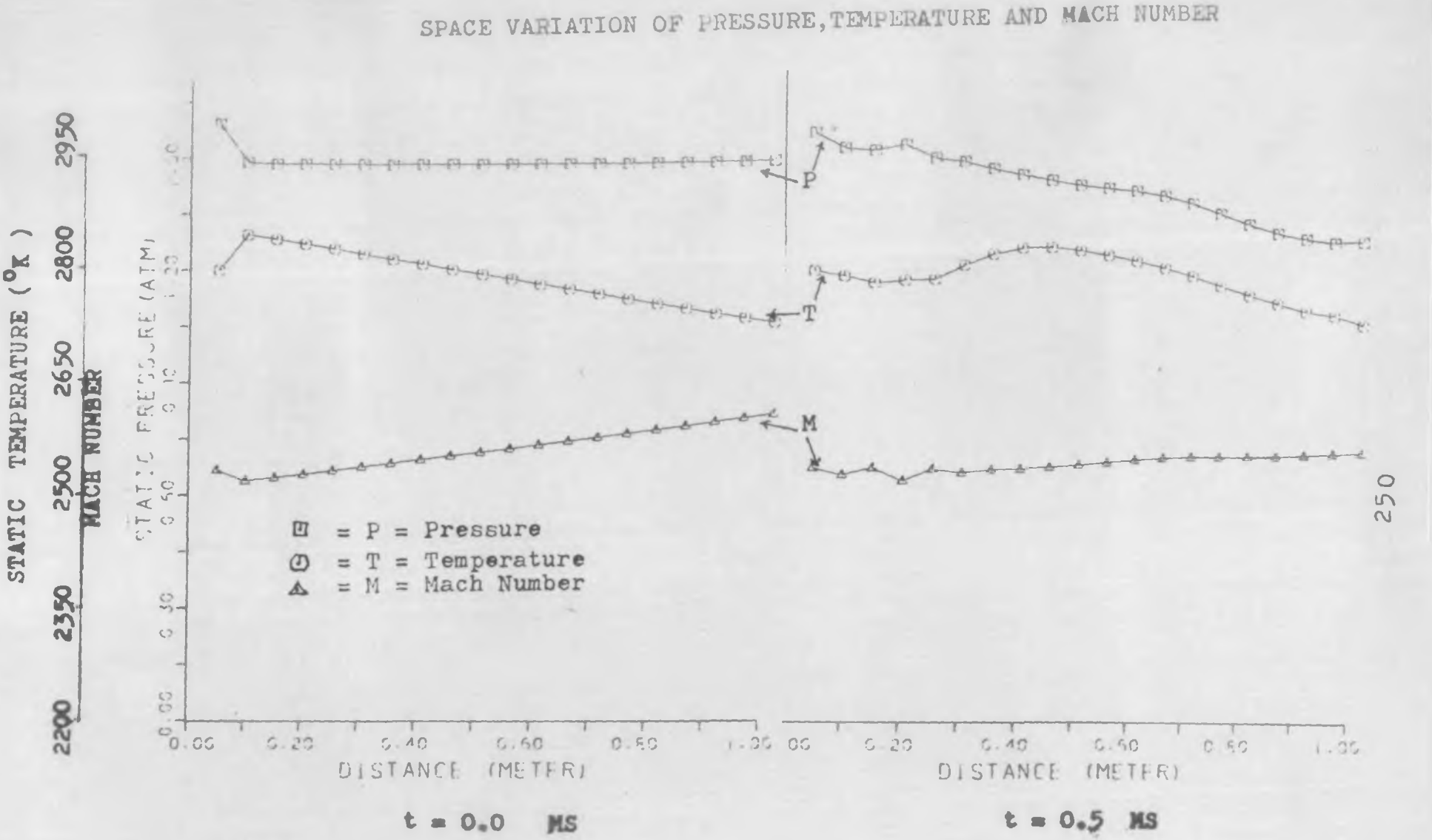

FIG. D - 5 STEP INCREASE IN LOAD

FIG. D - 6 STEP INCREASE IN LOAD

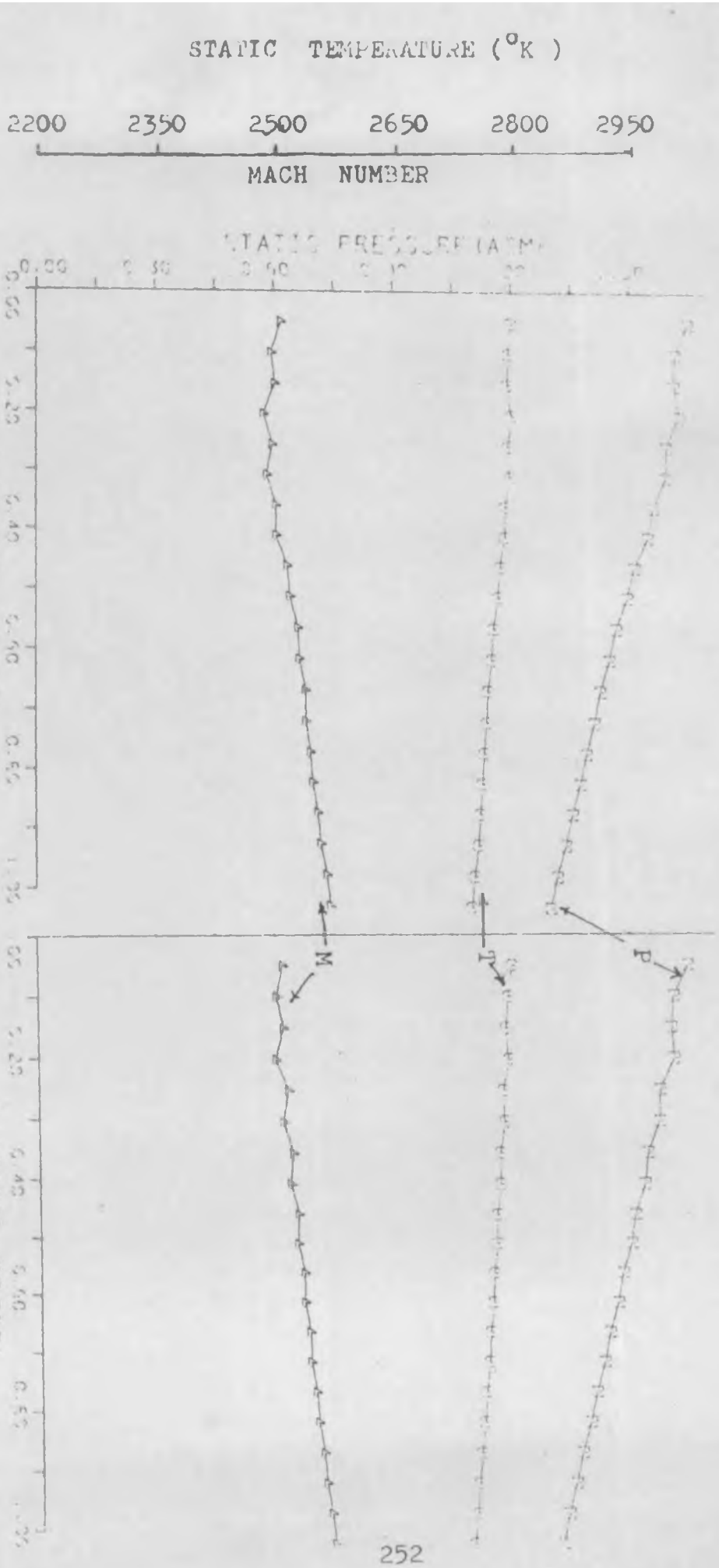

FIG. D - 7 STEP INCREASE IN LOAD

SPACE VARIATION OF PRESSURE, TEMPERATURE AND MACH NUMBER

FIG. D - 8 STEP DECREASE IN LOAD

t = 0.0 MS

t = 0.5 MS

FIG. D - 9 STEP DECREASE IN LOAD

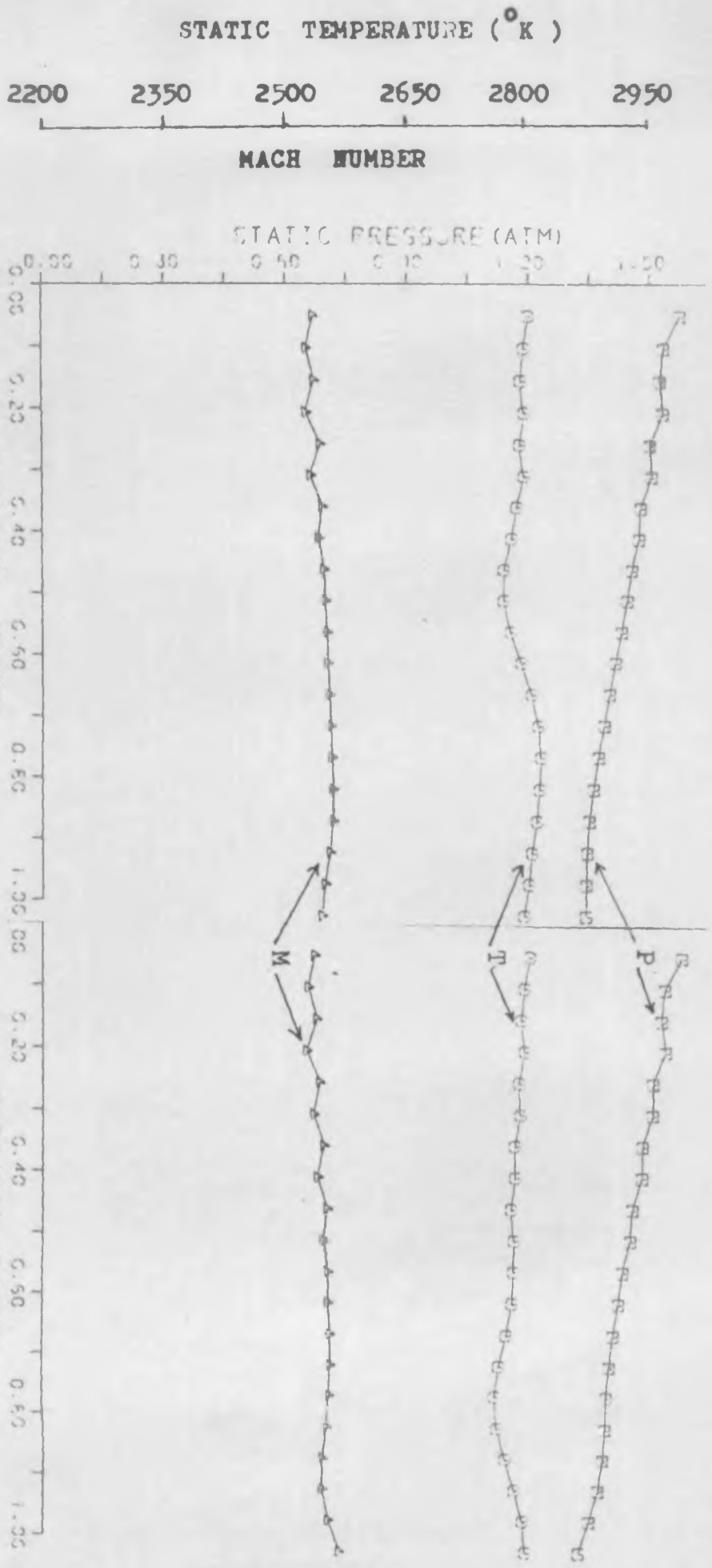

FIG. D - 10 STEP DECREASE IN LOAD

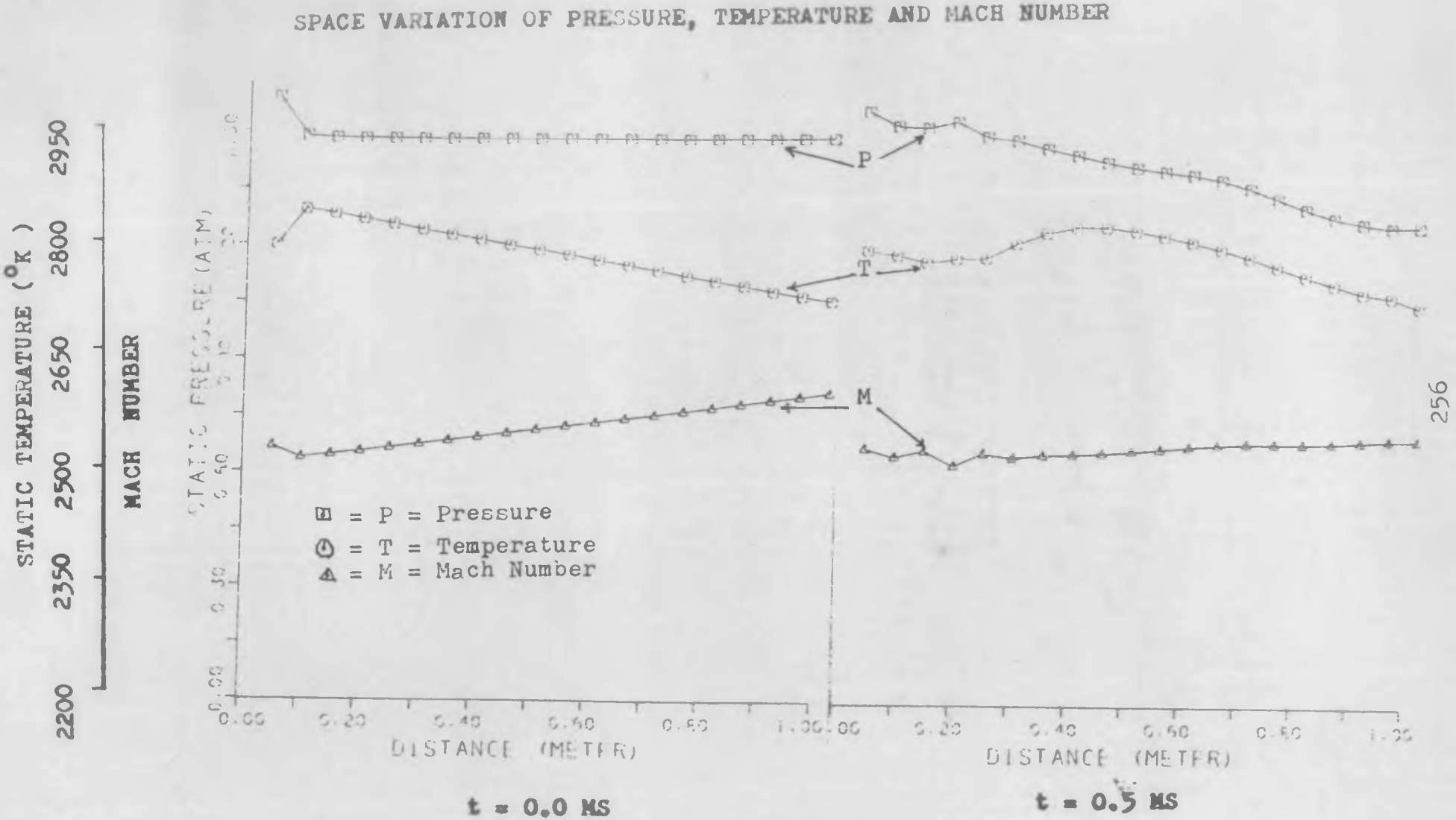

FIG. D-11 FULL LOAD TO SHORT CIRCUIT

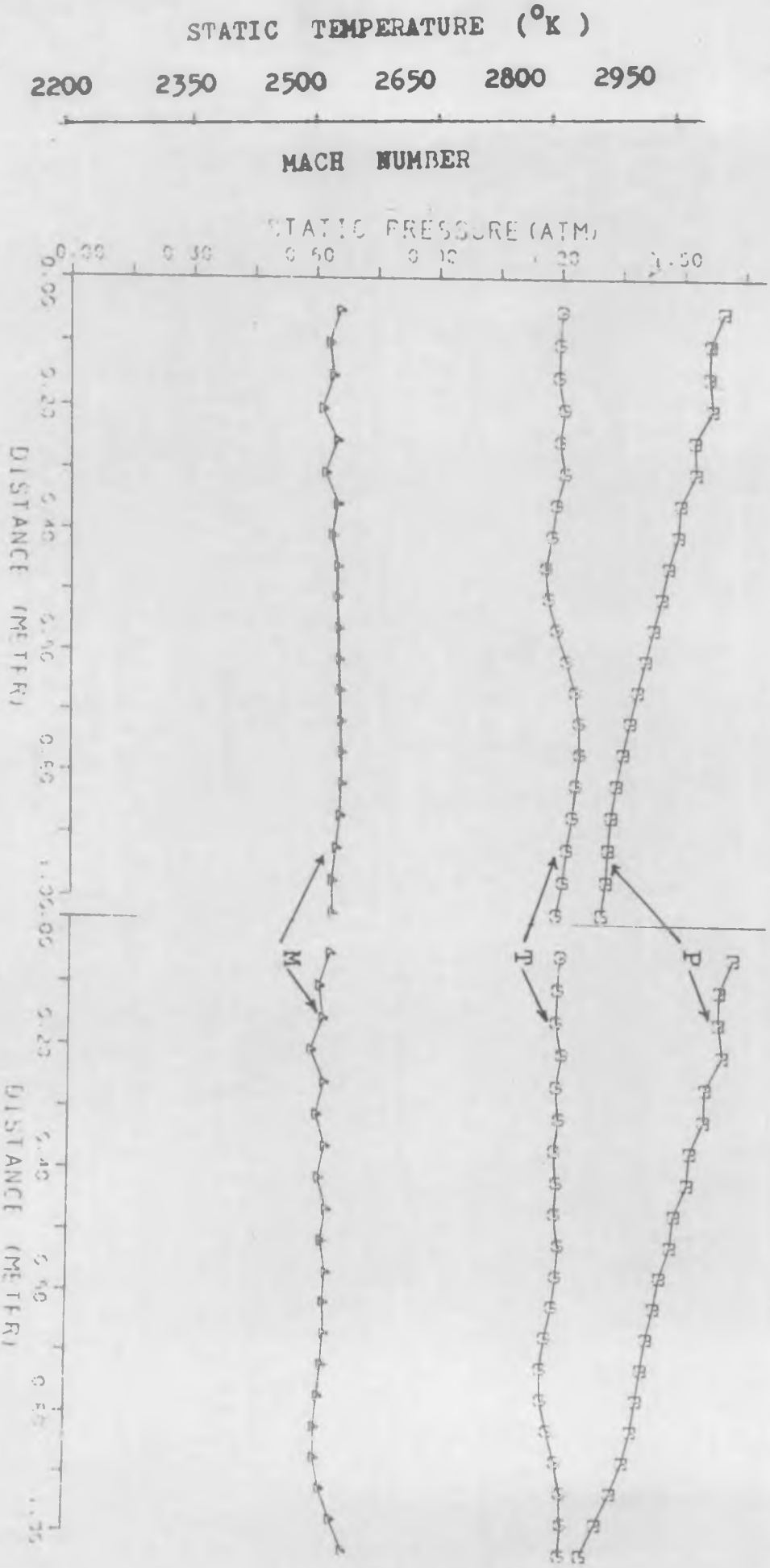

t = 1.0 MS

t = 1.5 MS

FIG. D - 12 FULL LOAD TO SHORT CIRCUIT

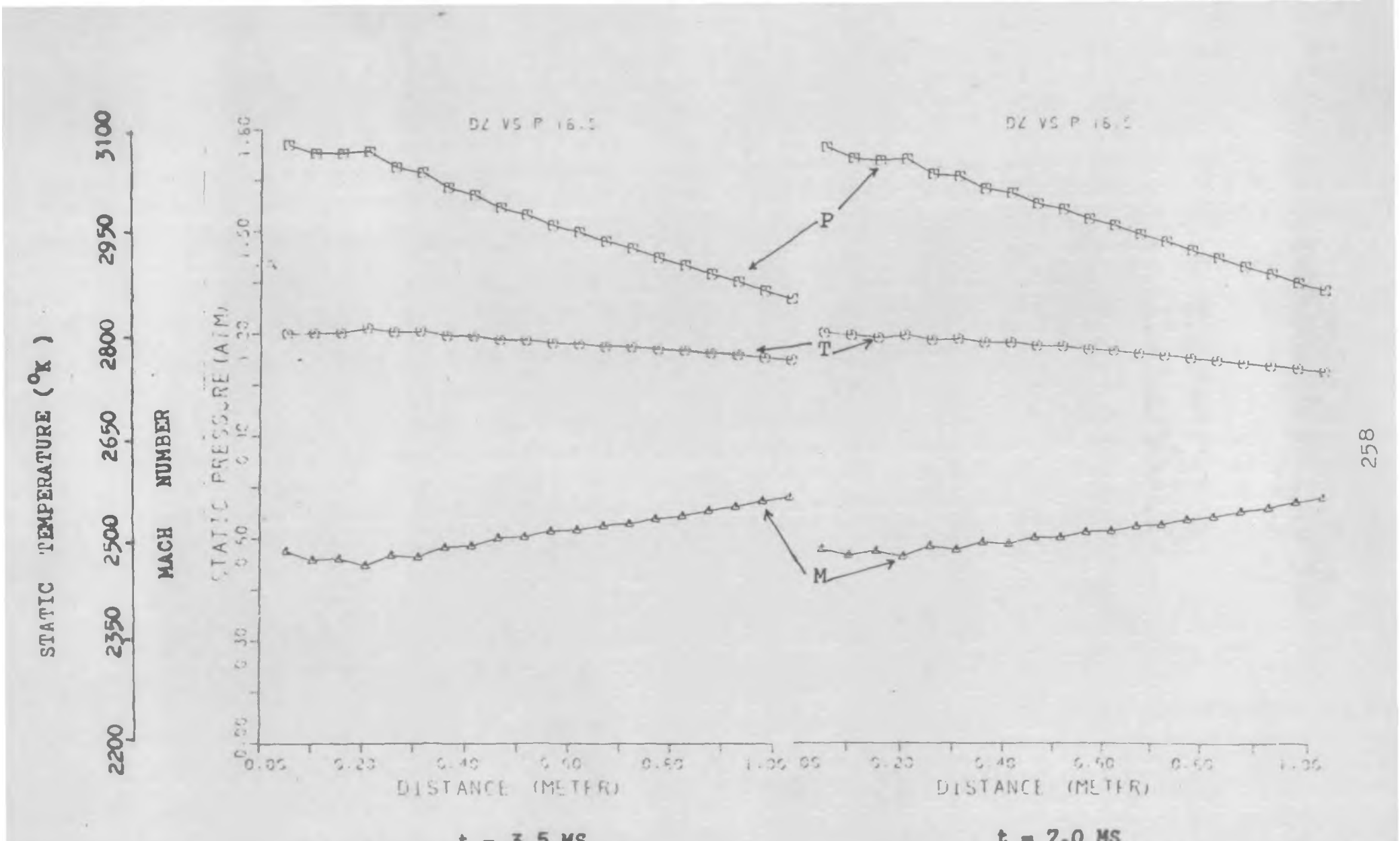

t = 3.5 MS

t = 7.0 MS

FIG. D - 13 FULL LOAD TO SHORT CIRCUIT

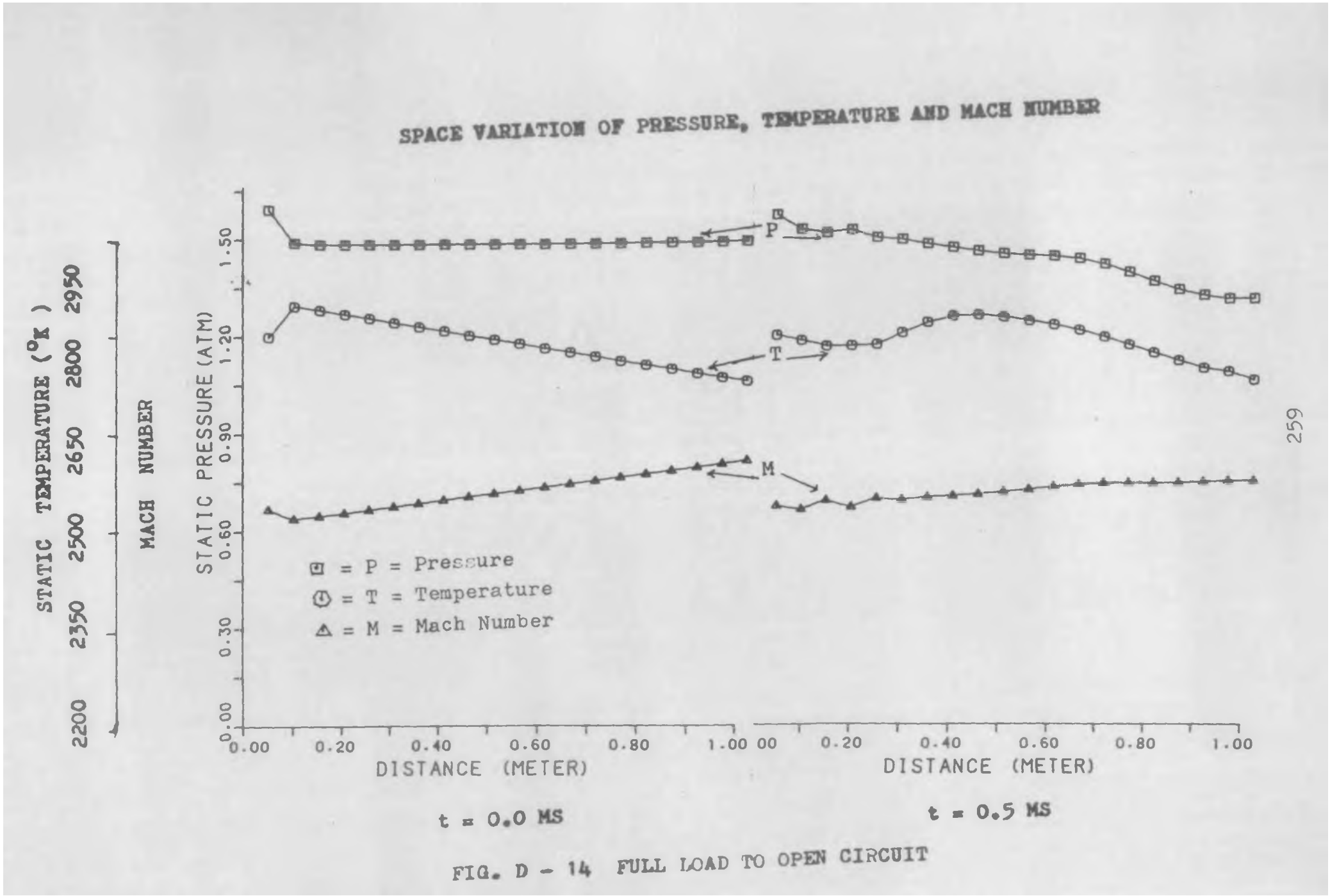

FIG. D - 14 FULL LOAD TO OPEN CIRCUIT

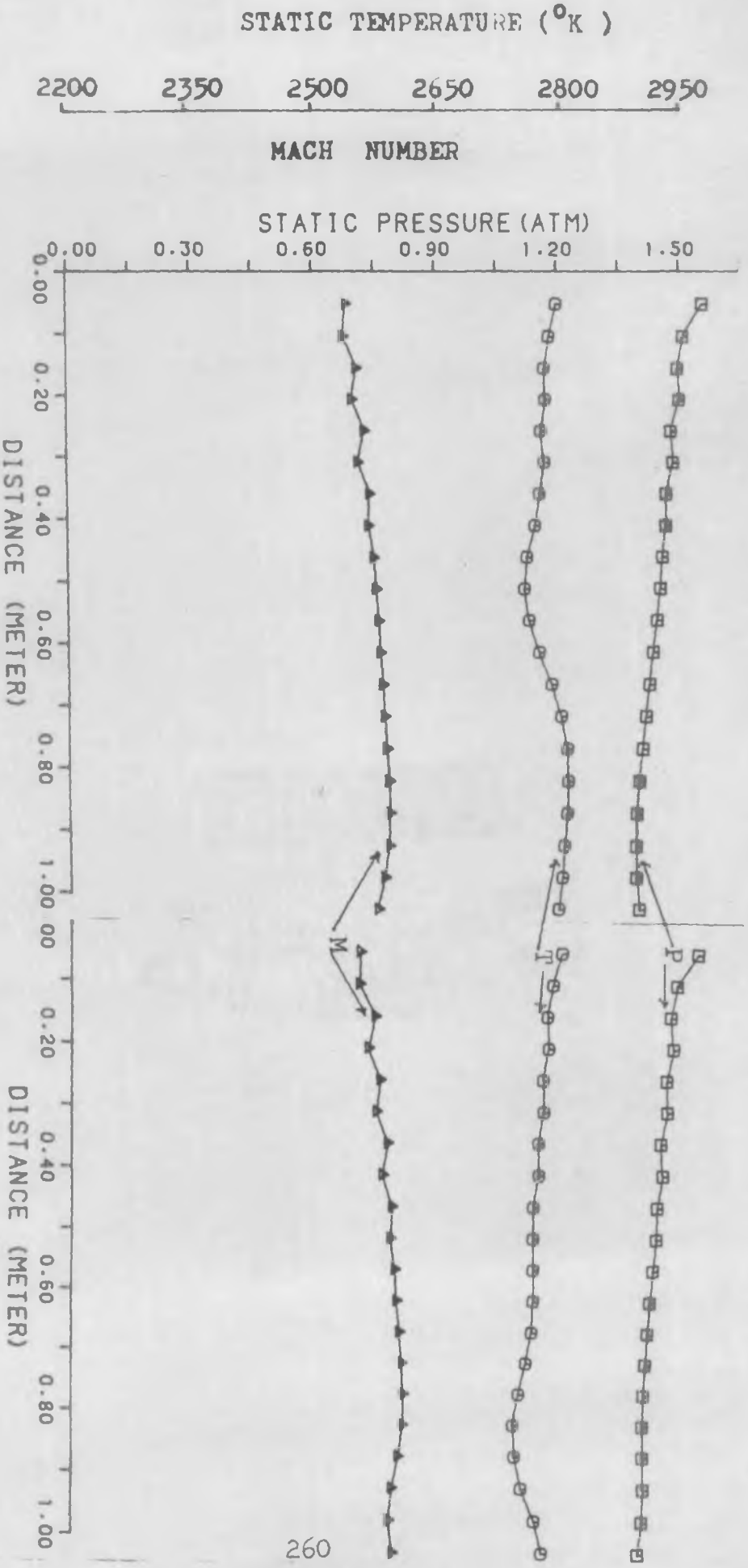

FIG. D - 15 FULL LOAD TO OPEN CIRCUIT

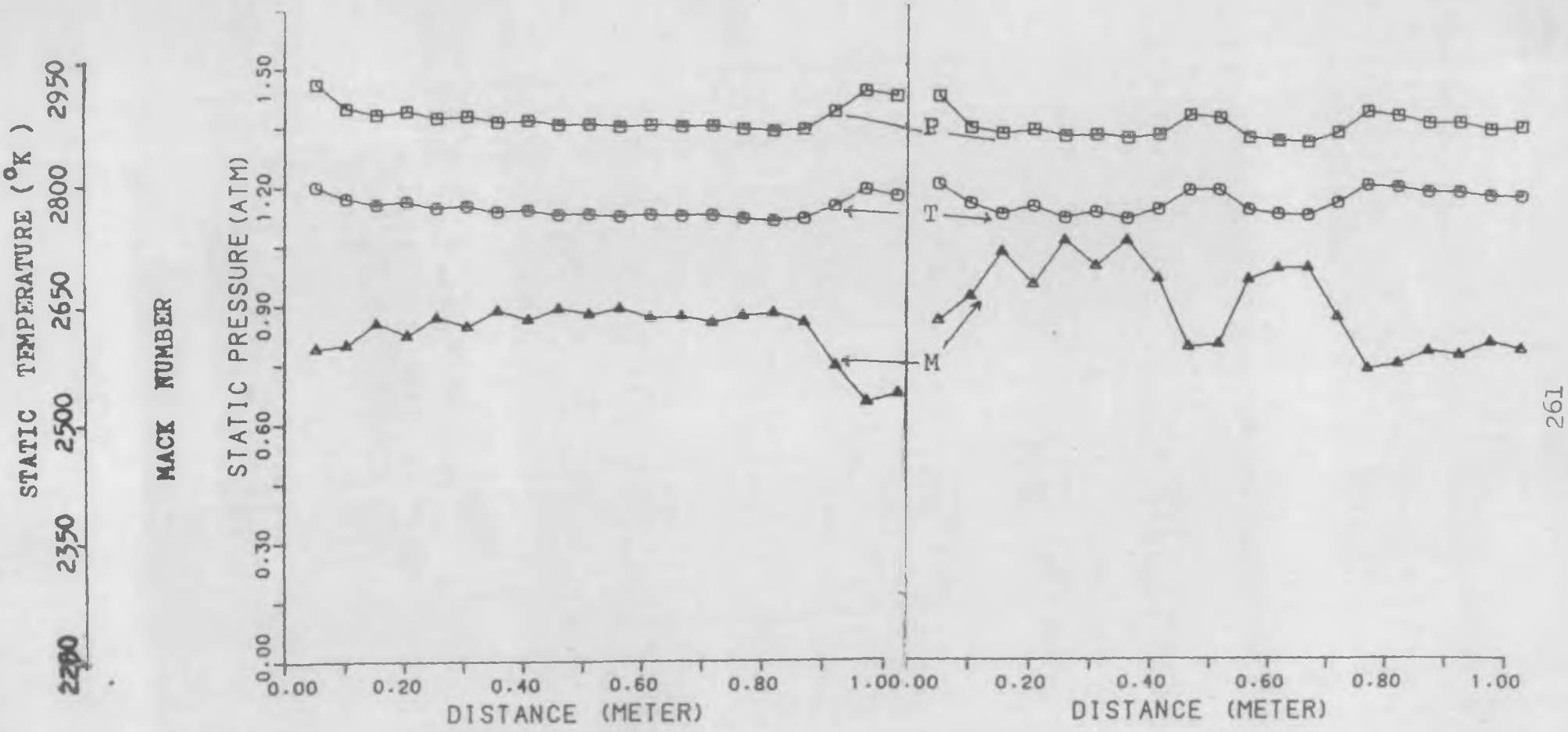

t = 3.5 MS

t = 7.0 MS

FIG. D - 16 FULL LOAD TO OPEN CIRCUIT

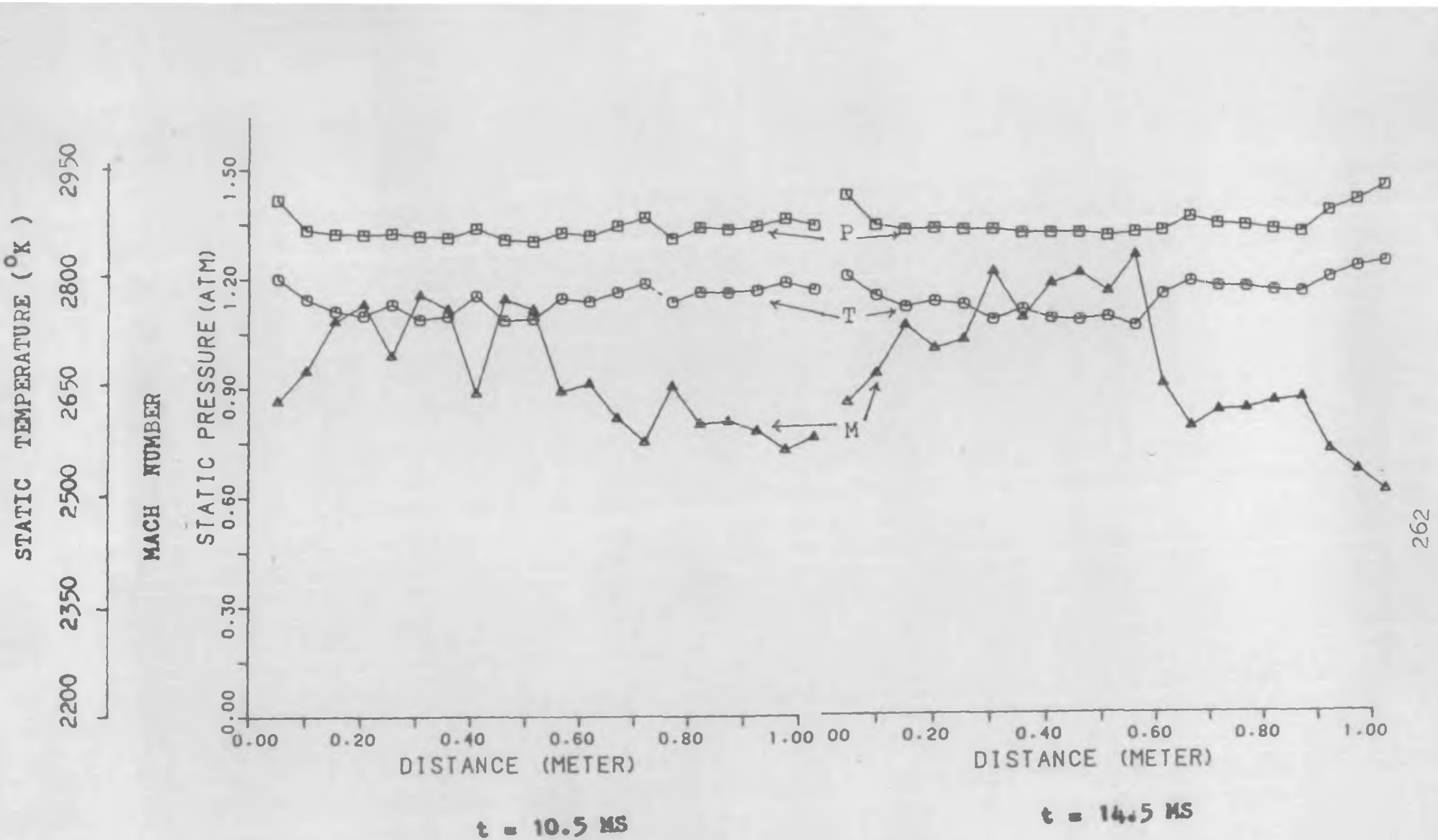

FIG. D-17 FULL LOAD TO OPEN CIRCUIT

CURRICULUM VITAE

1. PERSONAL DATA

(a) Name	MOHIBULLAH
(b) Date of birth	December 31st, 1950
(c) Present Occupation	Reader Department of Electrical Engineering A.M.U. Aligarh
(d) Address for correspondence	4 Teachers Hostel Near M.M. Hall Aligarh Muslim University Aligarh 202 002, UP (India)

2. ACADEMIC AND PROFESSIONAL QUALIFICATIONS

Examinations passed	Name of Board/University	Year	Division
High School	U.P. Board	1965	First
Pre-University	A.M.U. Aligarh	1966	First
B.Sc. (Engg.)	A.M.U. Aligarh	1971	First
M.Sc. (Engg.)	A.M.U. Aligarh	1975	First
Ph.D.+	A.M.U. Aligarh	To be submitted soon	

+Thesis Topic, Force Commutated Inverters for Conversion and Control of MHD Power.

Eight papers, out of the thesis have already been published and two have been communicated for publication.

3. PROFESSIONAL EXPERIENCE

(a) Taught B.E. (Evening Course) from January, 1972 to December 1972.

(b) Teaching under-graduate and post-graduate classes in theory and practicals both from December 1972 till date.

4. AWARDS/SCHOLARSHIPS RECEIVED

(a) University of Sydney Post Graduate Award from January, 1980 to December, 1983.

(b) Govt. of India University Grants Commission (UGC) Post Graduate Scholarship from August, 1971 to December, 1972.

(c) Govt. of India National Scholarship from August, 1965, to July, 1971.

5. RESEARCH EXPERIENCE

(a) Papers published/presented in National and International Conferences/Journals/Seminars and Symposium.

(b) Papers communicated/under preparation.

} As per list of publication attached.

(c) Guided undergraduate and post graduate projects.

6. CURRENT RESEARCH INTEREST

(a) Investigation of Transients in MHD Generator Inverter Link with Gasdynamic Coupling.

(b) Feasibility studies of Rewirable Fuse wire for protection of Semi-conductor Devices.

(c) Investigation of Electrical Transients in Transformers.

7. INTERNATIONAL CONFERENCES ATTENDED

(a) Ninth International Conference on MHD Electrical Power Generation, November, 17-22, 1986, Taskuba, Ibaraki,
JAPAN

(b) Specialists Meeting on Coal Fired MHD Power Generation, November 4-6, 1981, Sydney,
AUSTRALIA

(c) International Electric Energy Conference, November, 13-17, 1980, Sydney,
AUSTRALIA

LIST OF PUBLICATIONS

1. Analysis of a Force Commutated Inversion Scheme for supplying MHD Power to an A.C. System,
   Mohibullah, G.J. Sanders and S. Ramakrishnan,
   Eighth International Conference on MHD Electrical Power Generation, 12-18 September, 1983, Moscow (USSR).

2. Analytical and Experimental Investigations of a Force commutated MHD-Inverter link for Power Control to A.C. System,
   Mohibullah, S. Ramakrishnan, G.J. Sanders and H.K. Messerle, Ninth International Conference on MHD Electrical Power generation, November 17-21, 1986, Taskuba, Ibaraki, Japan.

3. Digital Simulation of Quasi Static Changes in the Fluid Dynamic Conditions of MHD Generator Inverter Link.
   Mohibullah, M. Salman Beg and M. Ayub, First Symposium on Electric Power System in Fast Developing Countries, March 21-24, 1987, King Saud University, Riyadh, Saudi Arabia.

4. Rewirable Water Fuse Protection for Semi Conductor Devices,
   Mohibullah and Ateeq A. Khan, Electrical India Journal, Vol. XXVII No. 22, November, 1987.

5. Magneto-hydrodynamic Energy for Electric Power Generation,
Mohibullah and M. Ahmad, XIth Annual Convention (ACE-84), I.E.E.E., Indian Council, December 4-9, 1984, Calcutta.

6. MHD Generation for Better Environmental Control and Cheaper Electrical Power,
Mohibullah, M. Salman Beg, M.S. Jameel Asghar and Prof. M.A. Jani, Indian Congress on Engineering and Environment (ICEE) November 10, 1985, New Delhi.

7. MHD Generator - Inverter Systems,
Mohibullah, M. Salman Beg and M.S. Jameel Asghar, Fourth National Power Systems Conference (NPSC 86), Feb. 15-17, 1986, Banaras.

8. MHD Thermal Power Plants,
Mohibullah, M. Salman Beg and M. Ayub, National Seminar on Recent Trends in Electrica Energy Systems, 21-23 May, 1986, New Delhi.

9. Coal Gas Fired MHD Power Plants - Technological Developments and Applications,
Mohibullah and M.A. Jani, Abstract Communicated to Energex 88 - International Energy Conference and Exposition, University of Al-Fateh, Tripoli, Libya.

10. Transient Response of MHD-Generator Inverter Link With Gas Dynamic Coupling,
Ready for submission to Tenth International Conference

on MHD Electrical Power Generation, 4-8 December, 1989, Tiruchirapalli, India.

11. Computerised Evaluation of Magnetising Inrush Current in Transformers,
Mohibullah and K.P. Basu, Electric Power System Research Journal, Vol. 2, No. 3, 1979, Switzerland.

12. Computation of Magnetising Inrush Current in Secondary of a Current Transformer.
Mohibullah, K.P. Basu and Prof. M.A. Jani, Journal of Institution of Instrumentation Scientists and Technologists (IIST), India, Vol. 6, No. 4, October, 1977.

13. Computation of Transient Current in the C.T. Secondary with Inductive Burden,
Prof. M.A. Jani, Mohibullah and K.P. Basu, Fourth All India Seminar on Instrumentation, November 2-3, 1985, Aligarh.

14. Measurement of Dynamic Magnetising Reactance of a Transformer,
Prof. M.A. Jani, M. Salman Beg, Mohibullah, M.S. Jameel Asghar, Fourth All India Seminar on Instrumentation, November 2-3, 1985, Aligarh.

15. Instant Controlled Switching of Transformers,
M. Salman Beg, Mohibullah and M. Ayub, National Seminar on Recent Trends in Electric Energy Systems, 21-23 May, 1986, New Delhi.

16. A Solid State Relay for Transformer Switching,
M. Salman Beg, Mohibullah and M.S. Jameel Asghar,
International Journal of Electronics, U.K. (Accepted).

17. A Circuit for Instant Controlled Switching,
M.S. Beg, Mohibullah and M.S. Jameel Asghar, International Journal of Electronics, Vol. 59, No. 4, PP 525-527 (UK).

18. A Solid State Three Step Distance Relay for EHV/UHV Lines,
M.S. Beg, Mohibullah and M.S. Jameel Asghar, Ninth National Systems Conference (NSC-85) December 21-23, 1985, Allahabad.

19. Speed Control of Squirrel Cage Induction Motor Using ON-OFF Control Scheme,
M. Ahmad and Mohibullah, Diamond Jubilee Symposium, March 8-10, 1979, Banaras.

20. Modelling of Polyphase Transformers for Computer Studies,
K.P. Basu and Mohibullah, All India Seminar on Computer Applications in Power Systems, November 14-18, 1978, Calcutta.

21. Effect of Parameter Variation on the Design and Optimisation of 3-Phase Induction Motor,
M. Ayub, M.S. Beg and Mohibullah, Abstract Communicated Fifth National Power Systems Conference, 8-10 September, 1988, Bangalore, India.